THE UNIVERSITY
of EDINBURGH

Markers of progression and regression in diabetic nephropathy – from animal models to human disease

Boris Bernhard Betz

A thesis submitted for the degree of Doctor of Philosophy

THE UNIVERSITY OF EDINBURGH

2017

DECLARATION

I hereby declare that this thesis has been composed by myself and has not been submitted for any other degree elsewhere. The work presented herein is my own and all referenced work and assistance given to me is duly acknowledged.

Signed ……. Date……

Boris Bernhard Betz

Student ID: 1202720

MRC/Centre for Inflammation Research, University of Edinburgh.

Certified that the present work entitled *''Markers of progression and regression in diabetic nephropathy – from animal models to human disease''* submitted to the University of Edinburgh in fulfilment of the requirement for the award of the Doctor of Philosophy, was carried out by Mr. Boris Bernhard Betz (1202720) under the supervision of Dr. Bryan Conway at Centre for Inflammation Research (CIR), QMRI, University of Edinburgh.

Signed…….. Date…….

Dr. Bryan Conway

BHF Centre for Cardiovascular Science, University of Edinburgh.

To my parents

ABSTRACT

Progression and regression of renal fibrosis is observed in patients with diabetic nephropathy (DN). The underlying pathways, especially those that promote regression of fibrosis, remain poorly understood in part due to the fact that most rodent DN models only mirror the early features of human DN. Another obstacle for optimizing treatment strategies is that albuminuria, the current gold standard biomarker of renal damage in DN, often lacks sensitivity and specificity for identification of those patients with diabetes who are at risk of a rapid decline in renal function. A novel DN model, in which diabetes was induced with streptozotocin in Cyp1a1mRen2 rats and hypertension was generated by inducing renin transgene expression with dietary indole-3-carbinol (I-3-C), mimicked many of the key biochemical, pathological and transcriptomic changes observed in the kidney of patients with DN. Recently, the model was extended to include a 'reversal phase' in which glycaemia was tightly controlled and blood pressure normalized for eight weeks after an 'injury phase' of 28 weeks. The present study aims to employ this novel rodent model to examine pathways activated in the kidney during and following reversal of hyperglycaemia and hypertension and to identify new biomarkers that might complement albuminuria in assessing risk of renal deterioration in patients with diabetes.

Methods

Tissue and urinary specimen from the Cyp1a1mRen 2 model of DN were analysed by realtime-PCR, Western-Blot, ELISA and staining techniques including immunohistochemistry, immunofluorescence and zymography. To establish in-situ

zymography a model of ureteric obstruction was used. Urinary peptidomic analysis as well as measurement of urinary exosomes and microparticles was performed in the model and in patients with DN utilizing liquid chromatography/tandem mass-spectrometry, nanoparticle tracking analysis (NTA) or flow cytometry.

Results

Tight control of blood glucose and blood pressure during an 8 week 'reversal phase' did not significantly reverse the degree of renal fibrosis accrued during a 28wk 'injury phase'. However, it did result in a reduction in expression of genes encoding myofibroblast markers and extracellular matrix (ECM) proteins. Genes that were up-regulated during both injury and reversal phases were implicated in adaptive immunity, phagocytosis, lysosomal processing and degradative metalloproteinases (MMPs). Paradoxically MMP activity was massively reduced during both injury and reversal phases. This may be due to an elevated level of tissue inhibitor of metalloproteinase-1 (TIMP-1) protein in both phases. After separating TIMP1 from MMP in renal tissue homogenates from animals of both the injury and reversal phases using gel electrophoresis, MMP activity was restored above that of controls.

For biomarker discovery peptidomic analysis was performed on urine from rats at baseline and during the injury and reversal phases of the Cyp1a1mRen2 model of DN and from patients with moderately advanced DN and from normal controls. The use of two different search and analyse tools (Maxquant, Progenesis QI) resulted in the discovery of significantly altered peptides in the urine in rodent and human DN. Further studies focused on peptides derived from those proteins for which the corresponding gene was similarly regulated in the DN model and in human DN.

Urinary epidermal growth factor (uEGF) matched these criteria as the reduction of excretion during the injury phase in the DN model was paralleled by reduced EGF protein expression in renal tissue.

Key biomarker candidates identified in the first two chapters were measured in urinary specimens of patients from the Edinburgh Type 2 Diabetes study (ET2DS) to test translational utility. MMP7 and other candidates, such as osteopontin or vascular endothelial growth factor (VEGF) were not of value in predicting renal outcomes. Reduced uEGF was significantly associated with increased mortality rate. In a subgroup of 642 study participants who were normoalbuminuric and had a preserved renal function at baseline, a lower uEGF to creatinine ratio was a risk factor for either developing an estimated glomerular filtration rate less than 60 ml/min per $1.73m^2$, rapid (over 5% per annum) decline in renal function or the combination of both. The latter remained significant after correction for other covariates. Addition of uEGF resulted in a marginal improvement in a model derived from traditional risk factors for predicting rapid decline and the composite end-point.

Urinary microparticle (20nm-1000nm) analysis was established in the rodent DN model and translated to patients with DN. Total urinary exosomes (20nm-100nm) or exosomes derived from specific renal cell types including podocytes and tubular cells, increased during the injury phase in the Cyp1a1mRen2 model followed by a decrease after reversal phase. In a pilot study comprising participants with advanced chronic kidney disease, the urinary exosome concentration correlated with renal function. In the ET2DS an increased exosome concentration at baseline indicated a higher risk for renal deterioration during four years follow-up even after correction for baseline eGFR. Urinary microvesicles (100nm-1000nm) concentration increased during the injury phase

in the DN model though correlation with renal function in humans was only significant if kidney-specific marker (podocalyxin) positive microvesicles were measured.

Conclusion

Normalisation of hyperglycaemia and hypertension in the DN model allows the study of genetic and protein regulation during the injury and reversal phases. ECM-production but not ECM-degradation genes are down-regulated during the reversal phase. The lack of reduction in ECM during the reversal phase might be caused by persistently reduced MMP activity due to the presence of TIMP-1. Targeting TIMP might be a treatment strategy to promote reduction of renal fibrosis.

For the first time, the analysis of urinary peptidomics was integrated with previous transcriptomic findings in the Cyp1a1mRen2 model and patients with DN for biomarker discovery. The approach was validated using different analysis tools and successfully identified candidate markers which were increased or reduced in DN. Candidates included uEGF, which identified patients with DN who were at risk of a rapid decline of renal function. Though the marker requires further confirmation in other cohorts, it might be especially useful for patients with type 2 diabetes, in whom renal decline is often uncoupled from the development of albuminuria.

Finally, the DN model helped to develop the methodology of microparticle analysis. For the first time a potential prognostic value of urinary exosome analysis in patients with diabetes has been demonstrated. Future work will include further optimisation of the methodologies, including labelling of microparticles with multiple antibodies and increasing study participant numbers.

SUMMARY

Diabetic Nephropathy (DN) increases the risk of cardiovascular death and end-stage renal failure, which necessitates dialysis or transplantation. It represents a huge economic burden for health care systems. In order to develop new treatment strategies it is mandatory to gain deeper insight into the mechanisms that promote damage and repair in the kidney. Moreover, novel biomarkers are needed to identify patients at high risk of rapid decline in renal function as the established marker, urinary albumin, fails to identify all patients at risk. Improved risk biomarkers may enable therapies to be targeted towards those who would benefit most.

This thesis examined a novel rat model of DN in which a combination of high blood pressure and high blood sugar reproduced the microscopic findings and gene expression patterns observed in the kidneys of patients with DN. To investigate repair mechanisms, blood pressure and blood sugar were tightly controlled for an additional 8 weeks (reversal phase) after a 28wk period of high blood pressure and high glucose levels (injury phase).

Tight control of blood pressure and blood sugar levels halts the progress of renal scarring by switching off genes that promote scar production. Whilst degradation of scar is attempted through increased production of enzymes called matrix metalloproteinases (MMPs), these appear to be blocked by Tissue inhibitor of metalloproteinases (TIMPs). Strategies to neutralise the inhibitory effect of TIMPs might promote renal repair in patients with DN.

To identify new biomarkers that predict renal prognosis, the identity and quantity of the peptides (small subunits of proteins) present in the urine of rats in the DN model

was analysed. A large number of peptides were excreted in higher or lower amounts in the urine of rats with high blood pressure and glucose compared with normal rats. One peptide originated from protein called epidermal growth factor (EGF), which was found to be decreased in the kidney and urine in rats with diabetes and hypertension

A panel of promising biomarker candidates identified in the rodent model of DN were examined for their ability to predict renal outcomes in patients with type 2 diabetes. Only one candidate, EGF, was able to predict renal outcomes even after the influence of other risk factors like baseline renal function, the amount of protein leak into the urine, sex, age or how tightly the patients' diabetes was controlled was taken into account.

Microparticles are small vesicles (<1 micrometre in diameter) released by cells either spontaneously or following induction by stimuli such as cellular damage. In the rodent DN model, increased urinary concentration of microparticles was associated with renal tissue damage. In patients with DN, the urinary concentration of very small (20-100 nanometres in diameter) microparticles, called exosomes, correlated not only with renal function but also seemed to be an indicator for future decline. Hence, microparticles might represent a new promising class of biomarkers.

In conclusion, using the novel rat DN model helped to dissect damaging and repair mechanisms in the kidney and to identify new potential biomarkers that predict renal outcome. Future work is needed to further expand the knowledge of repair mechanisms and to confirm the validity of the biomarkers to enable earlier and more efficient treatment of patients with diabetic nephropathy.

ACKNOWLEDGEMENTS

First of all, I would like to thank Dr. Bryan Conway for the opportunity to perform this work under his supervision. His exceptionally profound knowledge and constructive advice always helped me to make progress. The completion of this thesis would not have been possible without his guidance and feedback.

He also kindly provided the samples from the rodent Cyp1a1mRen2 diabetic nephropathy model.

Profound thanks to my second supervisor, Prof Jeremy Hughes, for his guidance, suggestions and active involvement during the whole project despite his professional commitments.

I want to thank all the members of the Phagocytosis group within the Centre for Inflammation Research for their support and advice. I really enjoyed the productive atmosphere in the group. I am deeply indebted to Carolynn Cairns for teaching me new laboratory techniques with an invaluable experienced guidance.

I am grateful to Spike Clay and Gary Borthwick for their help with the in vivo studies and to the team from the Histology Department for the processing of histological specimens.

Dr. Andrew Cronshaw has to be thankfully credited for patiently introducing me into the field of peptidomic analysis and for his assistance with the measurement of samples. The data analysis was supported by Dr. Jonathan Manning, who programmed an R-implementation for MaxQuant data and Douglas Lamont who helped me using Progenesis QI in the Proteomics Facility, University of Dundee.

Profound thanks to Professor Jackie Price for allowing me to work with the urinary specimens from the Edinburgh Type 2 Diabetes study. I also benefited from Professor Price's and Sara Jenks' advice on epidemiological issues.

I thank all participants of the RDS study for consenting to provide blood and urine samples. I am also thankful to all staff members from the Renal Diabetes and Renal Medicine Clinics of the Royal Infirmary of Edinburgh, who supported me during the recruitment and sample collection process.

My sincere thanks go to Dr. Margaret Paterson, Dr. Wilna Oosthuyzen and Dr. John Pound for helping me using the NanoSight LM10 and the Attune Flow Cytometer. Without their profound explanations and patient advice my work on these instruments would not have been possible.

Finally, I would like to thank my parents for their support, faith and encouragement.

ORAL PRESENTATIONS AND PUBLICATIONS

Oral Presentations

i. Boris Betz, Sara J. Jenks, Andrew D Cronshaw, Douglas J. Lamont, Carolynn Cairns, Jonathan R. Manning, John J. Mullins, Jeremy Hughes, Stella McLachlan, Mark W.J. Strachan, Jackie F. Price, Bryan R. Conway (2015) **Urinary peptidomics in a rodent model of diabetic nephropathy highlightsepidermal growth factor as a biomarker for renal deterioration in patients with type 2 diabetes**. Meeting 2015, The Scottish Renal Association, Dundee, UK

ii. Boris Betz, Wilna Oosthuyzen, John Pound, James Dear, Jeremy Hughes, Bryan Conway. (2014) **Profiling urinary exosomes in patients with Diabetes mellitus type 2 using the novel Nanosight Tracking Analysis (NTA) technique**. Autumn meeting 2014, The Scottish Renal Association, Edinburgh, UK

iii. Bryan R. Conway, Boris Betz, Tara A. Sheldrake, Jonathan R. Manning, Donald R. Dunbar, Jeremy Hughes, John J. Mullins (2013) **Identifying mechanisms that promote injury and repair in diabetic kidney disease using a novel rodent model**. Meeting 2013, European Diabetic Nephropathy Study Group, Barcelona, Spain

Publications

i. Conway B. R., Betz B., Sheldrake T. A., Manning J. R., Dunbar D. R., Dobyns A., Hughes J., Mullins J. J. (2014). **Tight blood glycaemic and blood pressure control in experimental diabetic nephropathy reduces extracellular matrix production without regression of fibrosis.** *Nephrology (Carlton) 19 (12): 802-813.*

ii. Betz B. B., Jenks, S. J., Cronshaw A. D., Lamont D. J., Cairns C., Manning J.R., Goddard J., Webb D. J., Mullins J. J., Hughes J., McLachlan, S., Strachan, M. W., Price, J. F., Conway, B. R. (2016) **Urinary peptidomics in a rodent model of diabetic nephropathy highlights epidermal growth factor as a biomarker for renal deterioration in patients with type 2 diabetes.** *Kidney Int 89(5): 1125-1135.*

iii. Betz, B. and B. R. Conway (2014). **Recent advances in animal models of diabetic nephropathy.** *Nephron Exp Nephrol 126(4): 191-195.*

iv. Betz, B. and B. R. Conway (2016). **An Update on the Use of Animal Models in Diabetic Nephropathy Research**. *Curr Diab Rep 16(2): 18.*

TABLE OF CONTENT

ABBREVIATIONS

Abbreviation	Full name
ACE-I	angiotensin converting enzyme inhibitors
ACR	albumin-to-creatinine ratio
AGE	glycolation end-products
ANG	angiotensin
ARB	Angiotensin II receptor blockers
BoM	Bodipy-Maleimide
BSA	bovine serum albumin
CE-MS	capillary electrophoresis mass spectrometry
CI	confidence interval
CKD	chronic kidney disease
CVD	cardiovascular disease
CysC	Cystatin C
DKD	diabetic kidney disease
DM	Diabetes mellitus
DN	diabetic nephropathy
ECM	extracellular matrix
eGFR	estimated glomerular filtration rate
ELISA	Enzyme-linked immunosorbent assay
ESRD	end-stage renal disease
ET2D study	Edinburgh Type 2 Diabetes study
EV	extracellular vesicles
FCM	flow cytometer
HTN	hypertension
IFN	interferon
IQR	interquartil range
LC-MS/MS	liquid chromatography tandem mass spectrometry
LDL	low-density lipoprotein
MALDI-TOF	Matrix-assisted laser desorption/ionization time of flight
mM	Milli molar
μM	Micro molar
MMP	matrix-metalloproteinase
MP	microparticles
MV	microvesicles
NF-κB	Nuclear factor kappa-light-chain-enhancer of activated B cells

NO	nitric oxide
NO	Nitric oxide
NTA	nanoparticle tracking analysis
OPN	osteopontin
PAS	periodic acid-Schiff
PBS	Phosphate-buffered saline
QC	quality control
Qdot	quantum dot
RAGE	receptors for glycolation end-products
ROS	reactive oxygen species
ROS	Reactive oxygen species
RT	room temperature
rt	reverse transcription
SD	standard deviation
SEM	standard deviation of the mean
SOP	standard operating procedure
STZ	streptozotocin
T1D	type 1 diabetes
T2D	type 2 diabetes
TFA	trifluoroacetic acid
TIMP	tissue inhibitor of metalloproteinases
TNF-α	Tumor necrosis factor- α
uEGF:Cr	urinary epidermal growth factor to creatinine ratio
ZDF	Zucker diabetic fatty

LIST OF TABLES

LIST OF FIGURES

1. INTRODUCTION

1.1 Diabetic nephropathy

1.1.1 Definition and Epidemiology

Epidemiology of Diabetes Mellitus and Diabetic Nephropathy

According to the International Diabetes Federation (IDF) the worldwide prevalence of diabetes is 8.8% which will rise to 10.5% in 2040, meaning that by then 640 million adult individuals will suffer from diabetes. In 2015, 14.5% of overall-mortality was diabetes related and 700 billion dollars (approximately 12% of the health care budget) was spent on the treatment of diabetes and its complications (source: www.idf.org). These dramatic numbers are largely caused by diabetes related end-organ complications such as cardiovascular disease or diabetic nephropathy (DN). In fact, 50% of patients with type 2 diabetes (T2D) have evidence of diabetes-related renal impairment(Parving, Lewis et al. 2006). This is in line with the UK Prospective Diabetes Study (UKPDS) in which 50% of participants developed renal impairment over 15 years with 29% experiencing incident CKD III (eGFR <60ml/min/1.73m^2)(Retnakaran, Cull et al. 2006). Regarding type 1 diabetes (T1D), the cumulative incidence over 30 years of developing renal impairment was up to 25%; of note, with intensified treatment (i.e. tight control of blood glucose and blood pressure levels) this rate declined markedly (Diabetes, Complications Trial/Epidemiology of Diabetes et al. 2009).

Among patients with T2D the prevalence of DN is much higher for certain ethnicities e.g. African American(Thomas, Cooper et al. 2016). In addition, many single nucleotide polymorphisms (SNPs) and chromosomal rearrangements have been

associated with altered risk of DN (Review by Conserva et al.) (Conserva, Gesualdo et al. 2016). Other factors linked with a higher risk of DN are obesity, smoking, anaemia, duration of diabetes, poor glycaemic control, advanced age and systemic hypertension(Macisaac, Ekinci et al. 2014, Thomas, Cooper et al. 2016).

Definition and Pathology

Both type 1 and type 2 diabetes cause renal end-organ damage and DN is defined by both clinical and pathological features. There are no pathognomonic lesions for DN though a typical histological constellation of lesions exists: glomerular lesions include basement membrane thickening, different levels of mesangial expansion and nodular to advanced glomerulosclerosis. Additionally tubular atrophy and interstitial fibrosis and inflammation, arteriolar hyalinosis and large vessel arteriosclerosis can be observed (Figure 1). The presence of these criteria can be used to indicate different disease stages that have been defined recently in a consensus conference (Tervaert, Mooyaart et al. 2010).

Clinically, albuminuria and a decline in renal function, as indicated by reduced glomerular filtration rate (GFR), are typical but not specific features of DN. While moderately increased albuminuria (2.5 mg/mmol [males], 3.5 mg/mmol [females] – 30 mg/mmol creatinine) is an important risk factor for the development of DN, severely increased albuminuria (>30 mg/mmol creatinine) and/or GFR below 60ml/min/1.73m^2 are the defining thresholds for overt diabetic nephropathy(Tuttle, Bakris et al. 2014), though not all patients with DN develop albuminuria at an early stage of the disease.

Figure 1: Renal Pathology in Diabetic Kidney Disease

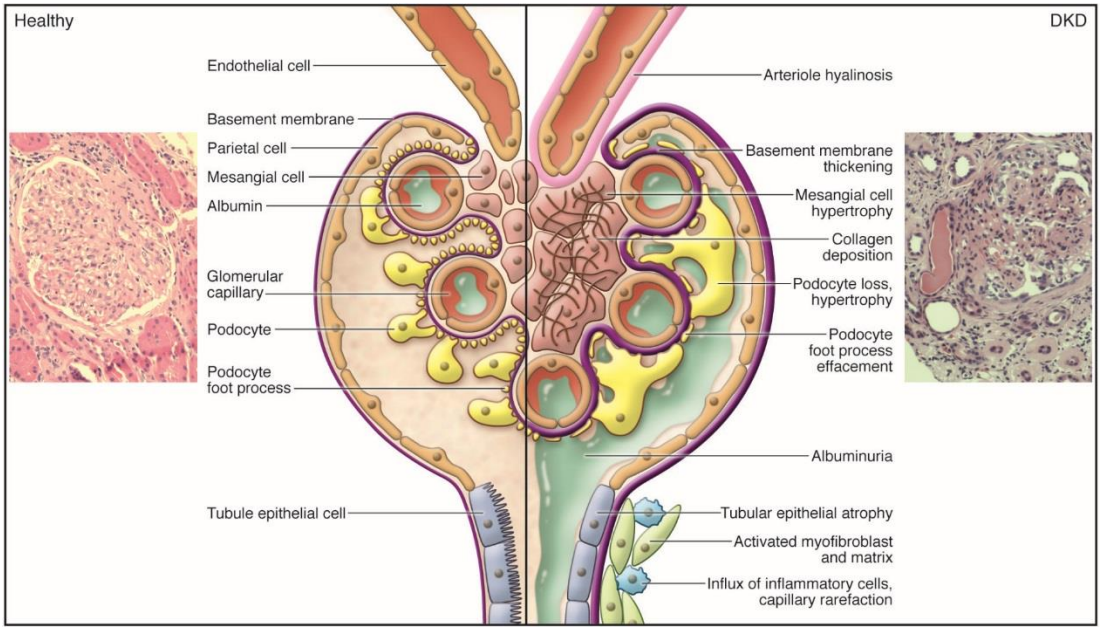

Figure 1 demonstrates the histology of a normal kidney and the pathological changes in the glomerulus and tubules. Also shown are two photos of a glomerulus from renal biopsy tissue from a healthy control and a patient with DKD (PAS stain). Original magnification, ×400. DKD, Diabetic kidney disease. Figure taken from Reidy et al (Reidy, Kang et al. 2014).

1.1.2 Pathophysiology

There is not a single pathophysiological pathway in DN but multiple mechanisms that interact with each other in a complex way. Only some of the arguably most important disease mechanisms that are also relevant for this work will be mentioned.

At an early stage high blood glucose causes glycosuria which together with glomerular hyperfiltration and hypertension result in renal enlargement characterized by tubular hypertrophy and hyperplasia. These factors also cause shear stress that activates intracellular pro-fibrotic pathways and contributes to glomerular basement membrane thickening and glomerulosclerosis.

Hyperglycaemia stimulates cellular matrix (ECM) expansion through both increased production of ECM and by inhibiting ECM degradation. Glycosylation of circulating

free amino acids produces advanced glycosylation end products (AGE) that bind to the cellular receptors for AGE (RAGE) to activate intracellular pro-fibrotic pathways. Hyperglycaemia also directly increases the intracellular glucose level (Heilig, Concepcion et al. 1995) which activates the polyol and protein kinase C (PKC) pathways and leads to the formation of intracellular AGEs. Non-enzymatic glycosylation of matrix proteins results in the development of cross-links that inhibit matrix degradation.

The endocrine vasoactive renin-angiotensin-aldosterone system plays an important role in the pathogenesis of intrarenal and systemic hypertension through the loss of autoregulation. Additionally, AT-II receptors might directly activate intracellular metabolic and pro-fibrotic pathways (Nagai, Yao et al. 2005).

The innate immune system has recently been reported to be involved in the pathogenesis of DN. For example, the complement cascade has been demonstrated to contribute to renal damage in a rodent model and increased expression and deposition of complement was detected in biopsies from patients with DN (Wada and Makino 2013, Wada and Nangaku 2013).

Endothelial deficiency of NO production is one of the key players in endothelial dysfunction. Effective endothelial NO synthase (eNOS) activity is diminished by reduced expression of the eNOS gene, post-translational modification of the protein or uncoupling leading to the production of superoxide anions and reactive oxygen species (ROS) instead of NO. Endothelial dysfunction might also cause dyslipidemia through impaired function of the enzyme lipoprotein lipase which in turn together

with increased ox-LDL levels is associated with local inflammation and macrophage infiltration.

Inflammation

As already indicated above, the metabolic, glycosylation and renin-angiotensin pathways are not separated from each other but might interact to promote progression of DN (Figure 2). For example, it is hypothesized that the cross-talking triangle between reactive oxygen species (ROS), protein kinase C and intracellular AGE can be maintained in an active state by any of the three aforementioned pathways (Kanwar, Sun et al. 2011). The activated triangle increases the expression of intracellular transcription factors such as nuclear factor kappa B (NF-κB) that in turn promote the process of inflammation.

Up-regulated transcription factors induce the production of cytokines. Cytokines contribute to inflammation via cell activation mediated by multiple pathways including the JAK/STAT pathway. The cytokines interleukin (IL)-1, -6, -10, -18 and TNF-α are increased in animal models and in renal biopsies from patients with DN. Cytokines are released by renal cells (endothelial, tubular, mesangial cells, and podocytes) but also by macrophages and T-cells that migrate into the kidney. While TNF-α is secreted by broadly pro-inflammatory Th1 cells, the increased expression of the modulatory IL-10 might point towards the presence of Th2 or regulatory T-cells (Treg), indicating an anti-inflammatory potential, but further studies are needed to investigate the role of T-cells in DN(Wada and Makino 2013).

Figure 2: Pathophysiological pathways in Diabetic Nephropathy

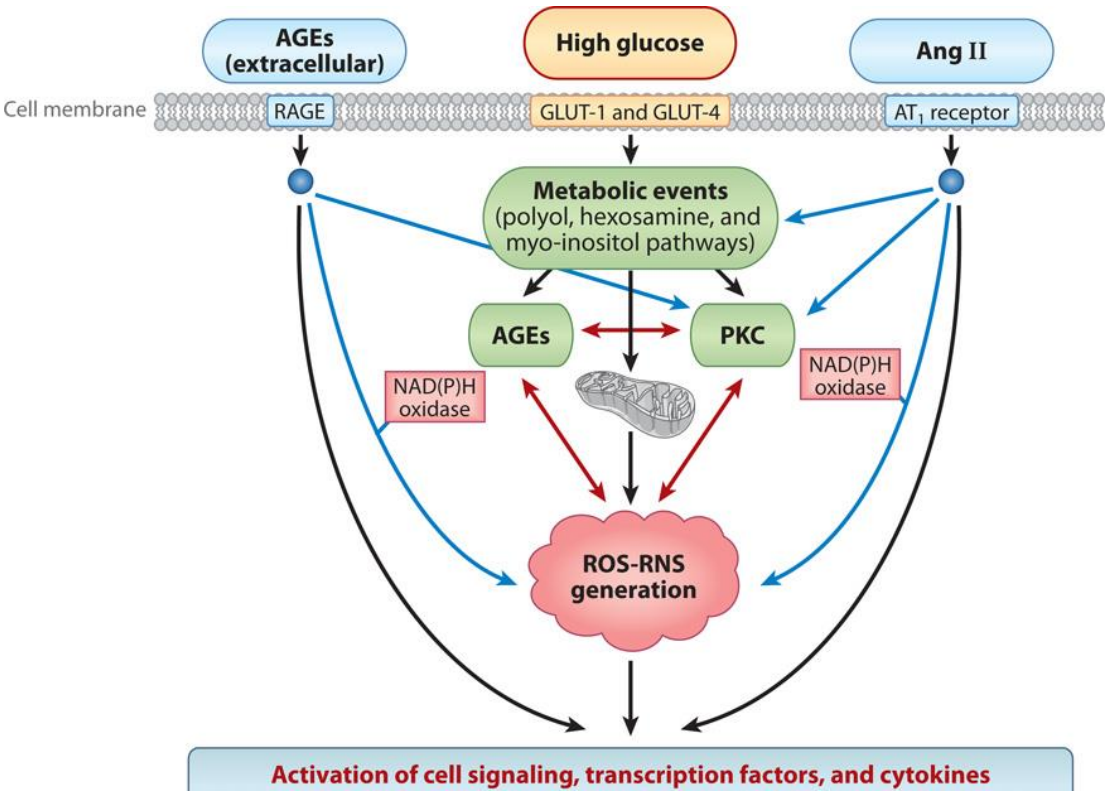

Figure 2. One common downstream pathway for three main pathologic factors for diabetic nephropathy. The figure highlights the hypothetical crosstalk between advanced glycation end products, hyperglycemia/metabolic changes and the renin-angiotensin II (Ang-II) system via protein kinase C (PKC), ROS (reactive oxygen species) and AGE and oxidative stress. AT1, Ang II receptor; GLUT, glucose transporter; RNS, reactive nitrogen species. Figure is shortened and taken from Kanwar et al.(Kanwar, Sun et al. 2011)

The presence of macrophages is a characteristic feature of DN in animal models and in human biopsies (Tesch 2010). After infiltration into renal tissue they may be polarised differently according to microenvironmental stimuli. Classically activated macrophages (M1) react to cellular injury and respond to cytokines such as IFN-γ and damage-associated molecular pattern molecules. They promote the inflammatory reaction by secreting chemokines, cytokines such as tumour necrosis factor-α (TNF-α), and reactive oxygen species (ROS) and recruit pro-inflammatory Th1 cells. M1 macrophages express a characteristic subset of markers such as MHC

Class 2 and inducible nitric oxide synthase (iNOS). M2 macrophages are "alternatively" activated by interleukins such as IL-4 or IL-13. They are immunoregulatory, secreting IL-10 and recruiting Th2 and Treg cells. Specific M2 markers are arginase-1 and mannose receptor(Braga, Agudelo et al. 2015) expression. M2 macrophages dampen the inflammatory process and are involved in the regulation of fibrosis process, what will be discussed below.

The expression of chemokines and adhesion molecules is pivotal for the migration of immune cells into the kidney. Expression of CCL2 and CXCL12 is increased in murine DN models and the glomerular up-regulation of CXCR13 has been demonstrated in STZ-induced diabetic rat kidneys (Kikuchi, Ikee et al. 2004). Osteopontin (OPN), another chemotactant molecule is overexpressed in renal tissue from rodent DN models and patients with DN (Kelly, Wilkinson-Berka et al. 2002, Li, Yang et al. 2003, Lorenzen, Shah et al. 2008, Nicholas, Liu et al. 2010, Woroniecka, Park et al. 2011). OPN seems to be a key player in macrophage and T-cell recruitment (Kelly, Wilkinson-Berka et al. 2002) and activation but also directly activates ECM related pathways in renal cells(Nicholas, Liu et al. 2010) and influences podocyte signalling and motility(Lorenzen, Shah et al. 2008). OPN deficient mice were protected against renal damage in a DN model(Lorenzen, Shah et al. 2008, Nicholas, Liu et al. 2010).

Fibrosis

Glomerulosclerosis and tubulointerstitial fibrosis represent the common final pathway of inflammation as well as other injurious mechanisms in DN. Fibrosis causes the disruption of cellular architecture, cellular damage and loss. Clinically,

fibrosis is associated with renal functional impairment and albuminuria. In general, fibrosis is triggered by tissue damage, for example due to inflammation, and part of the subsequent healing response aimed at repairing wounds and replacing damaged cells. However, very severe and/or prolonged injurious stimuli are likely to cause an excessive response resulting in tissue scarring. Histologically, fibrosis is an intercellular accumulation of ECM proteins consisting of mainly collagens (I and IV in the glomerulus, I and III in the tubulointerstitium) and fibronectin but also elastin, laminin, proteoglycans and non-collagenous glycoproteins. All these ECM proteins are mainly produced by myofibroblasts that also generate contractility by expressing smooth muscle proteins, namely the characteristic α-smooth muscle actin. In the glomerulus, myofibroblasts arise from *in situ* mesangial cells. In the tubulointerstitium several sources of myofibroblasts are discussed (Conway and Hughes 2012).

The first potential source for myofibroblasts is the recruitment of circulating fibrocytes. However, the importance of that pathway has been questioned at least in models of fibrosis caused by ureteral obstruction (Lin, Kisseleva et al. 2008). The second source is the epithelium to mesenchymal transition (EMT) as tubular epithelial cells transform into myofibroblasts and migrate into the interstitium. Recent lineage tracking studies have cast doubt on this pathway as a major contributor to myofibroblast accumulation and stress the importance of pericytes. (Kriz, Kaissling et al. 2011) (Humphreys, Lin et al. 2010). Pericytes are perivascular cells that are in close association with endothelial cells but may detach from the microvasculature and infiltrate the tubulointerstitium where they adopt a fibroblastic phenotype. As a side effect of pericyte detachment the denuded capillary vessels are

deprived of pericyte support and may perish which may result in microvascular loss and the promotion of further tissue damage secondary to hypoxia and ischaemia. Like pericytes, perivascular fibrocytes are platelet-like growth factor receptor-β^+ (PDGFR-β^+) and may also play a role in fibrosis. All these processes are induced by cytokines with transforming growth factor-β (TGF-β) being involved in most of them. TGF-β is secreted by alternatively activated (M2) macrophages and accumulation of myofibroblasts is associated with the presence of macrophages (Brosius 2008, Tesch 2010). Studies in regression of liver fibrosis suggest that a subset of "reparative" M2 macrophages is also a key player for resolution of fibrosis(Duffield, Forbes et al. 2005). These macrophages have not yet been fully characterized, but they seem to have markers of phagocytosis and lysosomal processing like Glycoprotein (transmembrane) nmb (Gpnmb)(Li, Castano et al. 2010, Ramachandran, Pellicoro et al. 2012). They might mediate ECM degradation by secretion of the matrix-metalloproteinases (Fallowfield, Mizuno et al. 2007).

Expansion of fibrosis is characterized by accumulation of ECM that results from an imbalance between ECM production by myofibroblasts and degradation of ECM by metalloproteinases (MMPs) and other proteases. The proteolytic activity of MMPs is zinc-dependent and a $Zinc^{++}$-binding site is a structurally common feature of all MMPs. MMPs can be categorised by their substrate specificity: collagenases (MMP1,8,13 & 18), gelatinases (MMP2 & 9), stromelysins (MMP3,10 & 11), matrilysins (MMP7 & 26), membrane-type matrix metalloproteinases (MT-MMP14-17, 24-25) and other MMPs (MMP12, 19-21, 23, 27 & 28) (Xu, Xiao et al. 2014). Except for MT-MMPs all MMPs are secreted into the extracellular space. While it is generally accepted that dysregulation of MMP expression and activity contributes to

progression of fibrosis in DN the exact mechanism and the role of individual MMPs remains unclear. The expression of MMPs is influenced by factors like NF-κB, TGF-β, ROS or the ERK1/2 MAPK pathway that are activated by hyperglycaemia and AGEs. The activity of MMPs is controlled by the blocking glycoproteins tissue-inhibitors of MMPs (TIMPs). There are discrepant reports about MMP tissue expression in patients with DN (e.g. MMP2) (Xu, Xiao et al. 2014). Also, MMP expression and function in rodent DN models seems to be different from human DN(Xu, Xiao et al. 2014). Of note, many of the animal DN models in which the MMP/TIMP pathways have been studied are related to an early stage of human DN. The failure to recapitulate advanced human DN might be one reason that prevents animal models from accurately reflecting the mechanisms of MMP/TIMP regulation in human diabetic kidney.

Systemic Hypertension and DN

While the pivotal role of intraglomerular hypertension and the renin-angiotensin system has been described before, an astonishing "experiment of nature" has demonstrated that systemic hypertension is not simply a consequence of renal failure but a prerequisite for the development and progression of renal DN(Berkman and Rifkin 1973, Beroniade, Lefebvre et al. 1987): In two patients with type 1 diabetes and systemic hypertension due to unilateral renal artery stenosis, the typical pathologic lesions of DN only developed in the kidney contralateral to the artery stenosis. The suggestion is that the renal artery stenosis protected the kidney from hypertension and the subsequent development of typical DN lesions (Figure 3).

The important role of systemic hypertension is also supported by the fact that subtle disturbances of physiological blood pressure regulation such as nocturnal “non-dipping” precedes the development of albuminuria and loss in eGFR in patients with diabetes(Lurbe, Redon et al. 2002, Agarwal and Andersen 2006). Furthermore only the combination of glycaemic and blood pressure control can effectively slow disease progression(Mogensen 1998) or even reverse albuminuria(Perkins, Ficociello et al. 2003) as described in the next paragraph.

Figure 3: An astonishing "experiment of nature"

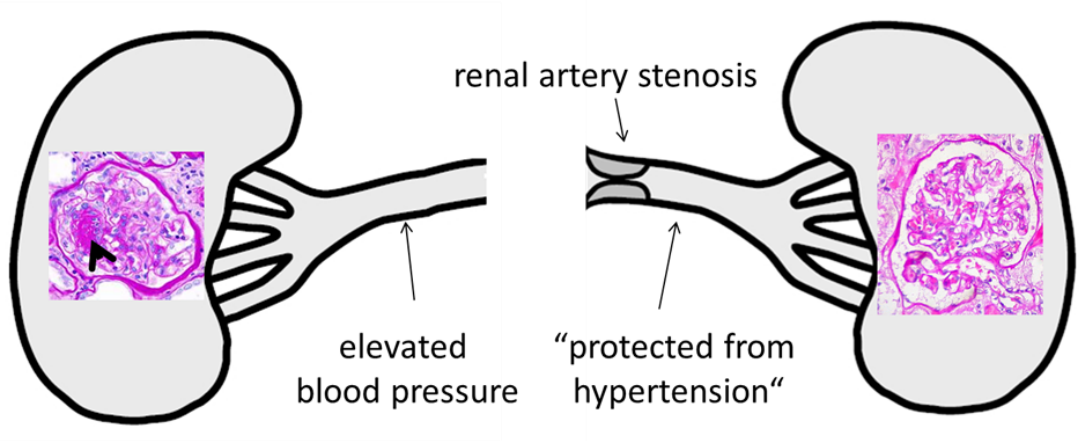

Figure 3. Schematic illustration of two exceptional case reports by Berkman et al. (Berkman and Rifkin 1973) and Beroniade et al. (Beroniade, Lefebvre et al. 1987). The unilateral renal artery stenosis protects the kidney from hypertension and preserves a normal glomerular architecture while diabetic glomerulosclerosis developed in the contralateral kidney (the arrowhead marks a nodular sclerotic [Kimmelstiel-Wilson] lesion). Two images of a glomerulus x400 PAS stain.

1.1.3 Prognosis and treatment

Treatment of DN

The major therapeutic goal is the prevention of DN. Lifestyle changes and stringent glycaemic control can avoid the progression from impaired glucose tolerance to T2D or from T2D without related complications to end-organ damage such as

DN(Molitch, Adler et al. 2015). Hallmarks in the therapy of DN include glycaemic, lipid and blood pressure control. For those with albuminuria, an ACE-I or an ARB is recommended, as the renin-angiotensin system also activates pathological pathways independent from hypertension (Molitch, Adler et al. 2015). There is some controversy about the target blood pressure. While the ADA (American Diabetes Association) has recently eased the target of systolic blood pressure to 140mmHg(American Diabetes 2016), the Kidney Disease Improving Global Outcomes guideline maintains the target systolic blood pressure of <130 mmHg for patients with moderate to severe albuminuria(KDIGO 2013). Though early results of the SPRINTtrial seemed to support the aim of strict blood pressure targets for the general population, the evidence level in DN is scarce and the aim is clinically hard to achieve(Tuttle, Bakris et al. 2014, Molitch, Adler et al. 2015). Only limited information about this controversy can be gained from experimental medicine as most animal DN models are normotensive.

Regression of DN

It has been thought for a long time that once renal damage is established in patients with diabetes mellitus this inevitably progresses to ESRD(Mogensen, Osterby et al. 1979). However this view has changed. With optimal control of blood glucose and blood pressure albuminuria can regress in almost half of patients with T2D(Perkins, Ficociello et al. 2003). Fioretto et al. demonstrated eventual regression of the typical histologic kidney lesions with restoration of almost normal glomerular structure and a marked reduction of collagen deposition in the tubulointerstitium in patients with T1D and moderate DN who underwent successful pancreas transplantation(Fioretto, Steffes et al. 1998, Fioretto, Sutherland et al. 2006). This regression however was

only visible 10 years after the transplant during which time period patients had been normoglycaemic and normotensive. The pathways underpinning such regression of DN remain poorly understood, at least in part for two reasons: first, there is no medical indication for serial biopsies in DN patients who respond to treatment; second, there are hardly any DN animal studies in which functional and histological regression upon intervention has been studied(Betz and Conway 2016).

Progression of DN to ESRD

A stringent therapeutic regime can delay the progression of DN and result in only a small percentage of patients developing ESRD. For example, less than 8% of patients developed ESRD over ten years in the STENO trial(Andresdottir, Jensen et al. 2014) and less than 1% in the intensive treatment group of the DCCT/EDIC trial(Diabetes, Complications Trial/Epidemiology of Diabetes et al. 2009). However, due to the high prevalence of diabetes mellitus, DN accounts for approximately 33% of all patients worldwide initiating RRT; in the USA, the rate exceeds 50%(Thomas, Cooper et al. 2016). According to the US renal data system (www.usrds.org), $30.9 billion had been spent on dialysis treatment in 2015 and the 5-year survival for patients with diabetes and ESRD is 42%. These figures underline the urgency to identify diabetic patients at risk of renal deterioration in order to optimize their therapeutic regime and prevent or delay further progression.

1.1.4 Biomarkers

Endpoints

End-stage renal disease (ESRD) as defined by an eGFR < 15ml/min/1.73m^2, the initiation of chronic renal replacement therapy or kidney transplantation are the most

relevant clinical renal endpoints in studies(Nguyen, Tarnow et al. 2008, Niewczas, Gohda et al. 2012). However, given the long-time course for these endpoints to develop, interventional studies in DN patients would take many years in order to achieve sufficient outcome numbers. Surrogate endpoints are therefore needed that are robustly associated with an increased risk of developing ESRD.

CKD III (eGFR < 60ml/min/1.73m^2) is part of the clinical definition for DN and is associated with an increased risk of metabolic and endocrine complications, a higher rate of drug dosing errors and a higher rate of cardiovascular disease (CVD) or death(KDIGO 2013). Many studies use CKD III as a renal endpoint, often called incident CKD(Perkins, Ficociello et al. 2010, Kim, Song et al. 2013, Macisaac, Ekinci et al. 2014). However, the risk of developing this endpoint depends upon the baseline eGFR and therefore requires a relatively homogenous study population and appropriate statistical adjustment.

The outcome "rapid progression of CKD" is characterized by a rapid and substantial loss of GFR. While the time for this loss in most studies is calculated/normalized per year of observation, there are discrepant definitions about the extent of GFR loss (Sheen and Sheu 2014). Some studies use an absolute number from 3 to 5 ml/min/1.73m^2/year(2013, Pena, Heinzel et al. 2015). Other studies calculate a relative loss of GFR per year ranging from 3.3% (Krolewski, Niewczas et al. 2014) to up to 20-30% (Ju, Nair et al. 2015, Looker, Colombo et al. 2015).

Albuminuria

Severe albuminuria (ACR>30mg/mmol) is an indicator for progression of CKD and increases the risk of ESRD, CVD, diabetes complications and death(Macisaac,

Ekinci et al. 2014, Molitch, Adler et al. 2015). However, not all diabetic patients with albuminuria develop DN and moderately increased albuminuria ("microalbuminuria") can even be reversed(Perkins, Ficociello et al. 2003, Perkins, Ficociello et al. 2010). On the other hand, many patients with DN exhibit a rapid decline in eGFR without developing significant albuminuria. In large T2D cohorts (UKPDS, RIACE, NHANES) 30-60% of patients with an eGFR <60ml/min/1.73m^2 did not have more than mildly increased albuminuria(Thomas, Cooper et al. 2016). Therefore, novel biomarkers for loss of eGFR are needed, especially in patients in whom standard risk factors such as albuminuria or impaired renal function are absent.

Alternative markers in diabetic nephropathy

It would exceed the scope of this introduction section to discuss the complete myriad of markers that have been tested to predict the risk of developing DN or of progression of the disease. There are, however, two promising marker categories of special interest.

As the inflammatory process is an early step in the development of DN these markers might precede albuminuria as an indicator of renal complications in diabetes. Transcription factors, cytokines and chemotactic factors are mediators of the inflammatory process. Indeed, serum concentrations of connective tissue growth factor (CTGF), soluble tumour-necrosis factor receptor (sTNFR) and osteopontin (OPN) are predictive for progressive renal function decline or ESRD in large cohorts of patients with T1D or T2D(Nguyen, Tarnow et al. 2008, Niewczas, Gohda et al.

2012, Gordin, Forsblom et al. 2014, Krolewski, Niewczas et al. 2014, Pena, Heinzel et al. 2015).

Since albuminuria is rather a marker of glomerular dysfunction, tubular markers might be complementary as tubulointerstitial damage is the best pathological prognostic hallmark in human DN(Gilbert and Cooper 1999). Cystatin C (CysC) is a ubiquitously secreted cellular metabolic by-product and serum CysC is superior to creatinine for estimation of renal function(Macisaac, Ekinci et al. 2014, Molitch, Adler et al. 2015). CysC is freely filtrated in the glomerulus and completely reabsorbed in the tubules. Increased urinary CysC might indicate tubular damage and Kim et al. have demonstrated that urinary CysC levels predict progression of DN(Kim, Song et al. 2013).

Renal expression and urinary secretion of kidney injury molecule 1 (KIM-1), neutrophil gelatinase-associated lipocalin (NGAL) and liver fatty acid binding protein (L-FABP) are increased in tubular damage. While two studies demonstrated a robust independent association between increased serum L-FABP and rapid renal deterioration and progression to ESRD in DKD(Kamijo-Ikemori, Sugaya et al. 2011, Araki, Haneda et al. 2013), another study examining L-FABP and studies assessing KIM-1 and NGAL had less convincing results(Conway, Manoharan et al. 2012, Nielsen, Reinhard et al. 2012, Chou, Lee et al. 2013, Mischak, Delles et al. 2015).

The Edinburgh Type 2 Diabetes Cohort

For clinical validation of biomarkers large cohorts of patients with diabetes are needed to achieve sufficient statistical power. These patients need to be followed for several years to assess long-term complications. Patients should be a homogenous

group regarding baseline clinical and epidemiological variables to reduce the influence of potential confounding factors. The Edinburgh Type 2 Diabetes Study comprises 1066 participants that have been demonstrated to be representative of elder men and women with type 2 diabetes in the Lothian area of Scotland, UK, and were followed for a period of four years. The study that will be further described in Materials and Methods section fulfils many of the mentioned requirements for biomarker validation studies.

1.2 Rodent models of diabetic nephropathy

1.2.1 Overview

Although DN is a long-term complication of diabetes that progresses for several years, animal models that develop DN within weeks to months are necessary to effectively study pathological pathways and the consequences of interventions. Over several decades an abundant number of rodent DN models have been published. The Diabetes Complications Consortium (DiaComp) defined functional and histological criteria that characterize the ideal model which should have a high congruency with human disease (Table 1) (Brosius 2008).

Remarkably, so far no rodent model meets all of the desired criteria. The inadequacy of current rodent DN models might be related inherently to the species employed or to the fact that pathophysiological pathways that are pivotal in human DN are not of importance in the models.

Table 1: Research criteria for validating progressive mice models of diabetic nephropathy according to the diabetes complications consortium (DiaComp).

Function	Greater than 50% decline in GFR over the lifetime of the animal
	Greater than 10-fold increase in albuminuria compared with controls for that strain at the same age and gender
Histology	advanced mesangial matrix expansion +/- nodular sclerosis and mesangiolysis
	any degree of arteriolar hyalinosis
	glomerular basement membrane thickening by 50% over baseline
	tubulointerstitial fibrosis

Table 1. Table adapted from diacomp.org and Brosius et al.(Brosius, Alpers et al. 2009)

Classical models and recent advances

The mandatory pathological pathway in animal models is the presence of hyperglycemia. This can be achieved by administration of streptozotocin (STZ) that is cytotoxic to beta-cells of the pancreas. These models therefore reflect type 1 diabetes characterized by the failure of insulin production. To imitate T2D, models such as the leptin deficient receptor db/db mice are utilized. These mice are hyperphagic and become obese, develop peripheral resistance to insulin, insufficient insulin production and consequently hyperglycemia(Qi, Fujita et al. 2005). However, as mentioned before, most of these models feature only the early histological and functional changes in DN (Figure 4). Of note the extent of histological and functional changes of DN depends on the mouse strain with DBA/2J mice and FVB mice much more prone to renal injury than C57BL/6J mice(Qi, Fujita et al. 2005, Betz and Conway 2016). These differences in strain susceptibility were capitalized on when the leptin deficient ob/ob mutation was crossed from C57BL/6J to the black and tan, brachyuric (BTBR) background(Hudkins, Pichaiwong et al. 2010). BTBR mice are naturally insulin resistant and in combination with the ob/ob mutation they develop

early hyperglycemia (six weeks of age) and their kidneys exhibit many histological and functional aspects of moderately advanced DN(Hudkins, Pichaiwong et al. 2010) in humans (Figure 4) and meet almost all criteria of the DiaComp (Table 1). However, these mice are difficult to breed and have a reduced life expectancy (high mortality after 24 weeks of age) which restricts the study of further progression in DN.

Figure 4: Classical models of DN and recent advances

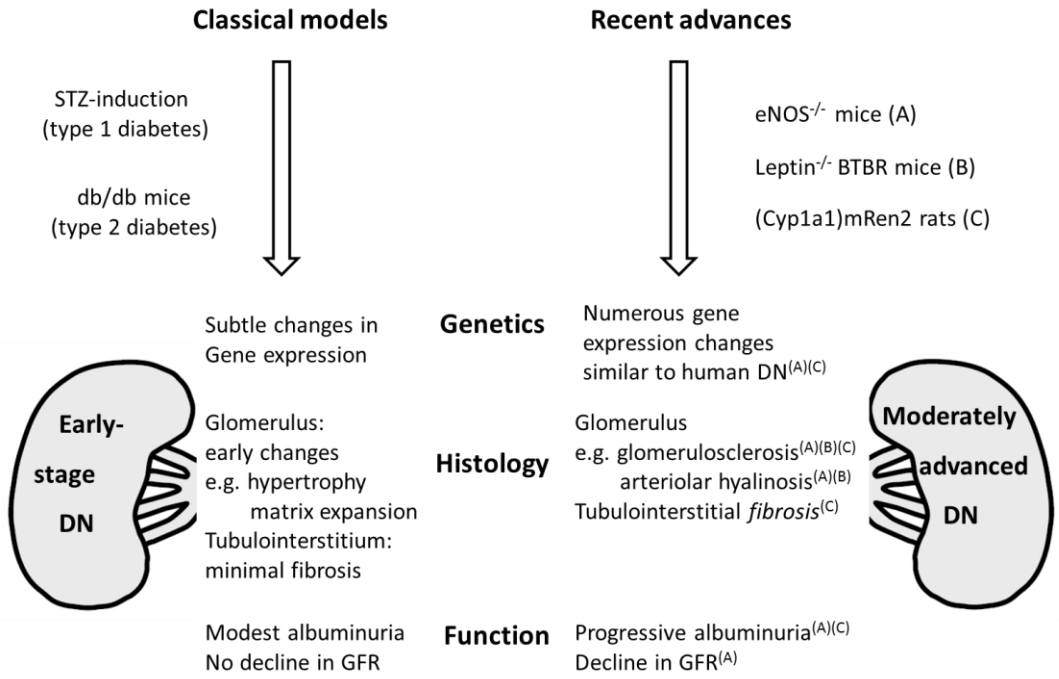

Figure 4. Schematic illustration of differences between classical models of DN and recent advances. Increased histological damage and functional impairment is achieved by the change of background strain or addition of systemic hypertension. Figure slightly adapted from Betz et al.(Betz and Conway 2014) STZ=Streptozotocin; db/db = leptin receptor mutation; ob/ob = leptin deficiency; BTBR = black and tan, brachyuric, Cyp1a1mRen2 = transgenic rats with the murine renin cDNA inserted under an inducible promoter, eNOS = endothelial nitric oxide synthase.

Another approach to increase the vulnerability of the kidney is to superimpose hypertension as hypertension seems to be a cornerstone in the development of human

DN(Berkman and Rifkin 1973, Beroniade, Lefebvre et al. 1987). Endothelial function is markedly compromised in db/db eNOS$^{-/-}$ mice and beside hypertension these mice exhibit early onset albuminuria, decreased GFR, arteriolar hyalinosis, mesangial expansion, mesangiolysis, and nodular glomerulosclerosis(Zhao, Wang et al. 2006). However there is only minimal tubulointerstitial fibrosis which is of concern as it is a key prognostic hallmark in human DN(Gilbert and Cooper 1999).

1.2.2 The Cyp1a1mRen2 model

Hypertension can be induced in transgenic mRen2 rats by the constitutive expression of murine renin cDNA(Kelly, Wilkinson-Berka et al. 1998). The injection of STZ in these rats seems to initiate advanced DN however the utility of this model is limited by the malignant phase hypertension (Hartner, Cordasic et al. 2007). This difficulty is overcome in Cyp1a1mRen2 rats in which the renin expression is under control of an inducible promoter. Supplementation of the diet with indole-3-carbinol (I-3-C) activates a cytochrome P4501a1 promoter which induces expression of the murine Ren2 gene to produce renin-dependent hypertension(Kantachuvesiri, Fleming et al. 2001). For the development of a DN model four experimental groups were (Conway, Rennie et al. 2012)studied: two groups (diabetes [DM] alone; diabetes and hypertension [DM+HTN]) were injected with a single dose of streptozotocin two weeks before the start of the experiment to induce diabetes mellitus. Two groups (HTN alone; DM+HTN) were fed with I-3-C to render them hypertensive. The control group remained untreated (Figure 5).

Figure 5: Experimental setting for the development of Cyp1a1mRen2 DN model

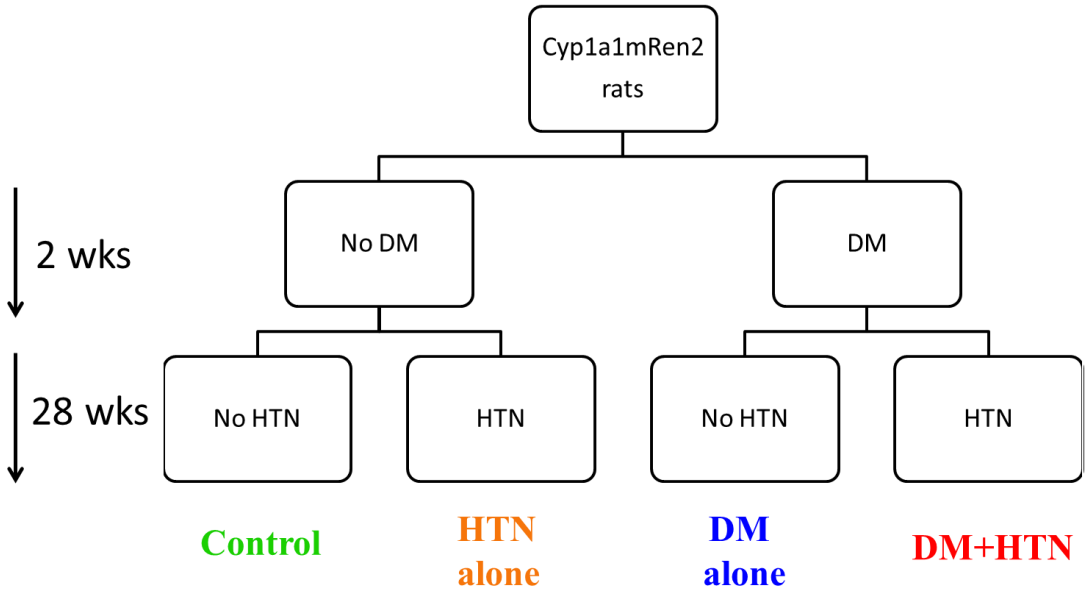

Figure 5. Schematic illustration of the experimental setting for the development of the Cyp1a1mRen2 DN model(Conway, Rennie et al. 2012). The different experimental groups are colour coded with DM=diabetes, HTN=hypertension.

During a period of 28 weeks animals developed severe hypertension, hyperglycaemia or both. Excretion of albumin in the urine (albuminuria) was slightly increased in the DM (14 -fold) or HTN (50-fold) groups. Interestingly, it was dramatically increased in the combinatorial DM+HTN group by more than 500 -fold in comparison to the control group. The increase was much higher than the albuminuria observed with DM and HTN alone supporting the hypothesis of the synergizing effects of diabetes and hypertension (Figure 6).

Figure 6: The Cyp1a1mRen2 DN model

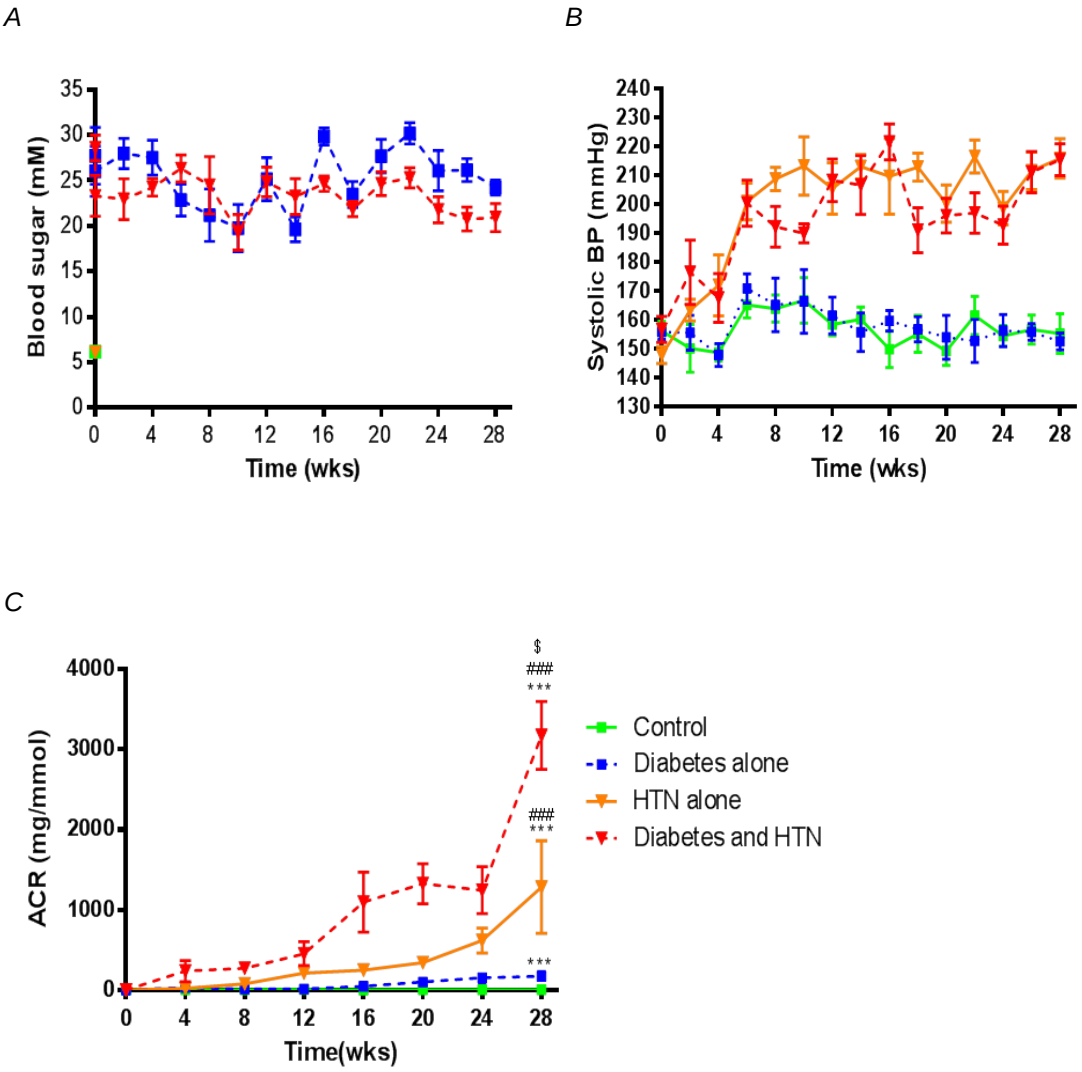

Figure 6. Serial blood glucose, systolic blood pressure and urinary albumin-to-creatinine (ACR) measurements during 28 weeks. The combination of hypertension and diabetes synergized to produce significantly more albuminuria than with DM or HTN alone. Data given are means +/- SEM. *** p<0.001 vs control, ### p<0.001 vs diabetes alone, $ <p0.05 vs hypertension alone. Figure adapted from Conway et al. (Conway, Rennie et al. 2012)

Figure 7: Histology in the Cyp1a1mRen2 DN model

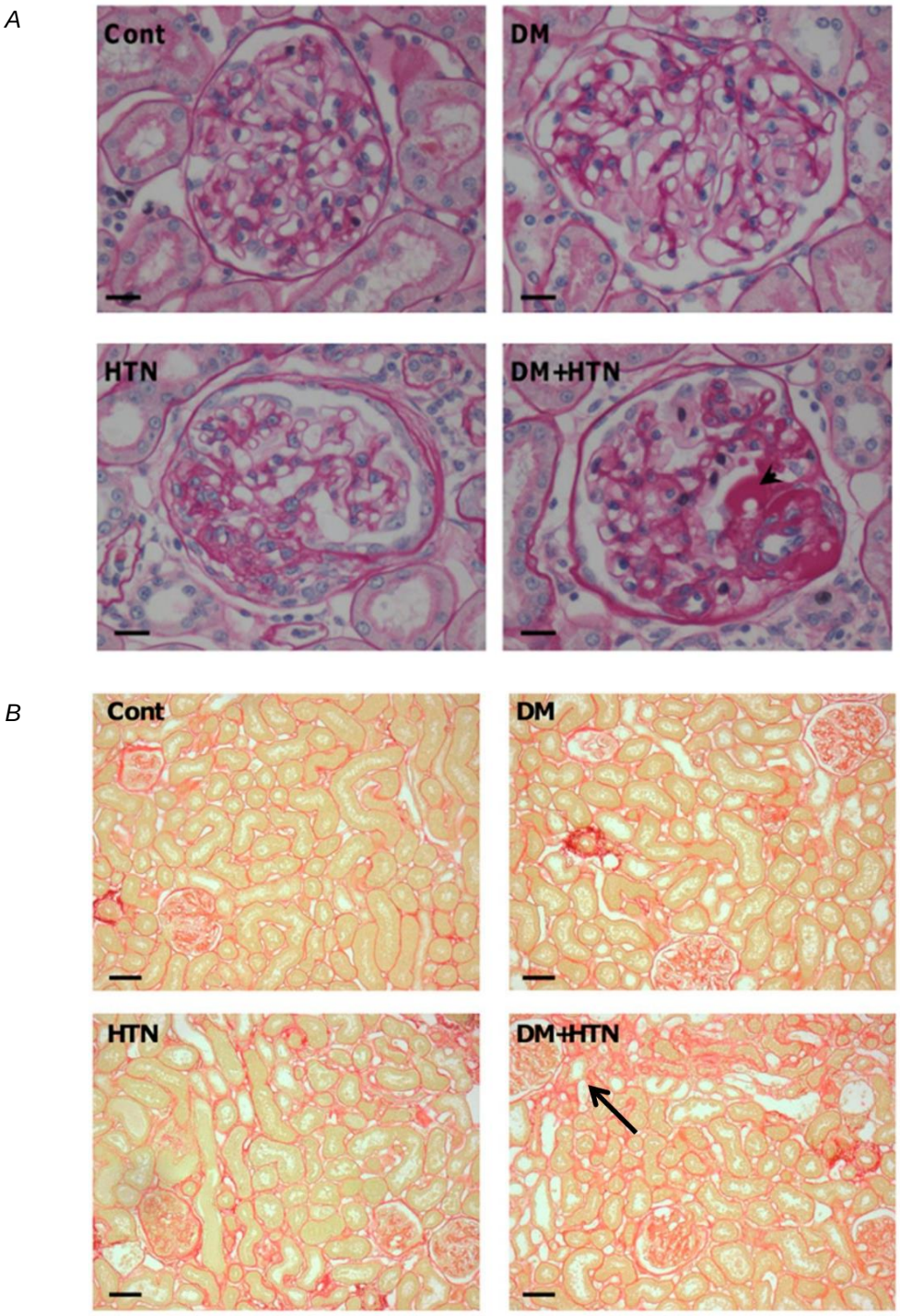

Figure 7. Representative images from periodic acid-Schiff staining (A) and picrosirius red staining (B) of the Cyp1a1mRen2 DN model. Glomeruli are highlighted in (A) with staining of the tubulointerstitium highlighted in (B). Only the combination of diabetes and hypertension promotes typical histological lesions. The arrowhead in (A) indicates a fibrin cap and the arrow in (B) highlights an area of tubulointerstitial fibrosis. Bars represent 25 μM in (A) and 50μM in (B). Figure adapted from Conway et al. (Conway, Rennie et al. 2012)

Histologically, in the DM alone group there was very little fibrosis present in the glomerulus and tubulointerstitium, and a non-significant increase in the glomerulosclerosis index in the HTN alone group. Concurrent diabetes and hypertension significantly increased both glomerulosclerosis and tubulointerstitial fibrosis indices compared to all other groups (Figure 7). The latter is especially remarkable as most rodent models of DN lack this feature that is both typical of and important in human diabetic nephropathy (Betz and Conway 2014).

1.2.3 Models of regression

In patients with moderate DN as mentioned above, the state of normotension and normo-glycaemia achieved by pancreas transplantation can, albeit after ten years, result in the regression of renal functional and histological alterations caused by DN(Fioretto, Steffes et al. 1998). The underlying pathways are as yet poorly understood, and there are only a few models that have been employed to identify factors promoting regression.

Pichaiwong et al. demonstrated that supplementation of leptin in a leptindeficient ob/ob BTBR mouse model induced normoglycaemia and regression of albuminuria and restoration of reduced GFR. Histologically, the extent of glomerulosclerosis and tubulointerstitial fibrosis decreased significantly (Pichaiwong, Hudkins et al. 2013).

Reversibility of DN in the Cyp1a1mRen2 model

In the Cyp1a1mRen2 DN model a reversal phase was created by normalizing blood pressure and controlling blood glucose levels for another 8 weeks (reversal phase)

after 28 weeks of hyperglycaemia and hypertension (injury phase) (Conway, Betz et al. 2014). This was achieved by increasing insulin therapy and stopping dietary supplementation with the Indole-3-Carbinol. Albuminuria decreased during reversal however it remained still significantly different from control (Figure 8).

Figure 8: The Cyp1a1mRen2 reversal DN model

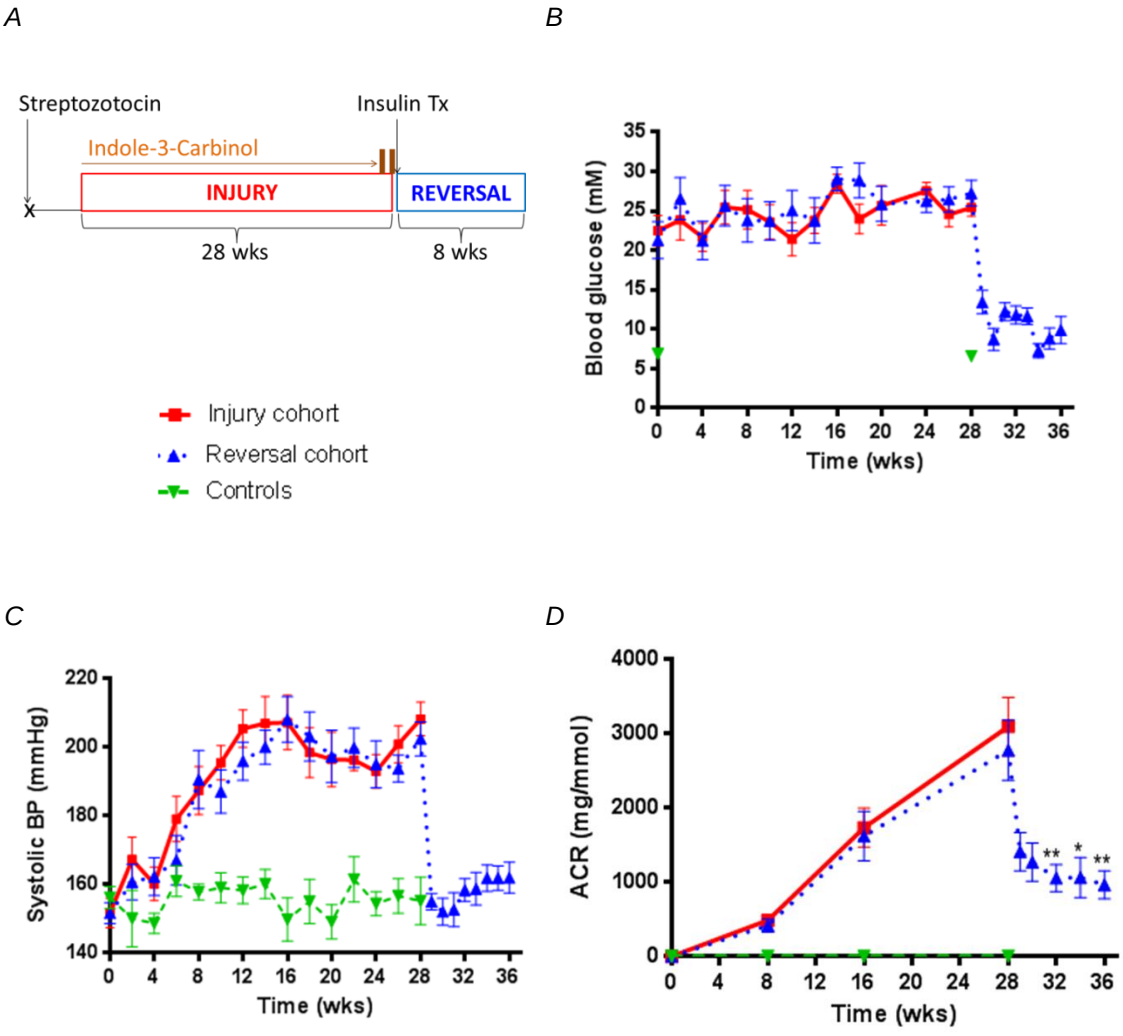

Figure 8. (A) Schematic illustration of the study design. (B) Blood glucose and (C) blood pressure are normalized during the eight week reversal phase while (C) albuminuria decreases but remains elevated compared to control. * p<0.05, ** p<0.01 vs peak injury. Data given are means +/- SEM. Figure adapted from Conway et al. (Conway, Betz et al. 2014)

Figure 9: Histology in the Cyp1a1mRen2 DN model

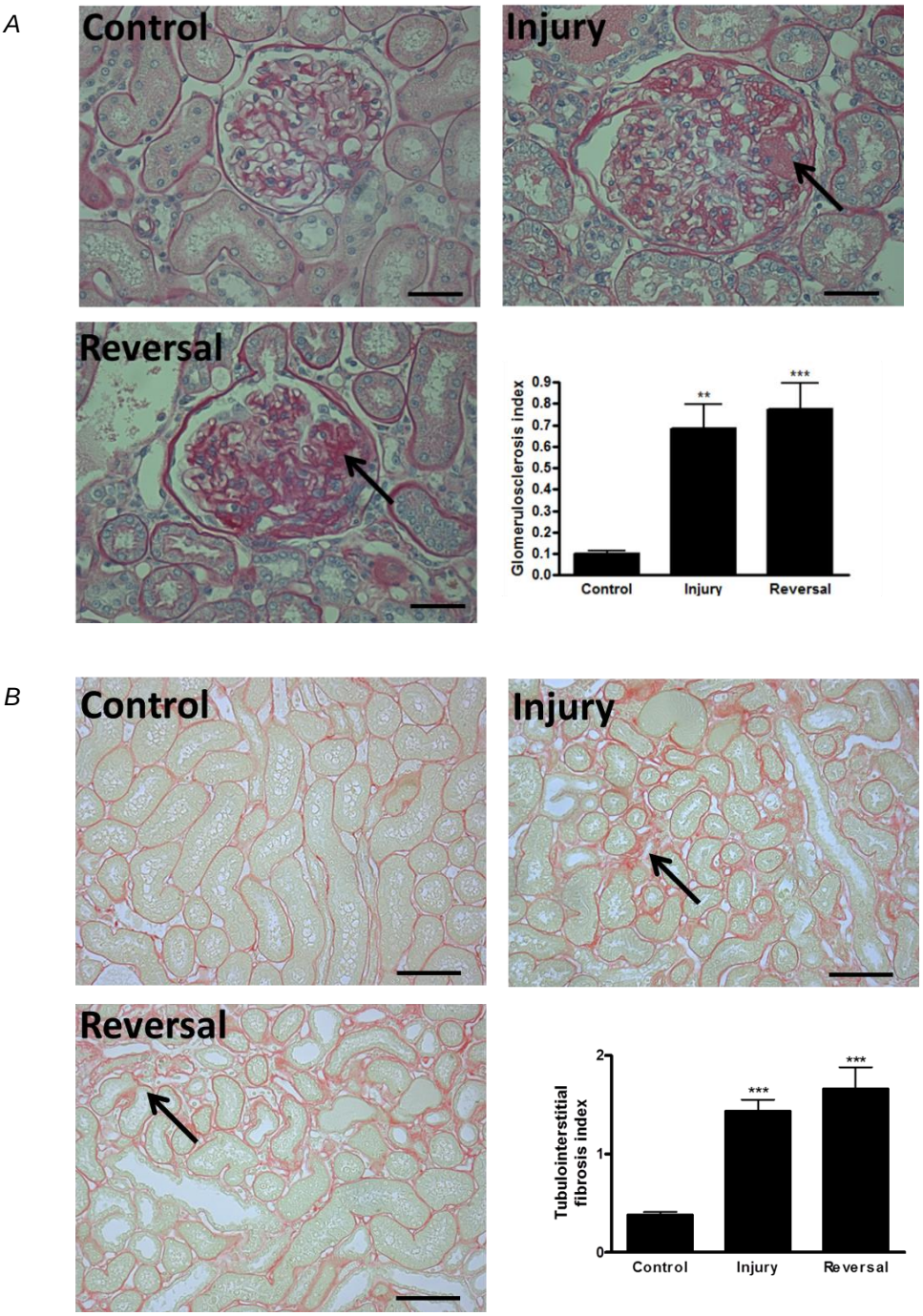

Figure 9. Representative images from (A) glomeruli and (B) tubulointerstitium of the Cyp1a1mRen2 DN model. The marked glomerulosclerosis (A, arrows) and tubulointerstitial fibrosis (B, arrows) remains unchanged after the reversal phase. The arrow indicates (A) a fibrin cap and (B) tubulointerstitial fibrosis. Bars represent (A) 20 μM and (B) 100μM with (A) periodic acid-Schiff staining and (B) picrosirius red staining. Data for the (A) glomerular and (B) tubulointerstitial fibrosis index are given as +/- SEM, ** $p<0.01$ and *** $p<0.001$. Figure adapted from Conway et al. (Conway, Betz et al. 2014)

However, eight weeks of relative normoglycaemia and normotension did not have any effect on the glomerulosclerosis index nor on tubulointerstitial fibrosis (Figure 9).

To assess changes in the molecular profile of the kidney during the reversal phase, a microarray chip analysis was performed in the control group, in the “injury” group after 28 weeks of DM+HTN and in the reversal group. The interpretation and validation of the results will be part of this work.

1.3 Integrative Biology in Diabetic Nephropathy

In order to further advance an in-depth understanding of a complex disease like DN an integrative biology approach has been proposed (Harder, Hodgin et al. 2015) (Mischak, Delles et al. 2015). Integrative biology aims to characterize the interplay of the heterogeneous multitude of factors involved in pathophysiology and disease progression. This approach tries to integrate the field of clinical research comprising molecular, histological phenotyping as well as outcome studies, the field of disease modeling including animal models and the field of systems biology (Figure 10). The term “systems biology” can be defined as an unbiased hypothesis-free discovery-based screening for disease related changes on different layers of the genome-phenome continuum. These layers include genomics, epigenomics, transcriptomics, proteomics and metabolomics. Beside the deeper understanding of known disease pathways and the discovery of novel pathways, integrative biology might also help to identify characteristic biomarkers of the most relevant disease pathways that might indicate the risk of disease progression.

Figure 10: The concept of integrative biology of DKD

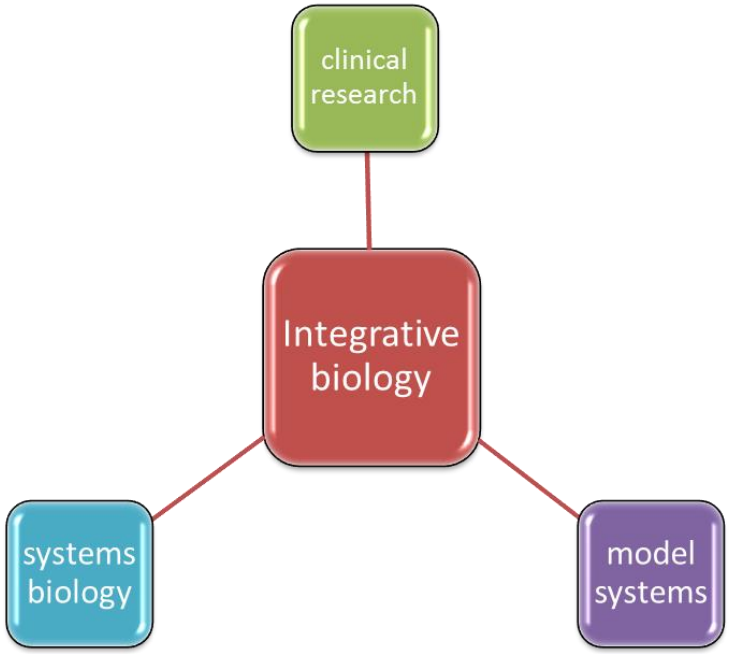

Figure 10. The concept of integrative biology in DKD. The scheme illustrates the concept of integrative biology that combines systems biology tools ("-omics") in model systems (animal, invitro studies) and in clinical research (outcomes, histology, molecular phenotyping) to analyze the complex pathophysiology of diabetic kidney disease (Harder, Hodgin et al. 2015).

1.3.1 Transcriptomic profiling

Genetic profiling can be performed in whole kidney tissue homogenates or via laser-capture technology of targeted areas (e.g. the glomeruli) in paraffin-fixed tissue sections (Lindenmeyer, Kretzler et al. 2007). Microarrays can analyse the expression of thousands of genes simultaneously, thereby drawing a very detailed molecular map of the kidney. There are now freely available online databases allowing researchers to compare their results with the molecular regulation from large disease cohorts. For diabetic nephropathy the database nephroseq (www.nephroseq.org)

comprises the transcriptomic results of several DN biopsy cohorts, such as Woroniecka et al. (Woroniecka, Park et al. 2011) and Ju et al. (Ju, Nair et al. 2015).

Hodgin et al. compared the glomerular transcriptome of kidney biopsies from patients with early type 2 DN with three murine DN models: the DBA/2 mouse with STZ induced diabetes, the C57BLKS db/db and eNOS-deficient C57BLKS db/db mouse(Hodgin, Nair et al. 2013). The eNOS-knockout mouse model most closely resembled the gene expression changes observed in the kidneys of patients with DN. Interestingly, many novel potential pathophysiological pathways of DN identified in human disease were only detected in one of the animal models. This indicates that researchers must carefully choose their DN model according to their target pathway for investigation.

The transcriptomic profiling in the Cyp1a1mRen2 DN model comprised the control, diabetes alone, HTN alone and the combination of diabetes and HTN groups (Figure 5). Since the analysis was made from snap-frozen whole tissue kidney it mainly reflects molecular regulation of the tubulointerstitium as glomeruli only account for a small part of kidney mass(Conway, Rennie et al. 2012). The vast majority of genes significantly up-regulated or down-regulated compared to control were present exclusively in the combined diabetes+HTN group; indeed, there were only a few genes dysregulated in the diabetes alone group (Figure 11). Similar to functional and histological parameters, the molecular regulation confirms the synergistic effect of concurrent HTN and diabetes. Up-regulated genes were enriched in pathways of inflammation, the innate and adaptive immune system, complement cascade and the ECM network. From all dysregulated genes, about 40% were similarly altered in the tubulointerstitium of patients with DN according to the Nephroseq biopsy database

(www.nephroseq.org). The congruency between moderately advanced human DN and the Cyp1a1mRen2 DN model on a histological, functional and molecular level renders the model highly suitable to translationally investigate relevant pathways and their related markers.

Figure 11: Patterns of renal gene expression changes in the Cyp1a1mRen2 DN model

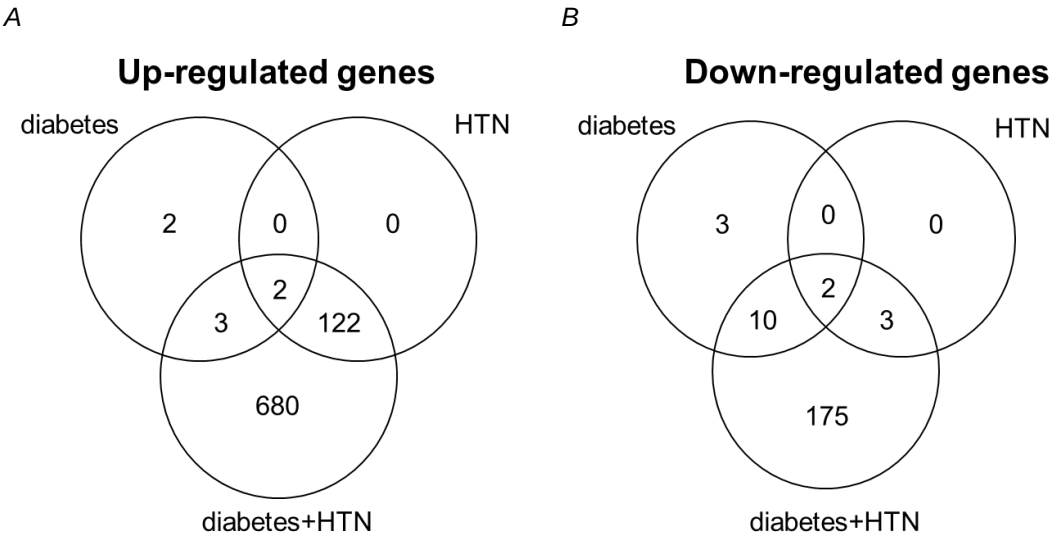

Figure 11. Venn diagrams demonstrate the number of genes (A) up-regulated or (B) downregulated more than 1.5-fold in the diabetes alone, HTN alone and combined diabetes & HTN groups in comparison with control animals at a corrected p<0.01. Figure adapted from Conway et al. (Conway, Rennie et al. 2012)

1.3.2 Proteomics & Peptidomics

Within the last decade there has been many reports published regarding the proteomics analysis of patients with diabetes mellitus for biomarker discovery (Mischak, Delles et al. 2015). In many of these studies urine was analyzed as it is easily accessible, relatively stable and pre-analytical preparation is less laborious than in blood. Finally, urine might be enriched with kidney specific components. In healthy persons almost 70% of urinary proteins originate from the kidney, therefore

some authors used the term “liquid kidney biopsy” (Klein, Bascands et al. 2016) (Pena, Mischak et al. 2016).

Bhensdadia et al. identified several potential biomarkers by comparing the urinary proteomics of patients with T2D and rapidly declining renal function with patients with T2D and stable renal function(Bhensdadia, Hunt et al. 2013). They then confirm that haptoglobin indeed predicts rapid decline in renal function in a large cohort of patients with T2D. In a commentary on the study, Brosius highlights that haptoglobin gene expression is also increased in patients with T2D and nephropathy compared to controls (Brosius and Pennathur 2013). Schlatzer et al. performed urinary proteomic analysis in streptozotocin-induced diabetic rats with a very stringent data analysis approach. However, when the methodology was transferred to humans with T2D, none of the markers from the animal model was chosen for the creation of a biomarker panel that indicated decline in renal function in patients with T2D(Schlatzer, Maahs et al. 2012).

Peptidomics focuses on the urinary peptide content, after removal of higher molecularweight proteins by filtration. Compared to proteomics, the analysis of peptidomics can be of pathophysiological advantage, for example, alterations in collagen fragments/peptides may indicate the (in)activity of metalloproteinases with specific cleavage sites(Maahs, Siwy et al. 2010) (Nkuipou-Kenfack, Bhat et al. 2015). Due to their small size serum peptides might pass through a minimally damaged glomerular filtration barrier while intact serum protein do not and therefore they could represent the first marker of impaired glomerular function. Moreover, peptides are more resistant to cleavage in the bladder than proteins (Klein, Bascands et al. 2016). Finally, the complete removal of high-molecular weight proteins from

the sample reduces analysis time by MS compared to proteomics in large study cohorts.

In 2009, Merchant et al. identified several peptide fragments that were altered in patients with T1D and early renal function decline compared to patients with stable renal function and they confirmed the increased expression of the parent proteins by immunohistochemistry on renal tissue sections from patients with T1D (Merchant, Perkins et al. 2009). Zurbig et al. demonstrate that a panel of 273 peptides (CKD273) can predict the development of DN in patients with T1 and T2D (Zurbig, Jerums et al. 2012). Recently, the CKD273 had been demonstrated to be independently associated with the risk for rapid decline in large cohort of CKD patients(Schanstra, Zurbig et al. 2015). The CKD273 panel comprises fragments from markers of renal pathophysiological processes such as clusterin, osteopontin and albumin; however the overwhelming majority (74%) of the peptides are collagen fragments. This underlines the importance of ECM expansion/turn-over in the development and progression of DN.

An important issue to be addressed in the urinary peptidomic analysis is the daily fluctuation in urine volume that necessitates a normalization process. Furthermore, the approaches for sample preparation (e.g. use of trypsin), measurement (e.g. LC-MS/MS vs CE-MS) and analysis (e.g. MaxQuant software vs MASCOTT) need to be standardised. The approach to these issues in the current work will be described in the Materials and Methods section and the comparison with different approaches from other studies will be mentioned in the discussion section.

1.4 Extracellular vesicles

Although the involvement of extracellular vesicles (EV) in pathophysiological pathways and their potential role as biomarkers had been previously suggested (Pisitkun, Shen et al. 2004), the field has recently gained much interest in kidney research, not least due to advances in the technologies employed for EV detection.

1.4.1 Definition

Extracellular vesicles (EV) is a term used to summarize all forms of membrane-bound vesicles. There is still no general consensus in the literature on nomenclature(Erdbrugger and Le 2016), however many authors categorize EVs into exosomes (20-100nm diameter), microvesicles (MV) (100-1000nm) and apoptotic bodies (>1000nm). Having been initially regarded to be "cell dust" it is now assumed that EVs play an important role in cell-to-cell communication (Burger, Schock et al. 2013) and activation (Oosthuyzen, Scullion et al. 2016) or have antibacterial properties(Hiemstra, Charles et al. 2014). Besides their size, EVs can be distinguished by their origin. The generation of exosomes starts with an invagination of the plasma membrane to form early endosomes, Intraluminal vesicles are formed within these endosomes by inward budding of the membrane. The resulting mature multivesicular bodies (MVB) are either degraded by merging with lysosomes or fuse with the plasma membrane thereby releasing exosomes into the extracellular space. Microvesicles, on the contrary, are formed by direct blebbing or outward budding from the plasma membrane (Figure 12). Both, exosomes and microvesicles carry surface markers of their parent cells with almost all microvesicles additionally expressing phosphatidylserine that is externalized during the generation

process(Thery, Ostrowski et al. 2009, Burger, Schock et al. 2013). Urinary exosomes contain proteins or mRNA species that are representative of all major segments of the nephron including: the glomerulus (eg. podocalyxin, nephrin), proximal (e.g. cubilin, aquaporin 1) and distal convoluted (e.g. sodium-chloride cotransporter) tubules, loop of Henle, and the collecting ducts (e.g. aquaporin 2) (Miranda, Bond et al. 2010, Salih, Zietse et al. 2014, Erdbrugger and Le 2016, Morrison, Bailey et al. 2016). Additionally, it has been demonstrated that extracellular vesicles are released upon stimuli associated with inflammation, cell stress and injury such as lipopolysaccharide, reactive oxygen species, tumor necrosis factor-*alpha* but also by hyperglycaemia, and advanced glycosylation end-products (Burger, Schock et al. 2013, Urbanelli, Magini et al. 2013, Salih, Zietse et al. 2014). As these factors are also involved in pathophysiological pathways of diabetic nephropathy (see above), the analysis of the urinary extracellular vesicle profile might present an attractive opportunity to detect and localize early cellular damage in DN. Alterations in the profile might even precede other markers like albuminuria.

1.4.2 Measurement

Standard methods for isolating exosomes from the urine require a large volume of urine (up to 200ml), are laborious (e.g. prolonged ultracentrifugation steps are required) and might affect sample quality as a loss of up to 40% of exosomes was suggested to occur during ultracentrifugation and purity was questioned for commercial EV precipitation approaches(Alvarez, Khosroheidari et al. 2012). Additional purification steps such as using a sucrose gradient result in a further reduction of the EV yield(Hogan, Johnson et al. 2014).

Figure 12: Cellular Release of extracellular vesicles and their measurement by Nanoparticle tracking

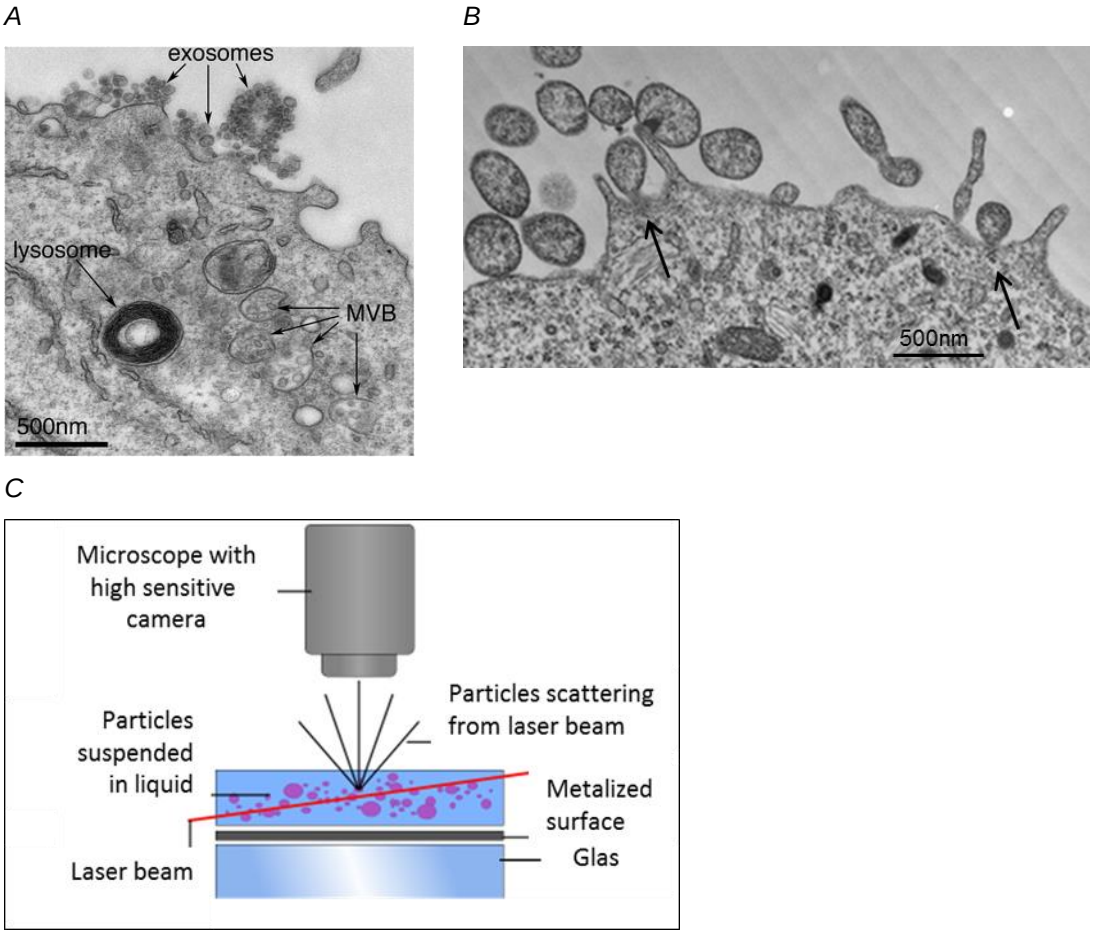

Figure 12. Transmission electron microscopy micrographs of cells A) releasing exosomes by the merging of a multivesicular body (MVB, arrow) that is packed with exosomes and the cellular membrane, B) releasing microvesicles by direct outward budding (arrows). Micrographs taken from Edgar(Edgar 2016) and Giusti et al. (Giusti, D'Ascenzo et al. 2013). C) Schematic illustration of nanoparticle tracking analysis (NTA). The light scattered from the particles is recorded by a digital camera and using the Stokes-Einstein equation particle size can be calculated. Picture taken from www.malvern.com

Immunoaffinity precipitation methods utilizing magnetic beads are restricted to exosomes that express the chosen surface marker(Kowal, Tkach et al. 2014). Therefore analysis of exosomes by current methods is unlikely to be readily translated into the clinic (Miranda, Bond et al. 2010, Dear 2014, Erdbrugger and Le 2016). A novel technology, nanoparticle tracking analysis (NTA) enables rapid and robust quantification of urinary exosomes(Dragovic, Gardiner et al. 2011,

Oosthuyzen, Sime et al. 2013). NTA is based on the principle that at a given temperature, the rate of Brownian motion of nanoparticles in solution is determined solely by their size as expressed in the Stokes-Einstein equation. In this method, laser light is directed at a fixed angle to particles in suspension, and the scattered light is captured using a microscope coupled with a high-sensitivity camera. By tracking the movement of individual particles over time, the software calculates their concentration and size (Figure 12). By incubating the sample with a fluorescently labelled antibody against an antigen expressed by a specific renal cell-type the number of exosomes released into the urine from the cell of interest may be determined. Major advantages of NTA are the small volume of urine (<1ml) required and the minimal processing of the urine sample prior to analysis.

Whilst the size detection threshold of flow cytometry (FCM) instruments is too high (200nm-400nm) for exosome analysis, the instruments cover most of the size range of microvesicles. FCM is the most commonly used technique for MV analysis (Erdbrugger and Le 2016) (van der Pol, Coumans et al. 2014). In FCM, the approach for gating of MVs differs between the studies, but many published protocols contain the use of a marker for externalized phosphatidylserine (Annexin V) and a restriction for particle size (<1µm and >100nm) (Burger, Thibodeau et al. 2014, Nielsen, Beck-Nielsen et al. 2014).

1.4.3 Extracellular vesicles in Chronic Kidney Disease

Since the seminal study from Pisitkun et al. that characterized the content of urinary exosomes, many studies have identified promising urinary exosome biomarker candidates for detection and prognosis of CKD and DN(Pisitkun, Shen et al. 2004,

Erdbrugger and Le 2016, Morrison, Bailey et al. 2016). WT-1 positive exosomes correlate with renal function (Kalani, Mohan et al. 2013). Podocalyxin positive microvesicles precede albuminuria in DN rat models(Burger, Thibodeau et al. 2014). Dipeptidyl peptidase-IV positive particles correlate with ACR in patients with T2D (Sun, Deng et al. 2012). Urinary exosomal miRNA145 might represent a marker of incipient DN in humans and animal models (Barutta, Tricarico et al. 2013). Regucalcin seems to be downregulated in renal tissue and in urinary exosomes in rodents and patients with DN(Zubiri, Posada-Ayala et al. 2015). Proteomic analysis of isolated exosomes seems to be a promising approach for biomarker detection, though validation studies have yet to be performed (Raimondo, Corbetta et al. 2013, Zubiri, Posada-Ayala et al. 2014). Of note, regarding microvesicles and renal diseases, there are only a few studies measuring MVs in the urine with most studies using blood samples instead (Erdbrugger and Le 2016) potentially due to the higher concentration of MVs in serum/plasma.

There are technical limitations for urinary EV analysis in large patient cohorts. Some studies apply a qualitative approach with the mere presence of the marker defining the diagnosis (Zubiri, Posada-Ayala et al. 2015). In other studies the large sample volume required (Barutta, Tricarico et al. 2013) or the time-consuming and technically difficult sample preparation or vesicle isolation procedure (Kalani, Mohan et al. 2013, Zubiri, Posada-Ayala et al. 2014) impedes their practical validation in large-scale study cohorts.

This work will investigate whether the methodologies of nanoparticle tracking analysis and flow cytometry could possibly overcome some of these obstacles.

1.5 Objectives

In this work the following questions are addressed.

i. Can the analysis of the transcriptome and pathological phenotype in a novel Cyp1a1mRen2 reversal DN model facilitate the study mechanisms of injury and repair and identify markers of translational potential?

ii. Can an integrative biology approach using urinary peptidomics confirm and complement the findings from (i)?

iii. Can the biomarker candidates derived from (i) and (ii) be confirmed in a large human T2D cohort?

iv. Can the measurement of urinary extracellular vesicles by NTA or FCM applied to human studies in a similar manner to conventional methodologies of biomarker measurement employed in (iii)?

Figure 13: Integrated objectives of the work

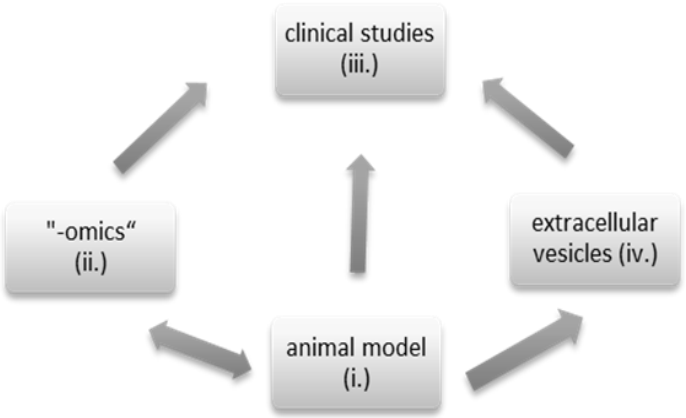

Figure 13. i. Transcriptomic analysis in the animal model and confirmation of the findings in renal tissue. ii. Peptidomics in urine from the animal model may identify non-invasive biomarkers of disease processes detected in the kidney in i. Similar studies in patients with DN generate novel biomarker candidates for further study in iii. large clinical cohorts. iv. analysis of extracellular vesicle profiles in the animal model may generate novel biomarkers which may then be tested in patients with DN (iii) i-iv refer to the objectives of this work (see above).

2. MATERIALS AND METHODS

All materials if not indicated otherwise were bought from Sigma (SigmaAldrich, Dorset, UK).

2.1 Animal models

The Cyp1a1mRen2 DN model and reversal DN model

It is important to point out that the studies on the Cyp1a1mRen2 model in the current thesis were performed on archived tissue from previous in vivo studies. These studies, including the initial description of the Cyp1a1mRen2 model of DN and the reversal model are described in detail in the introduction chapter and have been published (Conway, Rennie et al. 2012, Conway, Betz et al. 2014).

Kidney tissue and urinary specimens from these studies were stored at -80°C degree. I was allowed to use them for further analysis in this work courtesy of my supervisor Dr. Bryan Conway.

The reversible unilateral ureteric obstruction ([R-]UUO) model

The methodology of the irreversible and reversible UUO model has been published before in detail (Hesketh, Vernon et al. 2014). In brief, following midline laparotomy, the left ureter was identified and ligated. A silastic tube placed around the ureter proximal to the ligature to prevent dilatation. Ten days after the initial surgical intervention the animals in the UUO-group and sham group were culled. In the animals of the RUUO-group a reversal of the ureteric obstruction was performed by anastomosing the ureter directly into the bladder. The animals were culled 29 days after the reversal surgery.

The timeline of UUO and reversal phase are described in the result section. I together with my supervisor Dr. Bryan Conway planned and prepared the experiments. The surgery was performed by experimental animal surgeons, Gary Borthwick and Spike Clay, at the small animal facility, Queen's Medical Research Institute (QMRI), University of Edinburgh. Procedures were performed under UK Home Office licence and approved by the Animal Ethics Committee of the University of Edinburgh.

2.2 Immunohistochemistry (IHC) and Immunofluorescence

After the harvest, kidneys were fixed overnight in 4% paraformaldehyde with 0.1M phosphate buffer or methyl-Carnoy (60% ethanol, 30% chloroform, 10% glacial acetic acid; for ED-1, transgelin, CD3, WT-1).

They were embedded in paraffin wax and sectioned at 5μm thickness and placed on slides in the Histology Department of the QMRI, University of Edinburgh.

For most paraformaldehyde slides antigen retrieval was performed to break formalin induced protein cross-links that potentially mask antigenic sites. The slides boiled in TRIS-EDTA buffer (10mM Tris Base, 1mM EDTA, 0.05% Tween 20 at pH 9.0) for 15min and cooled by rinsing in water for another 30min thereafter. After deparaffinization of the slides in xylenes for two times 5min, the slides were rehydrated in serial dilutions of 100%, 90%, 75% and 50% of alcohol and washed. The slides were exposed to 2% hydrogen superoxide Peroxidase-Blocking solution (Dako, Glostrup, Denmark) for 15min on a shaker to block the endogenous peroxidase activity of the tissue and washed again. Slides were placed in Sequenza racks (Ted Pella, Altadena, CA, USA) prior to blocking and staining. An

Avidin/Biotin Blocking Kit (Vector Laboratories, Burlingame, CA, USA) was used to block avidin and biotin binding sites in the tissue according to the manufacturer's instructions. Then 3 drops of serum-free protein block (Dako) was put on the slides for 10min. They were incubated with 125µl of the primary antibody in antibody-diluent (Dako) at 4°C overnight. Next day, after washing with PBS, 125µl of the species-appropriate biotinylated secondary antibody in diluent for 30min was added on the slide at room temperature (RT) (see Table 1 for antibody details and concentrations). Following further washing steps, 3 drops/ per slide of R.T.U. Vectastain Elite ABC (Vector Laboratories) was applied for 30 minutes. Subsequent to three washing steps with PBS, 125µl of chromogen DAB solution (DAKO) was added to the slides for between 30 seconds to 3 minutes (depending on the antibodies applied) until brown staining was clearly visible. After another short wash, slides were counterstained for several seconds in haematoxylin and Scott's tap water (SigmaAldrich, provided by Histology Core Facility, QMRI, University of Edinburgh). Slides were dehydrated in serial increasing strength alcohol dilutions and alcohol was cleared by placing slides in xylene for 10 minutes thereafter. Finally coverslips were mounted on the slides with DPX mounting medium (SigmaAldrich).

Data collection and analysis

For every tissue section 8 images were taken using a Zeiss Axioskop microscope (Zeiss) and QImaging Micropublisher 3.3 RTV camera and QCapture Pro imaging software (QImaging, BC, Canada).

For collagen I&III positive staining was identified with ImageJ (NIH, Bethesda, MD, USA). The percentage positive staining was calculated as the number of positive

pixels (positive stained tissue area) divided by the total pixel number (total tissue area) using the colour deconvolution plugin of ImageJ. For total (ED-1$^+$), M1 phenotype (iNOS$^+$) and M2 phenotype (mannose receptor, MR$^+$) macrophages, the number of positive cells was counted in 20–30 ×400 tubulointerstitial fields/slide; for podocytes (WT-1$^+$) the number of positive cells was counted in 20-30 hilar glomerular cross-sections/slide. The resulting numbers were averaged for each animal. On each slide all glomeruli were counted for total glomeruli number per section. For 20-30 hilar glomeruli per slide the surface was measured by manually marking the glomerular tuft area using Adobe Photoshop CS5 (Adobe).

Table 2: List of antibodies for Western Blotting

Primary antibody **Specificity / Clonality / Isotype** **Manufacturer**	**Dilution**	**Secondary antibody** **Manufacturer** **(all biotinylated)**	**Dilution**
rabbit anti-collagen I mouse, rat / polyclonal / IgG Abcam / ab34710	1:300	goat anti-rabbit IgG Vector BA-1000	1:300
goat anti-collagen III mouse, rat / polyclonal / IgG SouthernBiotech / #1330-01	1:150	rabbit anti-goat IgG Vector BA-5000	1:300
goat anti-KIM-1 rat / polyclonal / IgG R&D Systems / AF3689	1:50	horse anti-goat IgG Vector BA-9500	1:300
goat anti-EGF rat/ polyclonal / IgG Santa Cruz Biotechnology / sc-1343	1:25	rabbit anti-goat IgG Vector BA-5000	1:300
mouse anti-ED-1 rat / monoclonal /IgG1 AbD Serotec / MCA341R	1:100	horse anti-mouse IgG Vector BA-2000	1:300
rabbit anti i-NOS rat / polyclonal / IgG Abcam / ab15323	1:2500	goat anti-rabbit IgG Vector BA-1000	1:300
rabbit anti mannose-receptor rat / polyclonal / IgG	1:1500	goat anti-rabbit IgG Vector BA-1000	1:300

Primary antibody **Specificity / Clonality / Isotype** **Manufacturer**	**Dilution**	**Secondary antibody** **Manufacturer** **(all biotinylated)**	**Dilution**
Abcam / ab64693			
rabbit anti transgelin rat / polyclonal / IgG Abcam / ab14106	1:8000	goat anti-rabbit IgG Vector BA-1000	1:300
rabbit anti WT-1 human / polyclonal / IgG Santa Cruz / sc-192	1:200	goat anti-rabbit IgG Vector BA-1000	1:300
mouse anti CD45RA rat / monoclonal / IgG1 AbD Serotec / MCA340GA	1:500	horse anti-mouse IgG Vector BA-2000	1:300
rabbit anti CD3 human / polyclonal / IgG DAKO / A0452	1:100	goat anti-rabbit IgG Vector BA-1000	1:300

Table 2. Details of the primary antibodies utilized for Western Blots including the respective secondary antibodies.

Immunofluorescent double staining

After dewaxing and rehydration (see above) the slide was exposed to 3 drops of serum-free protein block (Dako) for 10 minutes. Then it was incubated with rabbit anit-CD 3 (Dako) 1:200 in antibody diluent (Dako) at 4°C overnight. Next day, after washing with PBS, a secondary donkey anti-rabbit IgG Alexa Fluor 594 antibody (Life Technologies, ThermoFisher, Scientific, Paisley, UK) 1:300 in antibody-diluent was put on the slide for 50 minutes. After a subsequent washing and blocking step, the second primary antibody mouse anti CD45RA (Serotec) 1:200 in anti-body diluent (Dako) at 4°C with an overnight incubation was followed by the second secondary goat anti-mouse IgG Alexa Fluor 488 (Life Technologies) 1:300 in antibody-diluent with an incubation time of 50min. Finally, the slide was mounted with VectaShield mounting medium (Vector laboratories). Images were taken using a Zeiss Axioskop 2mot+ (Zeiss).

2.3 Homogenization of tissue samples

For downstream analysis a piece (20-30mg) of cortex was cut off from snap frozen kidney and placed directly into 300-600µl of the appropriate homogenate buffer for the downstream indication: Triton X 100/50mM Tris pH8/150mM NaCl for zymography and collagenase/gelatinase kit, RIPA buffer for Western-Blot (50mM Tris pH 7 – 8, 150 mM NaCl, 0.1% SDS [sodium dodecyl sulfate], 0.5% sodium deoxycholate, 1% Triton X 100 and a protease complete inhibitor mini cocktail [Roche, Basel, Switzerland]) or RA1 Lysis Buffer from Nucleospin RNA II kit (Macherey-Nagel, Duren, Germany) containing 1% beta-mercaptoethanol for PCR.

Tissue was homogenized with metal beads in a mixer mill MM200 tissue homogeniser (Retsch, Haan, Germany) at 30 Hz for 120 seconds.

For Western-Blot and the zymography/activity assays homogenate was then centrifuged at 10,000g for 10min at 4°C and the supernatant was further processed or stored at -20°C.

Measurement of protein content

Detergent compatible DC Protein Assay (Bio-Rad, Hercules, CA, USA) was used to determine the amount of protein/µl in kidney homogenates for normalization of samples. The assay is based on the methodology of Lowry in which divalent copper becomes monovalent by forming complexes with free peptides bonds and reacts with radicals from aromatic amino acids reducing the Folin reagent that returns blue colour. After all kit reagents (25µl alkaline copper tartrate and 500µl Folin reagent) and the sample (5µl) had been mixed together in a 96-well flat bottom microplate

(Corning, New York, NY, USA) the reaction lasts 15min and the photometric density can be measured by a microplate reader at 750nm wavelength. By the simultaneous measurement of standards (0, 0.2-1.5 mg/ml of bovine albumin [SigmaAldrich]) a standard curve can be calculated and the sample protein concentration interpolated from it.

2.4 rt-PCR

RNA extraction

The extraction was performed using the Nucleospin RNA II kit (Macherey-Nagel).

The homogenate in RAI buffer was transferred to a NucleoSpin Filter column with a syringe with a 0.9 mm needle (20 gauge) attached and spun at 11000g for 1min. After mixing with 350µl ethanol the filtrate was put on a NucleoSpin® RNA column with a silica membrane and processed in serial steps with membrane desalting buffer (MDB), DNase Reaction Buffer, RAW2 buffer and RA3 (2x times) buffer. The dried column was placed into a nuclease free collection tube and eluted with 60µl RNase-free water by spinning at 11000g for 60s and placed on ice.

cDNA synthesis by reverse transcription

The mRNA in the samples was quantified using a NanoDrop ND-1000 spectrophotometer (ThermoFisher Scientific, Cramlington, UK) at 340nm wavelength.

For reverse transcription into cDNA the high capacity cDNA reverse transcription (RT) kit (Applied Biosystems, Warrington, UK) was used according to manufacturer's instructions. In brief, 10µl mRNA in a concentration 0.1µg/µl were

mixed with 10µl master mix (RT buffer [volume: 2µl; final concentration: 1x], deoxyribonucleotide triphosphate [dNTP] mix (0.8µl; 4mM), RT Random primers [2µl; 1x], reverse transcriptase [1µl; 50U], RNase inhibitor [1µl], nuclease free water) [3.2µl]) in a 96-well reaction plate. The transcription was performed in a PTC-100 Thermal controller (MJ Research, Reno, NV, USA) for two hours at 37°C followed by a termination at 85°C.

Real-time polymerase chain reaction (RT PCR)

TaqMan inventoried primers and TaqMan Universal PCR master mix (Applied Biosystems) was used: 5ng cDNA from the sample were mixed with 1µl of 20x TaqMan inventoried primers and 10µl of 2x PCR master mix and diluted with ddH_2O to a total volume of 20µl in a fast 96 well reaction plate (ThermoFisher Scientific). Altogether 40 cycles (10min at 95°C for DNA polymerase activation, 15s at 95°C for melting, 1min at 60°C for annealing and extension) were run on a Applied Biosystems Fast Real time 7500 PCR machine. The following primers were used (Applied Biosystems): tagln:Rn01642285_g1; col1a1:Rn01463848_m1; fn:Rn00569575_m1; foxp3:Rn01525092_m1; mmp2:Rn01538170_m1; mmp7:Rn00689241_m1; mmp12:Rn00588640_m1; mmp14:RN00579172_m1; timp1:Rn01430873_g1; timp2:Rn00573232_m1; timp3:Rn00441826_m1; egf:Rn00563336 and the housekeeping gene TATA-binding protein: Rn01455648_m1. Each sample was run in triplicate for each gene and the mean calculated.

Data analysis

The SDS Software 1.3.1. was used for analysis. The threshold in the ΔR_n (normalized reporter with - without template) vs Cycle plot was set in the linear phase of the amplification curve excluding background noise at the first significant increase in ΔR_n . ΔC_T (threshold cycle) was determined for every sample by the software. The ΔC_T sample was calculated by subtracting the C_T of the housekeeping gene from the C_T of the gene of interest. Then the average ΔC_T of the reference group was subtracted from the ΔC_T of the other samples to determine the $\Delta\Delta C_T$ for each sample and the relative expression (RQ) is calculated as $2^{-\Delta\Delta Ct}$.

2.5 Western-Blot analysis

Gels are cast in an assembled Mini-PROTEAN Tetra system (Bio-Rad) with the 10% polyacrylamide gel mixed manually (For 2 gels: 29.2% Acrylamide, 6.67ml 0.8% Bisacrylamide (w/v), 5ml 0.4% SDS in 1.5M Tris-Cl pH 8.8, 8.33ml distilled water, 100µl 0.06% (w/v) APS, 10µl TEMED (v/v)). Homogenates were normalized for individual protein concentration, mixed with 5x laemmli sample buffer (60mM Tris-HCl pH 6.8, 2% SDS, 10% glycerol, 0.01% bromophenol blue) containing 5% (v/v) β-mercaptoethanol and boiled at 95°C for 10min. After the system had been filled inside with cathode buffer (50mM Tris, pH 8.6, 383.5mM glycine and 0.1% (w/v), SDS) and outside with anode buffer (50mM Tris, pH 8.6 containing 0.1% (w/v) SDS), samples (30µg protein) were loaded on the gel. Samples were separated at constant voltage 80V for 70min and then transferred on a polyvinylidene fluoride (PVDF) membrane (Amersham Hybond P 0.2, GE Healthcare LifeSciences, Little

Chalfont, UK) for 60min at 90 volts in transfer buffer (50mM TRIS, 383.5mM glycine, 20% (v/v) methanol). Afterwards the membrane was washed twice for 5 minutes in TBST (50mM TRIS pH 7.5, 150mM NaCl, 0.05% (v/v) Tween-20). Then it was blocked for one hour in 5% skim milk TBST followed by the incubation with the primary antibody (i.e. 1:000 rabbit anti-rat TIMP-1 [Biorbyt, Cambridge, UK] and 1:10000 rabbit anti-rat beta-actin [Abcam, Cambridge, UK] in 5% bovine serum albumin) at 4°C overnight. After two washing steps with TBST the secondary antibody horseradish peroxidase-conjugated anti-rabbit IgG (Dako) diluted in 5% skim milk TBS (at 1:2000 [TIMP-1] and 1:10000 [beta-actin]) was incubated for one hour at room temperature. After three wash steps with TBS, Pierce ECL Plus 2ml Substrate (ThermoFisher Scientific) was added on the drained membrane and incubated for 5min in the dark. ECL was carefully removed and the membrane was covered by a transparent foil and imaged on a Versadoc system (Bio-Rad). The densitometry was performed with Adobe Photoshop CS3 (Adobe, San Jose, CA, USA).

2.6 Gelatinase and Collagenase activity assay kits

Metalloproteinase activity was assessed using the EnzChek Gelatinase/Collagenase Assay Kit (Invitrogen, ThermoFisher Scientific, Paisley, UK). According to the manufacturer's instructions 100 µl of homogenates (at 1µg/1µl) were incubated with 20µl DQ gelatin or collagen (1mg/ml) respectively and 80µl of reaction buffer in the dark for 24 hours. DQ gelatin/collagen is so heavily labelled with the conjugate fluorescein that the fluorescence is quenched. Cleavage by collagenase and gelatinase releases fluorescent peptides and the fluorescence can be quantified by a

plate reader at excitation/emission=380nm/500nm. Fluorescent intensity from the released peptides correlates with the collagenase/gelatinase activity. For QC, additional measurements were performed with some samples spiked with a general metalloproteinase inhibitor (1,10-phenanthroline, monohydrate, 0.5 mM) or samples were completely replaced by reaction buffer.

2.7 Zymography

Gel zymography

For substrate zymography 10% polyacrylamide gels were manually cast like for Western-Blots, but in addition including either gelatin (1 mg/mL) or collagen (0.2 mg/mL). Tissue homogenates were mixed 1:1 with zymogram sample buffer containing 62.5mM Tris pH 6.8, 25% glycerol, 4% SDS and 0.01% Bromophenol Blue (Bio-Rad), loaded on the gels (40µl per lane at 2.5µg/µl) and separated by electrophoresis at a low constant voltage (40-60V) using PowerPac (Bio-Rad). The running buffer contained 25mM Tris, 192mM glycine, 0.1% SDS at a pH 8.3. After dismantling from the system, gels were washed twice with 2.5% Triton X-100 to remove SDS enabling protein renaturation followed by an incubation period for 48–72 h at 37°C in incubation buffer (50 mM Tris HCl, 0.15 M NaCl, 10 mM CaCl, [Bio-Rad]). Gels were stained with 0.05% Coomassie Brilliant Blue (VWR, Radnor, PA, USA) in 25% methanol/ 10% acetic acid/water and de-stained in aqueous 4% methanol/8% acetic acid. The gels were scanned using Li-Cor Odyssey and the band intensities were quantified on Software Odyssey v.3.0 (Li-Cor, Lincoln, NE, USA).

In-situ zymography

In-situ zymography was performed either on zinc-fixed paraffin-embedded or on frozen (-80°C) tissue sections generally based on the publications from Ahmed et al.(Ahmed, Haylor et al. 2007) and Hadler-Olsen et al.(Hadler-Olsen, Kanapathippillai et al. 2010) with modifications. Upon harvest, tissue was either snap frozen and mounted in Tissue Tek O.C.T (Sakura, VWR) or fixed in zinc-buffered fixative (ZBF) (BD Biosciences, Oxford, UK), for 24 hours at room temperature, dehydrated and paraffin-embedded. 8μm sections were cut in the Histology facility, QMRI, Univeristy of Edinburgh. For zymography cryo-sections were air dried for 10min at RT and washed for 10min in PBS to remove OCT. Zinc-fixed tissues were kept at 59°C overnight and deparaffinised in xylene. Then they were rehydrated in graded alcohol baths. 150-200μl of 2% DQ Gelatin (1mg/ml) substrate mixed in 50 mM Tris-HCl, 150 mM NaCl, 5 mM CaCl and 0.2 mM sodium azide (pH 7.6) was put on the sections. Subsequently, sections were incubated at 37°C in the dark in a humidified chamber for two hours. Then gelatin was removed by gentle washing in dH_2O followed by a fixation in 4% neutral-buffered formalin (40ml/L 37-40% Formaldehyde, Sodium phosphate, monobasic 4.0 g/L Sodium phosphate, dibasic (anhydrous) 6.5 g/L pH 7) for 10min in the dark. After another short wash sections were mounted with VectaShield mounting medium (Vector Laboratories), covered by a coverslip and kept in the dark. For analysis 5 images of the cortical area were taken per section using a Zeiss Axioskop 2mot+ (Zeiss, Jena, Germany) with an Hamamatsu Orca camera (Hamamatsu Photonics, Shizuoka, Japan). Whole image contrast/brightness was adjusted using Adobe Photoshop CS5 (Adobe). Analysis was performed using ImageJ (NIH) with the number of positive

pixels expressed as a percentage of the total number of pixels(Hesketh, Kluth et al. 2014).

For double staining, instead of mounting the section was washed in PBS and exposed to 125µl of serum-free protein block (Dako) for 10 minutes. Then it was incubated with rabbit anti-rat collagen I (Abcam) 1:300 in anti-body diluent (Dako) at 4°C overnight. Next day, after washing with PBS, a secondary donkey anti-rabbit IgG Alexa Fluor 586 (Life Technologies) 1:500 in antibody-diluent was put on the section for 50min. After a subsequent washing step, the section was mounted with VectaShield mounting medium. Images were taken using a Zeiss Axioskop 2mot+ (Zeiss).

2.8 Enzyme-linked immunosorbent assay (ELISA)

For ELISA in human studies the R&D Duoset Kits were used (detailed specification see Results) (R&D Systems, Abingdon, UK). R&D Duoset was also used for measurement of urinary Epidermal Growth Factor (EGF) in the rat. The ELISAs were performed according to the manufacturers` instructions with the exception that for EGF, Osteopontin and MMP-7 volumes of samples, standards and of all chemicals were halved. In brief, Corning 96 Well EIA/RIA clear flat bottom plates (Corning) were coated with capture antibody (100µl) overnight at RT. After three washes with PBS (Gibco, ThermoFisher Scientific) containing 0.05% Tween® (SigmaAldrich) plates were blocked with Reagent Diluent (1% BSA in PBS, R&D Systems) (400µl) for 1-2 hours. After another 3x wash steps, 100µl of samples or 100µl of standard concentrations that had been generated by serial dilution were

added to the plates for 2 hours. Following another three wash steps, plates were incubated with 100µl of detection antibody, washed three times and incubated with 100µl Streptavidin-HRP for 20 minutes in the dark. After another 3x washes, 100µl of 3,3',5,5'-Tetramethylbenzidin (SureBlue TMB, KPL, Gaithersburg, Maryland, USA) was added and this converted into a blue soluble product over 20 minutes. The reaction was stopped by adding 50µl 1N HCl which turned TMB into a yellow product. The optical density of each well was measured by a microplate reader at 450nm wavelength with a correction set at 570nm. The standard curve was calculated and the concentrations of the samples interpolated from the curve. The urinary TIMP1 (RayBiotech, Norcross, GA, USA) was performed according to the manufacturer's instructions that were similar to the ones described above.

2.9 Measurement of urinary peptidomics

Sample selection for urinary peptidomic analysis

All samples for the urinary peptidomic analysis had been stored at -80°C. These were urinary samples collected over 24 hours from the Cyp1a1mRen2 DN model(Conway, Rennie et al. 2012) including the control, diabetes mellitus (DM) alone, hypertension (HTN) alone and combined diabetes and hypertension (DM+HTN) groups. Additional samples were obtained from rats from the Cyp1a1mRen2 DN reversal model(Conway, Betz et al. 2014): these were serial samples from 24 hours urinary volume collections from the same animals at 3 time points: baseline, after 28 weeks injury phase (combined diabetes and hypertension) and after another 8 weeks reversal phase (reversal of hypertension and tight glycaemic control). All urinary samples were centrifuged at low speed (500g) for 5 mins to remove cellular debris.

Human samples were spot urine taken from RDS study participants that will be described in more detail below. Human "control" urine was taken with informed consent from healthy volunteers with no medical history of kidney related diseases.

Urinary protein separation by electrophoresis

After defrosting the samples (300µl) were mixed with acetonitrile (SigmaAldrich) 1:5 for precipitation and incubated overnight at 4°C. Then they were centrifuged for 40min at 4000g at 4°C. The supernatant was removed and the pellet re-suspended in solution buffer containing 0.05M 1,4-dithiothreitol (DTT). Protein was measured with the RC DC Protein Assay (Bio-Rad) according to the manufacturer's instructions. Select samples (300-500µl) were dialyzed against >500x volume of dialysis solution following the manufacturer's instructions using a Slide-A-Lyzer cassette with a 3.5-kDa molecular mass cutoff (ThermoFisher Scientific). Albumin was depleted from some samples using the Aurum Affi-Gel Blue Mini Column Kit (Bio-Rad) following the manufacturer's instructions. Samples were mixed 4:1 with 4xLDS buffer (Novex, ThermoFisher Scientific). 50µl of the sample was loaded onto a precast gel (4–20% Mini-PROTEAN TG Precast Protein Gel, Biorad) and run for approximately 1 hour at 150V in MES-Buffer (Novex). Afterwards the gel was washed twice in dH_2O for 15min. The gel was stained using GelCode Blue Stain Reagent (ThermoFisher Scientific) that is based on colloidal Coomassie dye G-250 followed by a de-staining step with dH_2O for two hours. The picture of the gel was taken by a smartphone camera (Samsung).

Sample preparation for urinary peptidome analysis

The methodology was published recently(Betz, Jenks et al. 2016): After thawing, 5% of the total 24hr urinary sample volume was centrifuged in Millipore Amicon Ultra-4 spin concentrators (Merck Millipore, Bellerica, MA, USA) with a 10kDa cut-off cellulose membrane at 3220g for 15min at 4°C. The resulting filtrate was acidified with 5% trifluoroacetic acid (TFA, SigmaAldrich) to pH4 and loaded onto a C8 StageTip. The StageTips had been assembled manually by placing small C8 membrane (C8 Empore Disks, 3M, Maplewood, MN, USA) into pipette tips(Rappsilber, Ishihama et al. 2003). The StageTip was wetted with 5µl MeOH, washed by loading 10µl 0.1% TFA and then the complete sample was subsequently loaded on the tip and centrifuged at low speed (500-2000g) for 1-5min. This was followed by two wash spins with 0.1% TFA. 40µl 80% acetonitrile in 0.1%TFA (v/v) was used to elute the peptides applying low speed centrifugation. The 40µl effluent was slightly warmed to evaporate acetonitrile. Then, the sample was re-suspended in 50mM ammonium bicarbonate to a volume of 50µl and reduced in 5mM DTT at 60°C for 15 min. Afterwards, samples were slowly cooled to room temperature. Iodoacetamide was added to a final concentration of 15mM and the sample was kept in the dark for 15min for alkylisation. The samples were incubated with trypsin at 2.5ng/µl overnight at 32°C to ensure the proteolytic digestion of high-molecular weight (HMW) peptides and small proteins up to 10kDa. The concern was these HMW components might otherwise not fly and fragment in the instrument and be difficult to detect by LC-MS/MS(Fliser, Novak et al. 2007). After incubation the sample was re-acidified with 1% TFA and loaded on a C18 StageTip that had been assembled in the same way as described above. The C18 StageTip loaded with the

sample could be frozen and stored at -80°C for later analysis or the sample could be further processed by eluting the sample with acetonitrile that was subsequently removed by vacuum evaporation(Ohta, Bukowski-Wills et al. 2010).

Matrix-assisted laser desorption/ionization – time of flight (MALDI-TOF)

For analysis using DE-STR MALDI-TOF MS Voyager (Applied Biosystems) 0.5µl of the sample was mixed with 0.5µl CHCA (alphaCyano-4-hydroxycinnamic acid) and dried on a 100 well MALDI sample plate. The laser intensity was set at 2200kW/cm^2. Roughly 200-300 shots from different regions of the spot were averaged. The resulting spectra were further processed automatically by using the "advanced baseline correction" option (degree 0.1, flexibility 0.5, peak width 16), "noise filter smooth" (set 0.7) and "noise removal" (set 2). Then data was exported to Mascot search engine (Matrix Science) for protein identification.

LC-MS/MS

The measurement on LC-MS/MS was performed with the assistance of Dr. Andrew Cronshaw, Proteomics Facility, School of Biological Sciences, University of Edinburgh, according to the following published procedure (Betz, Jenks et al. 2016): "5µl of the sample was loaded onto an Ultimate 3000 Series HPLC (Dionex) with a PicoTip Emitter (FS 360-100-8-N-20-C12, New Objective) in series with an LTQorbitrap mass spectrometer (ThermoFisher Scientific). The PicoTip Emitter was packed with Reprosil-Pur C18-AQ 3µm (Dr Maisch GmbH) to a length of 6.5-7.5cm. The PicoTip column was equilibrated with solvent A (0.5% acetic acid in 5% acetonitrile) and eluted with a linear gradient, from 0%B for 9min; from 0 to 20%B over 9 to 40min; from 20 to 80%B over 40 to 48min; solvent B (0.5% acetic acid in

99.5% acetonitrile), over 65min at a flow rate of 0.7µl/min for the first 9min and 0.3µl/min thereafter. Data dependent acquisition was controlled by Xcalibur software (ThermoFisher Scientific)."

2.10 Data analyses

Data analysis of urinary peptidomics using MaxQuant, Perseus and an in-house algorithm

For peak identification and label-free quantitation of raw data files from LC-MS/MS, the freely available software MaxQuant (version 1.4.1.2) was used (http://www.maxquant.org)(Cox and Mann 2008). MaxQuant automatically corrects for inaccuracies of retention times from peptides. Mass and intensity of the detected peaks were searched in in a species-specific way via Andromeda search engine that is downloaded at the same time. For the current study the FASTA file databases for "rattus norvegicus" (version 2013 containing 37202 sequences) and "homo sapiens" (version 2013 containing 154,578 sequences) were downloaded from UniProt Knowledgebase (www.uniprot.org). Each hit is scored by a peptide identification probability score. Programme settings in MaxQuant included: no enzyme specificity; mass accuracy window for precursor ion = 10 ppm (parts per million); mass accuracy window for fragment ions = 0.8Da; variable modification including only carbamidomethylation of cysteines and oxidation of methionine. The criteria for peptide identification were a mass accuracy of _10 ppm and a false detection rate (FDR) of p=0.05 to correct for multiple testing. From all peptides detected identical sequences with different charges were summarized. Peptides with a detection score below "50" had to be excluded to avoid false positive results. Obvious contaminants

like human keratin were removed. Finally, peptides were only further analysed when they were detected in a minimum of 3 samples from at least one group. Peptides were quantified by the individual peptide peak intensities expressed as relative abundance.

For human samples data were further statistically analysed by the freely available software Perseus 1.4.0.17 (http://www.perseus-framework.org)(Tyanova, Temu et al. 2016). A first quantitative correlation analysis in the Cyp1a1mRen2 reversal cohort was also done with Perseus. However, assessing differential representation of peptides quantitatively between sample groups was challenging due to a large number of missing values of individual peptide sequences. This made standard analysis by Perseus impossible. Therefore a non-parametric approach was chosen using a custom implementation of Rank Products in R-software. This implementation as an in-house algorithm was developed by Dr. John Manning, BHF CoRE Bioinformatics, University of Edinburgh. In brief, this programme generated lists of peptides that were significantly and consistently ranked highly in fold change between paired samples, irrespective of absolute values. This made a comparison between the relative abundance of peptides at baseline, injury and reversal possible.

Data analysis of urinary peptidomics using Progenesis QI

Progenesis QI software (version 4.0, Nonlinear Dynamics Limited, Newcastle upon Tyne, UK) was used to analyse the urinary peptidome of all groups from the Cyp1a1mRen2 DN model as published previously (Betz, Jenks et al. 2016) and based on the methodology by Atrih et al. (Atrih, Mudaliar et al. 2014): After import of the raw LC-MS/MS data and a visual check of the chromatograms for defects, the

alignment process was started with Progenesis QI automatically selecting a sample from the DM+HTN group as the most appropriate reference and aligning all other ion intensity maps to it with minimal manual corrections. The feature ions with charge states below 2+ or above 5+ were removed and the top five "ranks" for each feature were exported to MASCOT. The settings for the MASCOT search were "no enzyme" to avoid loss of natural peptides, a peptide tolerance of 6ppm and allowed modifications Carbamidomethyl, Dioxidation, Gln>pyro-Glu and Oxidation within the Uniprot "Rattus norvegicus" database as used above. Data were searched against a decoy database with the homology and an identity threshold FDR of <5%. Peptides above an ion score threshold of 50 (corresponding to p-value 0.05) were re-imported into the Progenesis QI software. For peptides with at least three hits per group the differences in peptide intensities between sample groups were calculated by the ANOVA test with a significance threshold of $p < 0.01$. The q-value threshold as a control for false positive p-values was set at 0.05. A q=0.05 for a peptide implies that 5% is the minimal FDR threshold at which the respective peptide will be significant, i.e. 5% of all significant tests will be false positive.

Estimations about the power in transcriptome and peptidome

The power to detect a difference of 50% in genetic up- or downregulation respectively between control vs injury or injury vs reversal group with an estimated SD between 0.25 to 0.3 after normalization is 0.81 (calculated by the freely available program G*Power, Version 3.1.9.2, University of Kiel, Germany).

The program MSstats (Version 2.4.0, Timothy Clough, Safia Thaminy, Susanne Ragg, Ruedi Aebersold, Olga Vitek. "Statistical protein quantification and

significance analysis in label-free LC-M experiments with complex designs" BMC Bioinformatics, 13:S16, 2012.) was used to estimate the necessary average fold change of difference in peptide abundance between the three groups in order to obtain a certain threshold of power. For this, several peptides that had been analyzed by Maxquant were uploaded into the R-based program and power-calculation was performed. On average, the difference in abundance has to be roughly 9.5fold in order to achieve 80% power.

Figure 13a: calculation of power in peptidomics

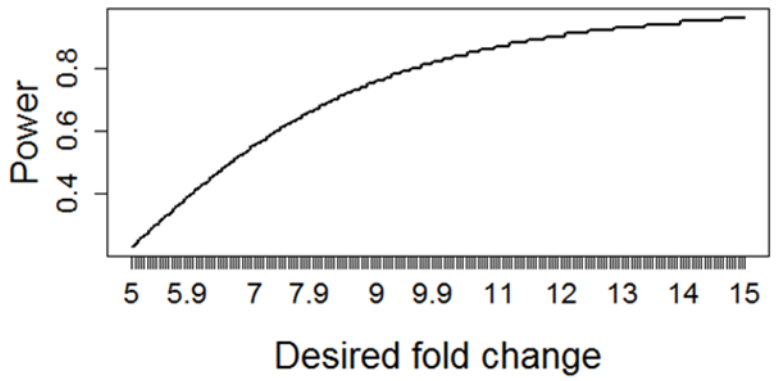

Figure 13a. Illustration of the correlation between increasing power and average fold changes in peptide abundances between groups with three groups, ten biological replicates per group and a False-Discovery-Rate=0.5 the power of 0.8 is achieved roughly at 9.5 times change in average.

When the program Progenesis QI was used instead of Maxquant, the power was calculated for each compound individually based on the abundance variance, the sample size and the difference between the group means. By reducing the threshold for p-value from 0.05 to 0.01 and thereby dismissing compounds with smaller differences between the groups and by defining a q-value of 0.05 almost all of the

peptides retained and especially those mentioned in the current work (like the peptide for the protein EGF and Osteopontin) had a power value above 0.8 (e.g. 96.5% in EGF for the comparison between the control and injury group). However, in future work new peptide candidates should be ensured to be above a defined power threshold like 0.8.

Data interpretation using freely available online databases

The parent proteins of identified peptides were entered into the STRING database v10.0 (Szklarczyk, Franceschini et al. 2015) (www.string-db.org) to assess interactions. Also STRING provided for the respective genes the most enriched biological processes based on Gene Ontology (GO) project data. In addition the expression of the respective genes in the kidney in the Cyp1a1mRen2 (Conway, Rennie et al. 2012, Conway, Betz et al. 2014) model and in biopsies from patients with diabetic nephropathy via the renal biopsy database nephroseq.org was compared with the relative urinary peptide abundance (Woroniecka, Park et al. 2011, Ju, Nair et al. 2015).

The genes that were exclusively up-regulated during injury phase and those that were up-regulated during injury and reversal phase were entered into the freely available database DAVID (Database for Annotation, Visualization and Integrated Discovery, National Institute of Allergy and Infectious Diseases, National Institutes of Health, Bethesda, MD, USA) (Huang da, Sherman et al. 2009) and the results from the analysis for KEGG (Kyoto Encyclopedia of Genes and Genomes) (Kanehisa, Sato et al. 2016) pathway and GO (Gene Ontology Consortium) (Gene Ontology 2015) databases are presented.

Statistical analysis in study cohorts

Means +/- standard deviation (SD) and medians with interquartile ranges (IR) were provided for parametric and non-parametric data respectively. The statistical tests used to compare each dataset are given in the results. In general, parametric tests t-test and ANOVA or non-parametric tests Mann-Whitney and Kruskal-Wallis were applied for comparison between two or several groups respectively. For correlations Spearman's rho (non-parametric) or Pearson's r (parametric) were calculated. Almost three quarters of ACR measurements (73%) in the ET2D study were below 0.5mg/mmol therefore the following 3 categories were used: <0.5mg/mmol; 0.5-1mg/mmol; 1-2.5mg/mmol (males) or 1-3.5mg/mmol (females).

For logistic regression analysis ACR was log transformed into log(ACR)+1 and similarly uEGF:creatinine, OPN:creatinine and MMP7:creatinine and the concentration of exosomes were log transformed. Linear regression analysis as well as Cox regression was calculated for the respective outcomes. The variables for which the regression analyses were adjusted are listed in the respective tables. A two-sided P-value < 0.05 was considered statistically significant unless explicitly stated otherwise in the text.

Most of the statistics and visualizations were performed on the SPSS package version 21 (SPSS Inc., Chicago, IL, USA) or on GraphPad Prism software version 6 (GraphPad Prism Software Inc., San Diego, CA, USA). AUC-ROC curves were calculated using Medcalc version 15.8 (MedCalc Software, Mariakerke, Belgium). For calculation of the Hosmer-Lemeshow test with visualization and the calculation of integrated discrimination improvement (IDI) the R-software (version 3.1.3., 2015, The R Foundation for Statistical Computing, Vienna, Austria) with the package

"PredictABEL" from Kundu at al. (Kundu, Aulchenko et al. 2011) was used. The functions that are based on the publication by Pickering et al. (Pickering and Endre 2012) were integrated into R-software to calculate $IDI_{event/non\text{-}event}$ including the graphical visualization.

2.11 The RDS and the ET2D study

The RDS study

To translate the findings from animal studies to the clinic, urinary samples from patients with (diabetic) chronic kidney diseases were required, ideally at different stages of the disease. A study with the title "Identification of biomarkers for pRogression and Regression in diabetic kidney DiseaSe" (RDS) was permitted to be performed as a clinical research project under the ethical approval of the "South East Scotland SAHSC BioResource" (REC reference 10/S1402/33). The study, which is still recruiting, includes the collection of outpatient samples from participating Diabetes/Renal clinics at the Royal Infirmary of Edinburgh and from healthy volunteers. Clinical data including renal parameters (e.g. creatinine and albumin in serum and urine) are recorded. As controls the following groups are additionally asked for participation: 1. patients with diabetes but without evidence of diabetic nephropathy (ACR<2.5mg/ml (males or <3.5mg/ml (females) and eGFR>60ml/min/1.73m^2) 2. patients with chronic kidney disease (CKD) of an aetiology other than DN and 3. healthy controls. It is planned over a period of 2-4 years to acquire serial samples and to monitor changes in renal function. These latter aspects are not part of this work.

The participants provided informed written consent and every patient was assigned an individual study number. The study information form and the consent form are attached in in the appendix.

Sample collection and storage for the RDS study

Samples were usually collected between 8-12am from non-fasting patients providing a "non-first-morning" urinary sample. The sample was immediately put on ice and within two hours centrifuged for 10min at 500g at 4°C. The resulting supernatant was aliquoted. To the aliquots for exosome measurement a proteinase inhibitor mix including PMSF [phenylmethylsulfonyl fluoride] (SigmaAldrich) at a final concentration 0.5mM and Leupeptin (SigmaAldrich) at 20μM was added. The samples were frozen down at -80°C.

The ET2D study

Urinary samples from the Edinburgh Type 2 Diabetes (ET2D) study were measured in this work. The samples were provided courtesy of Professor Jackie Price, Centre for Population Health Sciences, University of Edinburgh, and were defrosted on ice before measurement. The study protocol has been published in detail before(Price, Reynolds et al. 2008, Marioni, Strachan et al. 2010, Conway, Manoharan et al. 2012, Betz, Jenks et al. 2016). In short, in 2006, 1066 patients with T2D aged between 60 and 74 living in the Lothian, Scotland, UK area attended the research clinic to participate in the Edinburgh Type 2 Diabetes study. At baseline epidemiological data was collected and a blood sample was obtained for measurement of different clinical parameters including HbA_{1c} and serum creatinine for calculation of the estimated GFR (eGFR) by the CKD-EPI formula (Levey, Stevens et al. 2009). Patients

provided also a urine sample (978 samples [92%]) that was after measurement of albumin and creatinine stored at -20°C. After four years participants were invited for the follow-up visit that included similar procedures as described before. 75 (8%) participants (8%) had died before this invitation and another 137 participants (14%) did not attend. For these 212 patients eGFR was calculated based on the serum creatinine that was obtained from health records of their last outpatient clinic visit. Microalbuminuria was defined as an ACR>2.5 (male) mg /mmol or >3.5 (female) mg/mmol in two out of three consecutive measurements (Conway, Manoharan et al. 2012). Incident CKD III is defined as two measurements of eGFR <60ml/min/1.73m^2 with more than three months between the measurements (Betz, Jenks et al. 2016).

2.12 Nanopatricle Tracking Analysis (NTA)

The measurements were performed on a Nanosight LM10 machine (Malvern Instruments, Malvern, UK) with a sCMOS Camera, a 532 nm (green) laser and analysed by Nanosight software v2.3.017. In principle, a laser is directed at particles in solution and the scattered light from the particles is captured by a microscope with a digital camera. According to the Stokes-Einstein equation, the movement (Brownian motion) of free particles in liquid solely depends on their size if the temperature and viscosity are constant. Therefore, by calculating the velocity of tracked particles Nanosight Software can calculate the particle size.

Sample preparation

Human urinary samples from the RDS and the ET2D studies that had been stored at -80°C were slowly defrosted on ice. Samples were vortexed thoroughly to optimize the exosome recovery(Zhou, Yuen et al. 2006). Samples and standards were diluted 1:25 (ET2D) or 1:50 (RDS) with pre-filtered (syringe filters with 0.1um pore size, Millipore) PBS (GIBCO) or distilled water.

Urinary samples from rats were taken from aliquots of the 24hours collection of the Cyp1a1mRen2 reversal study(Conway, Betz et al. 2014). Since urine had been collected by keeping the rats in metabolic cages, some urine samples contained debris that was easily pelleted by a centrifugation step at 500g for 5min before further processing.

The best method to adequately normalize for differences in urinary concentration is a debated issue(Salih, Zietse et al. 2014). For most urinary biomarkers, normalization to urinary creatinine is calculated to compensate for variations caused by diurnal variations in urinary output. This approach has been applied in humans for the measurement of urinary exosomes (Oosthuyzen, Scullion et al. 2016). In general, human urinary output does normally not vary more than 100% or 150%. However, the urinary 24 hours output in the Cyp1amRen2 reversal model increases up to 1000% from baseline to injury. Normalization calculated after measurement could artificially create differences between the groups. Therefore urinary samples from the Cyp1a1mRen2 reversal DN model were beforehand normalized to the 24 hours volume, i.e. samples were diluted with filtered PBS according to their ratio to the sample with the highest volume.

Alternative normalization factors instead of urinary creatinine or 24 hours volume are the total exosome concentration or the use of “pan-exosome” markers. However, out of a number of the suggested housekeeping candidates (CD9, CD24, CD 81, TSG-101, ALIX) no consensus has been reached so far on the optimal choice(Salih, Zietse et al. 2014, Edgar 2016, Morrison, Bailey et al. 2016). Before measurement all samples were diluted 1:100. All samples were kept on ice after thawing. In addition, for each measurement the sample temperature was measured by Nanosight LM10 and integrated into the Brownian motion formula.

For the fluorescent measurement of Qdot (605nm) (Life Technologies) conjugated antibodies, 1000µl of sample volume was incubated with 1µl of the respective antibody for 20-30 minutes. The following antibodies were used: rabbit anti-nephrin (ABT319, Milipore, polyclonal IgG), rabbit anti-cubilin (ab65773, Abcam, polyclonal IgG), rabbit anti-aquaporin 2 (ab3274, Millipore, polyclonal IgG) and as isotype control a mouse IgG (Invitrogen).

Qdot conjugation with antibodies

Qdot fluorophores are nanocrystals (5nm-20nm) that contain in their core aggregates of atoms of a semiconductor material (cadmium mixed with selenium or tellurium) surrounded by a zinc sulphide shell. Biomolecules are attached to the coating polymer layer. Upon excitation their fluorescent emission results from the formation of stable excitons. In comparison to traditional fluorophores Qdots have a more intense brightness and longer photostability. The emission wavelength depends on the size of the Qdot.

The conjugation of antibodies was performed with the Qdot Antibody conjugation kit 605nm (Invitrogen) according to the manufacturer's instructions. In short, 500µl Qdots were activated by incubation with the amine-thiol crosslinker SMCC (N-Succinimidyl 4-(N-maleimidomethyl)cyclohexane-1-carboxylate) for 60min and the antibody (1mg/ml) in 300µl was reduced by incubation with DTT for 30min followed by binding to a dye labelled marker and by a desalting step using a desalting column. Thereafter Qdots and antibodies were incubated for 1 hour to conjugate. The process was quenched by addition of 2-mercaptoethanol for 30min. Subsequent to a concentration step by ultracentrifuging (7000rpm, 15min) the conjugate was purified by running through a separation media column. The resulting concentration of the conjugated Qdots is typically in the range of 1-2 µM.

Quality control

Before every measurement run on the Nanosight LM10, silica beads (Kisker Biotech, Steinfurt, Germany) with a size of 50nm and 100nm at a concentration of $1.9x10^8$ and $4.8x10^7$ respectively from a large stock of aliquots that had been prepared before were measured.

Calculations for total, intra- and inter-assay variation were based on "User verification of performance for precision and trueness; approved guideline – second edition." (Clinical and Laboratory Standards Institute. CLSI document EP15-A2. Wayne, PA, USA: CLSI; 2005) as described by Chesher (Chesher 2008) with slight adaptions. In brief, the within-laboratory precision expressed as standard deviation (SD) (S_t) by $\sqrt{\frac{n-1}{n} \times s_r^2 + s_b^2}$ with s_r being the repeatability and s_b the SD of means

for a period of days (n). Hereby is $s_b^2 = \frac{\sum_{d=1}^{D}(\overline{x}_d - \overline{\overline{x}})^2}{D-1}$ with D=number of days, $\overline{\overline{x}}$ average of all results and $\overline{x_d}$ average of all replicates on day d. $s_r = \sqrt{\frac{\sum_{d=1}^{D}\sum_{r=1}^{n}(x_{dr} - \overline{x_d})^2}{D(n-1)}}$ with D = total number of days, n = total number of replicates per day, x_{dr}=result for replicate r on day d, $\overline{x_d}$ = average of all replicates on day d. In this work eight days were taken for observation period. The coefficient of variation is calculated as the SD divided by the overall mean ($\overline{\overline{x}}$).

Instrument settings

For non-fluorescent light-scatter mode the standard camera level 16 was used. The gain was 512, the shutter 26 ms, threshold 10, minimal expected size and minimal track length were set as "auto". For the fluorescent mode (532nm laser with long-pass filter [430nm]) the detection threshold was set at 6.

Measurement of exosomes by NTA Technology

The optimal stage and focus for the camera was determined manually with the microscope (Gardiner, Ferreira et al. 2013). Before the measurements were recorded, 1ml of filtered PBS was inserted into the measurement chamber to confirm that there were no particles. Then approximately 0.6 ml of the diluted samples or standards were sequentially inserted into the measurement chamber of the Nanosight LM10 machine (Malvern Instruments, UK). For fluorescent measurement the level and position of the camera was checked in the light-scatter mode first before the long-pass filter (430nm) was used. For each measurement altogether three video sequences for 30 seconds were recorded as replicates. Between each replicate

measurement an additional 0.1ml-0.2ml of the sample were inserted into the chamber. Between each sample the chamber was rinsed with filtered water and PBS until no particles were visible.

For the analysis, the software tracks automatically the motion of particles in the recorded video sequences. From the velocity of particle movement the software calculates particle size based on the Stokes-Einstein equation and from the number of particles tracked the software calculates the concentration. The results are visualized in a size (x-axis) vs concentration (y-axis) plot. The total concentration for all particles between 20nm and 100nm was calculated as the area under curve ($AUC_{20\text{-}100nm}$) determined following the trapezoidal rule as published by Oosthuyzen et al. (Oosthuyzen, Sime et al. 2013, Oosthuyzen, Scullion et al. 2016).

2.13 Flow Cytometry (FCM)

For flow cytometry analysis the Attune (Life Technologies) Flow Cytometer that employs on acoustic focusing was used. This technique allows high flow rates and reduces background noise which is especially advantageous at low particle size range.

Sample preparation

For rat urine in the Cyp1a1mRen2 model, to compensate for the great variation in 24 hours urinary excretion, as described above, urine was pre-diluted in filtered (0.1 µm) PBS to an overall volume of 600µl with the samples diluted according to the ratio of their volume to the urine sample with highest 24 hours urinary volume.

For human urine 1 ml per sample was used and subsequently corrected for differences in urine concentration by reference to urinary creatinine. Microvesicles were isolated by differential centrifugation as described by Burger et al. (Burger, Thibodeau et al. 2014) with slight modifications: After a centrifugation at 2500g for 20min to remove large debris the supernatant was transferred to a fresh 2ml Eppendorf tube and centrifuged at 20,000g for 20min to pellet the microvesicles. Afterwards the exosomes containing supernatant (approximately 550µl (rats) or 950µl (humans) respectively) was removed and microvesicles remained in approximately 50 µl of residual diluted urine.

Quality control

Every sample run included an empty control (PBS without sample and dye) as well as Bodipy-Maleimide (BoM) without sample or sample without BoM. A performance test was run on a daily basis using Attune Performance Tracking Beads (Life Technologies) that contain a distinct mixture of beads of different sizes and fluorescent intensities at a final concentration of about $5x10^5$ /ml.

Instrument settings

For defining the size gate 200nm and 1000nm silica beads (Kisker) were used(van der Pol, Coumans et al. 2014). Serial dilutions were performed to exclude swarm detection. After preliminary optimizing experiments the following setting was used: For Side Scatter (SSC) the applied voltage was 3900mV, the threshold was 5. For Forward Scatter (FSC) the applied voltage was 3250mV and the threshold was 5. For the Blue laser (488nm) (530/30nm Filter) the voltage was set 1350mV.

Measurement of microvesicles by Attune FCM

Eppendorf tubes containing approximately 50µl of suspended microvesicles were mixed with 3µl (rats) or 5µl (humans) of freshly thawed and diluted aliquots of Bodipy-Maleimide (50µM) (BODIPY FL N-(2-Aminoethyl))Maleimide), Life Technologies) to a final concentration of 3-5µM BoM (Enjeti, Lincz et al. 2008). Some samples were incubated with 3µl Annexin V Pacific Blue (BioLegend, London, UK) and the calcium concentration was increased to about 2.5mmol/l to ensure binding of Annexin V. In the human study 1µl of mouse anit-podocalyxin IgG antibody (TRA-1-60R, monoclonal, PerCP-conjugate, 1mg/ml, Novus Biologicals, biotechne, Abingdon, UK, 1mg/ml) or 1µl of mouse IgG (monoclonal, PerCP-conjugate, 1 mg/ml, Novus Biologicals) as an isotype control was added. The sample was vortexed after addition of the respective antibodies, and kept for 60min in the dark. Subsequently samples were diluted with 130µl filtered (0.1 µm) PBS and measured. Measurement was performed at a flow rate of 25µl/min.

3. RESULTS

3.1 The Cyp1a1mRen2 Rat Model of Diabetic Nephropathy

3.1.1 Introduction

As mentioned before there are few models that mimic the pathological features of advanced human DN. One of them is the Cyp1a1mRen2 rat model that combines hyperglycaemia with hypertension resulting in marked albuminuria, renal fibrosis and transcriptomic changes that are similar to those observed in the kidney of patients with DN(Conway, Rennie et al. 2012). In order to study mechanisms that promote renal remodelling and markers that indicate regression of albuminuria and fibrosis the model was extended to include a 'reversal group' in which glycaemia was tightly controlled using insulin and blood pressure normalised after an injury period(Conway, Betz et al. 2014).

The analysis of this Cyp1a1mRen2 reversal DN model in this chapter was performed on archive tissue that was available to me from a previous study.

3.1.2 Pathological parameters of the reversal model

The key biochemical and pathological features of the model have been published previously(Conway, Betz et al. 2014) and are summarised in Table 3. Albuminuria increased in the diabetic and hypertensive rats (injury cohort) and decreased by more than 50% after eight weeks of tight blood glucose and blood pressure control (reversal cohort), although it remained persistently greater than in controls. After 28wks of diabetes and hypertension, the creatinine clearance was not significantly different when compared with controls and it remained unchanged following 8wks of

relative normalisation of glycaemia and blood pressure. The mean kidney:body weight ratio increased in the injury cohort compared with controls and while this fell significantly in the reversal cohort it remained significantly greater than in controls. There was a marked increase in the glomerulosclerosis and tubulointerstitial fibrosis indices in the injury cohort compared with controls and this remained persistently increased despite 8 weeks of tight glycaemic and blood pressure control.

As both increased glomerular volume and reduced numbers of glomeruli can be phenomena associated with advanced human DN (Review by Fioretto et al.(Fioretto and Mauer 2007)), these parameters were determined in the current model. There were no differences in the mean hilar glomerular cross-sectional area or the number of glomeruli per tissue section between the cohorts (Figure 14). A trend towards a reduction in the mean number of WT1 positive podocytes/hilar glomerular cross-section in the injury and reversal cohorts compared with control animals did not reach statistical significance ($p = 0.07$) (Figure 15).

Table 3: Parameters of the control and experimental groups

	mean (SD) or median (IQR)					
	Control (n=6)		**Injury (n=10)**		**Reversal (n=9)**	
Blood glucose (mM)	6.3	(0.8)	26.3[aa]	(7.4)	7[bb]	(0.9)
Systolic blood pressure (mmHg)	152	(11.9)	206[aa]	(12.5)	158[bb]	(15.8)
Albumin to creatinine ratio (ACR) (mg/mmol)	4.9	(3.3-5.7)	2962[aa]	(1681-4824)	847[ab]	(547-1463)
Urinary volume (ml/24h)	6.2	(5.2-7.6)	40.0[aa]	(25.0-70.0)	12[ab]	(9-15)
Creatinine clearance (ml/min)	2.37	(0.63)	2.34	(0.40)	2.59	(0.63)
Kidney weight (g)	1.38	(0.1)	1.64[a]	(0.21)	1.53	(0.19)
Body weight (g)	460	(25.5)	350[aa]	(39.5)	424[bb]	(33.2)
Kidney/body Weight (%)	0.30	(0.01)	0.47[aa]	(0.06)	0.36[ab]	(0.03)
Glomerulosclerosis index score (0-4)	0.10	(0.02)	0.71[a]	(0.10)	0.76[a]	(0.12)
Tubulointerstitial Fibrosis index score (0-4)	0.32	(0.01)	1.45[aa]	(0.08)	1.59[aa]	(0.20)

Table 3. Parameters of the Cyp1a1mRen2 model in controls, after 28 weeks of induced diabetes and hypertension (injury phase) and following 8 weeks of tight blood pressure and glucose control (reversal phase). The index score represents an average of all glomeruli /tubulointerstitial fields graded with 0: normal; grade 1: <25%; grade 2: 25–50%; grade 3: 50–75% and grade 4: >75% of area sclerosed/fibrosed. a $p<0.05$ and aa $p<0.001$ v control; b $p<0.05$ and bb $p<0.001$ v injury cohort.

Figure 14: Glomerular numbers and glomerular hilar areas

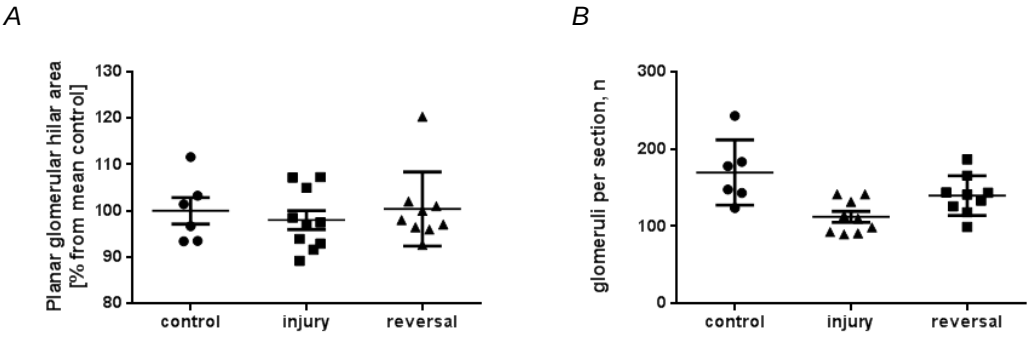

Figure 14. (A) The mean (±SEM) planar glomerular hilar areas and (B) the mean (±SEM) number of glomeruli per section was not altered between the control (n=6) injury (n=9) and reversal (n=9) groups. In (A) the glomerular area is expressed as % of the mean area from all controls

Figure 15: Quantification of WT-1 positive glomerular cell number

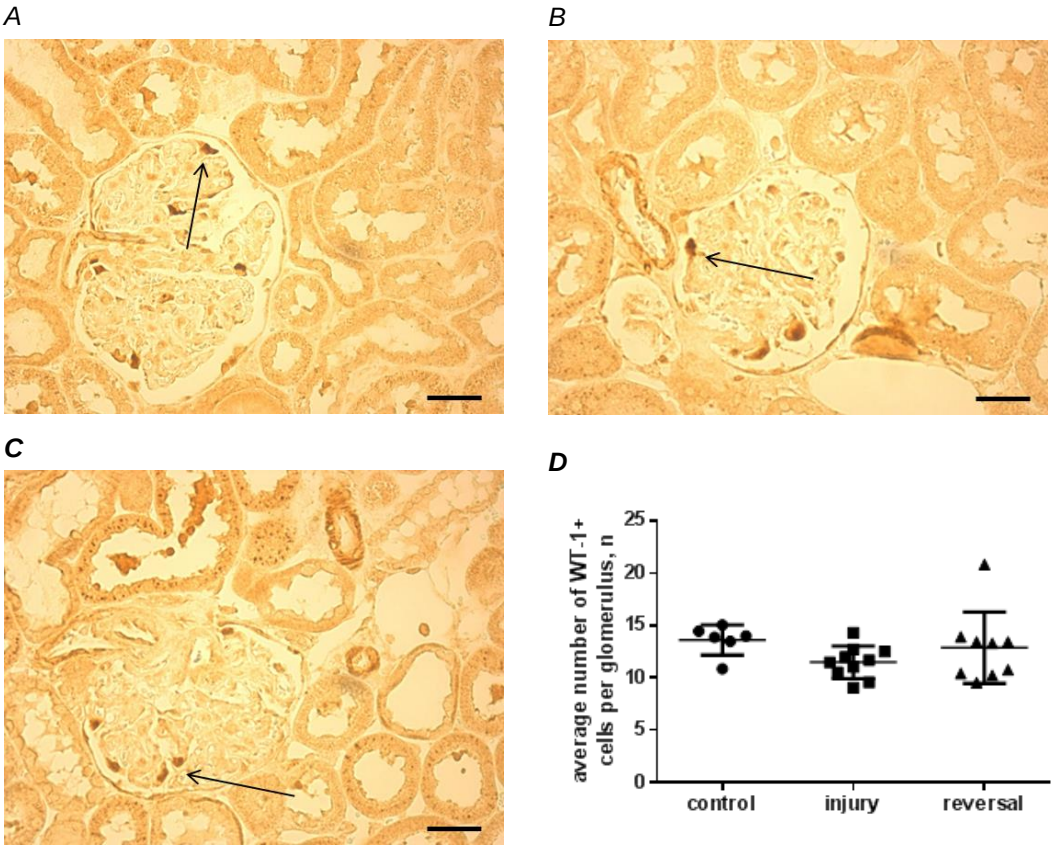

Figure 15. Tissue sections were immunostained for the well-established podocyte marker WT1. (A)-(C) Representative images of WT1 positive cells (arrows) in the glomeruli of control (n=6), injury (n=9) and reversal (n=9) groups. The scale bars represent 20 µM. (D) For each animal the mean number (+/-SEM) of WT1+ cells per glomerulus was calculated in the control, injury and reversal groups. There was a trend (p=0.07) towards a reduction in the injury group.

3.1.3 Genes upregulated specifically during injury phase

Of the 677 genes that were significantly upregulated in renal tissue of the injury group, 85 of these fell >50% towards control levels following 8 weeks of tight control of glycaemia and blood pressure (Appendix). The list was entered into DAVID (Database for Annotation, Visualization and Integrated Discovery, v6.8 Beta)(Huang da, Sherman et al. 2009) for functional annotations and the most significantly over-represented category (p-value) was cell signalling, followed by secreted and extracellular matrix (Table 4). This was also reflected by pathway analysis using DAVID and the KEGG (Kyoto Encyclopedia of Genes and Genomes) database(Kanehisa, Sato et al. 2016) with extracellular matrix-receptor interaction being the most over-represented pathway (Table 4) (Conway, Betz et al. 2014). Expression of the alpha-1 chain of collagen Type I (Col1a1) and transgelin (a marker of smooth muscle cells and myofibroblasts, similar to α-smooth muscle actin) genes were validated by realtime-PCR. Following 8 weeks of reversal of hyperglycaemia and hypertension there was a marked reduction in the mRNA levels of transgelin in the reversal group compared to the injury cohort (Figure 16). In control animals transgelin was restricted to arterial smooth muscle cells. The expression of transgelin increased significantly in the injury group in the glomerular compartment with a non-significant reduction in the reversal group (Figure 17). In the tubulointerstitial compartment transgelin staining was increased in both the injury and reversal cohorts (Figure 18). Thus, in contrast to transgelin mRNA expression that falls during the reversal phase, the immunohistochemistry results indicated that the tissue expression of transgelin protein was sustained.

Table 4: Analysis of genes upregulated specifically in the injury cohort

A

Functional Annotation	Gene Count	%	p-value	Benjamini-Hochberg
Signalling	46	59.7	5.30E-18	6.40E-16
Extracellular matrix	12	15.6	1.50E-12	8.90E-11
Secreted	24	31.2	5.70E-12	2.30E-10
Disulfide bond	31	40.3	7.50E-11	2.30E-09
Glycoprotein	30	39	9.40E-10	2.30E-08
Collagen	8	10.4	2.60E-09	5.30E-08

B

Pathway	Gene Count	%	p-value	Benjamini-Hochberg
ECM-receptor interaction	9	11.7	1.00E-08	7.70E-07
Protein digestion and absorption	8	10.4	2.20E-07	8.30E-06
PI3K-Akt signaling pathway	12	15.6	5.20E-07	1.30E-05

Table 4. List of (A) functional annotation categories and (B) pathways which are most significantly overrepresented amongst genes that are upregulated specifically in the injury cohort compared to control and reversal cohorts using the DAVID and KEGG databases. In both lists extracellular matrix genes are prominently represented. In (B) only pathways with $p<0.05$ were retained and pathways that were related to infections (e.g. Amoebiasis) were removed since they were not of interest in the current study.

Figure 16: Collagen I and transgelin gene expression

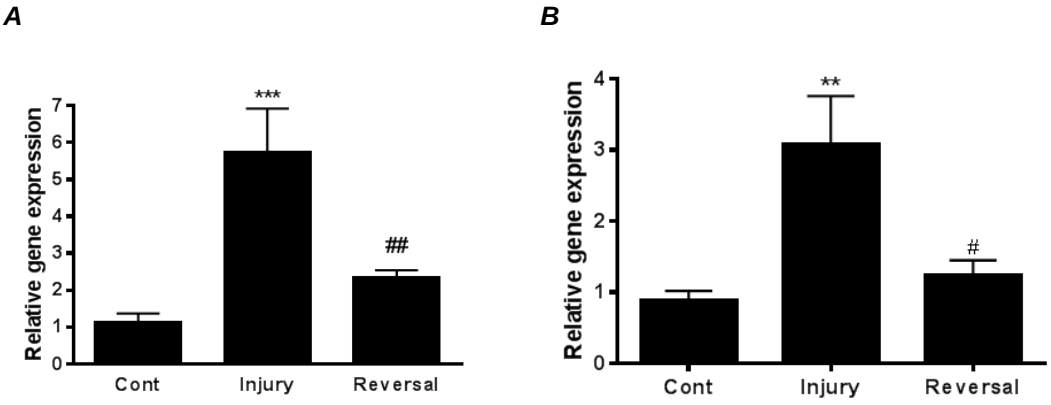

Figure 16. Relative gene expression of (A) alpha-1 chain of type I collagen that is a key component of the extracellular matrix and (B) transgelin that is an established marker for myofibroblasts Both genes validate the microarray results as they are significantly upregulated specifically in the injury cohort. Data is presented as mean±SEM. n=6 for all groups. **P < 0.01 and ***P < 0.001 vs controls; # P < 0.05 and ## P < 0.01 vs injury cohort.

Figure 17: Immunohistochemial staining and quantification of glomerular transgelin expression

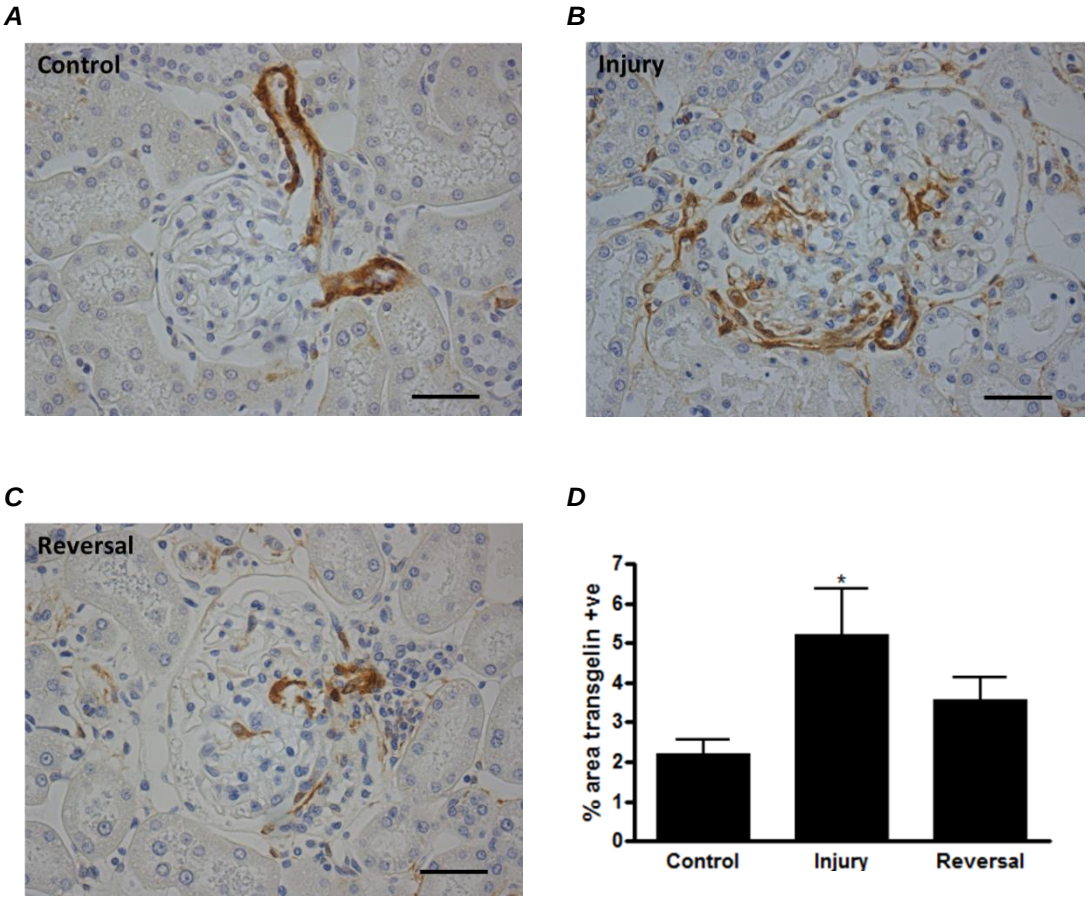

Figure 17. (A)-(C) Representative images of transgelin immunohistochemistry and (D) quantification of the area staining positive for transgelin in the glomerular compartment. Transgelin expression is increased in the injury cohort compared to controls while in the reversal (n=9) group transgelin expression is not significantly different from either the injury (n=10) or the control (n=6) groups. Data is presented as mean±SEM. Scale bars represent 50μM. *p<0.05 vs control.

Figure 18: Immunohistochemial staining and quantification of tubulointerstitial transgelin expression

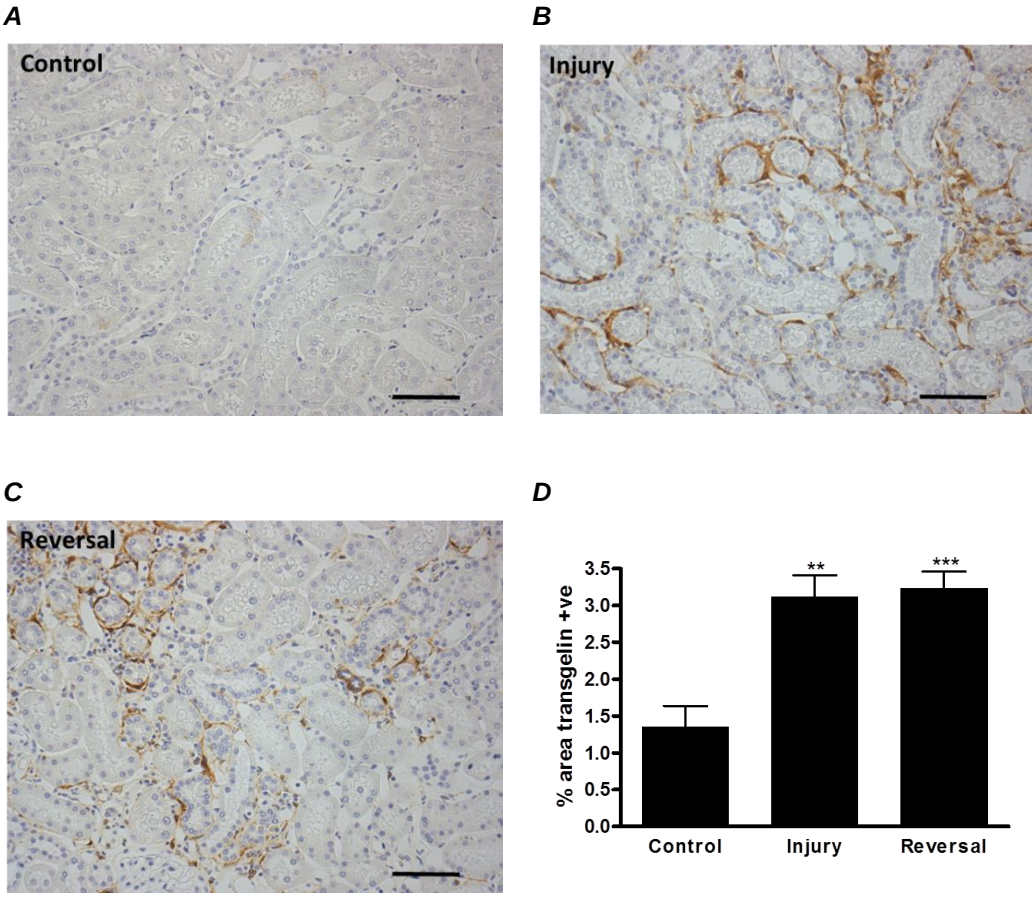

Figure 18. (A)-(C) Representative images of transgelin immunohistochemistry and (D) quantification of the area staining positive for transgelin in the tubulointerstitial compartment. There is significantly increased expression of transgelin in the injury (n=10) and reversal (n=9) cohorts compared to control (n=6). Data is presented as mean±SEM. Scale bars represent 100μM. **p<0.01 and ***p<0.001 vs control.

3.1.4 Genes upregulated during the injury and reversal phase

Amongst the 677 genes that were upregulated after 28 weeks of induced hypertension and hyperglycaemia, the expression of 314 genes either increased further or fell by <20% of peak values following 8 weeks of tight blood glucose and blood pressure control (Appendix). Analysis of the gene list by DAVID suggested that there was a significant over-representation of genes implicated in the annotation categories of innate and adaptive immunity as well as degradation of ECM. This was reflected by pathway analysis (Table 5). Consistent with the microarray data, real-time PCR confirmed that there was increased expression of the Foxp3 gene, a marker of regulatory T-cells (Tregs) in both the injury and reversal groups compared with controls. Aggregates of B-cells were also present during both injury and reversal and were typically located adjacent to blood vessels and associated with T-cells (Figure 19). An infiltration of $ED1^+$ macrophages was observed in the tubulointerstitium in both the injury and reversal cohorts, however there was no significant change in glomerular macrophage count (Figure 20). Immunostaining for inducible nitric oxide synthase (iNOS) and mannose receptor (MR) provided evidence supporting a switch in macrophage phenotype in the model. $iNOS^+$ cells that might represent classically activated macrophages were increased in the injury group (Figure 21), whereas MR^+ cells that might represent alternatively activated macrophages were identified in both the injury and reversal cohorts (Figure 22).

Table 5: Functional annotation and pathway analysis of upregulated genes during injury and reversal phase

A

Functional Annotation	Gene Count	%	p-value	Benjamini-Hochberg
Immunity	14	5	1.40E-05	2.80E-03
Signalling	69	24.5	4.60E-05	4.70E-03
Disulfide bond	52	18.4	5.20E-05	3.50E-03
Zymogen	10	3.5	1.60E-04	8.00E-03
Adaptive immunity	6	2.1	5.40E-04	2.20E-02
Phosphoprotein	78	27.7	5.70E-04	1.90E-02
Glycoprotein	48	17	1.50E-03	4.20E-02
Cytoplasm	50	17.7	5.10E-03	1.20E-01
Metalloprotease	6	2.1	1.10E-02	2.20E-01
Neurogenesis	7	2.5	1.70E-02	2.90E-01

B

Pathway	Gene Count	%	p-value	Benjamini-Hochberg
Primary immunodeficiency	8	2.8	5.50E-07	1.00E-04
Hematopoietic cell lineage	9	3.2	2.10E-05	1.90E-03
T cell receptor signalling pathway	10	3.5	2.30E-05	1.40E-03
Natural killer cell mediated cytotoxicity	9	3.2	7.70E-05	3.60E-03
Fc gamma R-mediated phagocytosis	8	2.8	2.20E-04	8.20E-03
Phagosome	9	3.2	7.60E-03	1.30E-01
NF-kappa B signaling pathway	6	2.1	9.40E-03	1.40E-01
Antigen processing and presentation	6	2.1	1.30E-02	1.70E-01
Cytokine-cytokine receptor interaction	8	2.8	3.70E-02	3.40E-01
Cell adhesion molecules (CAMs)	7	2.5	3.90E-02	3.20E-01

Table 5. List of (A) functional annotation categories and (B) pathways which are most significantly over-represented amongst genes that are upregulated in both the injury and the reversal cohort compared to control using DAVID and KEGG databases. Immunity and ECM degradation are annotation categories of interest while immunity pathways especially the T-cell signalling seems to be enriched with genes upregulated in injury and reversal groups. In (B) only pathways with $p>0.05$ were retained and for clarity pathways that were related to infections (e.g. Toxoplasmosis and Tuberculosis) were removed since they were not of interest in the current study.

Figure 19: Foxp3 gene expression and B cell localisation

A

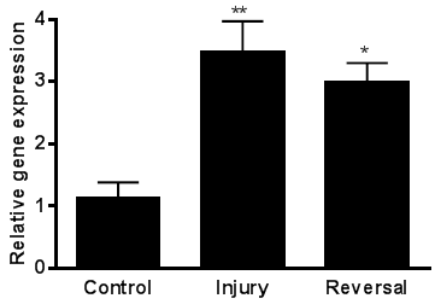

B

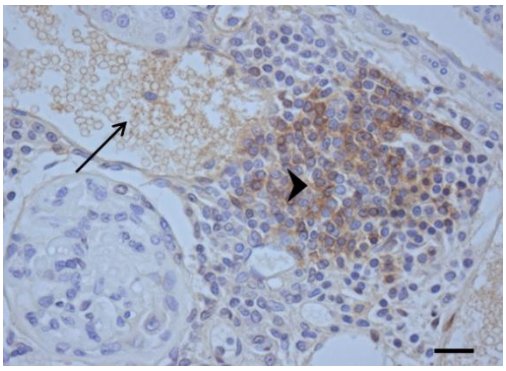

C

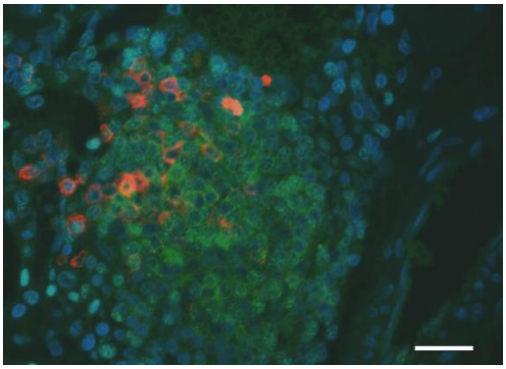

Figure 19. (A) Relative expression of the Foxp3 gene as a marker of regulatory T-cells is markedly increased in injury and reversal cohorts compared to controls, n=6 for all groups. Data is presented as mean±SEM, *p<0.05 and **p<0.01 vs controls. (B) and (C) Representative staining $CD45R^{+}$ cells in a reversal group animal demonstrates the persistence of B-cell aggregates (arrowhead in [B], green cells in [C]) in the renal cortex in the reversal cohort. B-cell aggregates are typically adjacent to blood vessels (B - arrowed) and associated with T-cells (C - red). In (C) CD45R coupled with Alexa Fluor 488 was used to stain B-cells and CD3 coupled with Alexa Fluor 568 to stain T-cells. Scale bars represent 25μM.

Figure 20: Quantification of ED-1 positive macrophage infiltration of glomeruli and the tubulointerstitium

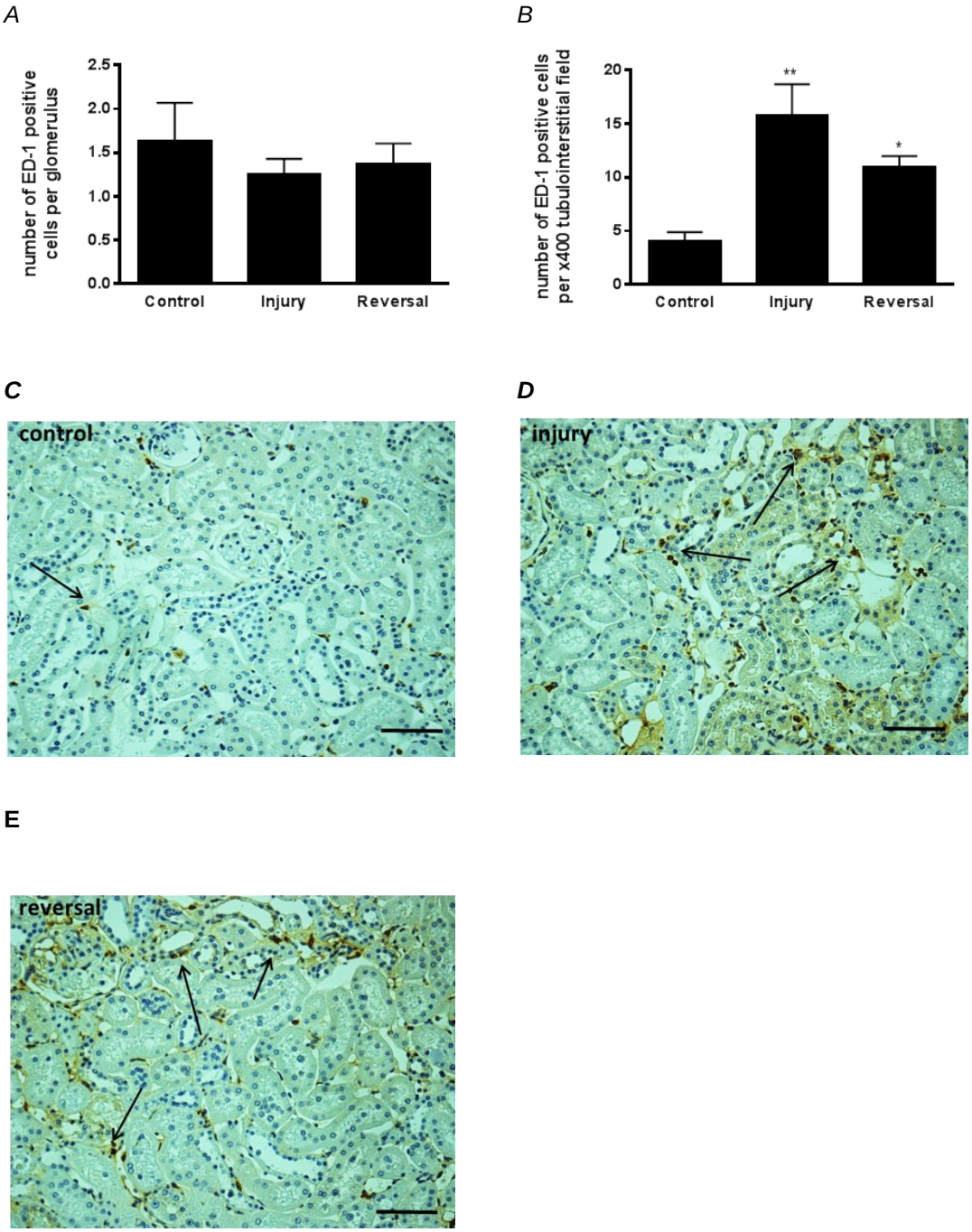

Figure 20. Tissue sections were stained for the macrophage marker ED-1 and the mean numbers of ED-1 positive cells (A) per glomerulus and (B) per x400 tubulointerstitial field were calculated and averaged for the control (n=6), injury (n=10) and reversal (n=9) groups. Representative images are depicted for each group with arrows indicating ED-1 positive cells in the tubulointerstitium. The scale bars represent 100 μM There was a significantly increased tubulointerstitial infiltration of ED-1 positive macrophages in the injury and reversal cohorts. Data is presented as mean±SEM. *$p<0.05$ and **$p<0.01$ vs controls.

Figure 21: Quantification of iNOS positive cell infiltration of the tubulointerstitium

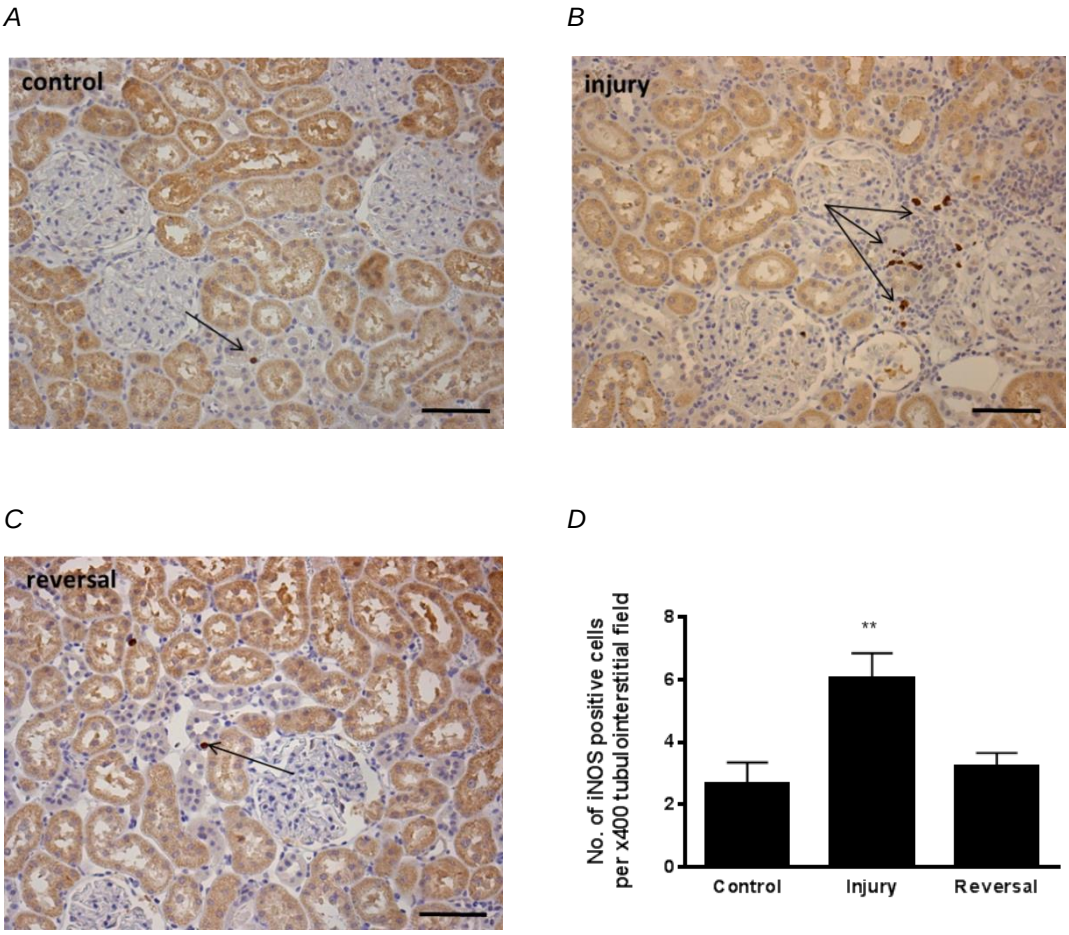

Figure 21. (A)-(C) Representative images of iNOS positive cells (arrows) for the control, injury and reversal groups. The scale bars represent 100 μM. (D) For each animal the mean number of iNOS +ve cells per x400 tubulointerstitial field was calculated and the mean (± SEM) averaged for the control (n=6), injury (n=10) and reversal (n=9) cohorts is provided. There was an increased infiltration of $iNOS^+$ cells in the injury group compared to control and reversal. ** $p<0.01$ vs all other groups.

Figure 22: Quantification of Mannose Receptor positive cell infiltration of the tubulointerstitium

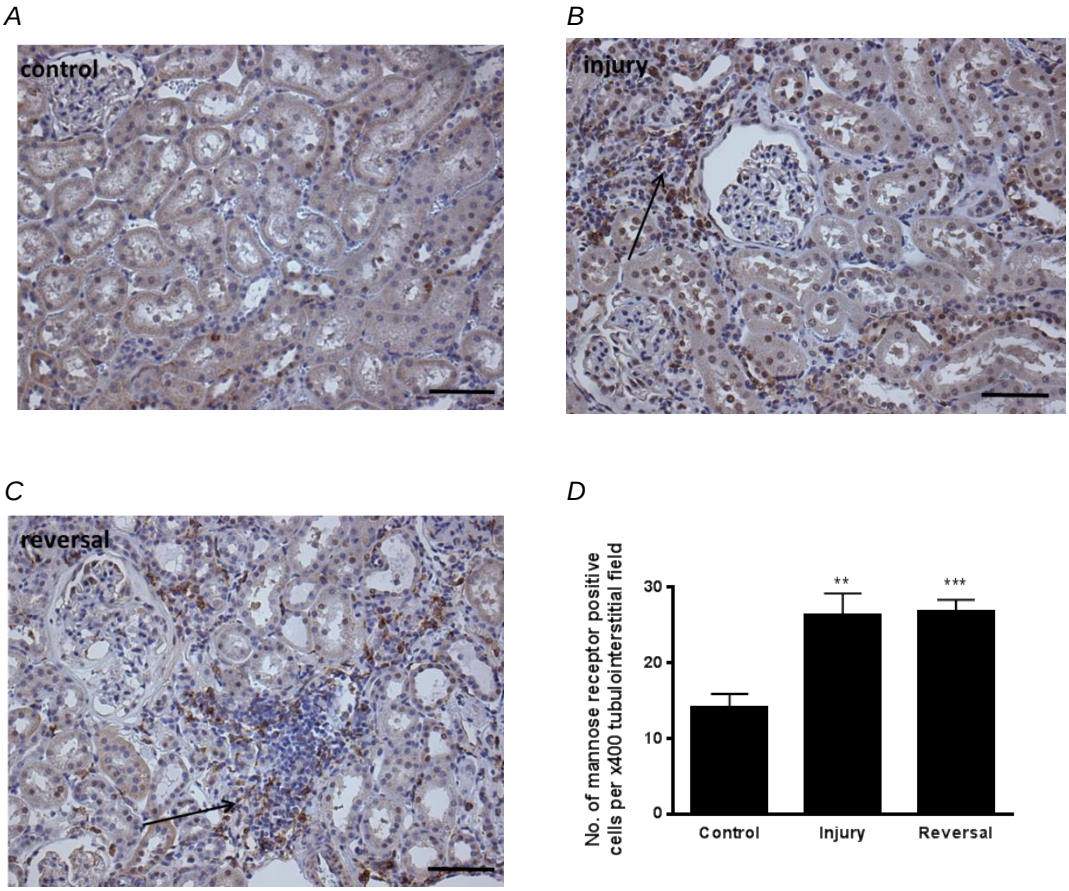

Figure 22. (A)-(C) Representative images of mannose receptor positive cells (arrows) for the control, injury and reversal groups. The scale bars represent 100 μM. (D) For each animal the mean number of mannose receptor +ve cells per x400 tubulointerstitial field was calculated and averaged. The mean (±SEM) for the control (n=6), injury (n=10) and reversal (n=9) cohorts is provided. There was an increased infiltration of mannose receptor +ve cells in the injury and reversal groups compared to controls. ** $p<0.01$ *** $p<0.001$ vs all other groups.

3.1.5 Regulation of factors for extracellular matrix degradation

Real-time PCR confirmed that the expression of multiple matrix metalloproteinase (MMP) genes was elevated in the injury group, with MMP-7 and MMP-12 being persistently elevated or further increased during reversal, whilst MMP-2 and MMP-14 levels returned towards control levels in the reversal group (Figure 23)

Despite the reduction in pro-fibrotic gene expression and persistent increase in the expression of some MMP genes in the reversal group, there was no reduction in glomerular or tubulointerstitial fibrosis evident (Table 3). It is recognised that MMP gene expression may not correlate with proteolytic activity due to the presence of endogenous inhibitors of enzyme activity. Hence, the biological activity of ECM degrading enzymes was assessed in each group. There was a paradoxical decrease in renal MMP activity in both injury and reversal groups as assessed by gelatinase and collagenase activity assays (Figure 24). Gene expression of tissue inhibitor of metalloproteinases (TIMP)-1 and to a lesser extent TIMP-2, were increased during injury, TIMP-3 expression was not significantly increased (Figure 25). TIMP-1 gene expression fell significantly in the reversal group but remained significantly higher than controls, whereas TIMP-2 expression in the reversal group was not different from either the control or injury groups. In contrast to the pattern of renal gene expression, urinary excretion of TIMP-1 protein increased significantly after 28 weeks of hypertension and hyperglycaemia and remained significantly elevated compared with controls despite 8 weeks of reversal of diabetes and hypertension. Expression of TIMP-1 protein in the renal cortex was persistently upregulated at a similar level in the injury and reversal groups (Figure 25).When TIMPs were physically separated from the MMPs using gel zymography, the gelatinase activity in both the injury and reversal cohorts tended to be greater than in controls and collagenase activity was significantly greater during reversal than in controls (Figure 26). This was in stark contrast to the reduced MMP activity in whole kidney lysates, when endogenous inhibitors may be complexed with the degradative enzymes.

Figure 23: Gene expression of metalloproteinases 2, 7, 12 and 14

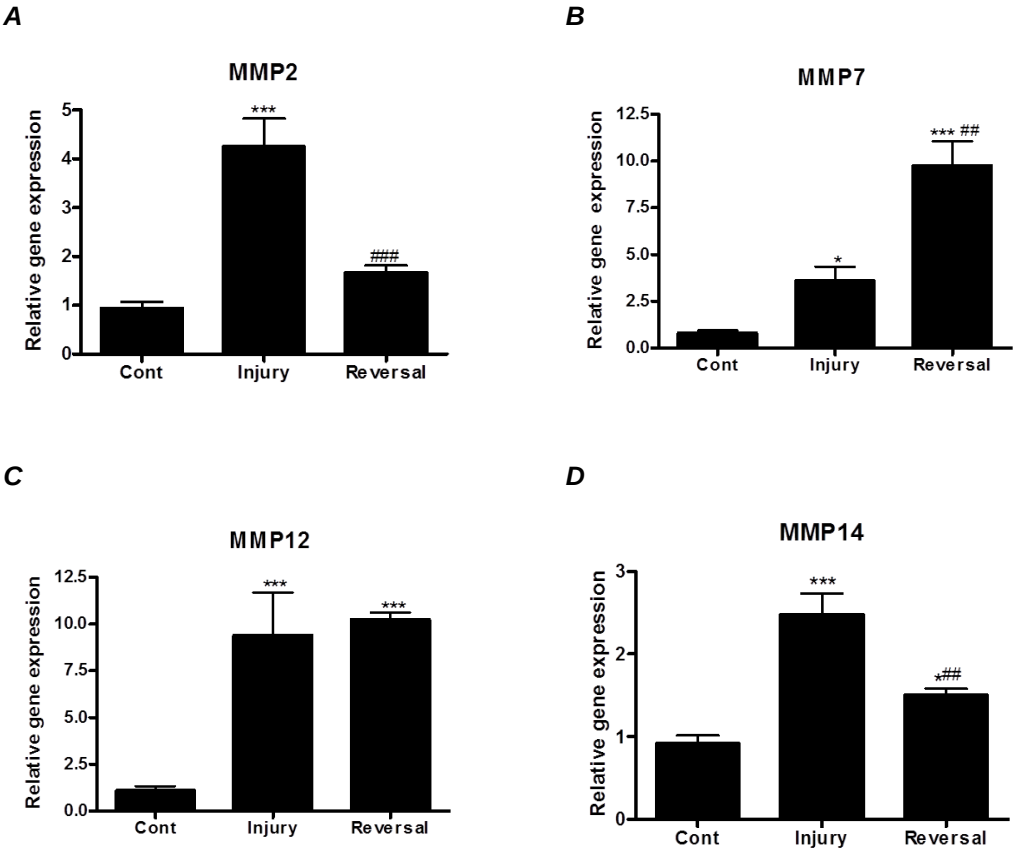

Figure 23. (A)-(D) The mean (±SEM) relative expression of the MMP-2, MMP-7, MMP-12 and MMP-14 genes was significantly increased in the injury and reversal groups compared to controls. n=6, * $p<0.05$, ** $p<0.01$ and *** $p<0.001$ vs control. ## $p<0.01$ and ### $p<0.001$ vs injury cohort.

Figure 24: Enzymatic activity of gelatinase and collagenase in renal cortical tissue homogenates

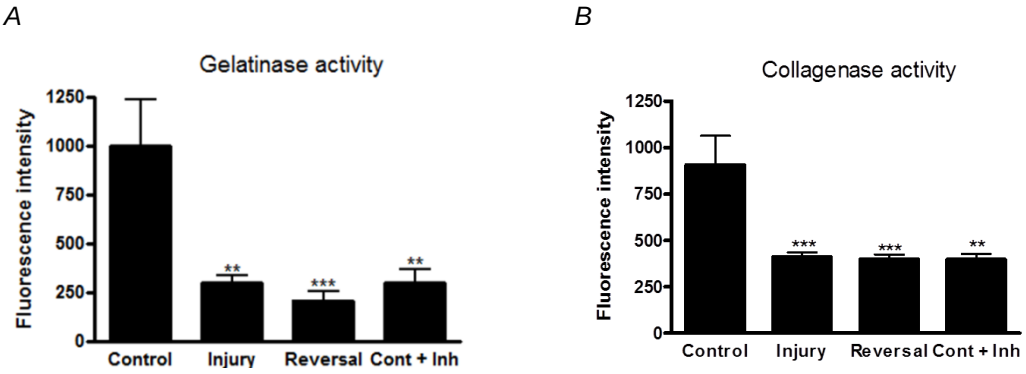

Figure 24. Mean (±SEM) activity in renal cortical kidney homogenates from the injury and reversal groups was markedly decreased for (A) Gelatinase and (B) Collagenase activity compared to control. For validation in every assay an enzymatic inhibitor was added. * $p<0.05$, ** $p<0.01$ and *** $p<0.001$ vs control, n=6 for all groups.

Figure 25: Molecular and biochemical expression of tissue inhibitor of metalloproteinases

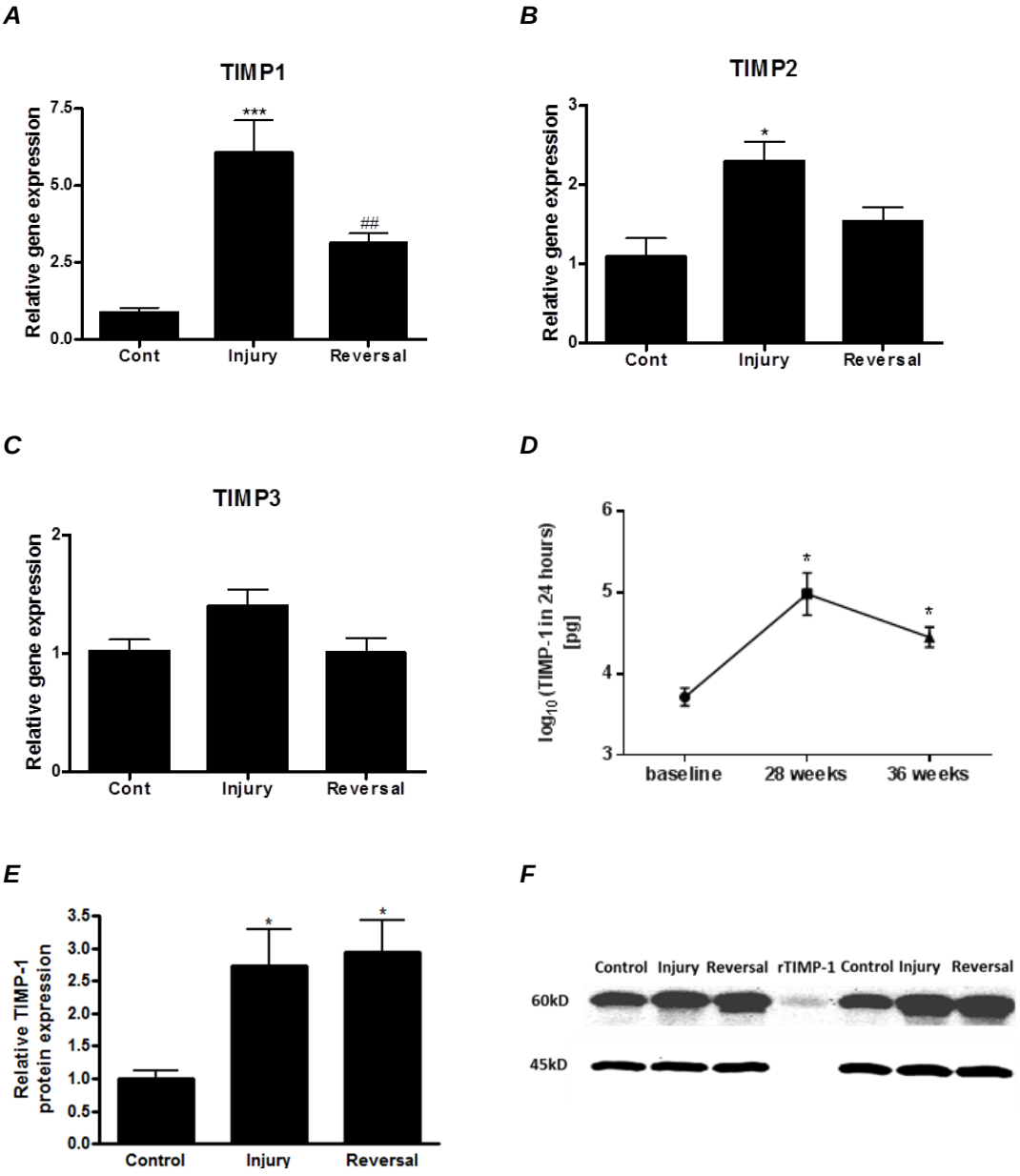

Figure 25. (A)-(C) Relative mean (±SEM) expression of (A) TIMP-1, (B) TIMP-2 but not (C) TIMP-3 genes was significantly increased in cortical tissue homogenates from the injury group but not the reversal group in comparison with controls (n=6 for all groups). (D) The mean (±SEM) 24 hour urinary TIMP-1 excretion in 5 animals from the reversal cohort was measured at 3 time points during the experiment. After 28 weeks of induced hypertension and hyperglycemia TIMP-1 excretion significantly increased compared to baseline and remained increased after 8 weeks of tight blood pressure and glycemic control. (E) Relative quantification of TIMP-1 protein by Western blotting with densitometry demonstrates increased expression in the renal cortex from injury and reversal animals compared to the controls (n=6 for all) Data is presented as mean±SEM. (F) Representative Western blot image with a positive control (rTIMP1, 60kDa. Beta-actin (45 kDa) was used for normalisation for protein loading. * $p<0.05$ vs control cohort.

Figure 26: Gelatinase and collagenase gel-zymography

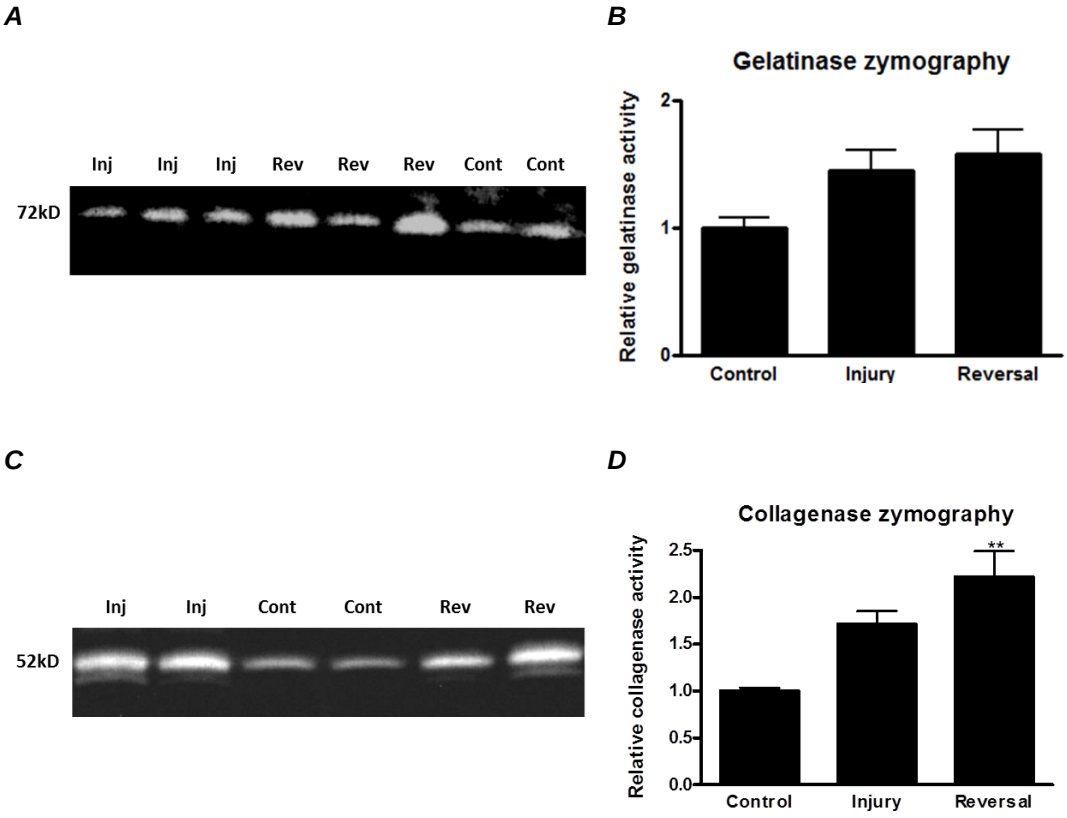

Figure 26. Representative images of gel-zymography demonstrating activity of (A) gelatinase (72kDa band) and (B) collagenase (52 kDa band) respectively in the control, injury and reversal groups. Gelatinase activity was non-significantly and collagenase was significantly increased in the reversal group. Data given are mean±SEM. n=6 for all groups. ** p<0.001

3.1.6 In situ zymography in a reversed UUO model

To assess the tissue localisation of MMP activity, a reversible unilateral ureteric obstruction (R-UUO) model(Hesketh, Vernon et al. 2014) was employed, as depicted schematically in Figure 27. Successful de-obstruction was confirmed visually by assessing the size and tension of the renal pelvis(Hesketh, Vernon et al. 2014).

Expression of type I collagen in the renal cortex by immunohistochemistry was markedly increased in the UUO group and remained elevated in the reversed UUO group compared to sham (Figure 28). Type III collagen expression was augmented in

the UUO group, and after reversal of UUO the expression of type III collagen remained markedly elevated but was not significantly different to either sham or UUO (Figure 29).

In situ zymography was performed on cryosections of kidneys from sham, UUO and reversed UUO groups. While there was homogenous tubulointerstitial enzymatic activity in sham animals, proteolytic activity for DQ-gelatine® in the UUO group and in the reversed UUO group fell dramatically resulting in focal islands of residual activity (Figure 30). When collagen I staining was performed alongside *in situ* zymography there was an inverse spatial correlation between collagen deposition and enzymatic activity as illustrated in Figure 31. When the expression of collagen I was compared with gelatinase activity from renal cortex lysates from each animal, an inverse correlation was apparent (Table 6). Similar results were observed with type III collagen and gelatinase activity, though this marginally failed to reach significance. Finally as some suggest that fibrosis develops more distinctly in polar renal regions than in the central region and resolves more easily in the latter(Cochrane, Kett et al. 2005), enzymatic activity analysis was divided into pictures taken from the polar and central region. Separate analysis confirmed a trend towards higher proteolytic activity in the central region of both UUO and R-UUO animals (Figure 32) compared to polar areas, however without reaching statistical significance mainly due to great variance of enzymatic activity in the central regions.

Figure 27: Experimental design of the reversal UUO study

A

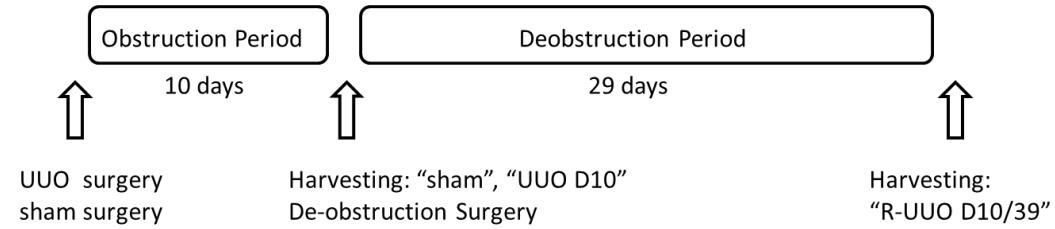

B

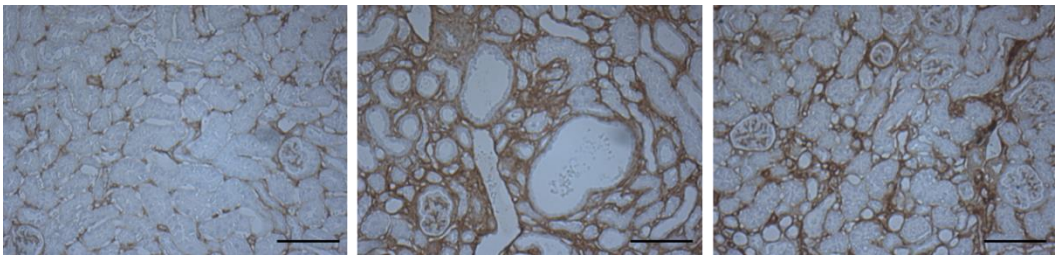

Figure 27. A) Illustration of experimental design for the reversal UUO study. Mice underwent unilateral ureteric obstruction (UUO) or sham surgery. After 10 days the UUO D10 and sham surgery groups were harvested whilst some mice underwent surgical reversal of UUO. The reversed UUO D10/39 group was harvested after 10 days of unilateral ureteric obstruction and another 29 days of de-obstruction. If not otherwise indicated numbers were n=6 for sham surgery controls and UUO D10 and n=3 for R-UUO D10/39. B) Representative pictures of collagen type III for control, UUO D10 and R-UUO 10/39 demonstrate many dilated tubules in the UUO D10 group but only very few in RUUO D10/39 group. Scale bars represent 200μM.

Figure 28: Immunohistochemical expression of Collagen I in the UUO reversal model

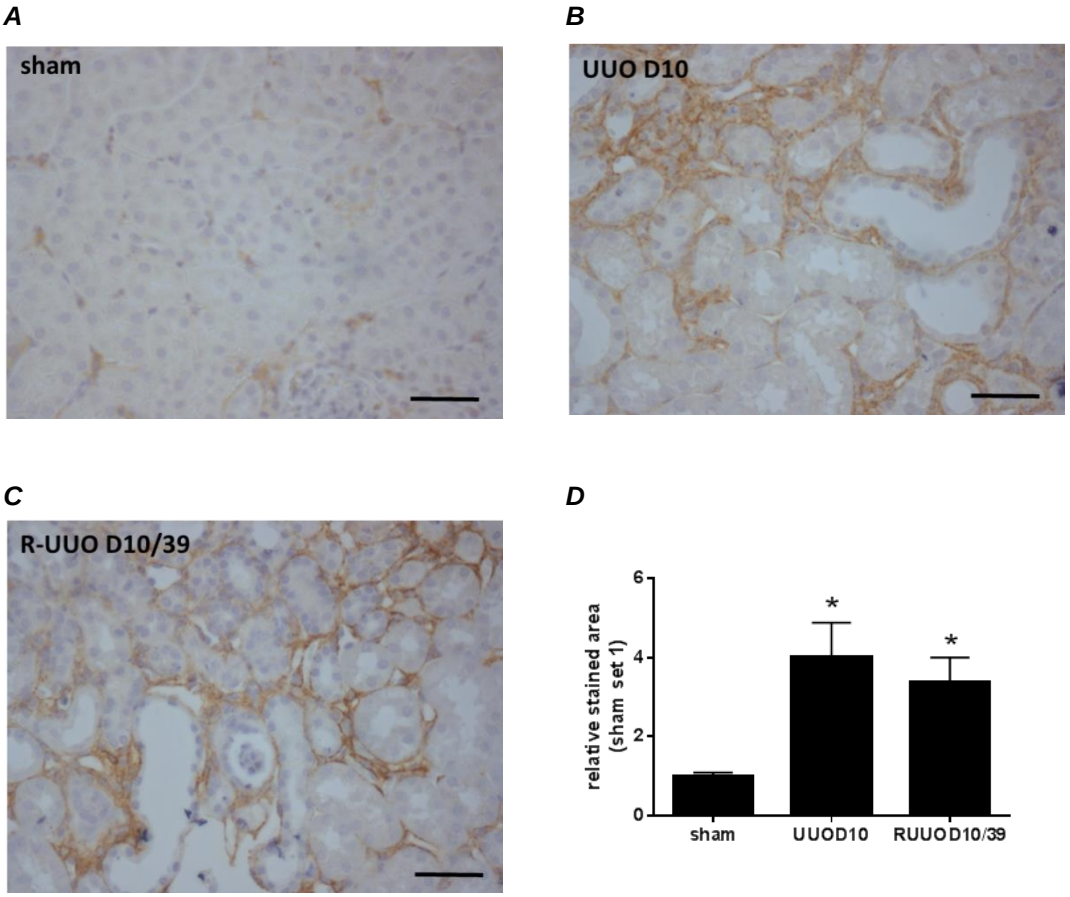

Figure 28. (A)-(C) Representative images of collagen type I immunohistochemistry and (D) quantification of mean (±SEM) area staining positive for collagen I in the tubulointerstitial compartment of each group. Mean (±SEM) collagen expression is increased in these two groups compared to control. Scale bars represent 100μM. *p<0.05 vs sham. n=6 for sham and UUO D10 and n=3 for R-UUO D10/39.

Figure 29: Immunohistochemical expression of Collagen III in the UUO reversal model

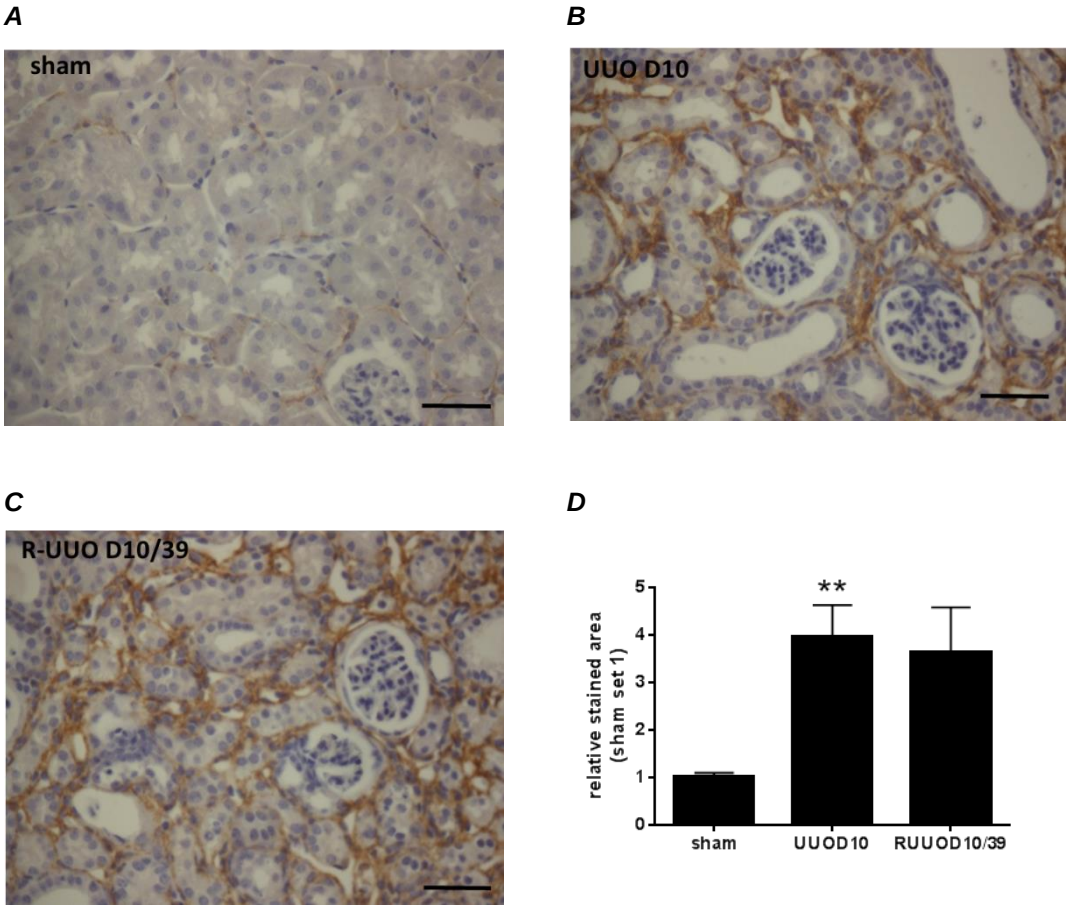

Figure 29. (A)-(C) Representative images of collagen type III immunohistochemistry and (D) quantification of the area staining positive for collagen III in the tubulointerstitial compartment of each group. There are many dilated tubules evident in the UUO D10 group but only few in RUUO D10/39. Mean (±SEM) collagen expression is increased in the UUO D10 group compared to control. Scale bars represent 100μM. **p<0.01 vs sham. n=6 for sham and UUO D10 and n=3 for R-UUO D10/39.

Figure 30: *In- situ* zymography in the UUO reversal model

A

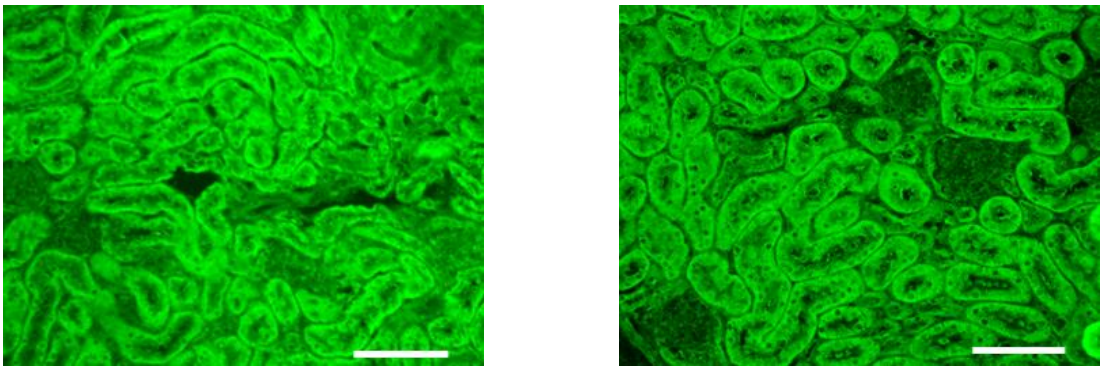

B

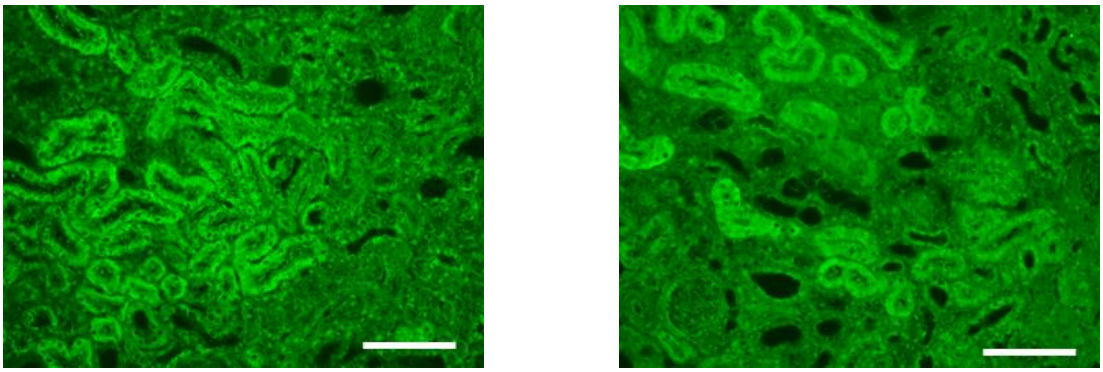

C

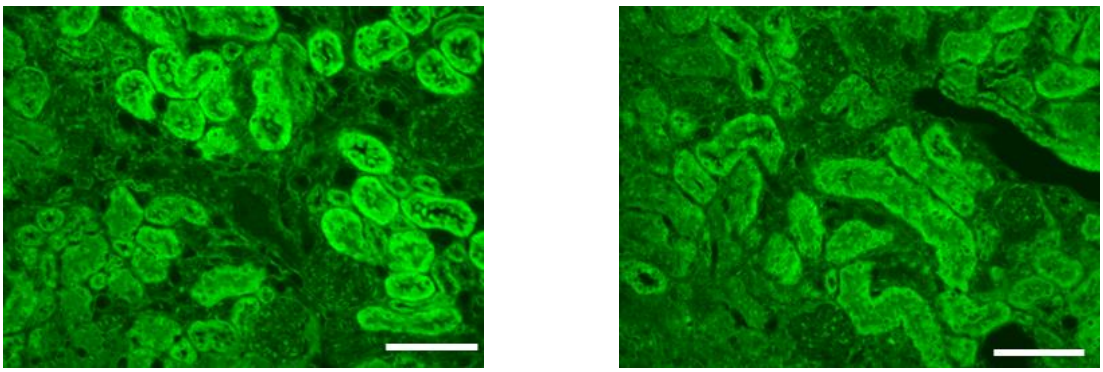

D

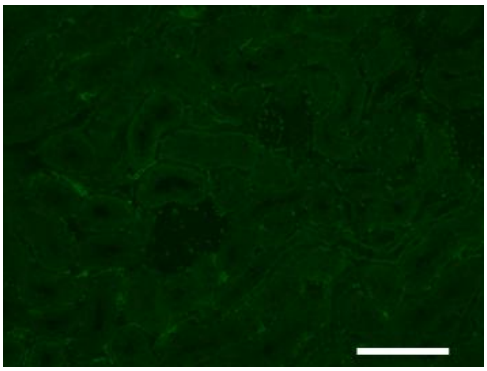

E

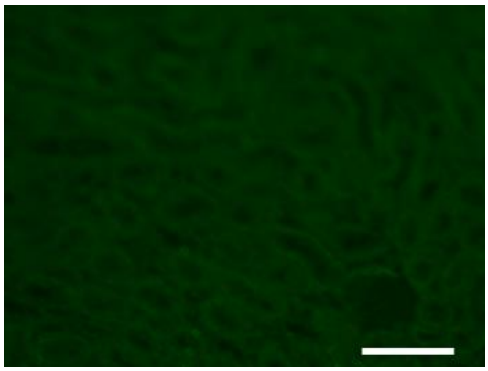

F

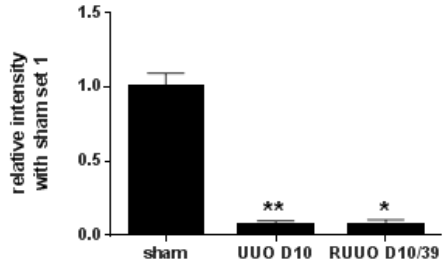

Figure 30. *In situ* zymography in murine kidneys. Representative pictures of *in situ* activity (bright green) utilizing a DQ-gelatine® substrate in kidneys from (A) sham animals, (B) animals after 10 days of renal obstruction (UUO D10) and (C) animals after an additional 28 days of following reversal of de-obstructed kidneysUUO (R-UUO D10/39). For comparison and validation one (D) sham animal section was treated without substrate whilst another tissue section from one (E) sham animal was incubated with a mixture comprising 20mM EDTA and 60mM 1,10 phenanthroline (inhibitors of MMP activity) added to the MMP substrate. (F) Quantification of proteolytic -activity by assessing the mean (±SEM) fluorescent intensities per section demonstrated a marked reduction of activity in the UUO D10 and RUUO D10/39 groups in comparison with control animals. n=6 for sham and UUO D10 and n=3 for R-UUO D10/39. Scale bars represent 200μM

Figure 31: *In situ* -zymography and collagen III immunostaining in the UUO model

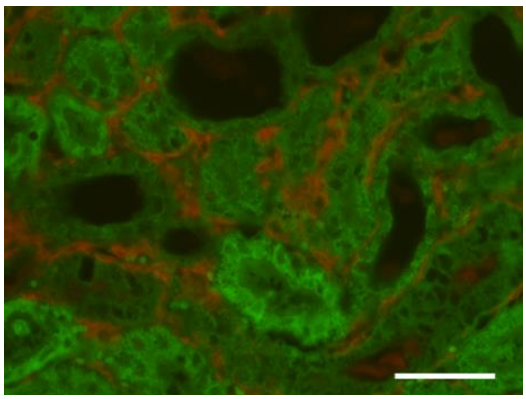

Figure 31. Representative photomicrograph of one section from a kidney obstructed for ten days that was first incubated with DQ-gelatine as substrate for zymography and then labelled for deposition of collagen type III (red) that was present in areas with little proteolytic activity (dim green). Scale bars represent 100μM.

Table 6: Correlation between collagen types I & III and proteolytic activity in the UUO reversal model

Spearman's rho	r	p
collagen I vs collagen III	0.81	0.011
collagen I vs proteolytic activity	-0.75	0.025
collagen III vs proteolytic activity	-0.66	0.059

Table 6. The extent of correlation between Collagen type I and III protein expression and proteolytic activity in animals from each group was compared using Spearman's Rank correlation. n=6 for sham and UUO D10 and n=3 for R-UUO D10/39.

Figure 32: *In -situe* Zymography ofin renal the polar and middle central regions of the obstructed or de-obstructed kidney using the UUO reversal model

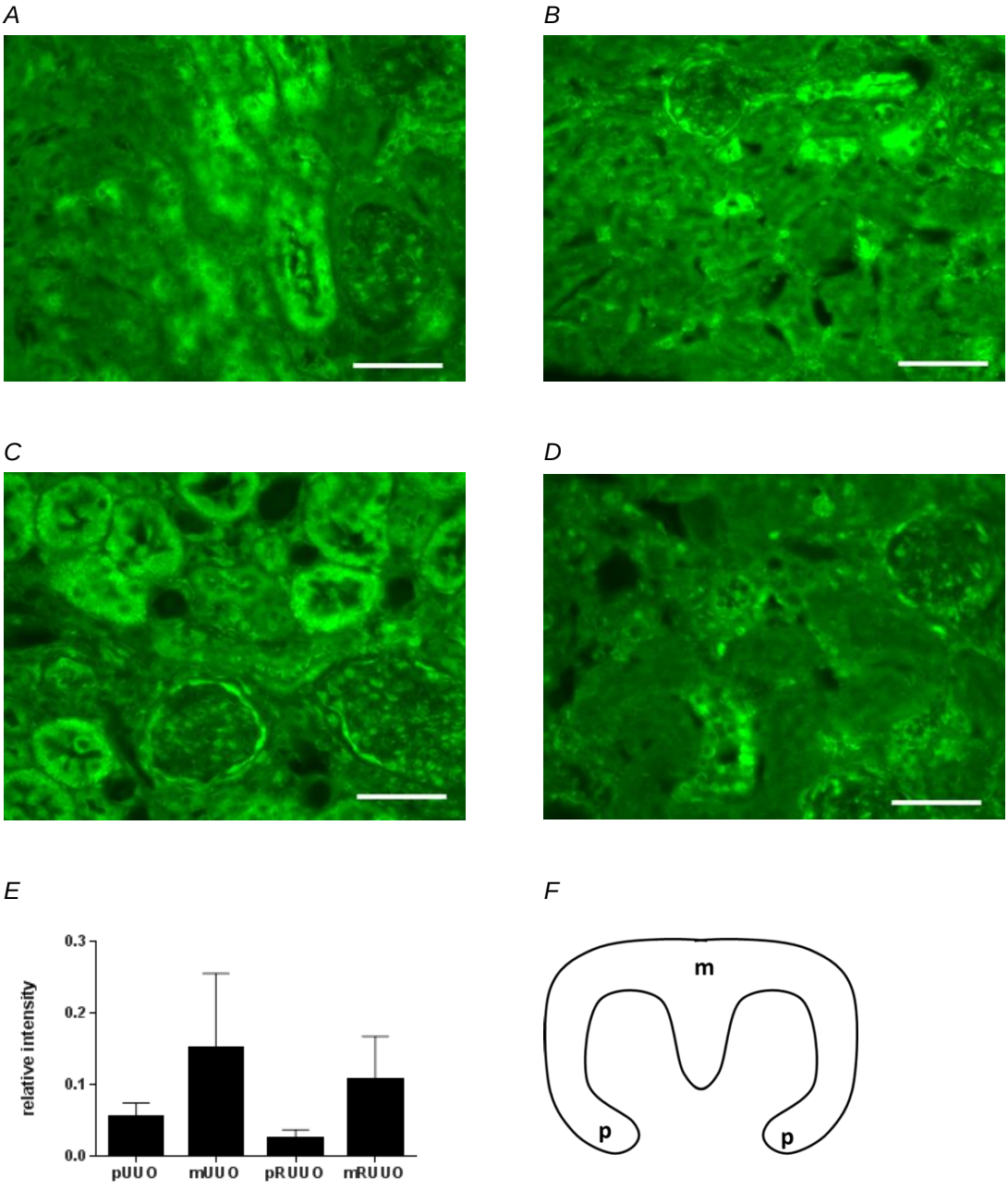

Figure 32. Representative images of in situ activity (bright green) utilizing a DQ-gelatine substrate in kidneys from UUO and reversed UUO animals in the (A,C) polar and (B,D) middle central region. (E) Quantification of proteolytic activity using fluorescent intensity from photomictographs from the respective region. There was a (non-significant) trend for more gelatinase activity in the central middle regions compared to the renal polar zones. (F) Schematic illustration of the localization of the “p” polar region and “m” middle central region. n=6 for UUOD10 and n=3 for R-UUO D10/39. Scale bars represent 100μM.

3.1.7 Discussion

Although regression of both albuminuria(Perkins, Ficociello et al. 2003) and renal fibrosis (Fioretto, Steffes et al. 1998, Fioretto, Sutherland et al. 2006) has been observed in patients with DN, the mechanisms that mediate repair in the diabetic kidney remain poorly understood. The current study represents an attempt to characterise the pathways that may promote regression of DN in a pathophysiologically relevant model.

Histopathological parameters of the Cyp1a1mRen2 rat reversal model

Previous studies in this model determined that tight control of the two major clinical risk factors for progression of DN, namely hyperglycaemia and hypertension, resulted in a marked reduction in albuminuria and renal hypertrophy. However, there was no evidence of resolution of established glomerulosclerosis or tubulointerstitial fibrosis, despite 8 weeks of relative normoglycaemia and normotension (Conway, Betz et al. 2014). There was an almost significant trend towards rarefaction of podocytes as an additional pathological marker of glomerular dysfunction that has been demonstrated in the Cyp1a1mRen2 model (Advani, Wiggins et al. 2011) and the leptin -deficient BTBR ob/ob mouse model (Pichaiwong, Hudkins et al. 2013). In the latter model of DN Pichaiwong et al. demonstrate not only functional (reduction of albuminuria) but also histopathological reversal of renal injury by supplementation of leptin. The difference in the degree of reversibility of histological features between these models might be related to differences in strain and species (BTBR mice vs Fischer rats) and to the pathophysiology of the model (leptin deficient type 2 diabetes vs streptozotocin-induced type 1 diabetes). The failure of

structural resolution in the current study might better reflect the time course of human disease, in that it takes ten years of normoglycaemia following pancreatic transplantation to achieve regression of glomerulosclerosis, with no improvement documented after five years (Fioretto, Steffes et al. 1998). Therefore one might speculate that a longer reversal period might not only have stopped progression of fibrosis but induced regression on a histological level.

Upregulation of "pro-fibrotic" genes specifically in the injury group

There were considerable alterations in genetic profile between the control, injury and reversal groups (Conway, Rennie et al. 2012, Conway, Betz et al. 2014). Prior to the study, it was hypothesized that the removal of injurious stimuli (hypertension and hyperglycaemia) might result in downregulation of genes promoting renal fibrosis and glomerulosclerosis. In support of this hypothesis, pathway analysis of the 85 genes that were specifically upregulated during injury, but which fell >50% towards control levels identified enrichment for functional categories and pathways implicated in fibrosis. Collagen is a major contributor to ECM and transgelin is a marker for myofibroblasts that play a key role in the production of ECM (Meran and Steadman 2011). The results of the pathway analysis together with the reduction in expression of col1a1 and transgelin genes in the reversal group suggest that normotension and normoglycaemia might be sufficient to switch off excess ECM production and halt progression of renal fibrosis. This is supported by the fact that there was no increase in glomerulosclerosis or tubulointerstitial fibrosis indices in the reversal compared with the injury group. However, transgelin was not reduced on a protein level in the kidneys from reversal animals. This might indicate that myofibroblasts remain in the kidney during the reversal phase. Kisseleva et al.

demonstrate that myofibroblasts remain in a quiescent state in the liver after pro-fibrotic stimuli had been removed (Kisseleva, Cong et al. 2012). However, this remains a highly speculative hypothesis in the current model, and it would necessitate future studies with a lineage tracing approach to be confident that this is indeed the case.

Upregulation of "immunity" genes in the injury and reversal groups

The majority of genes that were upregulated during injury remained upregulated in the reversal phase (Conway, Betz et al. 2014). It is possible that these were potentially reactive genes activated by the presence of renal structural damage rather than by external stimuli. Categorizing the genes using functional annotations and pathway analysis revealed that these genes were over-represented in pathways related to signalling, innate and adaptive immunity and phagocytosis, while pro-fibrotic pathways were not well represented. This suggests that there has been a switch away from ECM production towards degradation and that immune responses may be implicated.

Although the role of adaptive immunity in DN has not been fully understood yet, T- and B-cell infiltration has been documented in the kidneys of patients with DN as in the current experimental study (Cohen, Lindenmeyer et al. 2008). Regulatory T-cells have been attributed with anti-fibrotic effects (Gandolfo, Jang et al. 2009) and their marker foxp3 was upregulated in both injury and reversal groups. B-cells have been associated with a pro-fibrotic role e.g. via IL-6 or immunoglobulin production as the depletion of B-cells resulted in reduced fibrosis in liver fibrosis (Novobrantseva, Majeau et al. 2005) and renal allograft models (Tse, Johnston et al. 2015). Therefore

one might speculate that persistence of B-cells in the current model could be an explanation for the lack of reduction in fibrosis despite the removal of the damaging stimuli. Depleting B-cells during the injury and reversal phase might be a speculative but interesting treatment strategy in future studies.

While macrophages have been implicated in the pathogenesis of progressive DN (Chow, Nikolic-Paterson et al. 2004), it is now appreciated that a subset of 'reparative' macrophages exists, which are essential for resolution of fibrosis (Duffield, Forbes et al. 2005, Hadler-Olsen, Kanapathippillai et al. 2010). Specifically in the injury group the increase in $iNOS^+$ cells might indicate an infiltration of classically activated macrophages that might be involved in the pro-inflammatory process (Anders and Ryu 2011). Mannose receptor positive cells are increased in both the injury and reversal groups compared to control. This provides evidence for the presence of macrophages with anti-inflammatory properties (Anders and Ryu 2011). This is consistent with the transcriptomic changes observed in whole kidney cortex. In both injury and reversal groups there is upregulation of genes involved in matrix degradation (MMP12 see below), phagocytosis and lysosomal processing (Conway, Betz et al. 2014) and this may hint towards the presence of a reparative/fibrinolytic macrophage phenotype as has been observed in regression of liver fibrosis (Ramachandran, Pellicoro et al. 2012).

Upregulation of "fibrosis-degrading" genes and increased MMP activity is counteracted by TIMPs in the injury and reversal group

Matrix Metalloproteinases play an essential role in the breakdown of ECM though they have pleiotropic effects in DN (Xu, Xiao et al. 2014). In the current study,

microarray analysis identified that several MMP genes were upregulated during injury, and this was subsequently confirmed by real-time PCR for the gelatinase MMP2, the matrilysin MMP7, the macrophage specific MMP12 and the membrane specific MMP14. Review of other DN models shows conflicting reports about MMP expression (e.g. MMP2 (Xu, Xiao et al. 2014)) that could be caused by the use of different strains/species (e.g. MMP2 increased in Sprague-Dawley rat (McLennan, Kelly et al. 2002) but downregulated in Wistar rats (Sun, Wang et al. 2006) in STZ-induced DM) and diverse degrees of severity of DN (e.g. MMP7 upregulated in the current model of advanced DN but downregulated in rats following induction of diabetes alone (McLennan, Kelly et al. 2007)). Similarly, there are conflicting reports in human DN e.g. for MMP7 (McLennan, Kelly et al. 2007, Cohen, Lindenmeyer et al. 2008, Woroniecka, Park et al. 2011).

Though the expression of some upregulated MMPs reverted towards control levels in the reversal group, others stayed persistently elevated or increased even further. This prompted the hypothesis that in the reversal phase in which the progression of fibrosis was halted the scene was nevertheless set for degradation of ECM. However despite the increase in expression of multiple MMP genes there was failure of regression of ECM in the reversal group. This prompted further mechanistic investigations focusing on the biological activity of proteolytic enzymes.

Despite the upregulated MMP genes gelatinase and collagenase activity was markedly reduced in both the injury and reversal cohorts. This is in line with the study by Ahmed et al. who reported reduced MMP gelatinase and collagenase activity in a fibrotic rat kidney after a 5/6 nephrectomy (Ahmed, Haylor et al. 2007). It is also in line with earlier reports regarding reduced MMP-2 activity and increased

TIMP-2 expression in STZ-induced diabetic rodents (McLennan, Kelly et al. 2002, Sun, Wang et al. 2006, Takamiya, Fukami et al. 2013). The reduction in activity had been less marked in the latter two cited studies compared to the current study as the models utilized were associated with only modest DN (McLennan, Kelly et al. 2002, Sun, Wang et al. 2006).

In all of the aforementioned studies reduction in MMP activity was explained by increased expression of tissue-inhibitor-of-metalloproteinases (TIMP) 1 and/or 2. TIMPs are regarded to be the major inhibitors of MMPs and the TIMP/MMP balance regulates ECM degradation (Xu, Xiao et al. 2014). TIMP-1 and TIMP-2 have a similar mode of action by directly blocking MMPs and seem to compensate for each other (Kim, Oda et al. 2001). In the current study both TIMP-1 and -2 upregulation during injury was confirmed by rt-PCR with both declining in the reversal group but not to the level of controls. Unlike TIMP-1 and TIMP-2, TIMP-3 is associated with anti-fibrotic effects (Wang, Famulski et al. 2014) and remained unchanged throughout the experimental groups. In contrast to the gene expression pattern, there was no significant decline in urinary TIMP-1 excretion in the reversal phase compared to the injury phase. This was mirrored by similar TIMP-1 renal protein levels in the injury and reversal groups as assessed by western blotting. An increased level of TIMP-1/2 in DN rat kidney has been reported by others at both the gene expression and protein level (McLennan, Kelly et al. 2002, Sun, Wang et al. 2006, Thrailkill, Clay Bunn et al. 2009, Takamiya, Fukami et al. 2013), however this study for the first time demonstrates the gene-protein uncoupling after optimisation of blood pressure and glucose levels in DN. Gel zymography demonstrated that after physical separation from TIMP the activities of MMP-1 and MMP-2 were increased

in whole tissue homogenate in both the injury and reversal groups. The increased activity of MMP-2 in zymography is contradictory to the study by McLennan et al. who used a less severe rat DN model (induction of diabetes with STZ alone)(McLennan, Kelly et al. 2002), but in line with Takamiya et al. who used a mouse DN model(Takamiya, Fukami et al. 2013) and McKittrick et al. who demonstrate increased urinary MMP-2 and MMP-9 activity by using gel zymography in a rat DN model (McKittrick, Bogaert et al. 2011). In summary, these results demonstrate that it is necessary to assess renal expression of TIMP and MMP but also the degree of MMP activity to gain a fully functional picture of the dynamic degradation angle component in the ECM turn-over process.

TIMP upregulation is induced by the inflammatory and pro-fibrotic cytokines TGF-beta, IL-6, TNF-alpha and IL-4 (Khokha, Murthy et al. 2013). Moreover CTGF directly increases TIMP1 production in mesangial cells exposed to high glucose concentrations (McLennan, Wang et al. 2004). Intracellular regulation of TIMPs seems also to involve the pathways of protein kinase A, protein kinase C and MAPK (Li and Curry 2009). These factors could explain the upregulation of TIMP during the injury phase in the DM&HTN DN model. However, since inflammatory pathways are downregulated during reversal phase, alternative mechanisms may contribute to the persistent presence of TIMP.

TIMPs are bound to surface lipoprotein-related protein-1 at the cellular membrane followed by internalization and degradation. Blockade of this process could prolong bioactive half-life of TIMPs and significantly shift the balance of TIMP turnover (Yamamoto, Murphy et al. 2015). Recently Scilabra et al. reported that TIMP3 is

bound to a soluble form of lipoprotein-related protein-1 (sLRP-1) that prevents TIMP3 from endocytosis (Scilabra, Troeberg et al. 2013).

TIMP-1-v2 has been identified as an alternative splicing variant of TIMP-1 that might modify TIMP-1 expression in cancer cell lines (Obro, Lademann et al. 2008). A similar modification of TIMP1 might be present in renal cells.

Using the reversed UUO model for in-situ zymography

Having demonstrated that MMP activity is dependent on the amount of TIMP present, a logical next step would be to determine where in the kidney MMP activity and TIMP expression is observed. *In situ* zymography on kidney sections would be the method of choice to localise MMP activity *in vivo* and provide some additional mechanistic information. Firstly, it could confirm the *ex vivo* results from renal homogenates. Secondly, it would help to exactly locate focal areas of insufficient degradation (low MMP but high TIMP expression) enabling construction of an "activity map" in a renal tissue section. Thirdly, it can be utilized as a surrogate for TIMP expression since despite multiple attempts using several TIMP-1 antibodies, none worked in IHC. Similar problems have been reported by others (Ahmed, Haylor et al. 2007).

Unfortunately no cryosections or zinc fixed paraffin blocks (Hadler-Olsen, Kanapathippillai et al. 2010) were available from the current reversal model in which to perform *in situ* zymography. Since repeating the 38-weeks Cyp1a1mRen2 diabetic and hypertensive rat model was beyond the scope of the current study an alternative way of inducing a reversible stimulus for renal fibrosis was sought. A well-established (Hesketh, Vernon et al. 2014) model of reversible UUO was chosen.

Although the initiating stimulus for fibrosis is clearly different between the DN and UUO models, many of the downstream mechanisms converge to the final common pathways for renal fibrosis (Chevalier, Forbes et al. 2009) often accompanied by an inflammatory component.

Initially the model was planned to be performed on Fischer rats as utilised in the DN model (Conway, Rennie et al. 2012, Conway, Betz et al. 2014). However, the surgery procedure was associated with a high mortality rate. So after consultation with our local veterinarian the strain was changed to Sprague-Dawley rats. However, still some animals unexpectedly died after surgery. Therefore, it was hypothesized that the susceptibility of death could be species related and future studies should be carried out in mice.

The extension of the obstruction period to ten days was employed to ensure that a significant level of tubular fibrosis had developed before reversal was undertaken. Though de-obstruction surgery was successful as indicated by a decompressed renal pelvis and small slightly atrophic kidney, there was no measureable reduction of collagen expression by IHC. There are conflicting reports about the presence of resolution of fibrosis after a prolonged time of de-obstruction (Ito, Chen et al. 2004, Cochrane, Kett et al. 2005, Tapmeier, Brown et al. 2008). Differences in reversibility might be related to species or surgical technique (Hesketh, Vernon et al. 2014). The fact that the removal of the damaging stimulus did not result in reduction of fibrosis might increase comparability to the DN model.

In accordance with other studies in normal kidneys from sham animals there was a constant homogenous gelatinase activity in the tubular epithelium contrasted by

lower focal activity in the glomeruli (Ahmed, Haylor et al. 2007, Hadler-Olsen, Kanapathippillai et al. 2010). During obstruction and after de-obstruction gelatinase activity was dramatically reduced consistent with a marked expression of collagen. These findings are in line with Ahmed et al. who studied MMP activity by *in situ* zymography in a fibrotic 5/6 nephrectomy model (Ahmed, Haylor et al. 2007). The positive correlation between collagen deposition and reduced gelatinase activity supports the hypothesis that reduced MMP activity is responsible for the persistence of excess ECM. Since other studies demonstrate elevated MMP and TIMP expression and increased MMP activity following separation of the MMP and TIMP by gel zymography in UUO models (Iimura, Takahashi et al. 2004, Wang, Famulski et al. 2014) one might hypothesize that in the reversal phases of both the DN and UUO models, the blockade of MMP bioactivity by TIMP might be a key common pathophysiological pathway of sustained renal fibrosis.

We observed (unpublished) when performing the R-UUO model that some regions within the kidney progressed to fibrosis at different speed depending on the localization: Polar "regions" of the kidney seemed to undergo accelerated fibrosis in contrast to the "middle" or central region of the kidney. We hypothesized that the reduced blood flow in polar regions might be one possible explanation. Interestingly, a similar effect was reported by Cochrane et al. in their R-UUO model with the polar regions exhibiting excess ECM deposition while the middle regions had only subtle signs of renal damage (Cochrane, Kett et al. 2005). In the present study there was a non-significant tendency for increased gelatinase activity in the middle region compared to the polar region in both the obstructed and the de-obstructed kidney.

While this interesting observation requires further pathophysiological investigations in future UUO studies, it underlines the tight association between reduced gelatinase activity and renal fibrosis/collagen deposition and helps to validate the methodology of *in situ* zymography in the UUO model.

It remains

Limitations

The study has some limitations. Firstly, in the model both the hyperglycaemia and hypertension were reversed at the same time, so the individual extent to which each component contributed to the findings in the reversal group cannot be determined. While proteinuria was reduced during reversal, it did not return to baseline and the resultant low-grade tubular injury could have caused some of the gene/protein expression changes during the reversal phase. The UUO model typically does not cause sustained glomerular damage in contrast to the DN model (Conway, Rennie et al. 2012, Hesketh, Vernon et al. 2014). Therefore comparability of *in situ* zymography results between the two models is restricted to findings in the tubular compartment. Finally the description of regulation of MMPs and TIMPs and their associations allows only speculative hypotheses about pathological functions. However, the aim of the current study was to demonstrate that not only the induction of injurious stimuli but also their reversal might have an effect on TIMP/MMP regulation and ECM homeostasis. Since the model has broad congruency with human DN (Conway, Rennie et al. 2012) it may explain why the resolution of established human DN fibrosis takes so long even under strict normotension and normoglycemia (Fioretto, Steffes et al. 1998).

Finally, as indicated before, the technical microarray analysis is not part of this work. Nevertheless, since flaws in the technical performance can affect the results that were used in this work, some potential pitfalls will be mentioned briefly.

It is important to assure the quality of the extracted RNA by using a bioanalyzer (Agilent). Problems during the steps cDNA synthesis, amplification, labelling and hybridization can be detected by spiking with control material at different steps. Imaging artefacts during the staining process by air bubbles or solution impurities in the microarray cartridge can be detected by visual heat map inspection.

Another disadvantage that is hard to account for is that the thousands of individual genes were analysed under the same conditions though since molecular properties differ between RNA/DNA fragments and might require different conditions to achieve optimal results (Jaksik, Iwanaszko et al. 2015).

For normalization of the data the assumption has to be made that in general the total level of mRNA does not vary significantly among samples independent from the experimental conditions.

A specific threshold for fold change has to be chosen to separate pathophysiological potential relevant differences from biological and technical variation. The chosen threshold of 0.5 resulted in an acceptable power of 0.8 for detection as described in the “Materials and Methods” section. However relevant gene expression changes that fall beyond the chosen threshold are less likely to be detected.

3.1.8 Summary

Although Fioretto et. al. demonstrated 20 years ago that histological DN lesions are reversible little is known so far about the mechanisms that induce repair (Mauer and Fioretto 2013). Conway et al. demonstrated in the novel Cyp1a1mRen2 DN model that genes upregulated in DN enriched pathways associated with injury as well as with healing/repair (Conway, Rennie et al. 2012). From this, one might conclude that in DN pathologic stimuli activate inflammatory/injurious pathways resulting in tissue damage that in turn activates repair mechanisms. The analysis of the data presented suggests that activated injurious and reparative pathways co-exist in the DN model (Figure 33). Of interest, similar genetic patterns have been observed in human DN (Woroniecka, Park et al. 2011) (Ju, Nair et al. 2015). However, there is a caveat. Whether a gene has an injurious or a repair/protective function can depend on the species and the model chosen. This is reflected by conflicting studies claiming injurious or protective characteristics of some MMPs (e.g. MMP2 and 7) (Xu, Xiao et al. 2014). Targeting genes e.g. by knock-out may provide an ultimate answer about gene function, though compensatory mechanisms (e.g. TIMP-1 for TIMP-2 and vice-versa) can make interpretation difficult (Kim, Oda et al. 2001). Individual knock-out of the multitude of genes involved in DN might be a time-consuming task. The Cyp1a1mRen2 reversal DN model provides a general approach to dissect the involved genes and pathways. The removal of damaging stimuli might selectively silence injurious pathways whilst reparative pathways remain activated due to the persistent damaged tissue (Figure 33).

In this work this concept is epitomized in two pathological pathways of DN. First, there is the role of immune cells: During the injury phase, both M1 and M2

macrophage numbers are increased in the kidney, but during reversal phase only M2 macrophages remain increased. This underlines the assumed role of M2 macrophages in ECM regulation (Anders and Ryu 2011) (Duffield 2014). The persistent upregulation of T-reg cells during injury and reversal phase might indicate a reparative role for this lymphocyte subpopulation.

The second exemplary pathway is ECM regulation. In this chapter it was demonstrated that in a reversal Cyp1a1mRen2 rat model of DN the normalization of hypertension and hyperglycaemia seems to halt ECM production, although fibroblasts might persist in a quiescent state. However, the reduction of ECM is hampered by reduced MMP activity in contrast to the elevated MMP gene expression. The presence of TIMP-1 in both the injury and reversal groups might effectively block MMP activity (Figure 33). *In situ* zymography supports the spatial association between increased collagen deposition and reduced MMP activity. The increase in MMP activity following separation of TIMP and MMPs via gel electrophoresis suggests that strategies to block TIMP-MMP interaction in the diabetic kidney may increase MMP activity, which may facilitate regression of fibrosis. This hypothesis merits further investigation in future studies.

Figure 33: Hypothesized genetic regulation in the Cyp1a1mRen2 rat DN reversal model

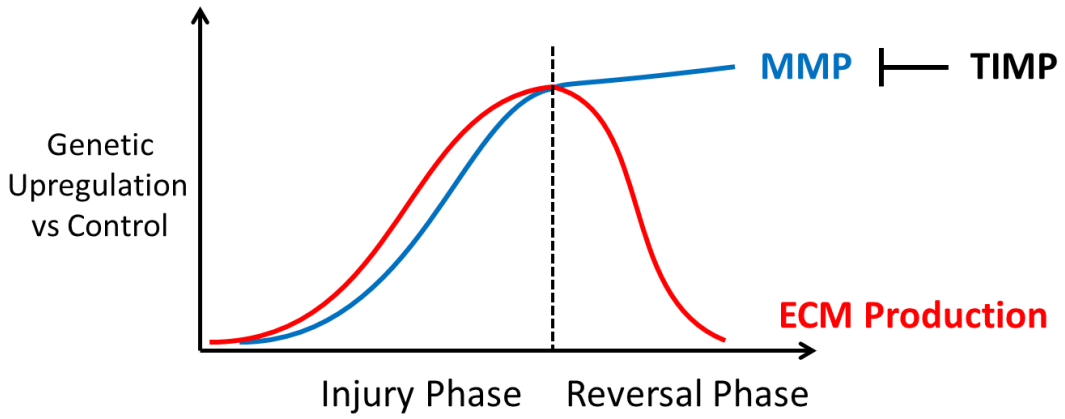

Figure 33. Schematic hypothesiszed illustration of genetic regulation in the Cyp1a1mRen2 rat DN reversal model and hypothesized pathological effects. During the injury phase characterized by hypertension and hyperglycaemia for 28 weeks the genes that are associated with both ECM production (red, e.g. collagens) and degradation (blue, e.g. MMPs) are up-regulated. Eight weeks of the reversal phase with normotension and normoglycaemia are sufficient to switch off the ECM production genes completely. ECM degradation genes remain up-regulated but MMP activity is effectively blocked by TIMP.

In conclusion, the Cyp1a1mRen2 reversal DN model supports the concept of a co-existence of injurious and reparative mechanisms in DN. The removal of injurious stimuli by inducing normotension and normoglycaemia (that is also the therapeutic target in human DN) silences injury pathways whilst the reparative ones persist - supposedly until a certain level of recovery is achieved what can last in humans more than 10 years.

3.2 Urinary peptidomics

3.2.1 Introduction

Previous studies in the Cyp1a1mRen2 rat model of DN confirmed that the model exhibited biochemical, pathological and transcriptomic changes consistent with human DN (Conway, Rennie et al. 2012). In the last chapter functional and pathway analysis of differentially expressed genes provided a deeper insight into the molecular basis of renal injury and repair processes within the model. The protein products of genes that were significantly altered during the injury and reversal phase could, if excreted into urine, be a potential source for non-invasive biomarkers that are informative regarding pathological renal processes. Albuminuria, the hitherto established biomarker in DN, is serum derived and more an indicator of glomerular leakage as a consequence of renal injury than a genuine marker of renal damage. Urine specimens from the rodent model and from a small human cohort of patients with DN were analysed by a non-biased so-called "shotgun" peptidomic approach to identify urinary markers that reflected the characteristic transcriptomic signature in DN.

3.2.2 Peptidomics in rat urine

Electrophoresis of rat urine

Preliminary experiments were performed to assess the quantity and nature of the proteins present in the urine of control rats and those with induced diabetes and hypertension (DM+HTN) for 28 weeks. Figure 1 demonstrates the pattern of proteins found in the urine from control rats and DM+HTN rats following separation by

electrophoresis with subsequent Coomassie Blue staining of the gel. While in control animals the dilution of the urine enabled clear protein separation, in DM+HTN rodents there was a broad band of approximately 66kDa, most likely albumin, which hampered further separation. This effect persisted even after serial dilutions. An overnight dialysis of the urine to remove the high salt content in urine only minimally improved separation of the proteins. Passing the urine through an albumin-specific immunoabsorption column did deplete the albumin from the sample, but also resulted in significant reduction of all other proteins (Figure 34).

Figure 34: Electrophoresis of urinary proteins from samples of the Cyp1a1mRen2 DN model

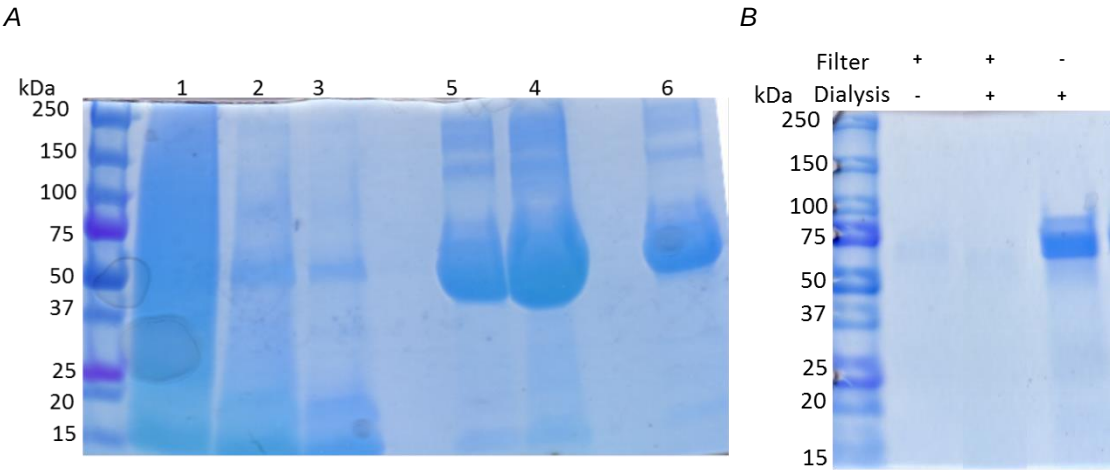

Figure 34. Electrophoresis of rat urine from control and DM+HTN samples and staining with Coomassie blue. A) Dilution of control urine samples resulted in a clear separation of bands, whereas resolution of bands in the DM+HTN samples was hampered by a large band at approximately 66kD (most likely albumin). Control sample (1) undiluted, (2) diluted 1:1, (3) diluted 1:5, and DM+HTN sample (4) undiluted, (5) diluted 1:1 , (6) diluted 1:5 . B) After albumin immunoabsorption filtering there were no clear protein bands visible. Pre-dialysis treatment of samples resulted in sharper but not more separated bands.

Peptidomic analysis from filtered rat urine

From the pilot studies described above, it became quickly apparent that the large amount of albumin specifically in the DM+HTN animals would swamp the signal from other proteins during mass spectrometry and hence another approach was necessary. The approach chosen was to focus on the peptidome and low molecular weight proteins after removing all high molecular weight proteins including albumin by passing the urine through a 10kD molecular weight filter.

The sample preparation protocol was designed with help from Dr Andrew Cronshaw, Proteomics Facility, School of Biological Sciences, University of Edinburgh and included several concentration steps after removal of most high molecular weight proteins by passing the urine through a 10kD molecular weight filter (Figure 35). The prepared samples were analysed by using MALDI-TOF mass spectrometry, and many peaks could be attributed to peptides. Using LC-MS/MS resulted in the detection of 10 times more peptides and was considered the preferred methodology.

Figure 35: Sample preparation scheme and comparison between MALDI-TOF/ and LC-MS/MS

A

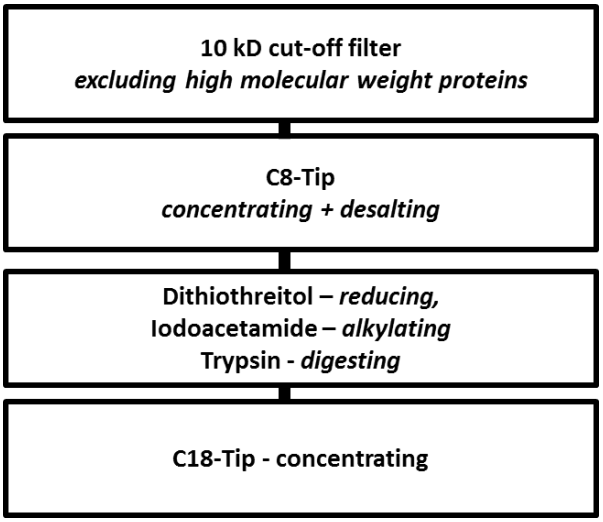

B

	MALDI-TOF	LC-MS/MS
control	**45**	**320**
injury	**85**	**954**

C

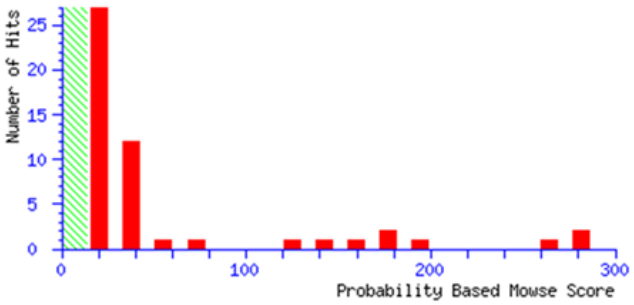

Figure 35. A) Schematic experimental protocol for isolation of low molecular weight proteins and peptides from whole urine. Italics indicate the rationale behind each stage in the process B) In one control and one DM+HTN, rat urinary analysis by LC-MS/MS was compared with MALDI-TOF MS. LC-MS/MS technology detects about 10 times more peptides than MALDI-TOF MS in both the control and the injury animal. C) Distribution of the probability scores for detected peptides in the urine from a DM+HTN rat using MALDI-TOF MS.

3.2.3 Characterisation of the urinary peptidome in the reversal DM+HTN model

Figure 36 displays the experimental design for urine collection in the reversal model. In 10 rats, urine was collected for 24 hours at the start of the experiment, after 28 weeks of combined induction of hypertension and diabetes mellitus (referred to as

injury phase) and after additional 8 weeks when both the diabetes and hypertension were tightly controlled (referred to as reversal phase). During the injury phase albuminuria and urinary volume were markedly increased compared with baseline (Table 7). After 8 weeks of reversal, both the urinary volume and albuminuria decreased significantly, however they remained significantly elevated compared with baseline levels (Table 7).

Typical base peak chromatograms demonstrate that the peptide profiles of animals within each treatment group appeared similar, while the profiles from animals from different groups were more divergent. This gave confidence in the analysis protocol. Raw data from LC-MS/MS were analysed using MaxQuant to identify the peptide sequences which best fitted the retention time and charge. Altogether more than 3200 different sequences were identified. Filtering steps as described in Figure 37 were applied to refine the search. Finally 1635 peptide sequences were selected for further analysis. For those, the probability score for detection peaked around 150. Roughly a third of the sequences were detected at all three experimental time points. Almost 60% of peptides were detected in the injury or reversal phases but not at baseline, with the majority of these being common to both the injury and reversal phases, underlining the similarity in the peptidome between these two phases. Conversely, only 2% (28) were unique to the baseline urine samples (Figure 37).

Figure 36: Time points of sample collection in the Cyp1a1mRen2 reversal DN model

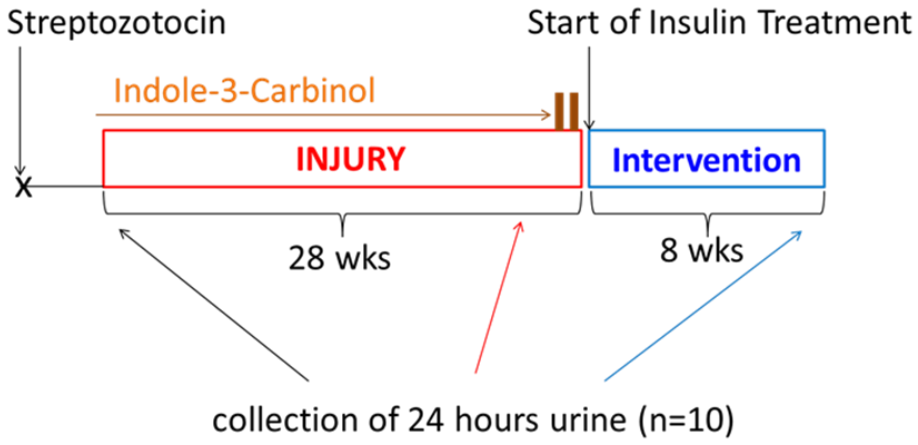

Figure 36. Schematic experimental design demonstrates the time points of urinary collection at week 0 (baseline), after 28 weeks of combined hypertension and diabetes mellitus (injury phase) and after an additional 8 weeks of tight glycaemic control and removal of dietary 1-3-C to reverse hypertension (reversal phase).

Table 7: Characteristics of the urine from the experimental phases

	mean (SD) or median (IQR)					
	Baseline week 0		injury phase week 28		reversal phase week 36	
albumin to creatinine ratio (ACR)	4	(2-5)	2198[a]	(1680-3417)	847[ab]	(547-1463)
urinary volume (ml/24h)	6	(4.8-8.2)	42.5[a]	(30.8-76.3)	12[ab]	(9-13.5)
creatinine-clearance	2.51	(0.69)	2.45	(0.31)	2.59	(0.55)

Table 7. Albuminuria and urinary volume are dramatically increased at week 28 (injury phase) compared to baseline and are decreased significantly at week 36 compared to injury phase. N=10. a $p<0.05$ and aa $p<0.001$ vs baseline; b $p<0.05$ and bb $p<0.001$ vs injury phase

Figure 37: MS/MS analysis from the Cyp1a1mRen reversal cohort

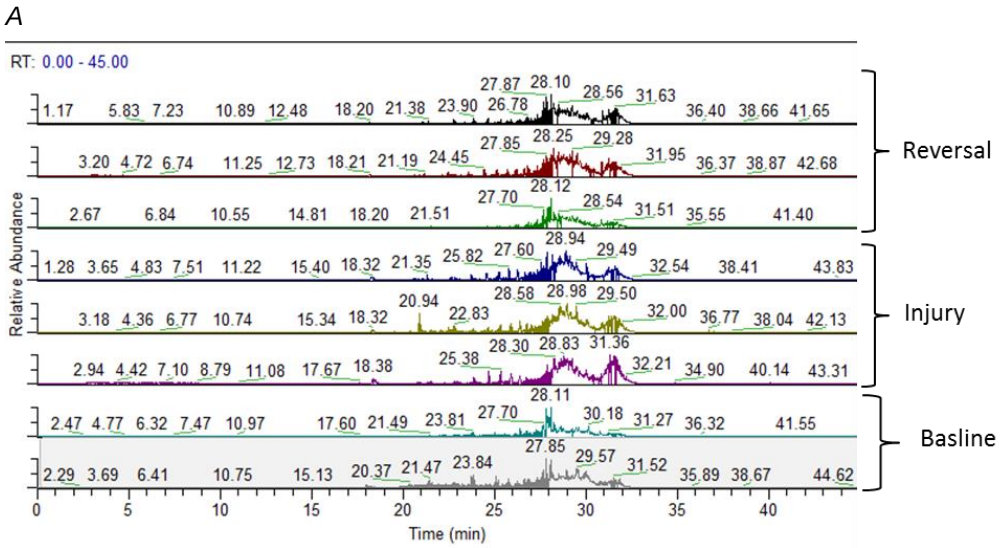

Figure 37. The MaxQuant software identifies and quantifies peptide sequences from MS-profiles. A) Typical MS profiles from urinary samples with base peaks and retention times.

There is a similar pattern profile between different animals from the same group, with the pattern from animals of different groups being more divergent. B) Flow-Chart of the processing steps to filter non-relevant peptides from the MaxQuant software output. From roughly 14000 initial hits about 12000 were retained after different charges of the same peptides were summarized. Removal of contaminants and a probability/detection score below 72 (with an false discovery rate of 0.05) resulted in approximately 4000 peptides. 1635 Peptides were retained after processing. C) The probability score indicates the likelihood that a peptide has been correctly identified. The diagram describes the distribution of probability scores (starting from a score of 72 as defined by an FDR threshold of 0.05) for the identified peptides. D) The venn diagram illustrates that roughly a third of all peptides had been detected in at least one animal at all three time points and almost half of the peptides were present during the injury and reversal phase only.

Correlation of urinary peptidomics in the experimental groups

For quantitation of peptides a label-free approach was utilized in which the height of the chromatographic peak corresponding to an individual peptide is proportional to the amount of peptide present in the sample. The relative abundance of each peptide was calculated by MaxQuant Software (see Materials and Methods) and is expressed as peak intensities. The patterns of relative peptide abundances in intensities were compared between two individual experimental phases. The strongest correlation was found between relative abundances of peptides present during the injury and reversal phases. There was a weak correlation between peptide abundances at baseline and the injury phase but a stronger correlation between baseline and reversal phase (Figure 38).

Figure 38: Correlation of peptide mean peak intensities between experimental phases

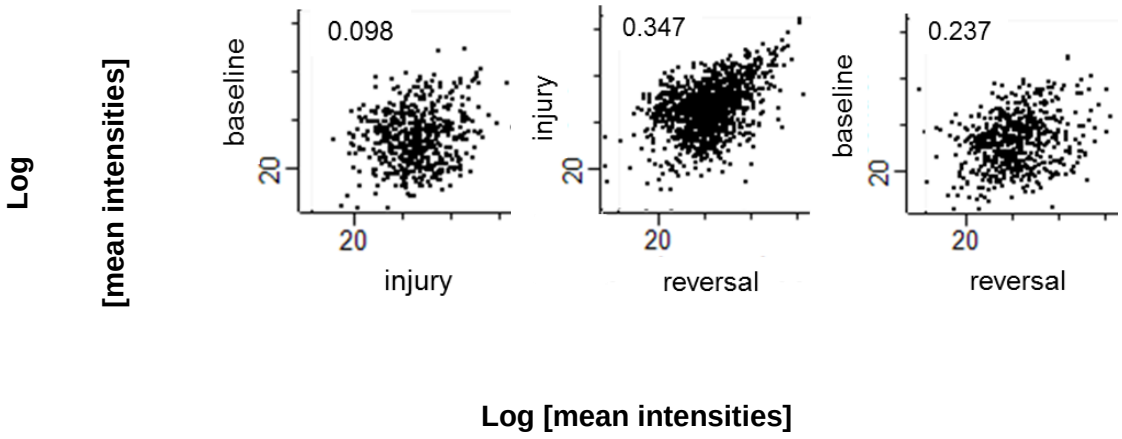

Figure 38. Scatter plots demonstrating the degree of correlation in mean peak intensities of the peptides between two different time points compared with the other time points. The strongest correlation was between the injury and reversal phases followed by the reversal and control phases, p-value for all coefficients <0.001.

Regulation of urinary peptidomics between all the experimental groups

To compare the signal from peptides across all three groups an in-house custom implementation of Rank Products in R-software was developed and applied as described in the Materials and Methods. Altogether 1290 peptides were detected at sufficient frequency among specimens in order to be included into analysis by the algorithm.

While the mean signal from most peptides did not change significantly between phases, 58 peptides had significantly increased peak intensities during the injury phase, 136 peptides had a decreased intensities during the injury phase compared to baseline. During reversal phase 42 peptides had decreased and 60 peptides increased peak intensities compared to the injury phase (Table 8).

Table 8: Peptides significantly changed in peak intensities between baseline and injury phase and injury and reversal phase

Direction: Baseline to injury	Direction: Injury to reversal	Number of peptides	Number of related proteins
increased	increased	3	2
increased	decreased	26	15
increased	unchanged	29	15
decreased	increased	13	11
decreased	decreased	3	1
decreased	unchanged	120	35
unchanged	increased	47	18
unchanged	decreased	13	7
unchanged	unchanged	1036	161

Table 8. Relative abundances from detected peptides are compared between baseline vs injury phase at week 28 and injury phase and reversal phase at week 36 using an in-house log-rank algorithm. The threshold for significant difference was $p<0.05$. Listed are number of unique peptides and the number of parent proteins. Since several peptides refer to the same parent proteins those can be present several times in the table. For 1290 from 1635 peptides (79%) were detected in enough animals at each time point to calculate a comparison. The relative abundance of most peptides (1036 from 1290) did not change significantly between time points. Some individual peptides and parent proteins are presented in the text or Figure 6 respectively. The complete list is added as an appendix.

Peptides with increased intensities during the injury phase were predominantly from serum derived proteins and were functionally associated with each other, such as albumin and apolipoproteins. Many of these peptides had decreased peak intensities from injury to reversal phase. Peptides with reduced peak intensities during the injury phase were often structural tubular or glomerular proteins (e.g. Uromodulin, Meprin A, Epidermal Growth Factor, Ezrin). During the reversal phase peptides with decreased peak intensities compared to the injury phase were related to serum

proteins (e.g. Apolipoproteins, serpins). Peptides with increased peak intensities in the reversal phase compared to injury phase were related to structural proteins and serum proteins (see Discussion) (Figure 39).

Analysis for biological processes enriched with parent proteins demonstrated that inflammatory/defence mechanisms were top ranked for peptides with increasing peak intensities from baseline to injury phase and with decreasing peak intensities from injury to reversal phase. Conversely, negative regulatory cell metabolism was top ranked among peptides with decreased peak intensities in injury phase compared to baseline but increased intensities in reversal phase compared to injury (Figure 39). There was a considerable overlap of parent proteins, genes and biological processes which is a caveat when interpreting the results.

RNA microarray data was available from renal cortex tissue of rats that were culled as control animals without further intervention, from rats that had undergone 28 weeks of hypertension and hyperglycaemia and from rats with an injury phase followed by a reversal phase (Conway, Betz et al. 2014). 9 out of the 74 parent proteins from urinary peptides which were significantly different between the phases were related to renal genes that had a similar regulation on a genetic level (Table 9). Those that were increased during the injury phase (7) at both gene and urinary peptide level comprised collagens, markers of renal damage (e.g. clusterin, osteopontin), complement cascade factors (c2, c3) and fibrinogen. The two peptides/genes reduced during injury were pro-epidermal growth factor and meprin A.

Figure 39: Parent proteins [gene symbols] from peptides significantly changed in peak intensities between baseline and injury phase and injury and reversal phase

A) Increased from Baseline to Injury phase

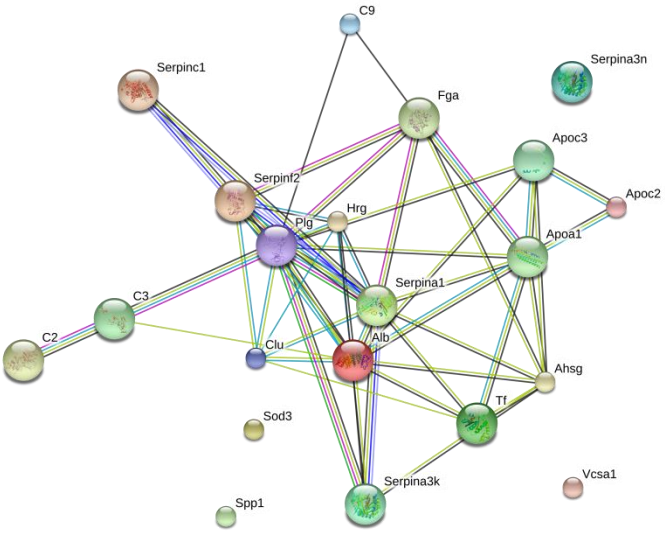

pathway ID	pathway description	observed gene count	FDR-adjusted p-value
GO:0006952	defence response	10	1.19E-08
GO:0051346	negative regulation of hydrolase activity	8	1.86E-08
GO:0006954	inflammatory response	8	3.63E-08
GO:0010951	negative regulation of endopeptidase activity	7	3.63E-08

B) Decreased from Injury to Reversal phase

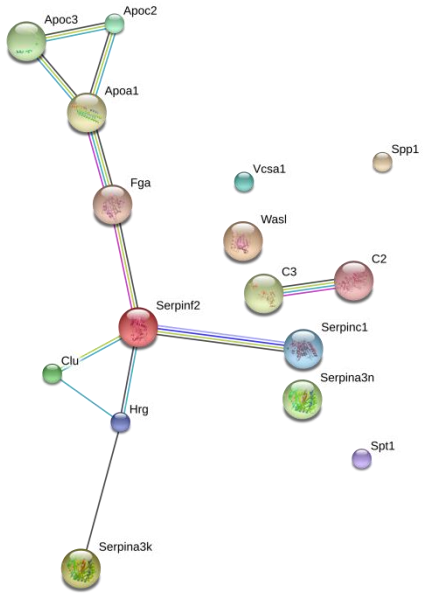

pathway ID	pathway description	observed gene count	FDR-adjusted p-value
GO:0051346	negative regulation of hydrolase activity	6	2.64E-05
GO:0010951	negative regulation of endopeptidase activity	5	8.75E-05
GO:0030162	regulation of proteolysis	6	9.26E-05
GO:0006952	defence response	6	0.000306

C) Decreased rom Baseline to Injury phase

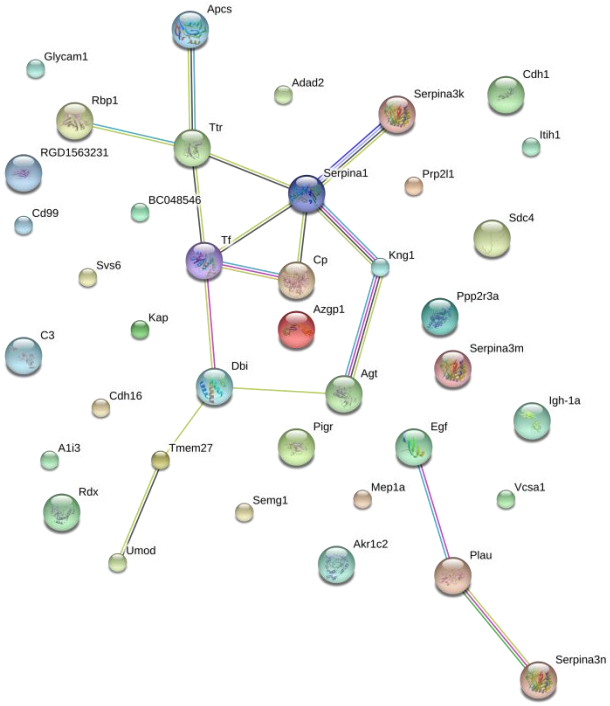

pathway ID	pathway description	observed gene count	FDR-adjusted p-value
GO:0010951	negative regulation of endopeptidase activity	9	2E-08
GO:0051346	negative regulation of hydrolase activity	10	2E-08
GO:0051248	negative regulation of protein metabolic process	10	1.48E-05
GO:0031324	negative regulation of cellular metabolic process	12	4.96E-05

D) Increased from Injury to Reversal phase

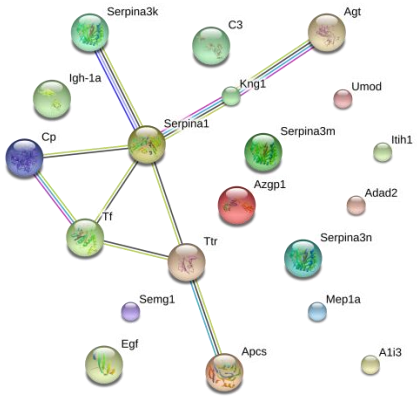

pathway ID	pathway description	observed gene count	FDR-adjusted p-value
GO:0051346	negative regulation of hydrolase activity	9	7.05E-10
GO:0010951	negative regulation of endopeptidase activity	8	8.83E-10
GO:0051248	negative regulation of protein metabolic process	9	1.17E-07
GO:0031324	negative regulation of cellular metabolic process	9	1.77E-05

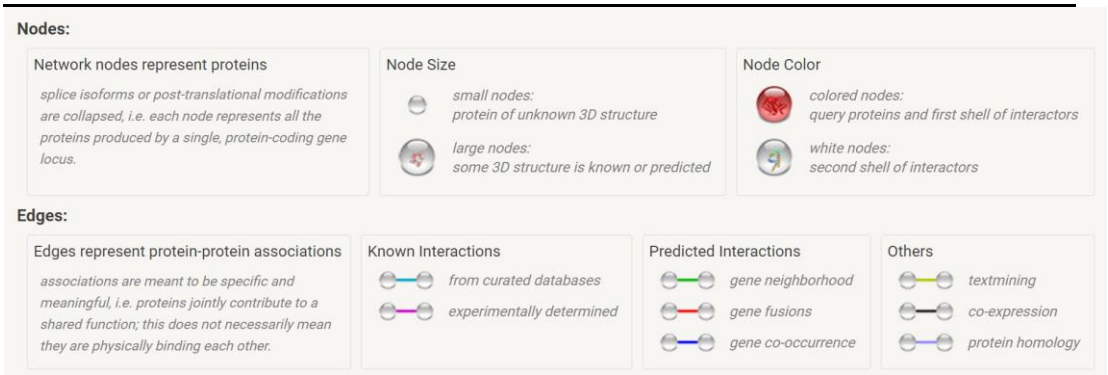

Figure 6. Illustration of functional protein associations from most parent proteins related to peptides with increased or decreased abundance in injury or reversal phase compared baseline or injury phase respectively using the String database (www.string-db.org). Proteins are represented by the gene symbol. The complete list of all peptides and related proteins is provided in the appendix. There were many associations between proteins in the category that were increased from baseline to injury. Most of them are serum proteins. Some of them were also present in the category that was decreased from injury to reversal indicating reduced glomerular leakage. There were few links between proteins in the category that was decreased from baseline to injury. Some of the structural proteins were present in the category that was increased from injury to reversal.

The top four biological processes (GO: Gene Ontology Consortium) are provided for each category according to false discovery rate (FDR) (www.string-db.org). Of note, similar to the

peptides there were some overlaps in the processes between the categories. Inflammatory mechanisms are ranked “top four” for being enriched with proteins from peptides increased during the injury phase compared to baseline phase. Conversely, these were among the “top four” to be decreased from injury to reversal phase. Negative regulatory processes of cell metabolism were enriched pathways from peptides with decreased peak intensities from baseline to injury and increased intensities from injury to reversal phase.

Table 9: Urinary peptides with similar regulation of related renal genes

Gene	Name	injury group vs control group	reversal group vs injury group
Clu	Clusterin	increased	unchanged
Col1a1	Collagen alpha-1(I) chain	increased	decreased
Col1a2	Collagen alpha-2(I) chain	increased	decreased
C3	Complement C3	increased	unchanged
C2	Complement C2	increased	unchanged
Fga	Fibrinogen alpha chain	increased	unchanged
Spp1	Osteopontin	increased	unchanged
Mep1a	Meprin A subunit alpha	decreased	increased
Egf	Pro-epidermal growth factor	decreased	unchanged

Table 9. The 254 peptides with significantly altered peptide peak intensities between the baseline, injury and reversal phases related to 74 unique proteins. These were compared with the genetic regulation assessed from the renal cortex of animals that were culled as controls, injury group or reversal group. A similar tendency in regulation compared to urinary proteins during baseline, injury and reversal phase was found for nine genes (12%).

3.2.4 Urinary peptides in patients with diabetic nephropathy and healthy controls

The methodology of urinary peptidomic analysis was applied to patients with diabetic nephropathy. Six healthy volunteers without a history of renal damage and ten patients with advanced chronic kidney disease from the renal and diabetic outpatients clinics of the Royal Infirmary of Edinburgh were analysed (Table 10).

After informed consent was received, a spot urine sample was collected and the proportion of the volume used for analysis was adjusted according to the urinary

creatinine to correct for differences in urinary concentration between the patients. Urine samples were processed as described in the previous paragraphs for the rodent studies. Altogether 1181 peptides were identified with almost 80% being detected exclusively in the DN group (Figure 40).

However many of those were only identified in one or two patients making it impossible to calculate statistical significance for differences in peptide peak intensities between the groups. 7 peptides, derived from seven parent proteins, had significantly less peak intensities in DN patients compared to healthy volunteers: These were Matrix Gla protein (MGP), Membrane-associated progesterone receptor component 1 (PGRMC1), Vascular endothelial growth factor A (VEGFA), Sodium/potassium-transporting ATPase subunit gamma (FXYD2), Angiopoietin-related protein 2 (ANGPTL2), CD59 glycoprotein (CD59) and Tetraspanin-9 (TSPAN9) (Figure 41).

Conversely, 120 peptides, derived from 47 unique parent proteins, were significantly more abundant in patients than in controls. These included many serum proteins (Apolipoprotein, Anti-thrombin) but also proteins associated with renal injury and fibrosis (Clusterin, Osteopontin) and collagens. In pathway analysis serum processes (e.g. platelet function) were the top ranked pathways.

Table 10: Characteristics of patients with DN and healthy controls

A

	Age	Gender	Stage CKD	eGFR
P1	44	M	IV	26.7
P2	65	M	IV	8.8
P3	82	M	V	37.8
P4	65	M	IV	6.3
P5	76	F	IV	19.1
P6	77	M	IIIb	27.0
P7	37	F	IV	17.8
P8	65	M	V	8.2
P9	41	M	IV	16.4
P10	74	M	IV	29.9

B

	Age	Gender	Stage CKD
C1	61	M	none
C2	71	M	none
C3	66	M	none
C4	38	F	none
C5	41	M	none
C6	34	M	none

Table 10. Urinary peptidomics were analysed in a discovery cohort comprising ten patients with diabetes and chronic kidney disease and six volunteers without medical history of renal disease.

Figure 40: Number of urinary peptides identified in patiens with DN and healthy volunteers

A *B*

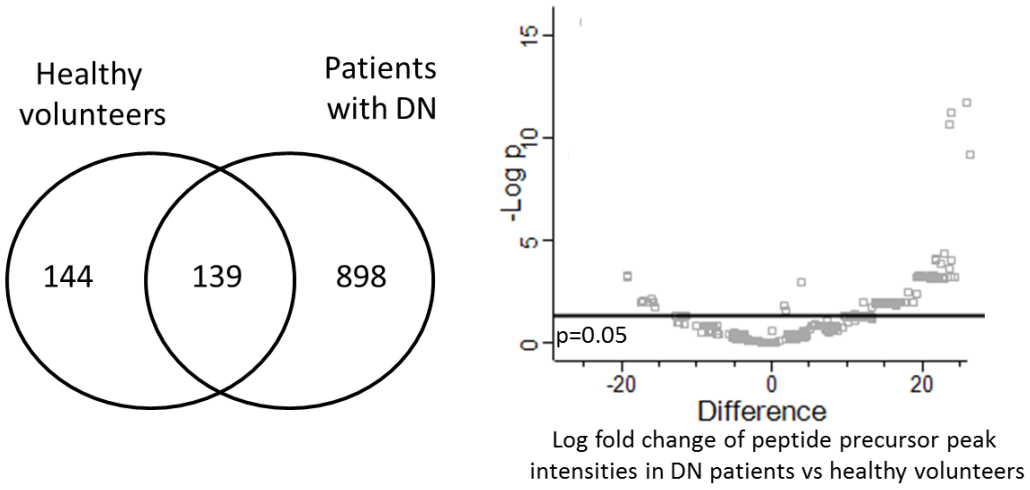

Figure 40. In the analysis of urinary specimens from patients with chronic kidney disease and from healthy controls A) most of the peptides detected were exclusively found in patients. B) The abundances from urinary peptides from DN patients were typically significantly increased compared to healthy volunteers.

Figure 41: Parent proteins [gene symbols] from peptides significantly changed in peak intensities between healthy volunteers and patients with DN

A

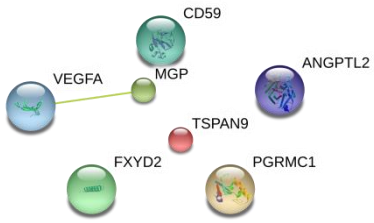

B

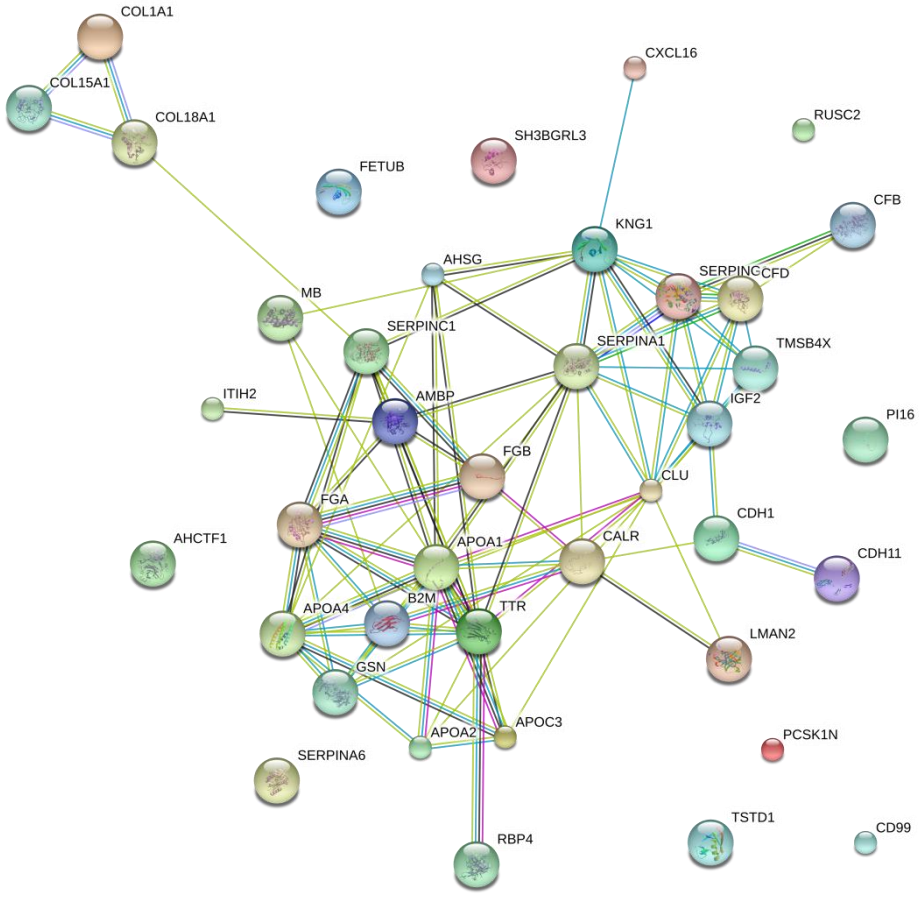

pathway ID	pathway description	observed gene count	FDR-adjusted p-value
GO.0002576	platelet degranulation	10	9.38E-12
GO.0030168	platelet activation	11	2.96E-09
GO.0016192	vesicle-mediated transport	17	1.40E-08
GO.0051346	negative regulation of hydrolase activity	12	1.66E-08

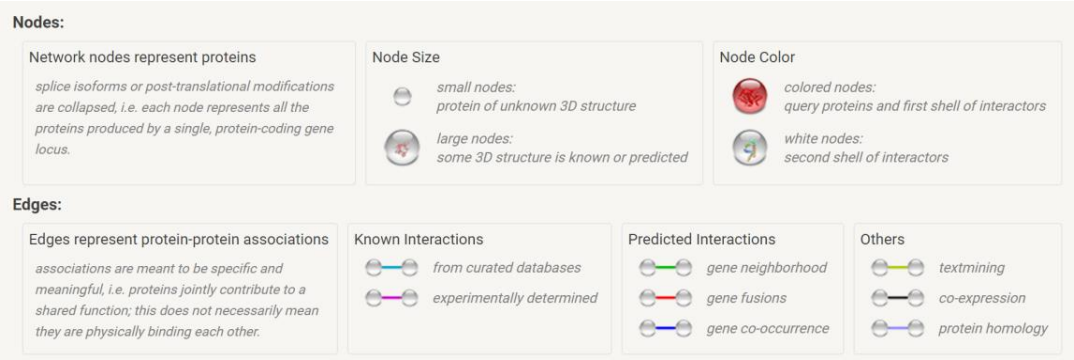

Figure 41. Parent proteins from peptides with (A) increased or (B) decreased peak intensities in patients with CKD compared to healthy volunteers were entered into the String database (www.string-db.org) for illustrating functional protein associations. Proteins are represented by the gene symbol. There are many associations between proteins with increased peptide intensities in CKD patients. Most of them are serum proteins indicating glomerular leakage. This is also underlined by the analysis of peptide/protein enriched biological processes. The top-ranked according to FDR (false discovery rate) biological processes all relate to serum related processes. The list of all peptides is provided in the Appendix.

3.2.5 Urinary peptidomic analysis in the DN model with Progenesis QI

In a previous study the effects of inducing diabetes (DM) or hypertension (HTN) alone versus the combination of induced diabetes and hypertension (DM+HTN) on the biochemical, pathological and transcriptomic features in the kidney had been compared and the experimental and clinical characteristics of the groups are published (Conway, Rennie et al. 2012). In order to extend these findings, peptidomic analysis of urine from each of the groups was performed. The data obtained from the LC-MS/MS was processed by Progenesis QI software from Nonlinear Dynamics (Figure 42). The software permits alignment of chromatograms from different sample runs to compensate for variation in the LC separation technique between runs (Figure 43).

After further processing, including removal of highly charged features, the complete dataset was exported to the Mascott search database for peptide identification.

Peptides were re-imported to Progenesis QI and matched with the relative abundance calculated from the peak intensities of the chromatograms. Subsequently data were analysed by principal component analysis (PCA) to visualise similarities and differences in the variation in the global urinary peptide profiles between animals. It is important to emphasize that bi-plot principal component analysis (PCA) was not calculated for identification of the components explaining the variation but rather as quality control to detect outliers as recommended by the developers of Progenesis QI (http://www.nonlinear.com/progenesis/qi/v2.0/faq/pca.aspx). In this process, all peptides contributed to the position of a sample within the matrix. In the PCA it was apparent that control and DM+HTN groups were well segregated from all the other groups implying that the combination of diabetes and hypertension was significantly different to induction of diabetes or hypertension alone (Figure 44).

The relative abundance that was calculated from the individual peak intensities of a peptide was considered to be significantly different when the p-value was below 0.01 and the q-value that corrects for multiple testing was below 0.05. Figure 42 summarizes the data processing in Progenesis QI (Figure 42).

Figure 42: Data processing in Progenesis QI

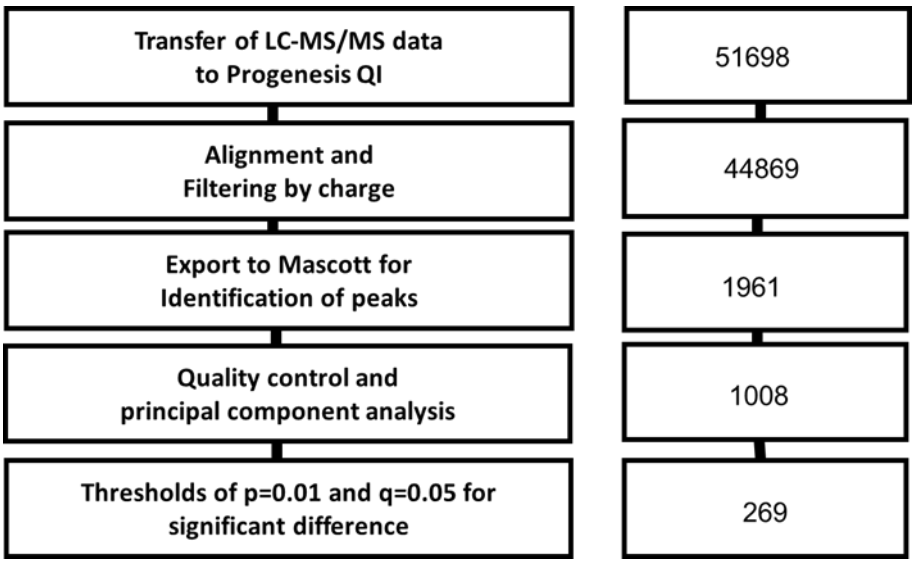

Figure 42. Schematic illustration of the most important steps using Progenesis QI for analysis of raw LC-MS/MS data. The right column lists the number of remaining peaks, features or peptides respectively after each step.

Figure 43: Alignment in Progenesis QI

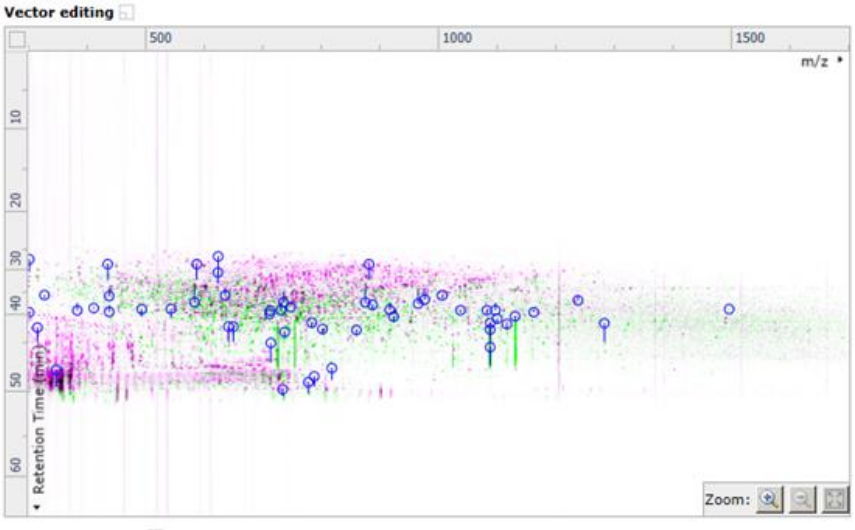

Figure 43. Representative screen shot illustrates the alignment process with peptides separated by retention time (y-axis) and m/z (x-axis). At the beginning a reference run to which all other runs were aligned was automatically chosen by Progenesis QI. Many peptides of the reference run (magenta) had been eluted earlier than the current run (green). Vectors (blue) can be set automatically and checked manually between individual peptides to align the entire peptidome.

Figure 44: Principal component analysis of the urinary peptidome from the Cyp1a1mRen2 DN model

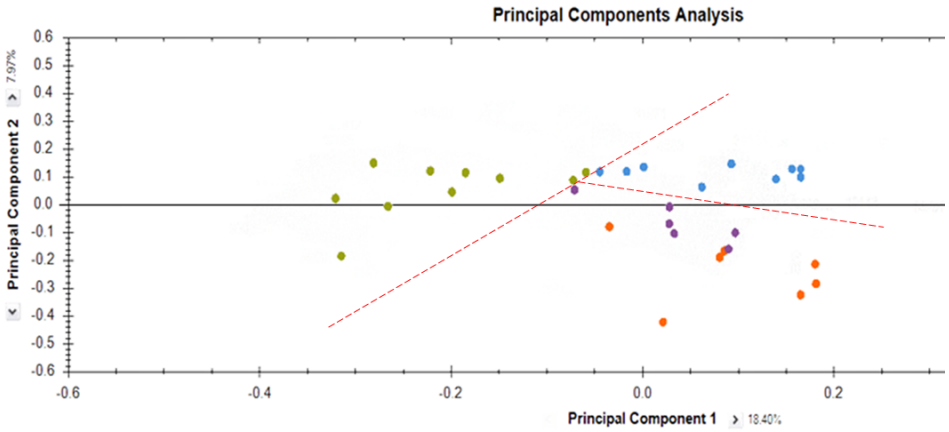

Figure 44. Principal component analysis of global urinary peptide profiles in the diabetic and/or hypertensive rat model. The plot shows principal component 1 (PC1) that is calculated from the combination of peptides explaining the most variation on X axis and principal component 2 (PC2) on Y axis for the combination of peptides explaining the second most variation. A blue dot summarizes all peptides from an urinary specimen from an animal of the control group (control), orange points denote specimens from the Hypertension alone group (HTN), violet data points denote specimens from the Diabetes mellitus alone group (DM) and green data points denote specimens from the combined (DM+HTN) injury model. There is an apparent clustering between the groups with the DM+HTN animals being separate from all other groups.

Urinary peptide profiles in the Cyp1a1mRen2 DN model

Altogether 269 peptides were identified to have significantly ($p<0.01$) increased peak intensities in at least one of the diabetes ± hypertensive groups compared with the control group. The distribution of these differentially excreted peptides mirrored the distribution of genes significantly increased in the renal cortex of diabetic ± hypertensive animals compared to control (see Introduction) (Conway, Rennie et al. 2012) (Figure 45). The complete list of peptides is given in the Appendix. The majority of peptides with increased peak intensities compared with controls were exclusively identified in the urine from the DM+HTN animals. A volcano plot illustrates the distribution of the peptides that were significantly different between the control and DM+HTN group (Figure 46).

Out of those peptides with increased peak intensities in the diabetes ± hypertensive groups compared with the control group were some of special interest because the genes encoding their parent proteins had been confirmed to be up-regulated in the renal cortex of the DN model and in kidney biopsies from patients with DN (Table 11). For comparison with molecular regulation in human DN the free online database nephroseq.org was used. Nephroseq.org contains the results of microarray analysis from many studies e.g. comparing gene regulation in DN biopsies with healthy controls (Woroniecka, Park et al. 2011).

Only 16 peptides were significantly decreased following induction of diabetes ± hypertension compared to controls. One of these peptides, derived from epidermal growth factor, was the only one for which a parallel reduction in the corresponding gene expression was observed in the renal cortex in both the DM+HTN rat model and in patients with DN (Table 12).

Figure 45: Peptides with significantly altered peak intensities in the DN model compared to control

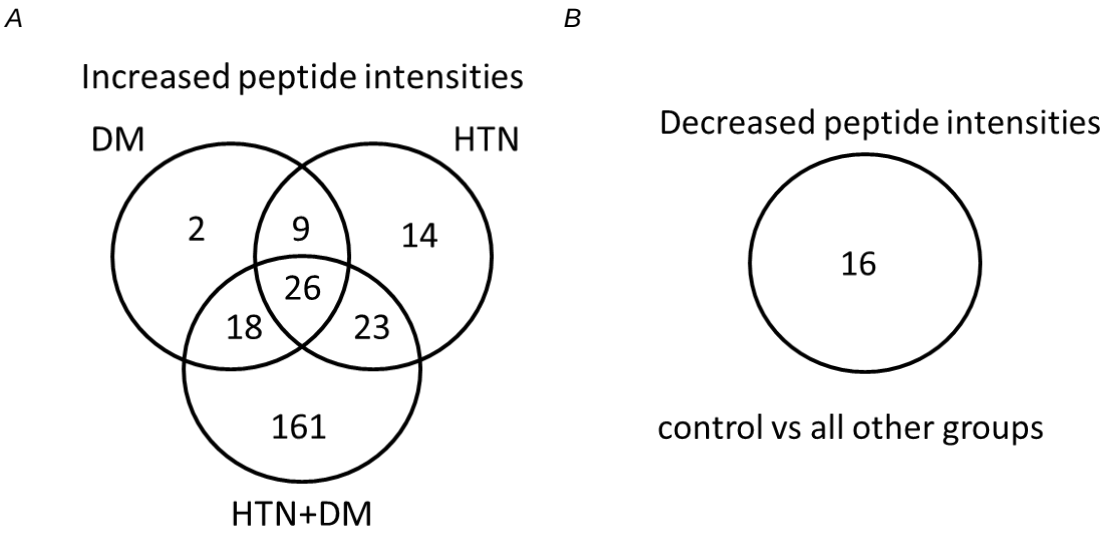

Figure 45. (A) Peptides in the hypertension alone (HTN), diabetes alone (DM) and injury (HTN+DM) groups that are significantly increased compared to control group. Most of them are significantly increased exclusively in the injury group. (B) Only 16 urinary peptides were increased in control animals. N=6-10.

Figure 46: Comparison of urinary peptidome between the control and the hypertension+ diabetes (HTN & DM) group of the Cyp1a1mRen2 DN model

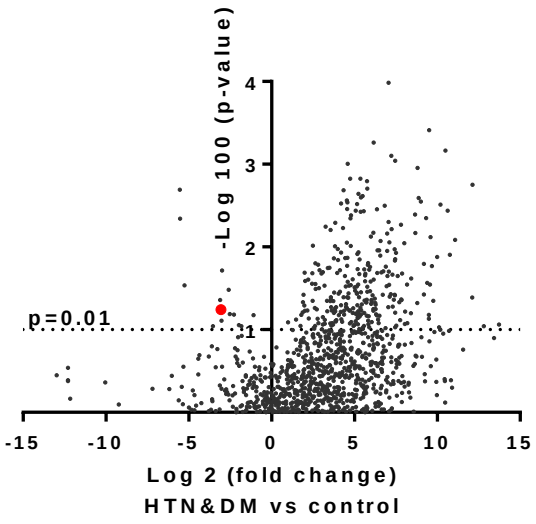

Figure 46. Volcano plot demonstrates the fold change (log2) in relative abundance (x-axis) plotted against the P-value (–log100, y-axis) for urinary peptides from the injury (DM+HTN) animal group compared with control animals. The dotted line represents p=0.01. The red dot indicates the pro-epidermal growth factor.

Table 11: Selected peptides with significantly increased relative peptide abundance in the injury group compared to control

Max fold change	P-value	Score	Protein ID	Sequence	Description
3.80E+03	5.20E-03	60.74	P04639	DNWDTLGSTVGR	Apolipoprotein A-I
6.56E+01	8.87E-09	51.63	M0RBF1	TLDPEHLGQGGVQRE	Complement C3 [*,#]
1.04E+02	8.65E-05	55.98	P08721	DAIDSAEKPDAIDSAERSDAIDSQASSK	Osteopontin [*,#]
4.38E+01	4.80E-04	95.99	F1LM19	VASVESASGEVLHSPK	Alpha-2-HS-glycoprotein
4.95E+02	1.36E-03	59.38	Q01177	LGSDVQQIAVTKL	Plasminogen
5.11E+01	3.43E-04	111.56	Q6P734	DSEVTSHSSQDPLVVQEGSR	Plasma protease C1 inhibitor [#]
1.21E+01	2.13E-05	100.37	P02454	DRGETGPAGPAGPIGPAG	Collagen alpha-1(I) chain [*,#]
1.35E+02	2.77E-05	98.52	P02770	TVDETYVPKEF	Serum albumin
7.43E+01	9.17E-03	73.3	P14480	EPPSLRPAPPPISGGGY	Fibrinogen beta chain [*]
7.59E+02	3.36E-03	52.59	P12346	SKDFQLFGSPLGK	Serotransferrin [*]
3.26E+02	7.37E-03	72.35	P05371	SLLNSLEEAK	Clusterin [*,#]
6.01E+01	3.22E-04	85.49	A1L114	DTGTTSEFIEAGGDIR	Fibrinogen alpha chain [*]
2.58E+01	4.69E-03	71.03	Q08420	DTGESGVDLADRLDLVEK	Extracellular superoxide dismutase [Cu-Zn] [#]

Table 11. Peptides of interest that had significantly ($p<0.01$) increased relative abundance in the DM+HTN group in comparison with controls. [*,#] Peptides for which the corresponding genes had similar changes in expression in renal tissue from the DM+HTN model ([*]) or from human DN biopsies ([#]) compared with respective controls.

Table 12: Selected peptides with significantly relative peptide abundance in the injury group compared to control

Max fold change	P-value	Score	Protein ID	Sequence	Description
-3.89E+01	1.13E-04	56.4	P08568	SPENSQEQP QQTNPEEKP PAPK	Submandibular gland secretory Glx-rich protein
-1.39E+02	6.44E-03	52.65	F1M959	VVHLHAQPG TENR	Pro-epidermal growth factor [*] [#]
6.59E+01	1.11E-04	61.37	Q63461	DQELTITSEAI R	Proline-rich protein
1.29E+02	4.82E-04	52.65	P02783	GGSFGEEAS EEISS	Seminal vesicle secretory protein 4

Table 12. Peptides of interest that had significantly ($p<0.01$) decreased relative abundance in the DM+HTN injury group in comparison with controls. Pro-epidermal growth factor was the only peptides for which the corresponding gene had similar change in expression in renal tissue from the DM+HTN model (*) or from human DN biopsies (#) compared with respective controls.

3.2.6 Validation of peptide regulation for the protein Epidermal Growth Factor

The regulation of the peptide representing Epidermal Growth Factor (EGF) was validated on a protein and gene level with material available from both the DN (Conway, Rennie et al. 2012) and the reversal (Conway, Betz et al. 2014) models. Excretion of urinary EGF (uEGF) declined early (8 weeks) after induction of hypertension and diabetes and remained at that level until week 28. After an additional eight weeks of reversal phase there was a slight increase with this time point being significantly different neither from baseline nor from 28 weeks. On a genetic level referring to the previously published microarray database (Conway, Betz et al. 2014) there was a significant decrease in EGF gene expression in the renal cortex during the injury phase compared with controls. There was a non-significant

trend for EGF gene expression to increase after the reversal phase. Polymerase chain reaction to confirm the results from microarray could only be performed in the control, DM alone, HTN alone and DM+HTN groups since tissue from the reversal group was not available. This demonstrated that expression of the EGF gene was reduced in the renal cortex of DM+HTN rats compared to controls (Figure 47).

Immunohistochemistry in renal tissues of the control group demonstrated ubiquitous expression of EGF in tubular cells (Figure 48). After 28 weeks of injury phase there was a focal reduction of EGF staining in atrophic and damaged kidney injury molecule-1 positive tubules (Figure 49).

Figure 47: Renal and urinary expression of epidermal growth factor in the Cyp1a1mRen2 DN model and the reversal cohort

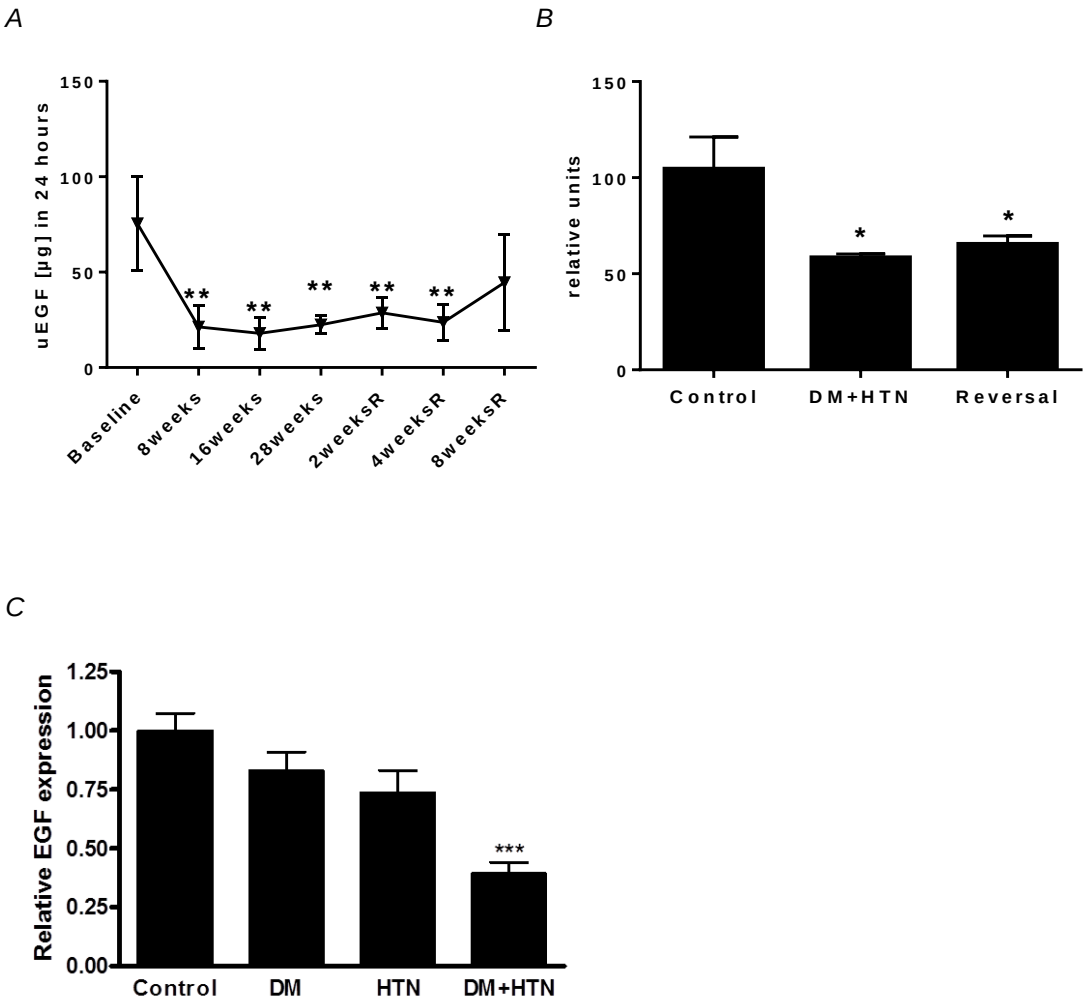

Figure 47. (A) In the Cyp1a1mRen2 reversal cohort the level of urinary EGF decreased significantly during the injury phase (Hypertension and Diabetes) and during the first four weeks of the reversal phase compared to baseline. Urine had been collected for 24 hours and measured uEGF concentration multiplied by urinary volume. n=10, ** = $p<0.01$ vs baseline. (B) Gene Microarray analysis in renal cortex from controls and animals at the end of the injury phase and after an additional reversal phase indicates significant down-regulation of the EGF gene. n=6. * = $p<0.05$ vs all others. (C) This was confirmed by rt-PCR with mRNA expression significantly reduced in the DM+HTN animals compared to control animals. n=6, *** $p<0.001$ v control

Figure 48: Staining for epidermal growth factor in sections from the Cyp1a1mRen2 reversal model

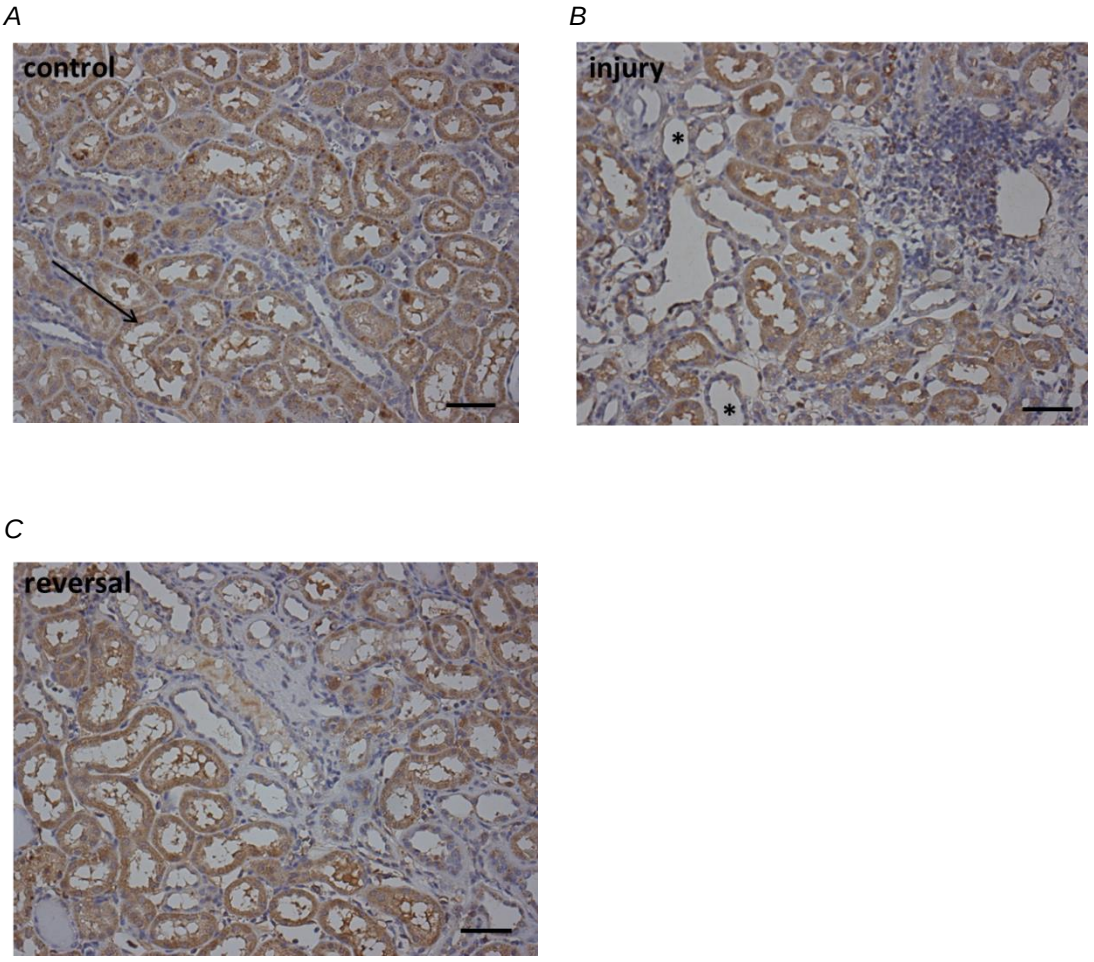

Figure 48. Representative photomicrographs from renal tissue cortex from a control, injury and reversal animal. EGF protein expression was reduced focally in injured tubules in the DM+HTN and reversal animals (asterisks) compared with uninjured tubules (arrow) and tubules of control animals. Bars represent 100 μM.

Figure 49: Staining for EGF and KIM-1 in sequential sections from the Cyp1a1mRen2 DN model

A

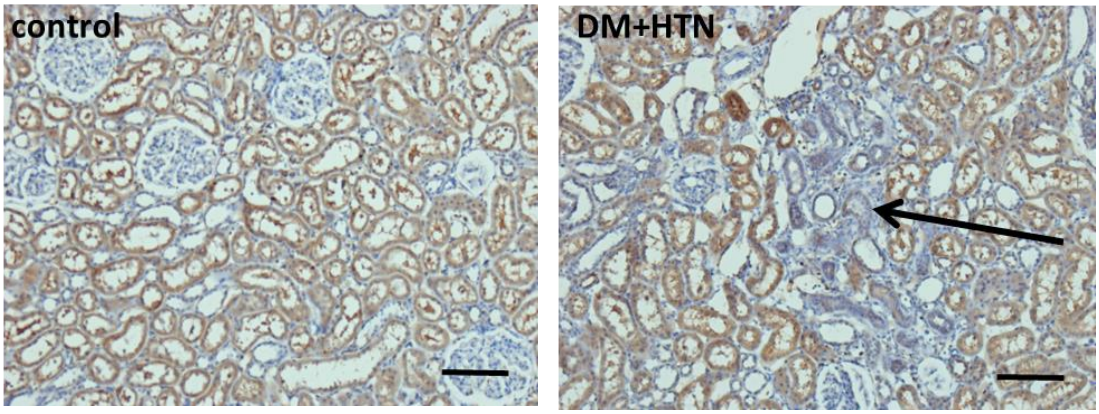

B

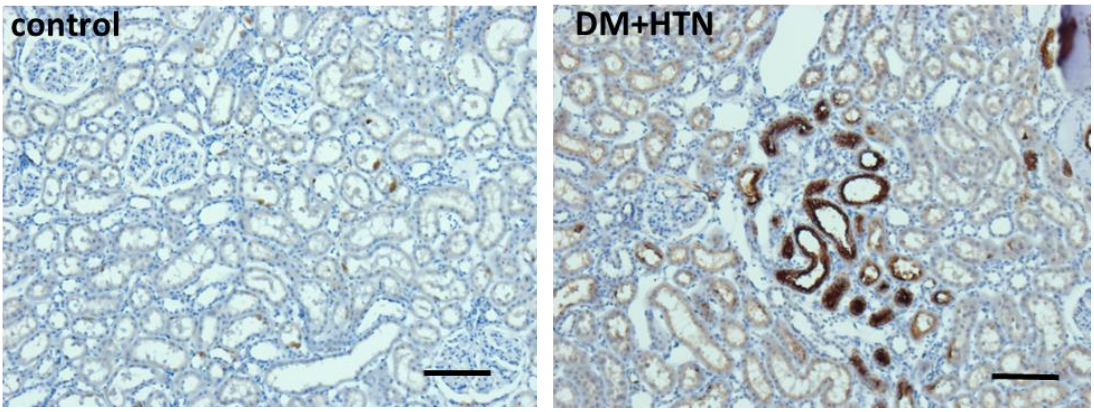

Figure 49. EGF and kidney injury molecule-1 (KIM-1) expression in sequential sections of renal cortex from control and DM+HTN animals (A) EGF protein expression was focally reduced especially in tubules in DM+HTN animals (arrow) (B) These tubules were injured as indicated by KIM-1 positivity (Betz, Jenks et al. 2016). Bars represent 100 μM.

3.2.7 Discussion

The aim of the experiments in this chapter was the identification of urinary peptides that may reflect the underlying pathophysiology in the DN kidney and which could hence be used as non-invasive biomarkers of disease and/or repair. Therefore a peptidomic approach in urinary specimens from the Cyp1a1mRen2 DN model was

combined with the transcriptomic profile of the model. In addition, a comparison with human DN was sought in order to strengthen the translational approach.

Preparation protocol

In a first attempt to analyse peptide sequences in urinary samples from the DN model a conventional electrophoresis separation strategy was performed, as described by Schlatzer et al. who investigated a rat DN model with only moderate albuminuria (Schlatzer, Dazard et al. 2009). Unfortunately, the very high albuminuria in the combined DM+HTN animals hampered clear protein separation. The interference from albumin and other "contaminants" such as salt is well described in the urinary proteomic field and Afkarian et al. tested several strategies to overcome these problems in human urine (Afkarian, Bhasin et al. 2010). In the current study, dialysis of the sample to reduce salt content did result in a slightly better separation, however albumin remained dominant. Depletion of albumin by using specific immunoabsorption columns resulted in an overall reduction of protein detected. These results are in line with those from Afkarian et al. (Afkarian, Bhasin et al. 2010). The option of increasing the volume of urine to compensate for the reduction in protein after immunoabsorption was not applicable given the limited volume of urine available in the rat DN model. In addition, Filip et al. reported limited success in the application of immunoabsorption columns in patients with CKD and macroalbuminuria (Filip, Vougas et al. 2015). Therefore the analysis of the urinary peptidome in the DN model seemed to be the preferable option. One hallmark in sample preparation for peptidomics is the removal of high-molecular weight proteins using a 10-20 kD cut-off filter thereby removing most of the overly abundant

albumin (app. 65 kD) (Merchant, Perkins et al. 2009, Good, Zurbig et al. 2010, Siwy, Zoja et al. 2012).

Comparison of analytical devices for peptidomics

The preparation of the samples was adapted to the technology available and was based on a modification of the in-house protocols of the Proteomics facility, Biology Department, University of Edinburgh and the protocol published by Rappsilber et al. (Rappsilber, Ishihama et al. 2003). The validity of preparation was tested initially using MALDI-TOF and a large number of peaks were detected consistent with successful identification of multiple peptides in the urine. After successful implementation of the protocol, samples were analysed by LC-MS/MS which resulted in a much higher number of detected peaks than MALDI-TOF. This is in line with other publications (Naseeb, Axelsson et al. 2015). Many other studies preferred to use CE-MS/MS over LC-MS/MS due to the following difficulties with LC-MS/MS analysis (Fliser, Novak et al. 2007, Mischak and Schanstra 2011, Klein, Bascands et al. 2016): 1. Long sample run time – however in the present study a relatively small number of samples had to be analysed. 2. Sensitivity to interfering compounds like salts - this was overcome in this work by including desalting and concentration steps into the preparation protocol 3. Problems in identification of larger peptides and low molecular weight proteins – in the present study the protease trypsin was used to make sure that all fragments are small enough to be detected.

The use of LC-MS/MS provides analytical depth which makes it suitable for biomarker discovery studies.(Fliser, Novak et al. 2007, Mischak and Schanstra 2011) Furthermore, peptidomic analysis in DN had already been performed by CE-MS/MS

in another model, (Siwy, Zoja et al. 2012) therefore by using LC-MS/MS the goal was to generate complementary data (Klein, Papadopoulos et al. 2014, Mischak, Delles et al. 2015).

In order to compensate for differences in diurnal excretion the use of albumin was not possible for obvious reasons. Other groups use housekeeping peptides(Good, Zurbig et al. 2010, Siwy, Zoja et al. 2012) but that approach depends on the detection of the respective peptides and is therefore restricted to the specific methodology (CE-MS). In the current study samples were pre-diluted according to their ratio with the largest 24 hour volume of the measurement run. Since the 24 hour volume was not available for the human samples, urinary creatinine was used as a surrogate parameter. Due to the large volume differences between the baseline and injury phase in the DN reversal model normalization before measurement was considered to preferable because measurement errors would have been multiplied if a mathematical correction was performed after measurement.

Peptidomics in the Cyp1a1mRen2 reversal DN model

In terms of qualitative analysis, the total number of peptides identified is close to those obtained by Siwy et al. who investigated urinary peptidomics in Zucker Diabetic fatty rats (Siwy, Zoja et al. 2012). The majority of peptides were detected in the DM+HTN phase with fewer in the reversal and baseline phases. This correlates well with differences in urinary albumin concentration between the experimental phases and is in line with the renal molecular expression as most genes were up-regulated during the injury phase followed by reversal phase compared to control (Conway, Betz et al. 2014).

Initial quantitative analysis was performed by two-group correlation using the program Perseus (max planck institute of biochemistry, Martinsried, Germany). The strongest correlation in peptide concentration was between the injury and reversal phases, in which the pattern of detected urinary peptides and up-regulated genes was similar. The moderate correlation between reversal and control phase might indicate a recovery effect following the removal of hypertension and hyperglycaemia.

Peptides with increased peak intensities during injury phase in the reversal DN model

Since Perseus is only able to perform a two paired comparison, an algorithm for determining the significance of differences in urinary peptide concentration between three groups was developed by Dr. Manning, University of Edinburgh (see Materials and Methods section). Most of the peptides did not change significantly during the three experimental stages. This again validates the methodical approach as many urinary proteins/peptides would be expected to be constantly excreted within the same species.

Many peptides with increased peak intensities in the urine during the injury phase and decreased during the reversal phase were derived from serum proteins such as apolipoproteins, urinary fibrinogen or histidine-rich glycoproteins. Hence, it is likely that many of these changes simply reflect reduced filtration from serum alongside the reduction in albuminuria during the reversal phase, rather than changes in protein expression within the kidney. In keeping with this the results from the microarray analysis of the renal cortex determined that there was no increase in apolipoprotein gene expression within the kidney. Other peptides with increased abundance during

the injury phase were derived from osteopontin and clusterin, which are well established markers in DN (Alter, Kretschmer et al. 2012, Korrapati, Shaner et al. 2012, Togashi and Miyamoto 2013). Osteopontin might play a pathophysiological role in DN as a macrophage chemoatactant (Kelly, Wilkinson-Berka et al. 2002). The expression of both the osteopontin and clusterin genes was upregulated in the renal cortex in this model suggesting that the increase in urinary osteopontin and clusterin might, at least in part, be due to increased production in the kidney. The presence of peptides from complement factors (C2, C3) in the urine could be easily explained by glomerular leakage. But interestingly microarray data indicates an upregulation of C2 and C3 in renal tissue during the injury phase in the DN model. A potential causative link between C3 accumulation and the development of DN has been discussed in the introduction section (Wada and Nangaku 2013). Further investigations are necessary to explore the potential role of complement components in DN.

Peptides with decreased abundances during injury phase in the reversal DN model

For two parent proteins from peptides with reduced peak intensities during the injury phase, pro-epidermal growth factor (EGF) and Meprin A subunit alpha, there was reduced expression of the corresponding genes in the renal cortex of rats specifically during injury period. EGF will be discussed in the following paragraphs. Meprin A (subunit alpha) is a metalloproteinase which belongs to the brush border membrane protein family in the kidney. Decrease of Meprin A peptide resonates with downregulation of the Meprin A gene in the kidney during injury. Matthew et al. confirm that Meprin A expression is reduced on a genetic and protein level in a rodent DN model, however paradoxically they report increased Meprin A urinary excretion. This was explained by a more intense decrease of renal Meprin B

compared to Meprin A in DN as Meprin B is necessary for the attachment of Meprin A to the brush border of tubular cells (Mathew, Futterweit et al. 2005).

Peptidomics in human kidney disease

In general, some but not many peptides were detected in both the human and rodent peptidome. Siwy et al. also report a low level of congruency in the urinary peptide profile from humans and rodents with DN (Siwy, Zoja et al. 2012).

One interesting peptide that has a reduced abundance in the urine of patients is vascular endothelial growth factor A (VEGF-A), which is constitutively expressed in tubular cells. As an angiogenic factor it may contribute to the maintenance of peritubular capillaries. Lindenmeyer et al. describe a distinct reduction of VEGF-A gene and protein expression in renal tissue biopsies from DN patients compared to healthy controls (Lindenmeyer, Kretzler et al. 2007). The list of parent proteins from urinary peptides that were increased in DN were enriched for serum proteins like Apolipoproteins and Alpha-2-glycoproteins, and this may reflect increase passage across a disrupted glomerular filtration barrier as it has been discussed in the rodent model. Similar to the rodent DN model, Osteopontin (SPP1), Clusterin (CLU) and Fibrinogen alpha chain (FGA) were identified as potential markers of renal damage. In addition, increased peak intensities of collagen peptides reflected results from the rodent reversal DN model. High levels of hepatocyte produced Fetuin-B (Fetub) that is assumed to impair actions of insulin, and C-X-C motif chemokine 16 (CXCL16), a scavenger receptor for oxidized low density lipoprotein and beta-2 microglobulin, have been reported to be increased in patients with diabetes (Aksun, Ozmen et al. 2004, Zhao, Wu et al. 2014, Meex, Hoy et al. 2015) . Retinol-binding protein 4

(RBP4), is not only produced by hepatocytes but released by tubular cells early upon damage (Norden, Lapsley et al. 2014) and has been reported to be elevated in serum and/or urine of patients with DN (Raila, Henze et al. 2007, Titan, Vieira et al. 2012). Taken together, analysis of the DN reversal model and urinary human DN, reveals interesting known and potential novel biomarkers with some of those corresponding with the transcriptomic findings from the DN model.

Peptidomics in the injury DN model using Progensis QI

Next the DN injury model (without reversal cohort) (Conway, Rennie et al. 2012) was analysed by a different program (Progenesis QI) to first validate the results obtained by MaxQuant and second to extend the list of promising biomarker candidates: using two different search algorithms (Andromeda vs Mascot) may extend the list of potential candidate markers since up to 25% of peptides/proteins might be exclusively identified by only one analytical programme (Merl, Ueffing et al. 2012).

Progenesis QI was used for data processing and label-free quantitation and the MASCOT search server for identification of peptides as performed by others in human urinary specimens (Rouillon, Zocevic et al. 2014, Beretov, Wasinger et al. 2015, Cantley, Colangelo et al. 2016). Progenesis QI offers the advantage of map alignment based on centroid data using user-set orientation marks to assign the same peptide feature in different runs for comparison. The analysis approach described by Atrih et al. was applied with slight adaptations (see Materials and Methods) (Atrih, Mudaliar et al. 2014).

Peptides with increased urinary peak intensities in the DN injury model

The distribution of peptides detected between the control, HTN, DM and HTN+DM groups resonates very closely with the distribution of the genes differentially expressed in the renal cortex in the same groups (see Introduction) (Conway, Rennie et al. 2012), thereby internally validating the results. For many parent proteins from urinary peptides with reduced or increased peak intensities in the HTN+DM group compared to control the corresponding genes were also up- or downregulated respectively. Furthermore, many of these genes were found to be similarly differentially expressed in the kidneys of patients with DN using data from the freely available online database "nephroseq.org" like osteopontin, clusterin and complement 3.

In addition, interesting novel candidate peptides/proteins biomarkers were detected. Increased serum superoxide dismutase (SOD) has been associated with micro- and microvasculature complications in diabetic patients. In addition, SOD1 is upregulated in renal biopsies from patients with DN, suggesting that the increased urinary SOD excretion may be derived from either the serum or kidney(Kimura, Hasegawa et al. 2003). Plasma protease C1 inhibitor is increased in human DN renal biopsies (www.nephroseq.org). Collagen I alpha chain has been detected by others in animal models of DN but seems to lack human translation(Siwy, Zoja et al. 2012).

Epidermal growth factor is decreased in urine and renal tissue in the DN injury model

Regarding parent proteins from peptides with significantly decreased peak intensities in the injury group, only epidermal growth factor (EGF) was reported to be

downregulated on a gene expression level in the kidney in both humans with DN and the rodent DN model. EGF is produced in the kidney by cells of the distal tubules. Hence, urinary EGF excretion could be indicative for functional tubular mass. Indeed, a dramatic reduction in urinary excretion of EGF has been observed in animal models of renal fibrosis (Thulesen, Jorgensen et al. 1997). In a model of early DN increased EGF levels are associated with reduced renal apoptosis (Kelly, Cox et al. 2002). In the Cyp1a1mRen2 DN model urinary EGF regulation was measured by ELISA, which largely confirmed the findings from urinary peptidomics. Correspondingly, renal cortex expression of the EGF gene was reduced in the DM+HTN group compared to control or DM and HTN alone in the Cyp1a1mRen2 DN model. A similar reduction in EGF protein expression was confirmed by immunohistochemical staining. However in contrast to uEGF that tends to increase during the reversal phase, renal expression of EGF remained downregulated in Cyp1a1mRen2 DN reversal model (microarray data). This discrepancy could be explained by leakage across an abnormal glomerular barrier in DN as an additional protein/peptide source. Another explanation might be the multiple possibilities of post-translational modification and proteolytic activity.

Limitations for biomarker discovery due to the techniques applied

In general, limitations of the techniques affect the stage of experimental design, they can be of procedural nature or issues can arise when raw data is processed and statistical analysis and interpretation of the results is performed:

1. Limitations - experimental design

Due to the limited accuracy of "shot-gun analyses" like transcriptome by microarrays and peptidomic/proteomics by LC-MS/MS all identified results require a confirmation by more accurate methods like PCR and ELISA (Dallas, Guerrero et al. 2015) (Jaksik, Iwanaszko et al. 2015).

For microarray, there is a selection of genes on the chip. Though the probes on the chip used in this work (Affymetrix Rat Genome 230 2.0 GeneChip) cover for more than 28,000 genes, the chip cannot be comprehensive for all the variants of alternative splicing at the pre-mRNA stage.

For peptidomics by LC-MS/MS there is no limitation for the number of peptide identification, however, the abundance of a few proteins/peptides mainly due to glomerular leakage in the injury group could mask those differences that a more subtle between the groups or inhibit the detection of peptides with very low concentration.

The reproducibility of the results in peptidomics is restricted to the same MS-platform as considerable variation has been reported when the same sample is analyzed with different MS techniques. Similarly, on the transcriptome level, reproducibility of the results depends on the microarray-chip utilized.

2. Limitations - experimental performance

Technical issues in the microarray array analysis have been discussed in Results Chapter 3.1.

A disadvantage for peptidomics/proteomics concerning sample quality is the potential degradation that might have started not only at the time of sample collection

but already in the bladder. However, literature indicates that urinary peptides are rather resistant against degradation (Klein, Bascands et al. 2016).

In urine salts and lipids might interfere with the LC-MS/MS analysis e.g. by dampening the ionization efficiency. The processes to remove these elements are elaborate and established but they are also time- and sample consuming and most likely reduce the reproducibility of the experiment.

Using a filter to separate higher molecular-weight proteins from peptides in urine is simple, fast and well-established approach; however, it has to be taken into account that the separation is incomplete with a slight leakage of larger proteins and loss of small peptides (Dallas, Guerrero et al. 2015).

Using a database searching engine (e.g. Mascot) for peptide identification performs well for most peptides but might a have sensitivity and accuracy issues (Merl, Ueffing et al. 2012). In this work the problem was reduced by combining two engines (Mascot and Maxquant/Andromeda), however, it has been demonstrated that incorporating identification by de-novo sequencing algorithms into database research could result in higher sensitivity and accuracy for peptide identification (Zhang, Xin et al. 2012).

In all peptidomics analysis normalization is crucial. In urinary peptidomics this can be achieved by correcting for creatinine or urinary 24hours volume. Due to the large differences in volume in the DM+HTN DN model between the control and injury groups. Small mistakes when adapting the large volumes might result in masking minute but significant differences in peptides abundances between the groups.

3. Limitations - data interpretation

Another disadvantage of the techniques chosen has been demonstrated by Ghazalpour et al.. They demonstrated that in mouse liver there is at best a moderate (50%) concordance between transcriptomic and proteomic expression changes (Ghazalpour, Bennett et al. 2011). This might limit the approach in this work to identify most promising biomarker candidates by referring to similar regulation of expression levels in renal genes and urinary peptides.

Astonishingly, there is a stronger association between clinical traits and transcriptomic regulation compared to protein regulation (Ghazalpour, Bennett et al. 2011). In the DM+HTN DN model there were much more significant differences between the individual groups control, DM alone, HTN alone and DM+HTN on the renal transcriptomic level than on the urinary peptidomic level. There are several possible explanations for this. Firstly, this could be explained by the experimental design as not tissue proteins/peptides but urinary peptides were related to renal transcripts. Changes in tissue protein level are not necessarily reflected in the urine that also contains a large number of proteins/peptides due to glomerular leakage. Secondly, as described above, accurate quantification by label-free LC-MS/MS is technically more challenging than microarray analysis. Thirdly, in the concept of "phenotypic buffering" the largest proportion of molecular variants is silent at the phenotypic level (Fu, Keurentjes et al. 2009). Fourthly, protein expression is not only affected by disease factors (e.g. hypertension and hyperglycemia) but also by numerous additional factors: translational efficiency, alternative splicing, assembly into complexes, covalent modification and degradation. For example, Clavo et al. have reported that the presence of upstream open reading frames (uORFs) reduces the translation of mRNA to protein for up to 50% (Calvo, Pagliarini et al. 2009).

Taking into consideration the limitations discussed in the previous paragraphs many candidate biomarkers were identified by analysing the renal transcriptome and the urinary peptidome in a rodent model and in patients with DN. Our group(Betz and Conway 2016) and leading groups in urinary peptidome research (Mischak, Delles et al. 2015, Klein, Bascands et al. 2016) suggest that results obtained from rodent models and human studies by "–omic" approaches should be compared and combined to redefine the evaluation of DN models. This might support researchers to select the most appropriate model for their specific research project and might thereby improve the translational application (Brosius, Alpers et al. 2009). The work of this chapter contributes to step one in the scheme for new biomarker/drug discovery as illustrated in Figure 50.

Figure 50: Schemata for the discovery of novel biomarkers

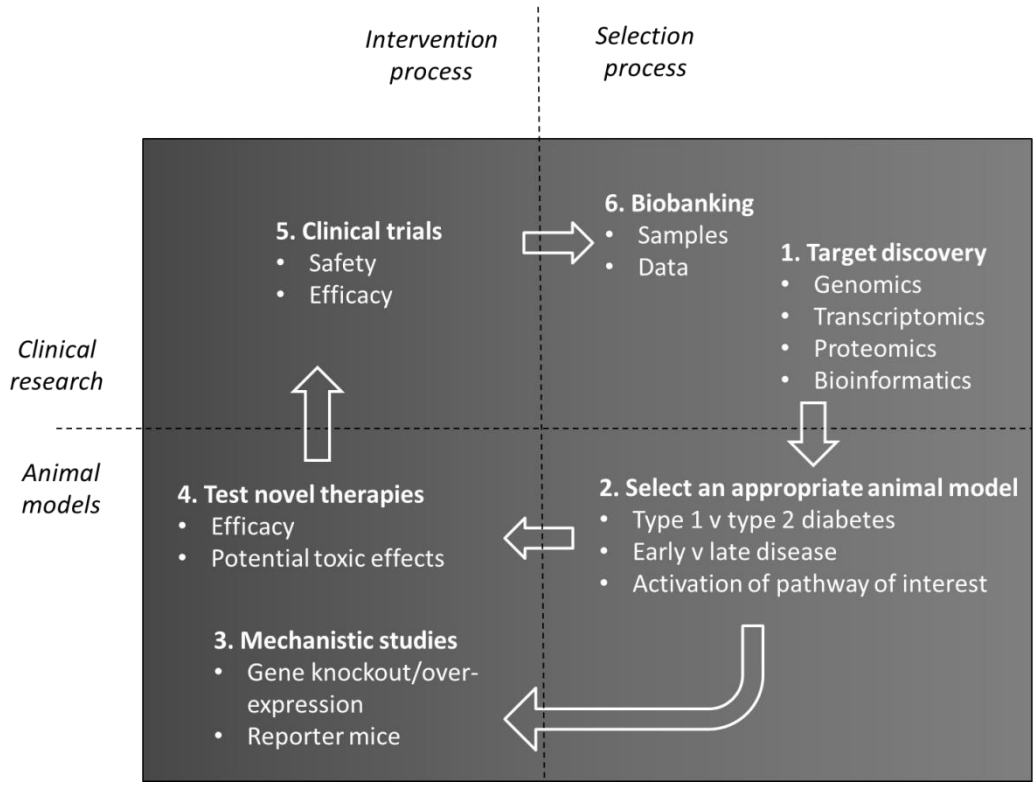

Figure 50. "Schemata for discovery of novel biomarker and therapeutic agents. 1. High-throughput, non-biased "-omic" approaches have identified hundreds of molecules that are associated with the development of human diabetic nephropathy. 2. Whether these molecules could be targeted to slow progression of nephropathy may be determined using the most appropriate animal model for the specific research question. 3. Genetically modified rodents may offer mechanistic insight and suggest whether development of a therapy is warranted. 4. Pharmaceutical agents may be tested for efficacy and potential side effects. 5. Therapies that are successful in robust animal studies may be taken forward into clinical trials. 6. Samples and data from these trials may be "biobanked" to provide further mechanistic insight toward refining therapies". (Figure and legend are taken from Betz et Conway, "An Update on the Use of Animal Models in Diabetic Nephropathy Research", Curr Diab Rep 16(2): 18.)

3.2.8 Summary

The present chapter describes:

- the development of a methodology for preparing, measuring and analysing the urinary peptidome utilizing highly sensitive LC-MS/MS technology

- the validation of the methodologic approach in several experimental cohorts

including the Cyp1a1mRen2 DN model with induction of DM alone, HTN alone or the combination DM+HTN, the DN reversal model and patients with DN.

- the identification of a candidate biomarker of tubular biomass, EGF, by two different analytical approaches (MaxQuant, Progenesis) and the validation of EGF protein regulation in urine and tissue.

The translational validation of uEGF will be part of the next chapter.

3.3 Urinary Biomarkers

3.3.1 Introduction

In the previous two chapters the Cyp1a1mRen2 reversal DN model helped to identify pathological pathways and proteins that might be involved in the progression of diabetic kidney disease. These proteins might be used as potential new non-invasive biomarkers indicating the risk of incident CKD or renal deterioration as the established marker albuminuria is often not present in patients with advanced DN. The candidate biomarkers were first tested in a small pilot study and then quantified in urine samples from the large well-defined Edinburgh Type 2 Diabetes Study (ET2D) cohort. (Price, Reynolds et al. 2008) The degree of correlation between the novel biomarkers and kidney function or previously tested urinary biomarkers was then assessed. The previously tested biomarkers include kidney injury molecule 1 (KIM-1) and Glycoprotein (Transmembrane) Nmb (Gpnmb) as potential indicators of disturbed tubular cellular integrity (Conway, Manoharan et al. 2012). Finally the predictive value of candidate biomarkers for renal deterioration was assessed.

3.3.2 Biomarker candidates for translational validation

Table 1 lists the biomarker candidates that were chosen from the previous chapters for validation in the human setting. Based on microarray data, all candidates were differentially expressed in the renal cortex in the rodent model and/or patients with DN compared with controls (Woroniecka, Park et al. 2011, Conway, Rennie et al. 2012, Conway, Betz et al. 2014). Some genes were increased (MMP7, OPN) with others decreased (EGF, VEGF). Similarly the corresponding peptides were increased (OPN) or decreased (EGF, VEGF) in the urine from DM+HTN rats or from patients

with DN. To assess the ability of the ELISAs to detect their target molecules in the urine, a pilot cohort was tested that comprised healthy volunteers (n=4) and patients (n=4) with CKD stage II, III, IV, V, respectively. For vascular endothelial growth factor-A (VEGF-A) no measureable signal in human urine samples could be detected although the standard curve worked well. All other biomarker candidates were robustly detected in the pilot urine samples and were taken to larger cohorts for further validation.

Table 13: Biomarker candidates tested in patients with diabetic nephropathy

Protein Candidate Biomarker	Rationale	ELISA R&D Systems	Pilot samples
Matrix Metalloproteinase 7 (MMP-7)	Genetics, Experimental Results	DY907	Detectable
Epidermal Growth Factor (EGF)	Genetics, Peptidomics (rodent)	DY236	Detectable
Osteopontin (OPN)	Genetics, Peptidomics (rodent)	DY1433	Detectable
Vascular Endothelial Growth Factor (VEGF)	Genetics, Peptidomics (human)	DY293B	Undetectable

Table 13. List of the urinary candidate biomarkers, the rationale for selecting (details see text), the respective ordering number of the ELISA kit in R&D Systems and the results of preliminary testing in urinary samples. The pilot cohort comprised healthy volunteers (sample number 1-4) and samples from patients with chronic kidney disease stage II III, IV and V (sample number 5-8).

Figure 51: Optical density (OD) readout for the VEGF ELISA

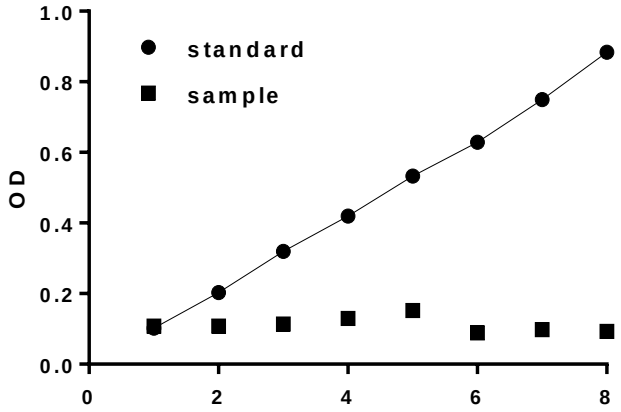

Figure 51. Vascular endothelial growth factor (VEGF) was largely below the threshold for robust detection in urinary samples from healthy participants (n=4) and patients with CKD II-V (n=4) by ELISA.

3.3.3 OPN and MMP7 in ET2D trial cohorts

A trial cohort from the Edinburgh Type 2 Diabetes Study was used for each of the candidates (Price, Reynolds et al. 2008). The study characteristics are described in more detail in the Material and Methods chapter. Urinary samples of the ET2D study were stored in 96-1ml-well plates, and for the test run several plates were defrosted. Since samples were sorted according to their anonymized study number each plate will have contained a random spread of patients with different severity of renal function. The baseline characteristics of the patients from the Edinburgh Type 2 Diabetes cohort used for each analysis are provided in Table 14. Urinary osteopontin and MMP7 concentration correlated positively with KIM-1, a marker of tubular injury, but not with albuminuria (Table 15).

In further analyses, the osteopontin and MMP7 concentration was referenced to urinary creatinine to correct for difference in urinary concentration. Urinary

osteopontin:creatinine ratio, but not urinary MMP7:creatinine ratio correlated with baseline GFR (Table 16, Figure 52) but both neither correlated with rate of renal decline nor were associated with death or eGFR after 4 years follow up (Table 17).

Table 14: Characteristics of the trial cohorts for OPN and MMP7

	OPN	**MMP 7**
n	423	748
urinary OPN : creatinine, ug/mmol	51.87 (22.62-127.56)	--
urinary MMP7 : creatinine, ug/mmol	--	2.63 (0.77-8.61)
age, years	67.5 (+/- 4.0)	67.9 (+/- 4.3)
male, n	236 (56%)	381 (51%)
eGFR, ml/min/1.73m^2	79.3 (+/- 17.0)	77.5 (+/- 18.6)
HbA1c, %	7.39 (+/- 1.0)	7.4 (+/- 1.1)
Duration of diabetes, years	7.57 (+/- 6.15)	8.25 (+/- 6.65)
Systolic blood pressure, mm Hg	133.2 (+/- 16.3)	133.5 (+/- 16.4)
Diastolic blood pressure, mm Hg	69.9 (+/- 9.3)	69.0 (+/- 9.1)
ACR, mg/mmol	1.09 (0.69-1.73)	1.18 (0.78-2.04)

Table 14. Characteristics of the cohorts in which urinary osteopontin (OPN) and metalloproteinase 7 (MMP7) were tested. Parameters are in mean and standard deviation or median and interquartile range as appropriate. N as given in the table.

Table 15: Correlation of OPN, MMP with other urinary renal markers

Spearman's rho	Osteopontin	MMP 7
Osteopontin	--	0.03
MMP 7	0.03	--
KIM 1	0.23*	0.1**
EGF	0.35*	0.08*
albumin	0.08	-0.04

Table 15. Correlation between urinary OPN and MMP7 and with other urinary markers of renal dysfunction. Correlation was calculated by Spearman's rho. * $p<0.05$, ** $p<0.01$

Table 16: Correlation of OPN and MMP with renal function

Pearson Correlation	Ln (urinary OPN : creatinine, ug/mmol)	Ln (urinary MMP7 : creatinine, ug/mmol)
eGFR, ml/min/1.73m^2	0.13*	0.05
Rate of change, ml/min/1.73m^2/year	0.03	-0.02

Table 16. Correlation of urinary OPN and MMP7 with baseline renal function (eGFR) and rate of change in renal function per year. OPN and MMP7 were rerferenced to urinary creatinine and logarithmized. Correlation was calculated by Pearson Correlation. * $p<0.05$

Figure 52: Visual correlation of OPN and MMP with renal function

A *B*

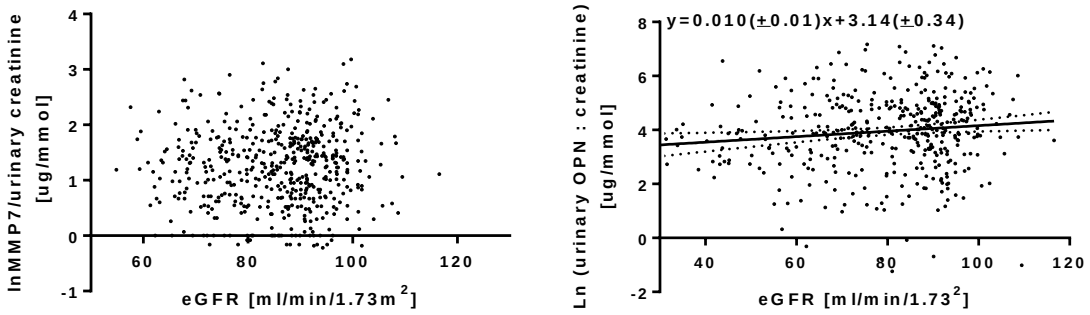

Figure 52. Scatterplot demonstrating the relationship between renal function and urinary MMP7 (n=748) or OPN (n=423) to creatinine ratios in patients from the Edinburgh Type 2 Diabetes Study. (A) Logarithmized urinary MMP7:creatinine did not but (B) logarithmized Osteopontin : creatinine did correlate with eGFR in the ET2D study cohort.

Table 17: Association of OPN and MMP with GFR after four years and mortality

Linear/Cox Regression		**Ln (urinary OPN : creatinine, ug/mmol)**	**Ln (urinary MMP7 : creatinine, ug/mmol)**
Year 4 GFR	**beta**	1.51	0.092
	CI	(0.253-2.761)	(-0.730-0.915)
death	**beta**	1.236	1.108
	CI	(0.906-1.687)	(0.958-1.282)

Table 17. For eGFR after four years univariable Linear Regression, and for death univariable Cox Regression was calculated. CI=95% confidence interval

3.3.4 uEGF in the ET2D study

uEGF and renal function in the ET2D study

Urinary EGF was measured in 978 patients from the ET2D study. The characteristics of the patient cohort before and after stratification into quartiles according to urinary EGF:creatinine ratio (uEGF:Cr) are listed in Table 18. While sex, age, HbA1c, duration of diabetes and systolic blood pressure did not differ between the quartiles, diastolic blood pressure was slightly but significantly lower in the quartile with lowest uEGF:Cr. Mean eGFR increased across the quartiles of uEGF:Cr. Indeed there was a highly significant correlation between uEGF:Cr and baseline eGFR (Figure 53). Although ACR tended to be higher in the lowest EGF-quartile (p=0.09), there was no significant association between uEGF and ACR (Figure 53). Urinary KIM-1:creatinine ratio (uKIM-1:Cr) increased with increasing quartiles of uEGF:Cr (Table 18). In a linear regression analysis, the association between log(uEGF:Cr) and eGFR at baseline remained significant after adjustment for other baseline variables (Table 19) The significant correlation between log(uEGF:Cr) and eGFR at four years did not persist after adjustment for eGFR and ACR, there was no association between log(uEGF:Cr) and the rate of decline in eGFR per year (Table 19).

Figure 53: Correlation of uEGF with renal function and albuminuria

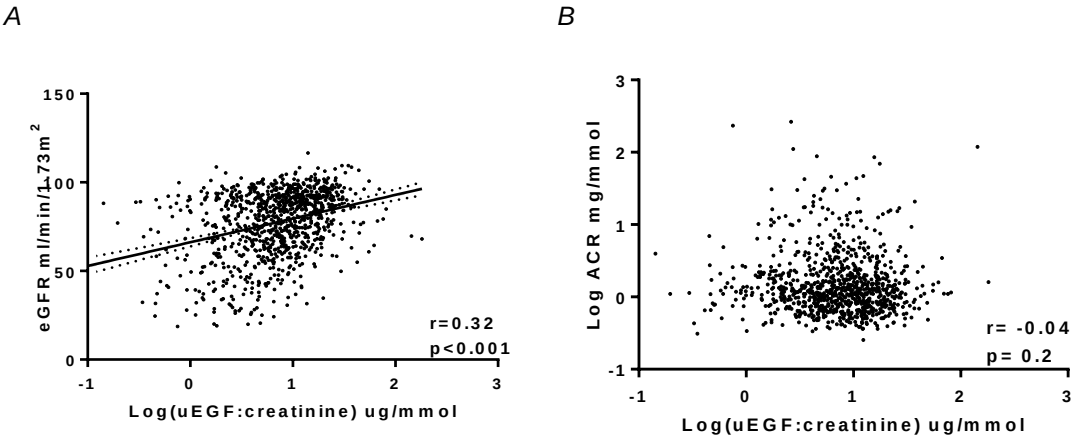

Figure 53. Urinary EGF:creatinine in the ET2D cohort correlated significantly with eGFR(A) but not ACR (B). The degree of correlation was assessed using Pearson correlation. In A) and C) a linear regression line is drawn with a 95 % confidence interval (dotted line).

Table 18: Characteristics of the ET2D study stratified into quartiles according to uEGF

	total (n=978)			Log(uEGF:creatinine) Quartiles												p-value
				I (n=244)			II (n=245)			III (n=245)			IV (n=244)			
male, n	517	%	53	125	%	51	131	%	53	138	%	56	123	%	50	0.56
age, years	67.84	(+/-)	4.23	68.14	(+/-)	4.30	68.17	(+/-)	4.29	67.61	(+/-)	4.00	67.46	(+/-)	4.30	0.15
eGFR, ml/min/1.73m^2	77.33	(+/-)	18.79	68.73	(+/-)	22.73	74.32	(+/-)	17.98	80.23	(+/-)	15.44	86.03	(+/-)	13.14	<0.01
HbA1c, %	7.39	(+/-)	1.10	7.43	(+/-)	1.09	7.41	(+/-)	1.06	7.32	(+/-)	0.98	7.42	(+/-)	1.25	0.72
Duration of diabetes, years	8.13	(+/-)	6.57	8.71	(+/-)	6.56	8.22	(+/-)	6.39	8.06	(+/-)	6.75	7.54	(+/-)	6.55	0.27
Systolic blood pressure, mm Hg	133.31	(+/-)	16.56	132.95	(+/-)	16.67	133.97	(+/-)	18.03	132.94	(+/-)	15.47	133.37	(+/-)	16.04	0.89
Diastolic blood pressure, mm Hg	68.95	(+/-)	9.05	67.44	(+/-)	9.30	69.59	(+/-)	9.17	69.61	(+/-)	8.48	69.15	(+/-)	9.12	0.02
ACR, mg/mmol	1.17	0.77-	2.02	1.28	0.88-	2.15	1.12	0.74-	2.17	1.13	0.72-	2.00	1.14	0.77-	1.74	0.09
urinary EGF : creatinine, ug/mmol	7.82	4.00-	13.38	2.18	1.36-	3.01	5.75	4.74-	6.67	10.43	8.97-	11.83	19.11	16.46-	24.81	<0.01
urinary KIM-1 : creatinine, ug/mmol	12.64	7.60-	22.88	11.29	7.60-	17.57	11.84	6.95-	22.47	12.67	7.63-	21.93	15.82	8.79-	32.83	<0.01
urinary Gpnmb : creatinine, ug/mmol	32.50	21.35-	50.96	32.28	20.03-	45.50	31.62	23.06-	49.30	33.03	20.61-	54.42	33.15	22.94-	53.73	0.31

Table 18. Detailed characteristics of the ET2D study cohort separated according to the quartiles of uEGF:creatinine ratio. Parameters are means (+/- standard deviation) or medians (inter-quartile range) as appropriate. p-values are calculated by ANOVA or Kruskal-Wallis test.

Table 19: Association of uEGF:creatinine ratio with eGFR at baseline, after four years and rate of decline in the ET2D study

	eGFR Baseline	eGFR 4 years	Rate of decline/year
Log (uEGF / creatinine) Unadjusted	13.4	11.9	-0.39
CI	(10.9 to 15.8)	(9.3 to 14.5)	(-0.95 to 0.16)
p-value	<0.001	<0.001	0.16
Log (uEGF / creatinine) adjusted*	11.8[a]	0.480[b]	--
CI	(9.4 to 14.2)	(-0.53 to 2.92)	--
p-value	<0.001	0.17	--

Table 19. Linear regression for eGFR at baseline, at 4 years and rate of decline per year with EGF:creatinine ratio as independent variable. [a]Adjustment for age, sex, BP(sys+dia), HbA1c, Duration of Diabetes, Log(ACR), Log(uKIM1:creatinine), Log(uGpnmb:creatinine). [b]Adjustment for the variables in model a and in addition baseline eGFR

uEGF and the risk of death in the ET2D study

Altogether 74 participants (7.6%) of the ET2D cohort died within four years. These participants were older, had a markedly lower baseline eGFR and uEGF:Cr, longer duration of diabetes and higher ACR and uKIM-1:Cr than those participants who survived (Table 8). In a Kaplan-Meyer analysis, participants in the lowest uEGF:Cr quartile had a significantly higher risk of death (Figure 54). In a Cox-Regression analysis the association between the quartile with lowest uEGF:Cr values and increased risk of death remained significant after adjustment for risk factors that were significantly different between death and survival (Table 20, Table 21).

Table 20: Characteristics of the ET2D study cohort are stratified for the endpoint death

	No (n=904)			Yes (n=74)			p-value
male, n	473	(%	52)	44	(%	59)	0.28
age, years	67.70	(+/-	4.18)	69.57	(+/-	4.42)	<0.01
eGFR, ml/min/1.73m^2	78.23	(+/-	18.07)	66.40	(+/-	23.57)	<0.01
HbA1c, %	7.39	(+/-	1.11)	7.39	(+/-	0.97)	0.98
Duration of diabetes, years	7.99	(+/-	6.47)	9.92	(+/)	7.46)	0.03
Systolic blood pressure, mm Hg	133.09	(+/-	16.37)	136.00	(+/-	18.64)	0.15
Diastolic blood pressure, mm Hg	69.10	(+/-	8.94)	67.05	(+/-	10.18)	0.09
ACR, mg/mmol	0.06	(-0.12	- 0.30)	0.21	(0.01	- 0.61)	<0.01
urinary EGF : creatinine, µg/mmol	0.90	(0.62	- 1.13)	0.74	(0.35	- 1.09)	0.02
urinary KIM-1 : creatinine, µg/mmol	12.23	(7.46	- 22.67)	15.68	(9.01	- 30.30)	0.02
urinary Gpnmb : creatinine, µg/mmol	32.09	(21.07	- 50.68)	37.53	(25.81	- 52.95)	0.09

Table 20. Characteristics of the ET2D study cohort are stratified for the endpoint death within four years. Parameters are expressed as mean (+/- standard deviation) or median (interquartile range). P-value for significant difference between the groups are given in the table and are calculated by T-test or Mann-Whitney test. Univariate and multivariate cox proportional hazards for death for the variables age, diastolic blood pressure, eGFR, ACR and KIM-1:creatinine and Gpnmb:creatinine in the ET2D cohort have already been published before (Conway, B. R., et al. (2012). "Measuring urinary tubular biomarkers in type 2 diabetes does not add prognostic value beyond established risk factors." Kidney Int 82(7): 812-818.).

Figure 54: Kaplan-Meyer Analysis of uEGF:Cr quartiles for the endpoint death in the ET2D study cohort

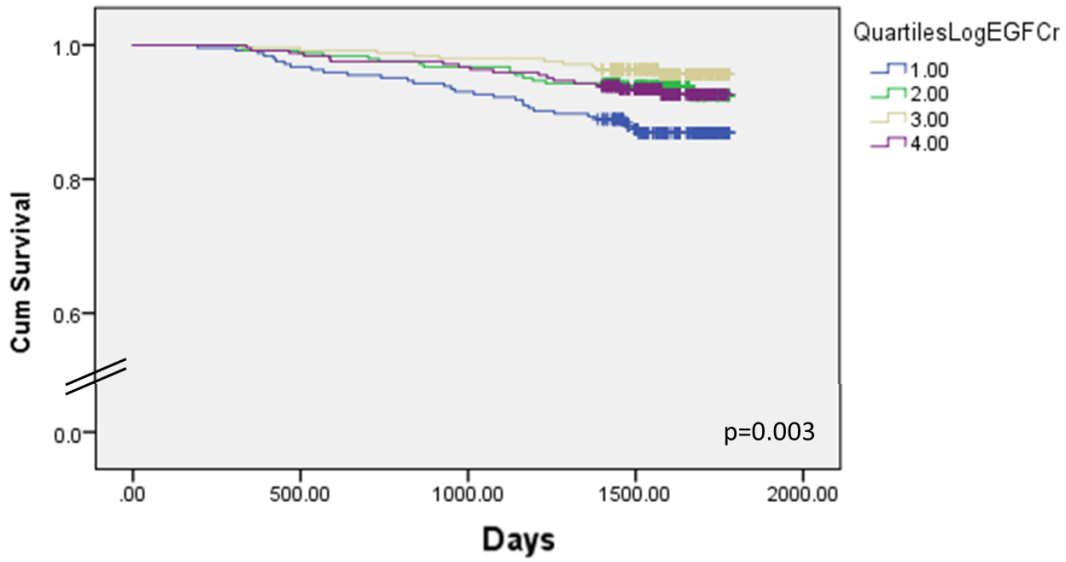

Figure 54. Kaplan-Meyer Analysis for the endpoint death in the ET2D-cohort stratified according to uEGF:creatinine quartiles. Study participants in the quartile with lowest uEGF:creatinine (blue=1) have a significantly increased risk of death during observation time.

Table 21: Association of uEGF with death in cox-regression analysis

	death
Log (uEGF:Cr) Quartile I, unadjusted	2.26
CI	(1.42 to 3.58)
p-value	0.001
Log (uEGF:Cr) Quartile I, adjusted*	1.76
CI	(1.04 to 2.96)
p-value	0.034

Table 21. Cox-Regression for the endpoint death with logarithmized uEGF:creatinine ratio as independent variable. In a multivariable analysis parameters which were significantly different for the outcome (refer to Table 8) were included: *=adjustment for age, eGFR, duration of diabetes, log (uKIM1:creatinine), log (ACR).

3.3.5 The ET2D subgroup of participants without "obvious renal damage"

From the 978 ET2D study participants with urinary EGF measurements, 642 (66%) had no indicators of chronic kidney disease at baseline as defined by eGFR≥60 ml/min/1.73m^2 and the absence of albuminuria (Stevens, Levin et al. 2013); this subgroup is referred to as "no obvious renal damage". A quarter of participants had eGFR<60 ml/min/1.73m^2, of those three quarters were normoalbuminuric. Ninety eight (10%) had an eGFR>60 ml/min/1.73m^2 and micro- or macroalbuminuria (Table 22).

The subgroup "no obvious renal damage" was stratified into tertiles according to log(uEGF:creatinine) (Table 23). eGFR was borderline significantly (p=0.051) higher in the tertile with highest uEGF:Cr and correlated weakly but significantly with uEGF:Cr (r=0.11, p<0.01). A significantly greater proportion of patients in the tertile with the highest uEGF:Cr had an ACR greater than 0.5 mg/mmol. The biomarkers urinary KIM-1 and Gpnmb were included in the subgroup analysis as they have only been characterized for the complete (albuminuric and non-albuminuric) ET2D study cohort before (Conway, Manoharan et al. 2012). Whilst Gpnmb:creatinine did not vary between tertiles, unexpectedly, uKIM-1:creatinine was significantly elevated in patients in the highest uEGF:Cr tertile.

Table 22: Classification of the ET2D cohort according to renal function and absence of albuminuria

ET2D (n=978)	eGFR ≥ 60 ml/min/1.73m^2 (n=740)	eGFR < 60 ml/min/1.73m^2 (n=238)
Normoalbuminuria	*642 (66%)*	175 (18%)
Micro-[1] /Macroalbuminuria[2]	98 (10%)	63 (6%)

Table 22. The ET2D study cohort was divided into four subgroups according to eGFR and the presence of proteinuria at baseline. [1] = ACR > 2.5 mg/mmol (males) and > 3.5 mg/mmol (females). [2] = ACR > 30 mg/mmol.

Table 23: Characteristics of the ET2D subgroup "without obvious renal damage"

	Mean (Total n=642)	T1 (n=214)	T2 (n=218)	T3 (n=210)	P
age, years	67.3 (+/- 4.1)	67.2 (+/- 4.1)	67.3 (+/- 3.9)	67.3 (+/- 4.4)	0.76
male, n	335 (52%)	112 (52%)	122 (56%)	101 (48%)	0.27
eGFR, ml/min/1.73m^2	85.9 (+/- 10.5)	84.8 (+/- 10.6)	85.7 (+/- 10.4)	87.3 (+/- 10.5)	0.51
HbA1c, %	7.33 (+/- 1.1)	7.33 (+/- 1.1)	7.34 (+/- 1.1)	7.33 (+/- 1.2)	0.99
Duration of diabetes, years	7.38 (+/- 5.9)	7.44 (+/- 5.4)	7.33 (+/- 5.9)	7.36 (+/- 6.4)	0.98
Systolic blood pressure, mm Hg	132.5 (+/- 15.3)	133.0 (+/- 15.9)	132.1 (+/- 15.0)	132.4 (+/- 15.0)	0.73
Diastolic blood pressure, mm Hg	69.3 (+/- 9.1)	69.1 (+/- 8.6)	69.9 (+/- 8.6)	68.8 (+/- 8.8)	0.57
ACR <0.5 / 0.5-1 / 1-2.5 (males) or 1-3.5 (females), mg/mmol, n (%)	466/72/104 (73%/11%/ 16%)	181/11/22 (85%/5%/ 10%)	148/26/44 (68%/12%/ 20%)	137/35/38 (65%/17%/ 18%)	<0.01
urinary KIM-1 : creatinine, µg/mmol	11.47 (7.19- 21.37)	10.06 (6.90- 14.72)	11.68 (7.17- 20.51)	14.16 (7.61-30.50)	<0.01
urinary Gpnmb : creatinine, µg/mmol	30.95 (20.12- 47.33)	30.62 (18.99- 40.28)	30.00 (20.19- 52.65)	31.54 (20.18- 49.13)	0.19

	Mean (Total n=642)	T1 (n=214)	T2 (n=218)	T3 (n=210)	P
urinary EGF : creatinine, µg/mmol	9.11 (4.60-15.24)	3.30 (1.90-4.60)	9.14 (7.55-10.99)	18.86 (15.53-24.16)	<0.01

Table 23. Characteristics of the 642 patients from the ET2D study who had no obvious renal damage at baseline (Table 22), classified according to tertiles of baseline uEGF:Cr. Parameters are in mean (+/-standard deviation) or median (interquartile range) as appropriate. Differences between groups were assessed by ANOVA, Kruskal-Wallis or χ^2 tests.p=p-value.

3.3.6 Association of urinary EGF, KIM-1 and Gpnmb with renal endpoints

During follow-up, 91 of the 642 patients (14%) developed an eGFR<60ml/min/1.73m^2 and 133 (21%) suffered from a rapid decline in eGFR (>5% per annum). Altogether 161 (25%) participants developed either endpoint, with 63 (10%) matching both criteria (Table 24). The frequency of endpoints was higher in patients from the lowest uEGF:Cr tertile.

When stratifying patients according to whether or not they developed the composite endpoint, there were significant differences in the baseline characteristics between the groups including: renal function (eGFR), age, sex, systolic blood pressure, duration of diabetes, HbA1c, ACR and uEGF:Cr and Gpnmb:creatinine (Table 25). Results were similar when stratification was performed for either outcome alone with ACR ceasing to be significantly different and KIM-1:creatinine being significantly different for incident CKD III (Table 26, Table 27). Kaplan-Meier analysis demonstrated that patients in the tertile with the lowest uEGF concentration at baseline had a significantly higher risk of developing an eGFR<60ml/min/1.73m^2 during the follow-up period, whilst patients in the tertile with lowest

Gpnmb:creatinine concentration had a significantly lower risk for incident CKD III. Conversely, tertiles of baseline ACR and uKIM-1 were not significantly associated with incident stage 3 CKD (Figure 55). Log(uKIM-1:creatinine), Log(uGpnmb:creatinine) Log(uEGF:creatinine) were significantly associated with incident eGFR<60ml/min/1.73m^2 (Table 28). Only uEGF:Cr had also a significant association with rapid decline in renal function or the combination of either outcome. After adjustment for baseline characteristics (eGFR, age, gender, ACR, HbA1c, duration of diabetes, systolic and diastolic blood pressure) the associations between uGpnmb:Cr and incident CKD III and the associations between uEGF:Cr and all outcomes remained significant.

Table 24: Classification of the ET2D subgroup "without obvious renal damage" by end points and log(uEGF:creatinine) tertiles

Log (uEGF:Cr) in tertiles	total (n=642)	T1 (n=214)	T2 (n=218)	T3 (n=210)	p-value
>5% decline in eGFR/year	133 (21%)	55 (41%)	42 (32%)	36 (27%)	0.076
Incident GFR<60ml/min/1.73m^2	91 (14%)	44 (48%)	26 (27%)	21 (23%)	0.004
Incident eGFR<60ml/min/1.73m^2 and/or >5% decline in eGFR/year	161 (25%)	73 (45%)	48 (30%)	40 (25%)	0.001

Table 24. Absolute frequency (percentage of total) of the outcomes decline in eGFR of more than 5% per year, incident eGFR<60ml/min/1.73m^2 and the combination of either or both end points in patients from the ET2D study subgroup with "no obvious renal damage" at baseline, stratified into log(uEGF:creatinine) tertiles. P-values for significant differences are given in the table and are calculated by χ^2 test.

Table 25: Stratification of the ET2D subgroup "without obvious renal damage" by the combination of the outcomes Incident eGFR<60ml/min/1.73m^2 or >5% decline in eGFR/year

Incident eGFR<60ml/min/1.73m^2 and/or >5% decline in eGFR/year	No (n= 481)	Yes (n= 161)	p-value
age, years	66.9 (+/- 4.1)	68.7 (+/- 3.9)	<0.01
male, n (%)	274 (57%)	61 (38%)	<0.01
eGFR, ml/min/1.73m^2	87.5 (+/- 10.0)	81.1 (+/- 10.6)	<0.01
HbA1c, %	7.27 (+/- 1.1)	7.54 (+/- 1.3)	0.02
Duration of diabetes, years	7.04 (+/- 5.8)	8.38 (+/- 6.2)	<0.01
Systolic blood pressure, mm Hg	131.9 (+/- 14.5)	135.1 (+/- 17.1)	0.03
Diastolic blood pressure, mm Hg	69.7 (+/- 8.6)	68.4 (+/- 9.3)	0.10
urinary EGF : creatinine, µg/mmol	10.17 (5.06-16.46)	6.42 (3.29-12.96)	<0.01
ACR <0.5 / 0.5-1 / 1-2.5 (males) or 1-3.5mg/mmol (females), n (%)	355/58/68 (74%/12%/14%)	111/14/36 (69%/9%/22%)	0.04
urinary KIM-1 : creatinine, µg/mmol	11.23 (6.85-21.72)	11.96 (8.08-21.24)	0.11
urinary Gpnmb : creatinine, µg/mmol	29.68 (19.13-46.39)	33.58 (23.59-52.40)	<0.01

Table 25. Characteristics of the ET2D study subgroup "without obvious renal damage" at baseline (Table 10) stratified according to whether they met the combined endpoint of incident eGFR<60ml/min/1.73m^2 and/or >5% decline in eGFR/year. Parameters are expressed in mean (+/- standard deviation) or median (interquartile range) as appropriate. P-values for differences between the groups are given in the table and are calculated by T-test, Mann-Whitney test or Chi^2 test.

Table 26: Stratification of the ET2D subgroup "without obvious renal damage" by the outcome >5% decline in eGFR/year

>5% decline in eGFR/year	No (n= 509)	Yes (n= 133)	p-value
age, years	66.9 (+/- 4.1)	68.7 (+/- 3.9)	<0.01
male, n	287 (56%)	48 (36%)	0.02
eGFR, ml/min/1.73m^2	86.5 (+/- 10.8)	83.8 (+/- 9.3)	<0.01
HbA1c, %	7.25 (+/- 1.0)	7.64 (+/- 1.4)	<0.01
Duration of diabetes, years	7.12 (+/- 5.86)	8.35 (+/- 6.18)	0.03
Systolic blood pressure, mm Hg	131.7 (+/- 14.5)	136.6 (+/- 17.4)	0.01
Diastolic blood pressure, mm Hg	69.5 (+/- 8.6)	69.0 (+/- 9.2)	0.56
urinary EGF : creatinine, µg/mmol	9.39 (4.84-16.17)	7.99 (3.45-13.62)	0.01
ACR <0.5 / 0.5-1 / 1-2.5 (males) or 1-3.5mg/mmol (females), n (%)	373/61/75 (73%/12%/15%)	93/11/29 (70%/8%/22%)	0.10
urinary KIM-1 : creatinine, µg/mmol	11.39 (6.91-20.79)	11.96 (8.04-22.27)	0.16
urinary Gpnmb : creatinine, µg/mmol	29.94 (19.85-46.27)	33.80 (22.07-55.30)	0.03

Table 26. Characteristics of the ET2D study subgroup "without obvious renal damage" (Table 10) at baseline are stratified according to the endpoint >5% decline in eGFR/year. Parameters are expressed in mean (+/- standard deviation) or median (interquartile range) as appropriate. P-values for differences between the groups are given in the table and are calculated by T-test,Mann-Whitney test or Chi^2 test.

Table 27: Stratification of the ET2D subgroup "without obvious renal damage" by the outcome Incident eGFR<60ml/min/1.73m^2

Incident eGFR<60ml/min/1.73m^2	No (n= 551)	Yes (n= 91)	p-value
age, years	67.0 (+/- 4.1)	69.1 (+/- 3.9)	<0.01
male, n	298 (54%)	37(41%)	0.02
eGFR, ml/min/1.73m^2	87.7 (+/- 9.7)	75.2 (+/- 9.0)	<0.01
HbA1c, %	7.32 (+/- 1.14)	7.39 (+/- 1.06)	0.57
Duration of diabetes, years	7.11 (+/- 5.72)	8.98 (+/- 7.0)	0.02
Systolic blood pressure, mm Hg	132.6 (+/- 15.1)	133.0 (+/- 16.1)	0.83
Diastolic blood pressure, mm Hg	69.8 (+/- 8.7)	67.1 (+/- 8.9)	<0.01
urinary EGF : creatinine, ug/mmol	9.52 (4.85-16.01)	6.16 (3.16-11.38)	<0.01
ACR <0.5 / 0.5-1 / 1-2.5 (males) or 1-3.5mg/mmol (females), n (%)	405/62/84 (74%/11%/15%)	61/10/20 (67%/11%/22%)	0.21
urinary KIM-1 : creatinine, ug/mmol	11.23 (6.92-20.60)	13.05 (8.40-27.13)	0.03
urinary Gpnmb : creatinine, ug/mmol	29.94 (19.52-46.37)	33.65 (24.85-56.54)	<0.01

Table 27. Characteristics of the ET2D study subgroup (Table 10) are stratified according to the endpoint incident eGFR<60ml/min/1.73m^2. Parameters are expressed in mean (standard deviation) or median (interquartile-range) as appropriate. P-values for differences between the groups are given in the table and are calculated by T-test, Mann-Whitney test or Chi^2 test.

Figure 55: Kaplan-Meier analysis for the endpoint Incident eGFR<60ml/min/1.73m^2 in the ET2D subgroup "without obvious renal damage"

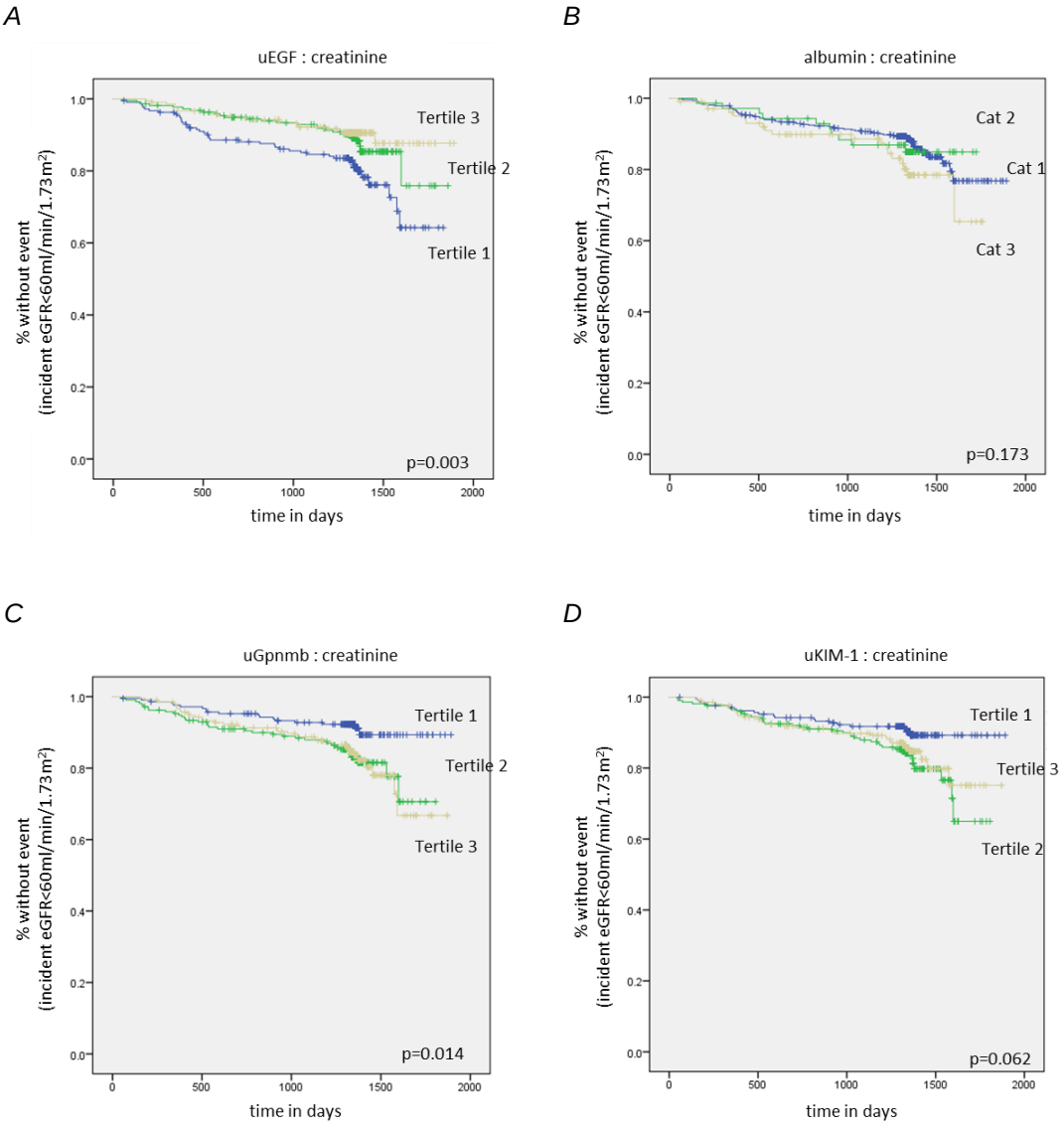

Figure 55. Kaplan-Meier analysis for the outcome "incident eGFR<60ml/min/1.73m^2" in the ET2D-subgroup "without obvious renal damage" at baseline (Table 10) stratified to (A) uEGF:creatinine, (C) uGpnmb:creatinine and (D) uKIM-1:creatinine tertiles. (B) ACR was stratified into the categories <0.5 (Cat1)/ 0.5-1 (Cat2) / 1-2.5 (males) or 1-3.5mg/mmol (females) mg/mmol (Cat3). p-value as indicated.

Table 28: Association of urinary EGF, KIM-1 and Gpnmb with renal outcomes in the ET2D subgroup "without obvious renal damage"

	≥ 5% decline in eGFR/year	Incident eGFR<60ml/min/1.73m^2	combined endpoints 4 years
Log (KIM-1 / creatinine) unadjusted	1.344	1.770	1.358
95% CI	(0.827 to 2.813)	(1.023 to 3.062)	(0.860 to 2.144)
p-value	0.233	0.041	0.189
Log (KIM-1 / creatinine) adjusted*	0.905	1.910	1.037
95% CI	(0.524 to 1.562)	(0.983 to 3.708)	(0.614 to 1.751)
p-value	0.719	0.056	0.892
Log (Gpnmb / creatinine) unadjusted	2.105	3.120	2.435
95% CI	(1.050 to 4.219)	(1.392 to 6.996)	(1.263 to 4.697)
p-value	0.036	0.006	0.008
Log (Gpnmb / creatinine) adjusted*	1.038	3.058	1.522
95% CI	(0.462 to 2.332)	(1.034 to 9.044)	(0.689 to 3.363)
p-value	0.928	0.043	0.299
Log (uEGF / creatinine) unadjusted	0.542	0.487	0.450
95% CI	(0.349 to 0.840)	(0.297 to 0.799)	(0.296 to 0.683)
p-value	0.006	0.004	<0.001
Log (uEGF / creatinine) adjusted*	0.444	0.480	0.382
95% CI	(0.273 to 0.722)	(0.256 to 0.899)	(0.236 to 0.618)
p-value	0.001	0.022	<0.001

Table 28. Binary logistic regression for the outcomes decline in eGFR of more than 5% per year, incident eGFR<60ml/min/1.73m^2 and the combination of either outcome with logarithmized KIM-1:creatinine, Gpnmb:creatinine or uEGF:creatinine ratio as independent variables. *In a multivariable analysis the following parameters were included: sex, age, eGFR, BP (systolic+diastolic), HbA1c, duration of diabetes, ACR. CI = Confidence interval

3.3.7 uEGF and risk prediction models

A key aim was to assess whether the addition of log (uEGF:creatinine) improves prediction of renal outcomes above and beyond traditional risk factors. Hence a reference model that included traditional risk factors (age, gender, eGFR, ACR, duration of diabetes, HbA1c, systolic and diastolic blood pressure) was compared to a model that included these risk factors, but in addition incorporated log (uEGF:Cr). To test how well the two models fitted the data the Homser-Lemeshow goodness of fit analysis was used. Patients were stratified into deciles according to their predicted risk calculated by the model. The extent of the differences between the observed risk and the predicted risk for every decile defines the calibration quality of the model. The model is well calibrated if the difference between calculated and observed risk is not significant ($p>0.05$).The Homser-Lemeshow test statistic (Kundu, Aulchenko et al. 2011) confirmed that all models fulfilled the goodness of fit criteria as the null-hypothesis (the "model does not fit") was rejected (Table 29, Figure 56).

Compared to the reference model the addition of log (uEGF:Cr) resulted in a small increase in AUC-ROC (Table 30), which was not significant (e.g. $p=0.07$ for the combined end-point, Figure 57).

Calculating the Integrated Discrimination Improvement (IDI)(Pickering and Endre 2012) there was a significant increase of IDI when log (uEGF:Cr) was added to the reference models for the endpoint rapid decline in eGFR and the combined outcome (0.017 and 0.023 respectively). The differences resulted mainly from an increase in IDI_{events} (0.014 and 0.017 respectively). The addition of log(uEGF:Cr) did not

significantly alter the IDI for incident eGFR<60ml/min/1.73m^2 alone (Table 31, Figure 58).

Table 29: Hosmer-Lemeshow goodness of fit analysis of the prediction models with or without EGF for renal outcomes in the ET2D study

p-value	≥ 5% decline in eGFR/year	Incident eGFR<60ml/min/1.73m^2	combined endpoint 4 years
ROC-AUC REF	0.166	0.95	0.177
ROC-AUC REF+EGF	0.704	0.99	0.300

Table 29. Hosmer-Lemeshow goodness of fit analysis tests the calibration (details provided in the text) of the reference model (REF) including sex, age, eGFR, BP(systolic+diastolic), HbA1c, Duration of Diabetes, ACR(logarithmized) and the reference model additionally including Log(uEGF:Cr) for all outcomes by comparing the predicted and the observed risk. All patients are stratified into deciles according to their predicted risk calculated by the respective model. P-values above 0.05 indicate that the models are well calibrated. ROC-AUC = area under the receiver operating characteristic curve, REF=refrence model

Figure 56: Graphical illustration of the Hosmer-Lemeshow goodness of fit analysis

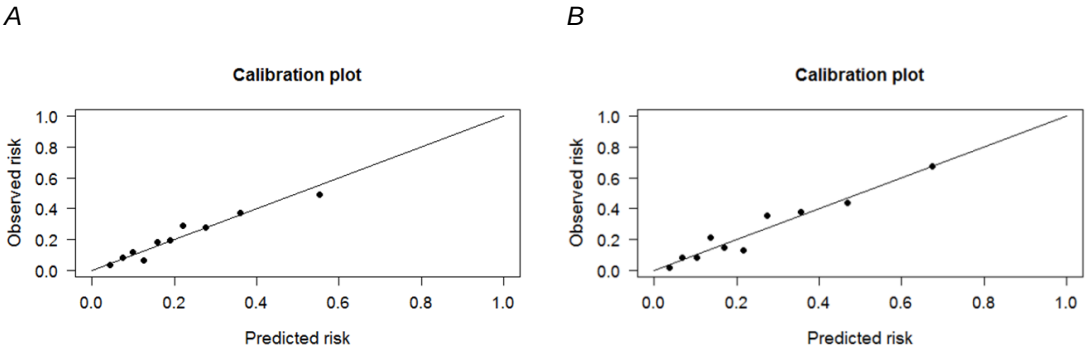

Figure 56. Graphical illustration of the calibration plots for the combined endpoints from the Hosmer-Lemeshow goodness of fit analysis for the reference model (A) without [REF] and (B) with uEGF [REF+EGF]. Patients are stratified into deciles according to their predicted risk calculated by the respective model.

Table 30: ROC-AUC with and without uEGF for renal outcomes in the ET2D study

	≥ 5% decline in eGFR/year	Incident eGFR<60ml/min/1.73m^2	combined endpoint 4 years
ROC-AUC EGF	0.570	0.605	0.601
(95% CI)	(0.530 to 0.608)	(0.566 to 0.643)	(0.562 to 0.639)
ROC-AUC REF	0.722	0.853	0.761
(95% CI)	(0.673 to 0.771)	(0.811 to 0.896)	(0.718 to 0.804)
ROC-AUC EGF+REF	0.740	0.855	0.777
(95% CI)	(0.693 to 0.787)	(0.812 to 0.897)	(0.735 to 0.818)

Table 30. Analysis of the Receiver operating characteristics – area under curve (ROC-AUC) of log(uEGF:creatinine), a reference model (REF) including sex, age, eGFR, BP (sys+dia), HbA1c, Duration of Diabetes, ACR (logarithmized) and the combination of both for the renal outcomes in the ET2D subgroup "without obvious renal damage". CI =Confidence Interval.

Figure 57: ROC graph with and without uEGF for the combined renal endpoint

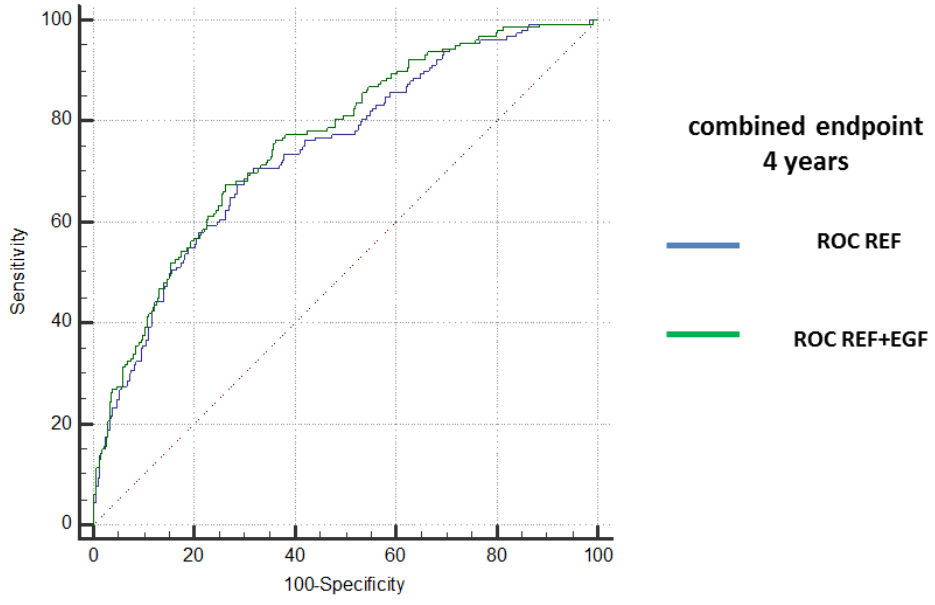

Figure 57. Graphical illustration of the receiver operating charcteristic (ROC) curve comparing the reference model without (ROC REF, green line) and with log(uEGF:creatinine) (ROC REF+EGF, blue line) for the combined endpoint in the ET2D subgroup "without obvious renal damage" at baseline.

Table 31: Integrated Discrimination Improvement (IDI) for prediction models including uEGF compared to model without uEGF for renal outcomes of the ET2D study

	≥ 5% decline in eGFR/year	Incident eGFR<60ml/min/1.73m^2	combined endpoint 4 years
IDI (CI)	0.017 (0.004 to 0.030)	0.011 (-0.001 to 0.023)	0.023 (0.009 to 0.037)
Relative IDI	14.8%	4.61%	13.5%
IDI (events)	0.014 (0.001 to 0.026)	0.009 (-0.002 to 0.021)	0.017 (0.005 to 0.030)
IDI (non-events)	0.003 (-9e-04 to 0.008)	0.002 (-0.001 to 0.004)	0.006 (1e-04 to 0.012)

Table 31. Absolut and relative integrated discrimination improvement (IDI) and IDI for events and non-events when log(uEGF:creatinine) is added to the reference model including sex, age, eGFR, BP(systolic+diastolic), HbA1c, Duration of Diabetes, ACR(logarithmized) . CI = 95% Confidence Interval. IDI is calculated for all renal outcomes in the ET2D subgroup "without obvious renal damage" at baseline.

Figure 58: Graphical illustration of the IDI_{events} and $IDI_{non\text{-}events}$ comparing the reference model without and with uEGF

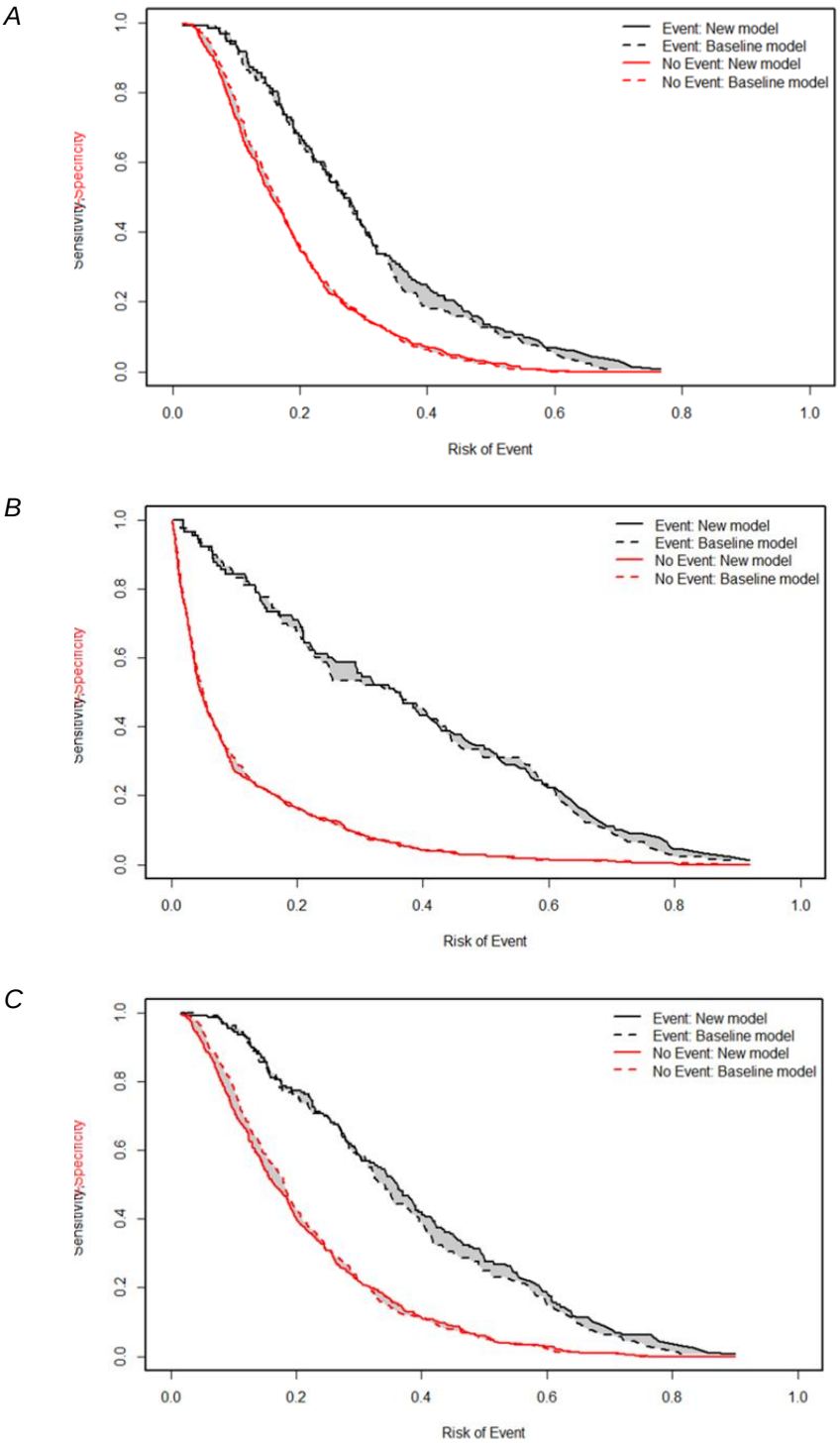

Figure 58. Graphical illustration of the Integrated discrimination improvement for events (IDI_{events}, black) and for non-events ($IDI_{non\text{-}events}$, red) comparing the reference model (REF) without (dotted line) and with log(uEGF:creatinine) (solid line) for the endpoints >5% decline in eGFR/year (A), Incident eGFR<60ml/min/1.73m^2 (B)and the combination of both endpoints after four years (C) in ET2D subgroup “without obvious renal damage” at baseline.

3.3.8 Discussion

In this chapter several candidate urinary biomarkers identified from patterns of gene expression or urinary peptidomics in the Cyp1a1mRen2 rat model of DN were tested for their ability to predict renal outcomes in patients with type 2 diabetes.

MMP7

The rationale for choosing MMP7 was based on the molecular and immunohistochemistry findings from this group(Conway, Betz et al. 2014) and a potential role for MMP7 in the homeostasis of ECM synthesis and degradation in diabetic nephropathy has been described before (Maahs, Siwy et al. 2010, Xu, Xiao et al. 2014, Mischak, Delles et al. 2015). However, there are conflicting results about MMP-7 expression in renal tissue in diabetic nephropathy. McLennan et al. demonstrate reduced molecular expression in both rodent STZ-induced and human DN (n=7)(McLennan, Kelly et al. 2007), whilst Woroniecka et al. and Ju et al. demonstrate an increased molecular MMP7 expression in renal biopsies of patients with DN (n=44 and n=17 respectively)(Woroniecka, Park et al. 2011, Ju, Nair et al. 2015). . In the current study, the uMMP7:creatinine ratio did not correlate with either baseline renal function, rate of change in renal function or albuminuria in patients with type 2 diabetes. Ban et al. demonstrate an increase in serum MMP7 with decreasing eGFR, increasing albuminuria or increasing cardiac dysfunction(Ban, Twigg et al. 2010). A possible explanation for the lack of association with urinary MMP7 and renal parameters might be that urinary MMP7 concentration is derived from two sources, serum and kidney. In albuminuric patients the disruption of the glomerular filtration barrier might cause increased excretion of MMP7. Increased

serum MMP7 in DN patients (Ban, Twigg et al. 2010, Kadoglou, Sailer et al. 2014) and decreased renal MMP7 could compensate for each other in urinary excretion.

There was a weak positive correlation of MMP7 with EGF. In the kidney, MMP7 is mainly expressed in tubular cells(He, Tan et al. 2012). Therefore, reduced MMP7 excretion might reflect a loss of renal tubular mass similar to EGF. However this hypothesis requires further experimental and clinical proof.

Osteopontin

Osteopontin (OPN) was weakly positively correlated with baseline renal function. This finding was unexpected as OPN is known to be involved in the genesis of albuminuria (Lorenzen, Shah et al. 2008) and the inflammatory response in DN(Zhang, Shek et al. 2010). Expression of the OPN gene is upregulated in the renal cortex of patients with DN compared to healthy donors (Woroniecka, Park et al. 2011, Ju, Nair et al. 2015). In patients with type 1 and type 2 diabetes elevated serum levels of OPN have been associated with an increased risk of diabetic nephropathy and rapid decline in renal function (Gordin, Forsblom et al. 2014, Looker, Colombo et al. 2015). A very weak positive correlation between urinary OPN and eGFR has previously been reported in a large cohort of patients with type 2 diabetes (O'Seaghdha, Hwang et al. 2013). As it has been demonstrated in the previous chapter, urinary peptide fragments of OPN are increased in the renal injury group of the Cyp1a1mRen2 DN model. One explanation for this discrepancy between human DN and rat models might be due species related differences as has been reported previously for collagen isoforms (Siwy, Zoja et al. 2012). Urinary OPN is reduced in patients with IgA-Nephropathy, however a 34 kD fragment resulting from cleavage

by serine proteases such as thrombin is increased compared to healthy controls (Gang, Ueki et al. 2001). This fragment was only detected by immunoblot but not by ELISA. Therefore, serine protease activity which is altered in DN (Kolset, Reinholt et al. 2012) might be reducing the non-fragmented urinary OPN concentration in diabetic nephropathy.

Vascular endothelial growth factor A (VEGF-A)

While most studies have focused on biomarkers that are excreted at higher levels in the urine of patients with DN compared to controls, those that are down-regulated may be more likely to reflect intrinsic renal pathophysiology than alterations in passage across a damaged glomerular filtration barrier.

VEGF-A is an attractive candidate biomarker, as expression of the VEGF-A gene was down-regulated in the renal cortex of the Cyp1a1mRen2 model(Conway, Rennie et al. 2012) and in patients with DN compared to healthy donors(Woroniecka, Park et al. 2011, Ju, Nair et al. 2015). Furthermore, VEGF-derived peptides had decreased abundance in patients with DN versus controls (previous chapter). Unfortunately, no signal from the parent protein could be detected by the commercial ELISA used, despite the standards working effectively. It cannot be excluded that ELISA kits from other companies targeting other epitopes of the protein might result in a detectable signal.

Rationale for EGF from previous rodent and human studies

Similar to VEGF EGF is down-regulated in the Cyp1a1mRen2 DN model on a transcriptional level and urinary peptides of EGF are reduced (previous chapter).

A reduction of EGF levels in tissue and urine has also been reported in other rodent models of chronic kidney disease (Thulesen, Jorgensen et al. 1997, Kelly, Cox et al. 2002, Siwy, Zoja et al. 2012). Consistent with the results from the animal models, a reduction in renal gene and protein EGF expression has also been observed in the renal tubulointerstitium in patients with DN (Lindenmeyer, Kretzler et al. 2007, Woroniecka, Park et al. 2011).

EGF is constitutively produced in the kidney by tubular cells, therefore urinary EGF concentration could be a surrogate for functional tubular mass. Lindenmeyer et al. hypothesized that since EGF acts as a growth factor on tubular cells the reduced EGF production in DN might also be an important pathophysiological factor for progressive renal damage(Lindenmeyer, Kretzler et al. 2007). This is consistent with the focal reduction in EGF expression in atrophic and injured tubules observed in the diabetic and hypertensive Cyp1a1mRen2 rats (previous chapter).

EGF correlates with renal function and is associated with mortality in the ET2D cohort

The uKIM-1:creatinine ratio increased progressively across quartiles of uEGF:Cr (Conway, Manoharan et al. 2012). The correlation between uEGF and KIM-1 remained significant even after removal of urinary creatinine as a correction factor ($r=0.341$ $p<0.001$, Spearman correlation). This was unexpected, given the inverse correlation between EGF and KIM-1 in rodent renal tissue. There is at the moment no explanation for this paradoxical correlation but possibly the presence of higher uEGF indicates more renal mass and tubular cells that can - upon damage - express KIM-1 as an early marker of injury(Bonventre 2009).

There was a strong positive correlation between uEGF:creatinine and renal function in the ET2D cohort, but not with ACR. Several studies have investigated the urinary concentration of EGF in patients with DN, almost always reporting a robust positive correlation with renal function but with conflicting results concerning the correlation with albuminuria (Dagogo-Jack, Marshall et al. 1989, Mathiesen, Nexo et al. 1989, Lev-Ran, Hwang et al. 1990, Kawaguchi, Kamiya et al. 1993, ter Meulen, Bilo et al. 1994, Torffvit, Jorgensen et al. 1998). However, all these studies had only limited patient numbers.

None of the studies aforementioned had evaluated the use of uEGF:creatinine as a prognostic biomarker. Whilst for the first time uEGF:creatinine has been demonstrated as a potential independent risk factor for all-cause mortality - what needs confirmation in larger study cohorts - uEGF:creatinine was not associated with the rate of decline in eGFR in the ET2D study cohort. Recently, Ju et al. demonstrated that the uEGF:creainine ratio predicts a marked decline in renal function (40% within 2-4 years) and end-stage renal disease in three large cohorts comprising patients with moderately to severely advanced CKD defined by reduced GFR and/or albuminuria(Ju, Nair et al. 2015). In contrast to the present study, there was a wide spectrum of aetiologies for CKD (including 50% with IgA Nephropathy) with only a minority of patients suffering from DN. The endpoints utilized in the study from Ju et al. were not applicable to the current study because after 4 years in the ET2D cohort only 4 patients (0.4%) had ESRD and 41 patients (4.2%) had a decline in eGFR of more than 40%.

EGF is associated with renal functional decline in normoalbuminuric ET2D patients

While 24% of patients in the ET2D study had eGFR<60ml/min/1.73m^2, only a quarter (6%) of these had evidence of micro-/macroalbuminuria. Hence, it is imperative to find prognostic biomarkers that predict the development of renal disease in those patients with type 2 diabetes and no microalbuminuria(Retnakaran, Cull et al. 2006). To this end the potential of uEGF:Cr to predict renal outcomes in the subgroups of 642 patients with eGFR>60ml/min/1.73m^2 and no albuminuria at baseline was assessed.

In these 642 patients with preserved renal function, the positive correlation of uEGF:creatinine ratio and baseline eGFR in patients was much weaker ($r=0.11$, $p<0.01$) than before when all participants with a broader range of renal function were included. The incidence of end-stage renal disease was too low to be used as a renal end-point, therefore incidence of new onset CKD (eGFR<60 ml/min/1.73m^2) was employed as a key outcome measure. One caveat about using an eGFR threshold as a renal endpoint is that those starting with an eGFR of, for example, 64 ml/min/1.73m^2 are much more likely to meet the end-point than those starting at 85 ml/min/1.73m^2. This is consistent with the fact that the mean eGFR in those developing CKD III was 75.2 ml/min/1.73m^2 versus 87.7 ml/min/1.73m^2 in those whose renal function remained in the normal range. Hence an additional endpoint based on rate of decline in renal function was used. The endpoint of a >5% decline in eGFR/year has been used as an indicator for renal deterioration in addition to incident CKD III by previous studies (Park, Shlipak et al. 2012, Driver, Shlipak et al. 2014) and the incidence rates in the current study were concordant with those reported in the Multi-Ethnic Study of Atherosclerosis.(Park, Shlipak et al. 2012)

When the cohort was stratified according to renal endpoints, as anticipated, classical risk factors for renal deterioration in patients with type 2 diabetes were higher in those who progressed (Retnakaran, Cull et al. 2006). However, albumin was relatively poor at predicting either rate of decline in renal function or new onset eGFR <60 ml/min/1.73m^2. This again highlights the importance of identifying additional predictors of renal outcomes in patients with type 2 diabetes and normoalbuminuria. Moreover that might reflect the heterogeneity of renal injury in type 2 diabetes with hypertension, dyslipidaemia and loss of autoregulation being essential additional contributors to renal damage besides hyperglycaemia (Mogensen 2003). These additional renal risk factors can be found with variable severity in T2D patients. Nosadini al. demonstrate in a group of patients with type 2 diabetes who had all a similar level of renal function and microalbuminuria, that the extent of glomerular damage varied considerably within the group and was a risk for renal deterioration(Nosadini, Velussi et al. 2000). Recently, Fufaa at al. demonstrated in Amercian Indians with type 2 diabetes that a histological glomerulopathy index is independent from albuminuria for prediction rapid renal function loss (Fufaa, Weil et al. 2016). Both aforementioned pathological studies did not investigate tubulointerstitial fibrosis (TIF) in detail though the severity of TIF can be an even more useful indicator for renal deterioration in DN than glomerular observations(Gilbert and Cooper 1999). EGF as a marker of tubular mass might provide precious information about the extent of tubular cell loss due to TIF and complement albuminuria especially in patients with type 2 diabetes.

Indeed, in the current study the lowest tertile of uEGF:creatinine but not microalbuminuria identified patients to be at risk of incident eGFR

<60ml/min/1.73m^2. uEGF was also associated with the combined outcome of incident CKD or rapid decline in renal function independently from albuminuria, eGFR and other risk factors.

The addition of uEGF/Cr ratio to a panel of established risk factors resulted only in a very modest increase in the ROC-AUC. However the comparison between ROC-AUCs of prediction models with and without the potential risk factor might be insensitive for small but actually significant improvements especially if the underlying model is already strong (Cook 2008, Parikh and Thiessen-Philbrook 2014). The index of discrimination improvement (IDI) is an alternative metric that summarizes the changes in calculated risk for every individual with event (IDI_{event}) and without event ($IDI_{non\text{-}event}$) when applying the new prediction model compared to the old model. The total IDI is the sum of IDI_{event} and $IDI_{non\text{-}event}$. However there is no established criterion regarding how a significantly positive increase in IDI should be statistically interpreted (Parikh and Thiessen-Philbrook 2014). For this, the relative IDI is calculated that is the absolute IDI divided by the discrimination slope of the reference model. It has been suggested that an IDI is relevant if the relative IDI > 1/number of variables in the reference model(Parikh and Thiessen-Philbrook 2014). In the current study, this is the case for the endpoints rapid decline in eGFR and the combination of rapid decline and incident CKD III (14.8% and 13.5% > 12.5%). In conclusion, although by logistic regression analysis uEGF:Cr was highly significantly associated with all three endpoints after adjustment for known risk factors, it seems to add predictive value beyond the reference model only for the endpoints of rapid decline in eGFR and the combined outcome.

uKIM-1 and uGpnmb in the normoalbuminuric ET2D cohort with eGFR>60 ml/min/1.73^2

Kidney injury molecule 1 and Glycoprotein Transmembrane nmb have been characterized in the ET2D cohort before and no prognostic value in addition to established risk factors had been found (Conway, Manoharan et al. 2012). However, their potential predictive value has not been investigated in the subgroup of patients with normoalbuminuria and preserved renal function. In Kaplan-Meier analysis urinary KIM-1:Cr did not predict renal decline. The failure of KIM-1 to be a relevant predictor of decline in eGFR is in line with most of the previous reports (Conway, Manoharan et al. 2012, Park, Shlipak et al. 2012, O'Seaghdha, Hwang et al. 2013). In both Kaplan-Meier analysis and binary logistic regression uGpnmb was associated with incident eGFR<60 ml/min/1.73^2 even after multivariate adjustment. For the first time, elevated urinary Gpnmb:creatinine is demonstrated to be an independent predictive marker for renal deterioration in patients with type 2 Diabetes. As a marker of renal repair(Li, Castano et al. 2010) elevated uGpnmb might indicate increased tubular damage/fibrosis that is an important predictor of renal function (Gilbert and Cooper 1999).

Limitations

Some limitations for the ET2D cohort and the endpoints need to be mentioned. Since biopsies were rarely performed in the ET2D study patients, the histological cause for decline in renal function and incident CKD cannot be determined. For assessment of decline in renal function only two timepoints for eGFR measurement were used whereas linear regression based on multiple eGFR measurements may provide a more accurate measure of rate of decline in renal function. Additionally, only a

single measurement of uEGF was assessed since 4 year follow up urinary samples had not been available. Those who died were not included in the endpoint calculations and this might have introduced survival bias, though the mortality was rather low (7.6%). Finally the homogeneity of the study cohort (Caucasians, type 2 diabetes, older age) restricts generalization of the marker uEGF to other patient groups.

Since a loss of 5% eGFR per year resulted in a minimum loss of GFR of 12 ml/min/1.73m^2 during a four year period for patients with a baseline eGFR of 60 ml/min/1.73m^2, all study participants who matched the endpoint fulfilled the NICE (National Institute for Healthcare and Excellence) criteria for progression of CKD from 2008: In the version of 2008 one definition for progressive CKD is "a decline in eGFR of >10 ml/min/1.73m^2 within 5 years" (NICE 2014). However, in the NICE guideline for CKD from 2014 this definition and the term "progressive" CKD have been removed. The new definition refers to "accelerated progression of CKD" as a "sustained decrease in GFR of 25% or more and a change in GFR category within 12 months or a sustained decrease in GFR of 15 ml/min/1.73 m2 per year" (NICE 2014). Therefore the chosen endpoint of 5% loss in eGFR per year does not single out patients with "accelerated progression of CKD" as defined by the new NICE guideline from 2014. However, the chosen endpoint has been used for progression of CKD in studies before and had been associated with increased risk for CVD outcomes (Shlipak, Katz et al. 2009, Park, Shlipak et al. 2012, Driver, Shlipak et al. 2014).

3.3.9 Summary

In this chapter a panel of biomarker candidates generated by a rodent model of DN were examined for their utility in predicting renal outcomes in patients with type 2 diabetes. The laborious process of biomarker-selection and its correlation with the amount of time, effort and materials/samples utilized has been nicely illustrated by Leichtle et al. as the "biomarkers bottleneck"(Leichtle, Dufour et al. 2013) (Figure 59). From the biomarker candidates tested, only one, uEGF:Cr, could be identified to be of potential clinical value but requires validation in in other populations, including those with type 1 diabetes.

Figure 59: "Biomarker bottleneck"

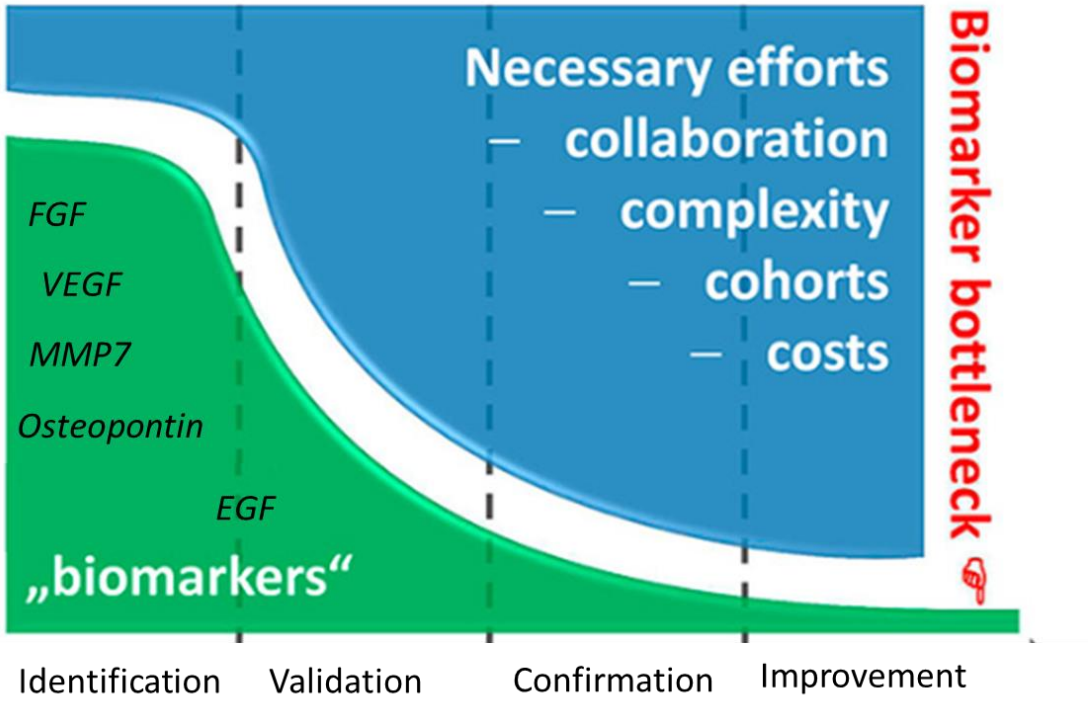

Figure 59. Steps in of biomarker discovery: Each stage in the biomarker development process results in a significant loss of candidates and an exponential increase in time, sample cohorts, epidemiological calculation and cost. Adapted from Leichtle et al., SMW, 2013.

3.4 Urinary Extracellular Vesicles

3.4.1 Introduction

The last chapter focused on the translational validation of biomarker candidate proteins by conventional measurement techniques (ELISA). The proteins had been selected based upon findings from the transcriptome and urinary peptidome of the Cyp1a1mRen2 DN model. Analysis of the ontology categories that were enriched with genes up-regulated in the kidney during injury phase compared to baseline identified the exosome pathway to be amongst the most significantly enriched (Table 32). Extracellular vesicles categories were also highly enriched with genes related to urinary peptides with increased relative abundance during injury phase in the Cyp1a1mRen2 model and from patients with DN (Table 33).

Extracellular vesicles are defined by their size (1µm) and can be further divided into exosomes (20-100nm) and microvesicles (100-1000nm) and in their cellular generation process (see Introduction section). Though they are present at high concentrations in all body fluids the established process for measuring EVs required hitherto large sample volumes (e.g. several hundred millilitres of urine), long preparation time (e.g. several hours for exosomes) and specialized equipment (Ultracentrifuge). Therefore, their application as biomarkers in large cohorts like DM patients was limited as this necessitates a brief, high-throughput methodology.

The nanoparticle tracking analysis (NanoSight LM10) and flow-cytometry using acoustic focusing (Attune Flow Cytometer) might allow quick and reproducible quantification of EVs in small samples volumes.

The aim of following chapter is to explore the possibilities but as well the potential pitfalls of these novel techniques for EV measurement. After being established in the Cyp1a1mRen2 DN model the methodology will be tested in human samples that had been collected in the Diabetes and Renal Medicine outpatients clinics (Renal DiseaseS (RDS) Study) and (for exosomes) in samples from the ET2D cohort (Figure 60).

Finally, when measurements in the following paragraphs are carried out by NanoSight LM 10 on unstained urinary specimens the appropriate term to use would be "total urinary unlabelled exosome-like particles concentration" since no confirmatory electron-microscopy was performed. For the cause of simplicity and clarity the term "total exosome concentration" will be used with the reader reminded of the limitation mentioned here.

Table 32: Ontology analysis from genes up-regulated in the Cyp1a1mRen2 DN model

Ontology	gene count	%	FDR-adjusted p-value
extracellular matrix	30	8.356546	5.39E-17
proteinaceous extracellular matrix	23	6.406685	2.01E-07
extracellular space	55	15.32033	3.25E-07
cell surface	33	9.192201	5.42E-06
extracellular exosome	84	23.39833	2.48E-05

Table 32. "Top 5" (according to p-value) list of ontology categories which are most significantly overrepresented amongst genes that are up-regulated in the kidney in the injury cohort compared to control using DAVID and QuickGo ontology databases. The extracellular exosome category was of interest as it accounted for the most gene counts of all categories. Only categories with $p<0.01$ and a gene count > 20 were retained. FDR = false discovery rate calculated with **Benjamini-Hochberg formula.**

Table 33: Ontology analysis from genes related to urinary peptides with increased relative abundance in rodent and human DN

A

pathway ID	Ontology	gene count	FDR-adjusted p-value
GO:0005615	extracellular space	24	2.49E-21
GO:0005576	extracellular region	31	5.48E-20
GO:0044421	extracellular region part	24	3.66E-14
GO:0072562	*blood microparticle*	*7*	*3.28E-10*
GO:0031988	*membrane-bounded vesicle*	*15*	*0.0000184*

B

pathway ID	Ontology	gene count	FDR-adjusted p-value
GO:0005615	extracellular space	30	5.37E-26
GO:0070062	*extracellular exosome*	34	2.89E-22
GO:0072562	*blood microparticle*	14	2.34E-20
GO:0031988	*membrane-bounded vesicle*	34	1.84E-19
GO:0044421	extracellular region part	32	6.25E-16

Table 33. List of ontology categories which are most significantly enriched for genes related to urinary peptides with increased abundance from the injury group of A) the Cyp1a1mRen2 DN model and B) from human DN. The STRING v10.0 database (www.string-db.org) and QuickGo ontology database are used. Extracellular vesicle pathways are among the top five when sorted for lowest false discovery rate in both species. FDR = false discovery rate calculated with **Benjamini-Hochberg formula.**

Figure 60: Overview of NTA and FCM measurements

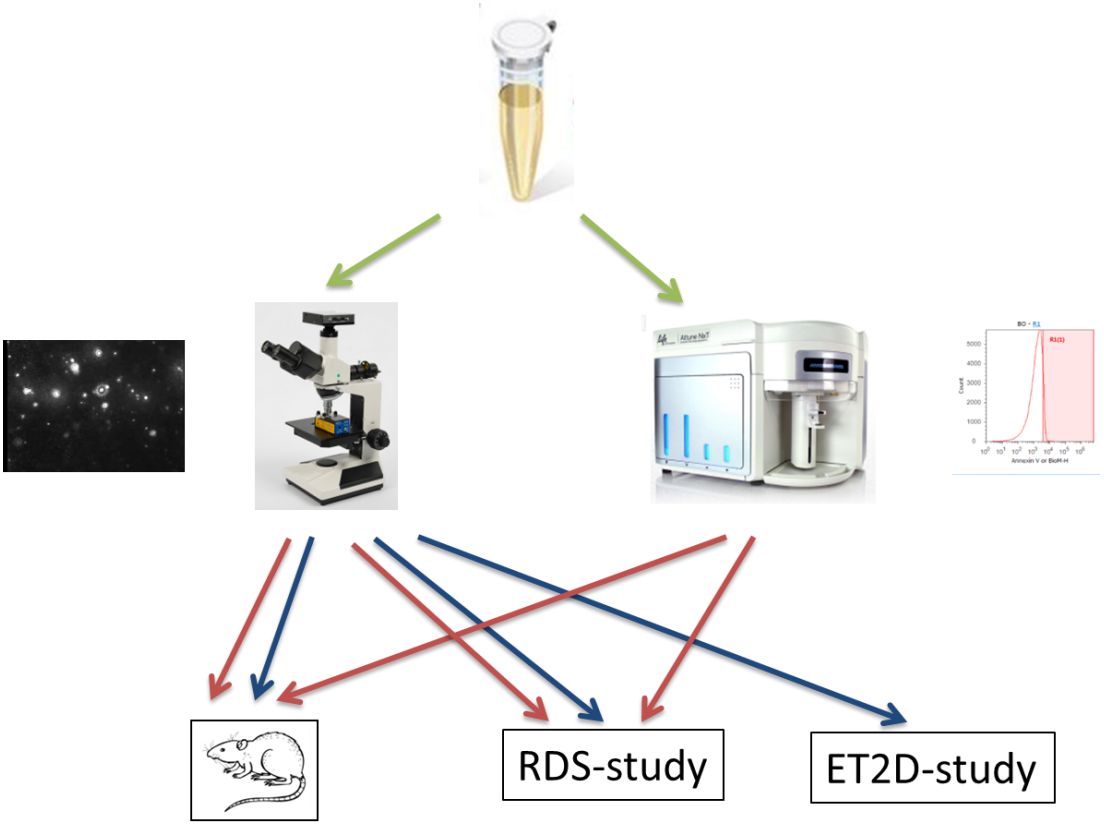

Figure 60. Schematic summary of experiments performed in this chapter: Urinary microparticles were measured using different methodologies in samples from rats and humans with different degree of renal impairment. The concentrations in the exosomal range (20nm-100nm; blue arrows) and in the microvesicular range (300nm-1000nm, red arrows) were determined by NanoSight using Nanotracking technology. Bodipy-Maleimide positive microvesicles were measured by the dedicated Attune flow cytometer. Arrows point to the analysed cohorts: the rat Cyp1a1mRen2 DN model, samples from the ”renal diseases“ study and in the Edinburgh type 2 Diabetes study.

3.4.2 Assessing conditions for measurement of urinary exosomes concentration

As published before there is an approximately 10-fold increase in the 24 hours urinary volume between rats after 28 weeks of injury (DM+HTN) phase compared to control (Figure 61). Generally, there are two ways for compensating for differences in urinary volume. First, measurements are corrected by urinary creatinine and this approach is especially appropriate when the 24 hours volume is not known or volume

fluctuations are expected to be in a moderate range. Due to high differences in urinary volume in the Cyp1a1mRen2 DN model it seemed more appropriate to pre-dilute urinary samples before measurement, rather than measuring first and correcting later. Hence urine samples were diluted by a factor equivalent to the ratio between the 24hr volume from each rat to the rat with the highest 24hr volume. Dilution medium was PBS filtered through a 100µm filter and checked for the absence of signal on the NanoSight. Therefore, a much smaller volume of control samples was used for measurements compared to injury samples. This approach was chosen for all animal experiments. For human studies the 24 hours urinary volume was not known and a correction for urinary creatinine was applied.

A laser with 540nm excitation coupled with a long-pass filter allows the application of antibodies conjugated to fluorophores to identify exosomes with specific surface antigens. Qdots are fluorescent nanocrystals (15-20nm) that can be conjugated with specific antibodies. Due to their small size and bright but narrow long-lasting emission spectrum Qdots are well suited for application in the NanoSight LM10(Dragovic, Gardiner et al. 2011, Oosthuyzen, Sime et al. 2013).

The optimal time for incubating the urine with antibodies bound to Qdots was evaluated first. From two animals two urinary samples each collected at baseline and after 28 weeks of injury phase were incubated with Aquaporin2 conjugated with Qdots for several time periods. A signal was already present within 15-20 minutes and peaked after roughly 35-45 minutes with a sharp decline after 5 hours (Figure 61). The results were similar when other antibodies conjugated to the same Qdot (540nm) were used (data not shown). The Coefficient of variation was approximately 20% for the first two time-points (20mins and 40mins) and 35% for

70-80 minutes based on triplicate readings. Repeating a measurement 8 times after an incubation of 40 minutes in one injury (DM+HTN) phase urinary sample reduced the coefficient of variation to 16%. Using IgG Rabbit as isotype control demonstrated a signal about 5-8% of the sample (Figure 61). Since measurements of total urinary exosome concentration in large study cohorts required several runs on different days, the intra-, inter- and total variability (imprecision) were calculated using aliquots of silica beads of a known size and a known concentration. Formulas of for the calculations are further specified in the Materials & Methods section. For three replicates performed daily across 8 days the intra-assay CV (coefficient of variation) was 14.34%, the inter-assay CV was 10.63% and the total (=within-laboratory) CV was 17.62% (Figure 61).

Figure 61: Quality control for NTA measurements

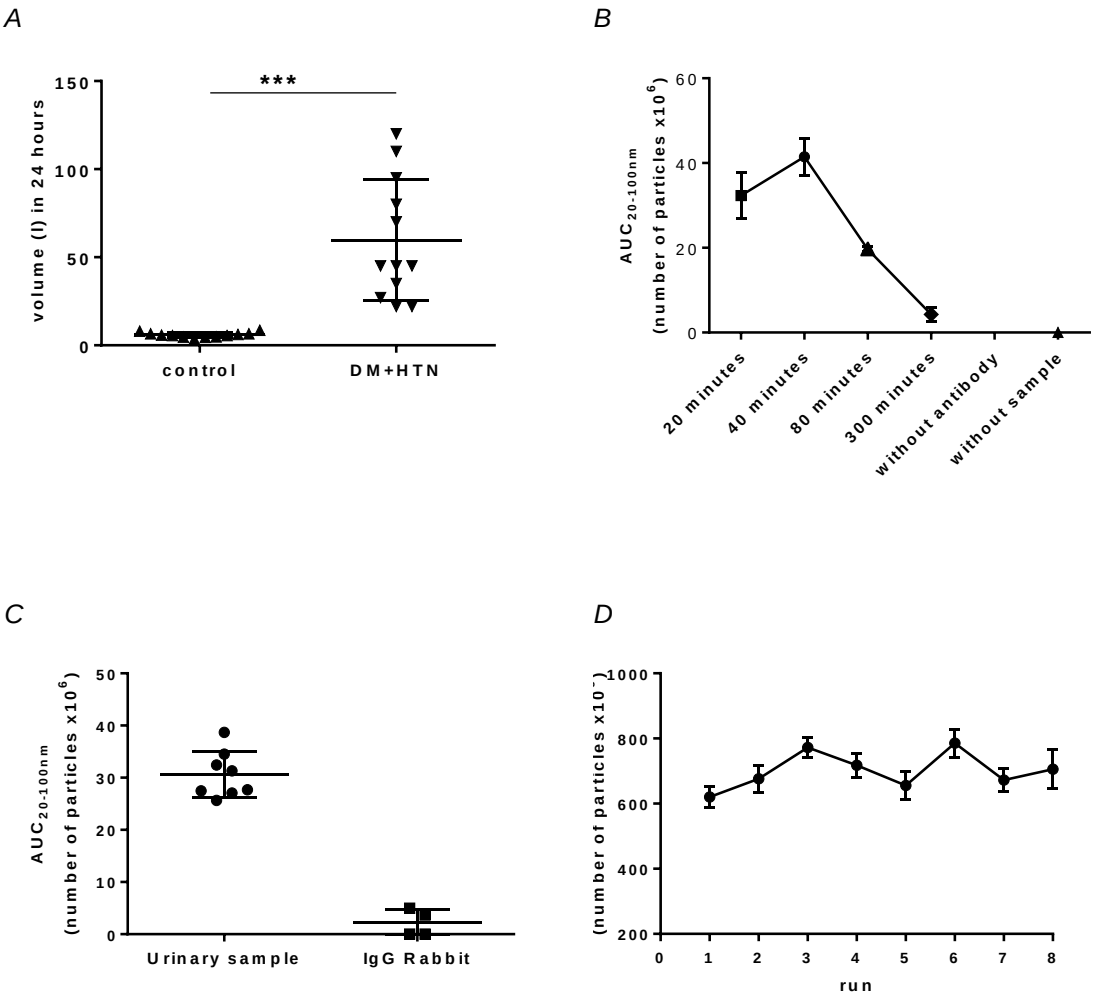

Figure 61. A) Urinary volume within 24 hours in the injury group from the Cyp1a1mRen2 model was ten times higher than in the control group. n=12 in each group, ***=p<0.001, B) 30-40 minutes seemed to be an ideal incubation period for binding of Aquaporin2 antibody conjugated to Qdots to urinary exosomes (n=4 with two baseline and two injury phase (HTN+DM) samples, all measurements in triplicates). C) Incubation (40 min) of an Isotype (IgG Rabbit) conjugated to Qdots does not result in a relevant signal compared to Aquaporin2. Measurements are performed on urine from one injury animal (n=1) (HTN+DM) and are repeated 8 times (Aquaporin2) for calculation of intra-assay precision or 4 times (Isotype). D) For calculation of inter- and intra- assay precision average AUC of aliquots from silica beads of fixed size and concentration were measured before each day with 6-8 repeats a day.

3.4.3 Urinary exosome concentrations in the DM+HTN rat model

Total and cell-specific exosome concentration in the urine samples from the Cyp1a1mRen2 DN reversal model (Conway, Betz et al. 2014) collected at baseline and injury phase (28 weeks) was assessed initially using the NanoSight. Total (unlabelled) exosome concentration increased almost 4-fold in the injury phase in comparison to baseline. Similarly the concentration of nephrin^{+} (a podocyte marker) and cubilin^{+} (a proximal tubular marker) exosomes rose more than 50% in the injury period compared to baseline. To a lesser extent, but still significantly different, Aquaporin 2^{+} (AQP2) (a collecting duct marker) exosomes were at a higher concentration during injury than in baseline (Figure 3). Consistently, cell-specific exosomes were at lower concentrations than total exosomes. After 8 weeks of reversal of hyperglycaemia and hypertension only the total exosome concentration fell significantly whilst Nephrin^{+}, Cubilin^{+} and AQP2^{+} exosome concentrations tended to decline, but were not significantly different from either the injury phase or from baseline.

Total exosome concentration and albuminuria:creatinine ratio were significantly positively correlated with each other when injury and reversal groups were combined or when the reversal group was analysed individually to avoid group bias (Figure 62).

Figure 62: NTA measurement in the Cyp1a1mRen2 DN model

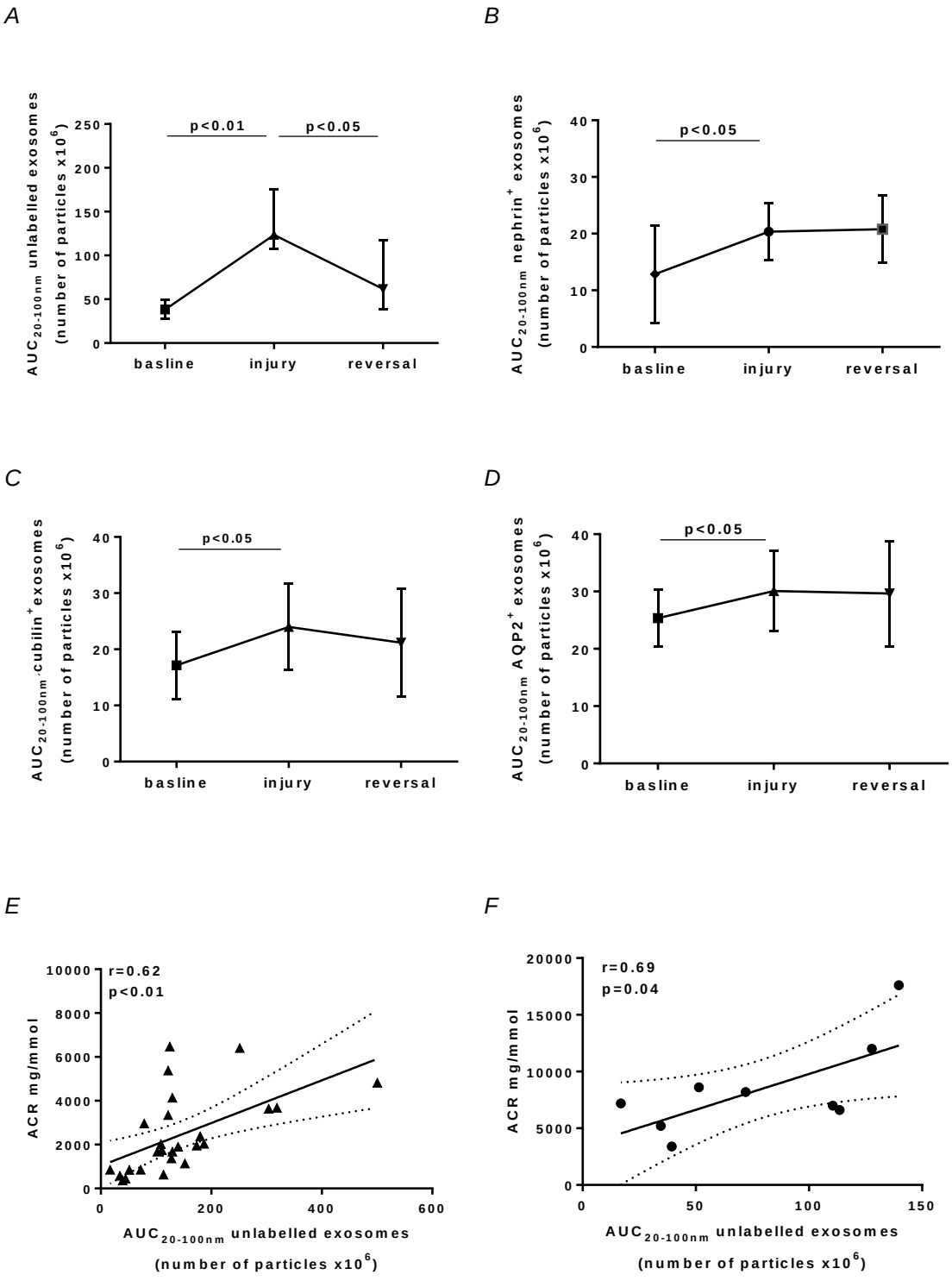

Figure 62. Urinary A) total, B) Nephrin +ve, C) Cubilin +ve and D) Aquaporin 2 +ve exosome concentrations in the Cyp1a1mRen2 reversal DN model increase at the end of the injury phase (28 weeks HTN+DM) compared with baseline but only the total exosome concentration decreases significantly from injury to reversal phase (additional 8 weeks with

normotension and normoglycemia). Neither the total nor cell-specific exosome concentration in the reversal phase was significantly different from baseline. Significant positive Pearson correlation was observed between ACR and urinary total exosome concentration from E) injury and reversal phase (n=20) and F) only reversal phase (n=10). Concentration is expressed in area under curve concentration (AUC) and injected sample volumes are corrected for 24 hours urinary volume, n=10. . In E) and F) a linear regression line is drawn with a 95 % confidence interval (dotted line). Data is presented as median (IQR).

3.4.4 Urinary exosome concentrations in the RDS study

Characteristics of patients from the RDS study

To evaluate whether the results from the DM+HTN rat model could be translated towards clinical practice, urinary specimens were collected from 151 patients at the Renal Medicine and Renal Diabetes outpatient clinics at the Royal Infirmary, Edinburgh. The pilot study had been approved as part the South East Scotland SAHSC Human Annotated BioResource bank (see Materials and Methodes and Appendix for consent form and patient information). The characteristics of the patients are depicted in Table 34.

Mean age was 63 years and two thirds of participants were male. The patients had a wide range of renal function, with 30% having normal renal function and 42% with severe renal failure (CKD 4 or 5). The primary aetiologies of chronic kidney disease in the patients are given in Table 35, with diabetic nephropathy being by far the most common cause of CKD.

Table 34: Patient characteristics in the RDS study

Participants, n	151
age, years	63 (+/-13)
male, n	98 (64.9%)
eGFR, ml/min/1.73m2	36.2 (22.6 - 66.3)
GFR > 60 ml/min (CKD I&II), n	45 (30%)
GFR <= 60 ml/min, GFR => 30 ml/min, (CKD III), n	43 (29%)
GFR < 30 ml/min (CKD IV&V), n	63 (42%)
ACR, mg/mmol	29.7 (3.8 - 107.7)
uCystatin C : uCreatinine, µg/mmol	70 (29 – 330)
Hemoglobin, g/L	120 (+/-22)
LDL Cholesterol, mmol/L	4.2 (3.6 - 5.2)
$AUC_{20\text{-}100nm}$, 106 / l / mmol creatinine	6.1 (3.6 – 12.5)

Table 34. Patient characteristics of the pilot RDS (RenalDiseaseS) study. Values are given as count number (with percentage from total), as mean (with standard deviation) or as median (with quartiles) depending on the Kolmogorov-Smirnov test for normal distribution. The total unlabelled exsosome concentration $AUC_{20\text{-}100nm}$ was logarithmized and corrected for urinary creatinine. eGFR=estimated glomerular filtration rate, CKD=chronic kidney disease with stage, ACR=urinary albumin to creatinine ratio, uEGF=urinary epidermal growth factor.

Table 35: Aetiology of chronic kidney disease in the RDS study

Diabetic Nephropathy (with or without hypertension)	70 (46.4%)
Other Glomerulonephritis	26 (17.2%)
Hypertension (without DN)	13 (8.5%)
Vasculitis	8 (5.3%)
IgA-Nephrophathy	6 (4.0%)
Lupus-Nephritis	5 (3.3%)
Interstitial Nephritis	6 (4.0%)
other/unknown reason for CKD	17 (11.3%)

Table 35. Primary aetiology of chronic kidney disease in patients from the RDS-study (number, with percentage of total).

Correlation of urinary exosome concentration with markers of renal function

Total urinary exosome concentration correlated weakly with urinary creatinine. There was a moderate correlation between total exosome concentration and urinary albumin and urinary cystatin C, a biomarker of renal damage (see Discussion below) (Figure 63).

Participants were divided into groups of approximately equal number according to their renal function: minor to moderately advanced chronic kidney disease (CKD) stage I-IIIa (eGFR >= 45ml/min, n=68) or severe CKD stage IIIb-V (eGFR =< 45ml/min, n=83). Total exosome concentration tended to be higher in the CKD IIIb-V group while urinary creatinine was significantly lower. The ratio between urinary exosomes and urinary creatinine was significantly different between those with CKD I-IIIa and those with CKD IIIb-V (Figure 64).

Figure 63: Correlation of total exosome concentration with urinary markers in the RDS study

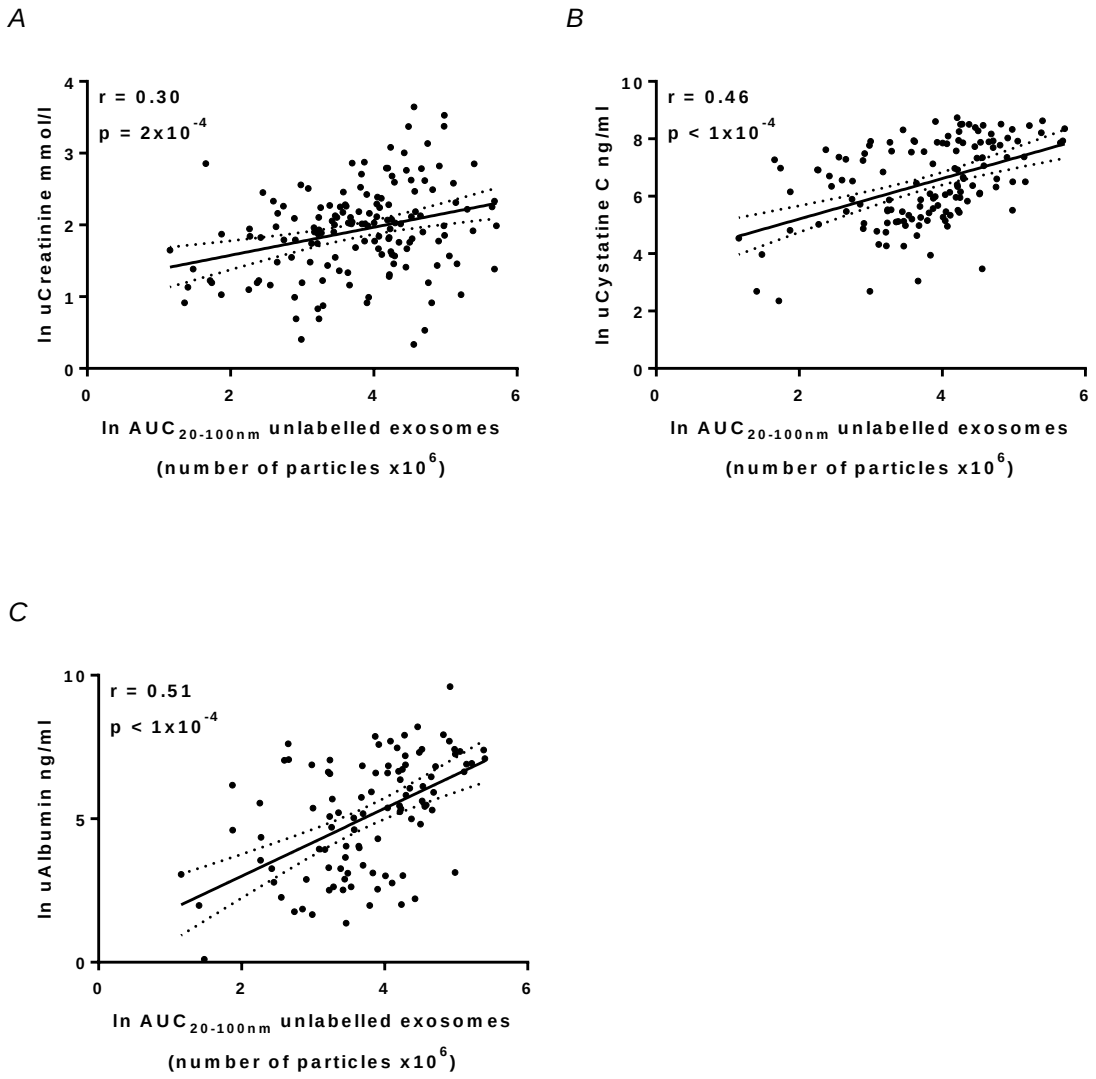

Figure 63. Pearson correlation between total exosome concentration and A) urinary creatinine, B) urinary Cystatin C and C) urinary albumin (all log-transformed). Exosome concentration is expressed in area under curve concentration (AUC), in each group. In B) and C) a linear regression line is drawn with a 95 % confidence interval (dotted line).

Figure 64: Correlation of total exosome concentration with renal function in the RDS study

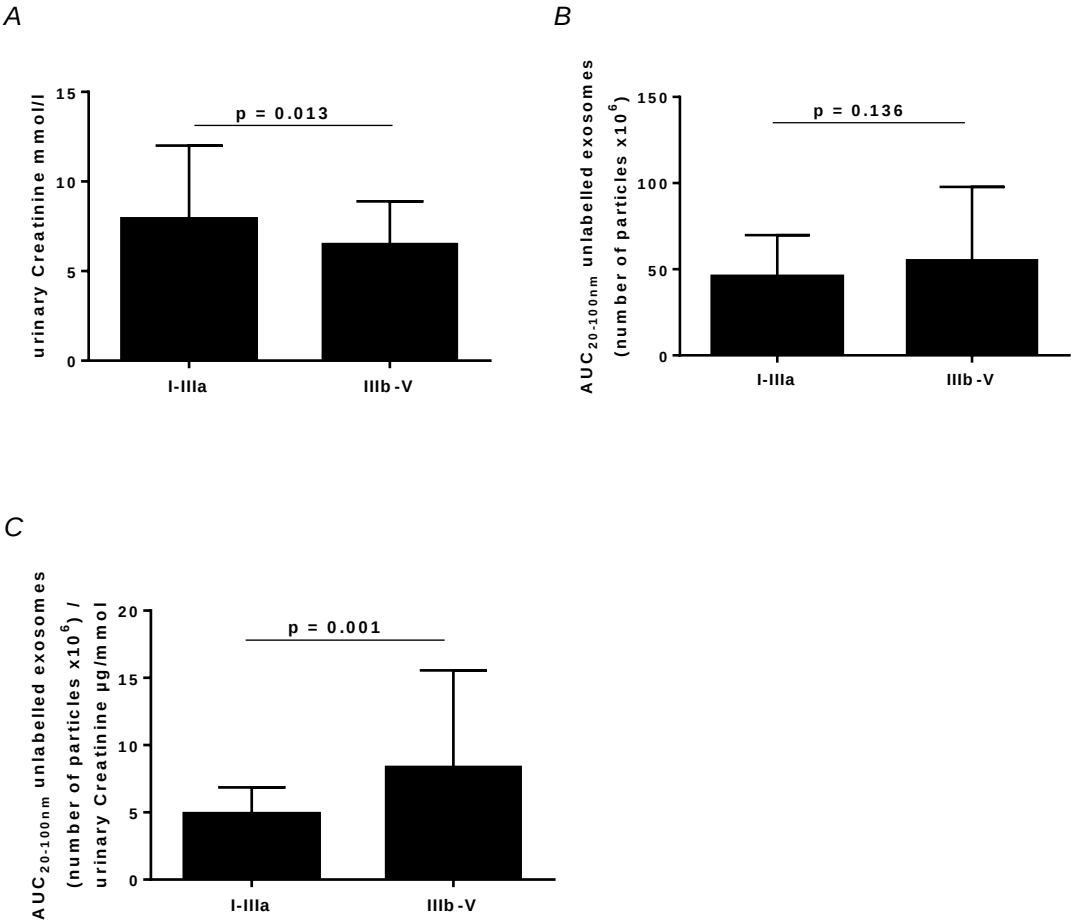

Figure 64. A) Median (IQR) Urinary creatinine is decreased in patients with advanced CKD (stage IIIb-V, n=83) compared to patients with preserved renal function (CKD stage I-IIIa, n=68). Median (IQR) total exosome concentration is increased in patients with advanced CKD non-significantly before (B) but significantly after correction for urinary creatinine (C). Mann-Whitney-U test.

$AQP2^+$: $CD24^+$ exosome ratio and markers of renal function

To determine their cellular origin urinary exosomes were stained with antibodies against nephrin, cubilin, aquaporin 2 and CD24 (a potential pan-exosome marker) coupled to a Qdot fluorophore. Unfortunately the antibodies against nephrin and cubilin did not produce a robust signal on human urine on the NanoSight and were not further analysed. The AQP2 positive exosome concentrations were normalized

for the CD24 positive exosomes as described previously (Oosthuyzen, Sime et al. 2013). The AQP 2 : CD 24 ratio was negatively correlated with renal function (defined by eGFR) and positively with urinary Cystatin C : creatinine ratio as a potential marker for renal damage. There was no correlation of the AQP 2 : CD 24 ratio with urinary creatinine indicating that urinary volume had no major effect on the ratio (Figure 65).

Figure 65: AQP2$^+$:CD24$^+$ exosome ratio in the RDS study

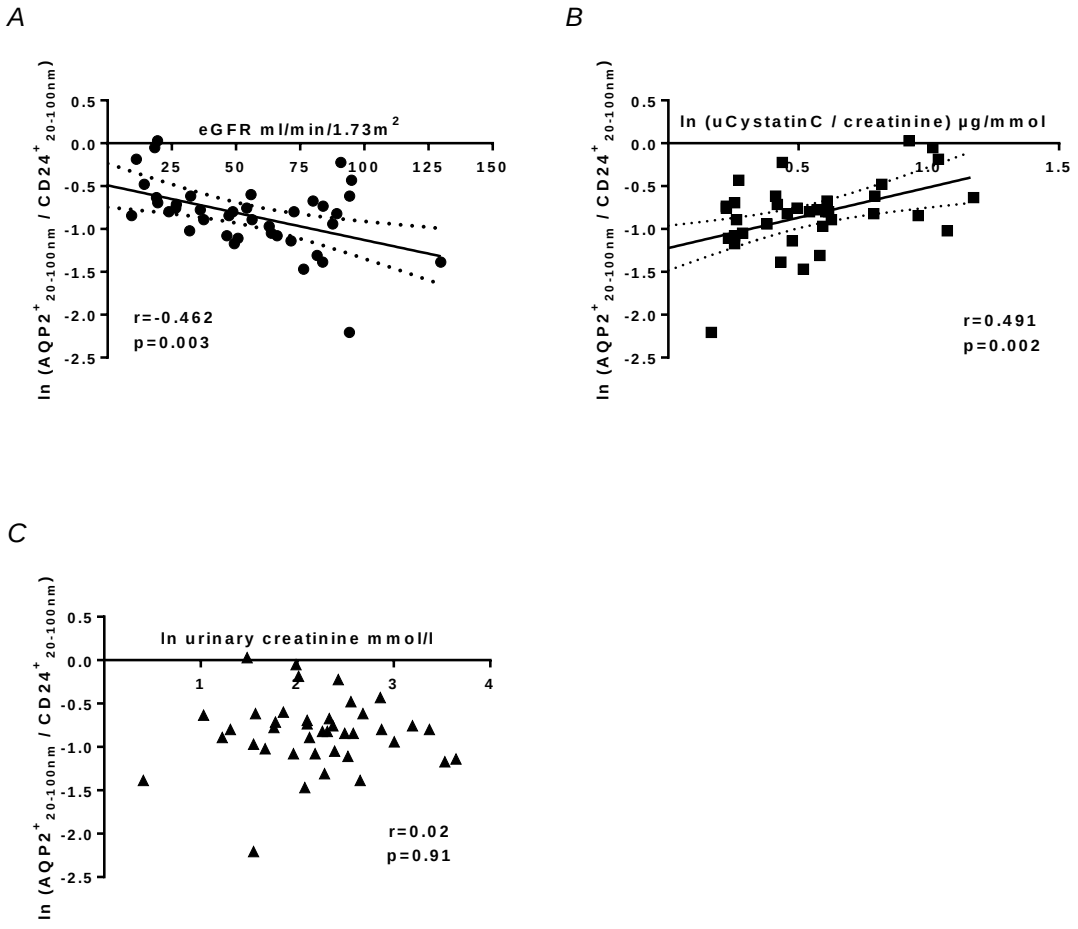

Figure 65. Ratio of AUC for aquaporin 2$^+$ exosomes (20nm-100nm) to CD24 positive exosomes correlates A) with estimated Glomerular filtration rate (negatively) and B) with urinary Cystatin C : creatinine ratio (positively). But it does not correlate with urinary creatinine (C). n = 41. Pearson correlation. . In A) and B) a linear regression line is drawn with a 95 % confidence interval (dotted line).

3.4.5 Total urinary exosomes concentration in a subset of the ET2D study

Total urinary exosome concentration was measured in a subset of 128 participants randomly selected from the Edinburgh Type 2 Diabetes (ET2D) subpopulation comprising 642 patients with preserved renal function (eGFR >60 ml/min/1.73m^2) and no evidence of micro- or macroalbuminuria (<2.5 mg/mmol men or <3.5 mg/mmol) at baseline (see previous Results chapter). The characteristics of this subset (20%) are listed in Table 36 and were not significantly different from the profile of all 642 patients from the ET2D study who had no evidence of renal disease at baseline (Results Chapter 3) except for duration of diabetes (5.0 years in the subset vs 7.4 years in the whole cohort). After categorising the patients into tertiles according to the urinary total exosome concentration corrected for creatinine the baseline characteristics in each tertile were not significantly different except for tubular injury marker urinary KIM-1 and total exosome concentration (Table 36).

The total urinary exosome concentration corrected for creatinine weakly but significantly correlated positively with the KIM-1:Cr ratio, there was no association with urinary EGF:Cr as a marker of tubular mass (Figure 66).

Table 36: Subset of the ET2D study divided into tertiles according to the unlabelled exosome concentration

	Mean (Total n=128)	T1 (n=42)	T2 (n=43)	T3 (n=43)	P-value
age, years	67 (+/-4)	66 (+/-4)	66 (+/-4)	67 (+/-4)	0.53
male, n	67 (52%)	24 (57%)	22 (51%)	21 (49%)	0.73
eGFR, ml/min/1.73m^2	86.7 (+/-9.8)	85.7 (+/-9.7)	89.1 (+/-9.0)	85.2 (+/-10.4)	0.14
HbA1c, %	7.1 (6.5 – 7.5)	7.0 (6.6 – 7.3)	7.1 (6.6 – 7.7)	7.1 (6.5 – 7.5)	0.70
Duration of diabetes, years	5.0 (3.0 - 9.2)	5.0 (3.0 - 10.0)	5.0 (2.0 - 8.5)	6.0 (4.0 - 11)	0.27
Systolic blood pressure, mm Hg	134 (+/-15)	135 (+/-15)	132 (+/-16)	134 (+/-13)	0.70
Diastolic blood pressure, mm Hg	69 (+/-8)	70 (+/-8)	67 (+/-8)	68 (+/-8)	0.28
ACR 0.5-2.5 (males) or 0.5-3.5 mg/mmol (females), n (%)	32 (25%)	10 (24%)	11 (26%)	11 (26%)	0.98
urinary creatinine, mmol/l	7.1 (4.9 – 9.8)	7.1 (4.9 – 9.9)	7.0 (5.1 – 10.3)	7.1 (4.6 – 8.6)	0.58
Log (urinary KIM-1 :creatinine), µg/mmol	1.14 (+/-0.34)	1.04 (+/-0.34)	1.07 (+/-0.33)	1.31 (+/-0.28)	<0.01
Log (urinary EGF:creatinine), µg/mmol	0.91 (+/-0.40)	0.94 (+/-0.42)	0.93 (+/-0.36)	0.85 (+/-0.41)	0.56
Ln $AUC_{20\text{-}100nm}$ (number of particles x106) : uCreatinine, mmol	1.46 (+/-0.96)	0.41 (+/-0.56)	1.46 (+/-0.24)	2.49 (+/-0.47)	<0.01

Table 36. A) Patient characteristics of the subset of the Edinburgh Type 2 Diabetes Study in which urinary total exosome concentration was measured. Only patients with an eGFR>60 ml/min/1.73m2 and without albuminuria (ACR <2.5mg/mmol or <3.5 mg/mmol for females) were included. Values are given as count number (with percentage from total), as mean (with standard deviation) or as median (with quartiles) depending on the Kolmogorov-Smirnov test for normal distribution. When participants were stratified into tertiles according to total exosome concentration corrected for urinary creatinine, there was no significant difference regarding the other variables except for the renal injury marker KIM-1. Variables were compared between the groups by ANOVA or Kruskal-Wallis test.

Figure 66: Correlation of total exosome concentration and urinary markers in the ET2D subset

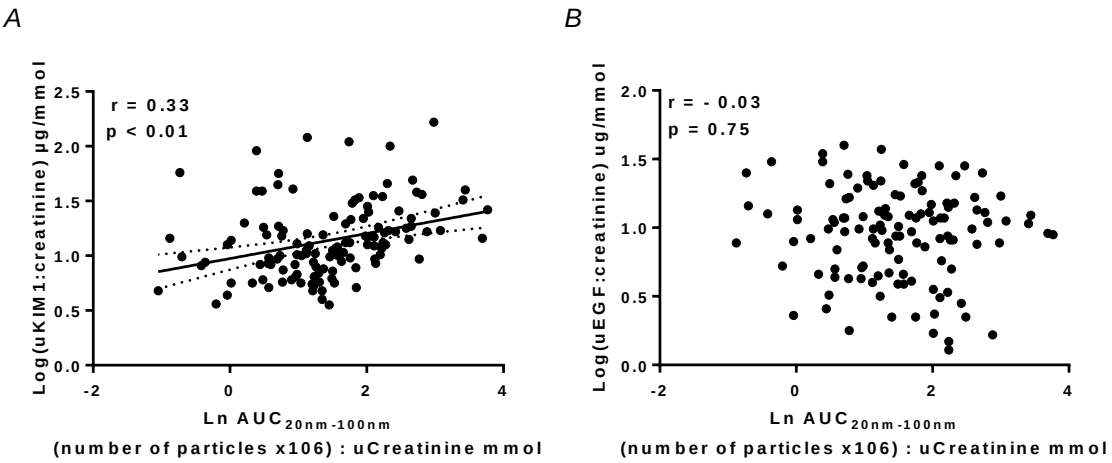

Figure 66. Total exosome concentration corrected for creatinine correlated significantly with urinary KIM1 : creatinine (A) but not with EGF:creatinine in a subset of patients from the ET2D study who had no evidence of CKD at baseline. Pearson correlation had been calculated after all variables had been log-transformed. In A) a linear regression line is drawn with a 95 % confidence interval (dotted line).

Urinary exosome concentration could predict incident CKD III

Study participants in the upper third of urinary total exosome:creatinine ratio had a significantly higher risk of developing CKD III over a period of 4 years (22 out of 128 patients) as defined by new onset eGFR<60 ml/min/1.73m^2 compared to participants in the lower two thirds. The presence of ACR >0.5mg/mmol did not indicate a higher risk for developing CKD III. On the other hand the risk for developing micro- or macroalbuminuria (>2.5 mg/mmol male, >3.5mg/mmol female) (27 patients in four years) was not associated with the total exosome concentration but with the presence of ACR >0.5mg/mmol at baseline (Figure 67).

Figure 67: Kaplan Meier Curves for total exosome concentration and ACR for the outcome incident CKD III and micro-/macroalbuminuria

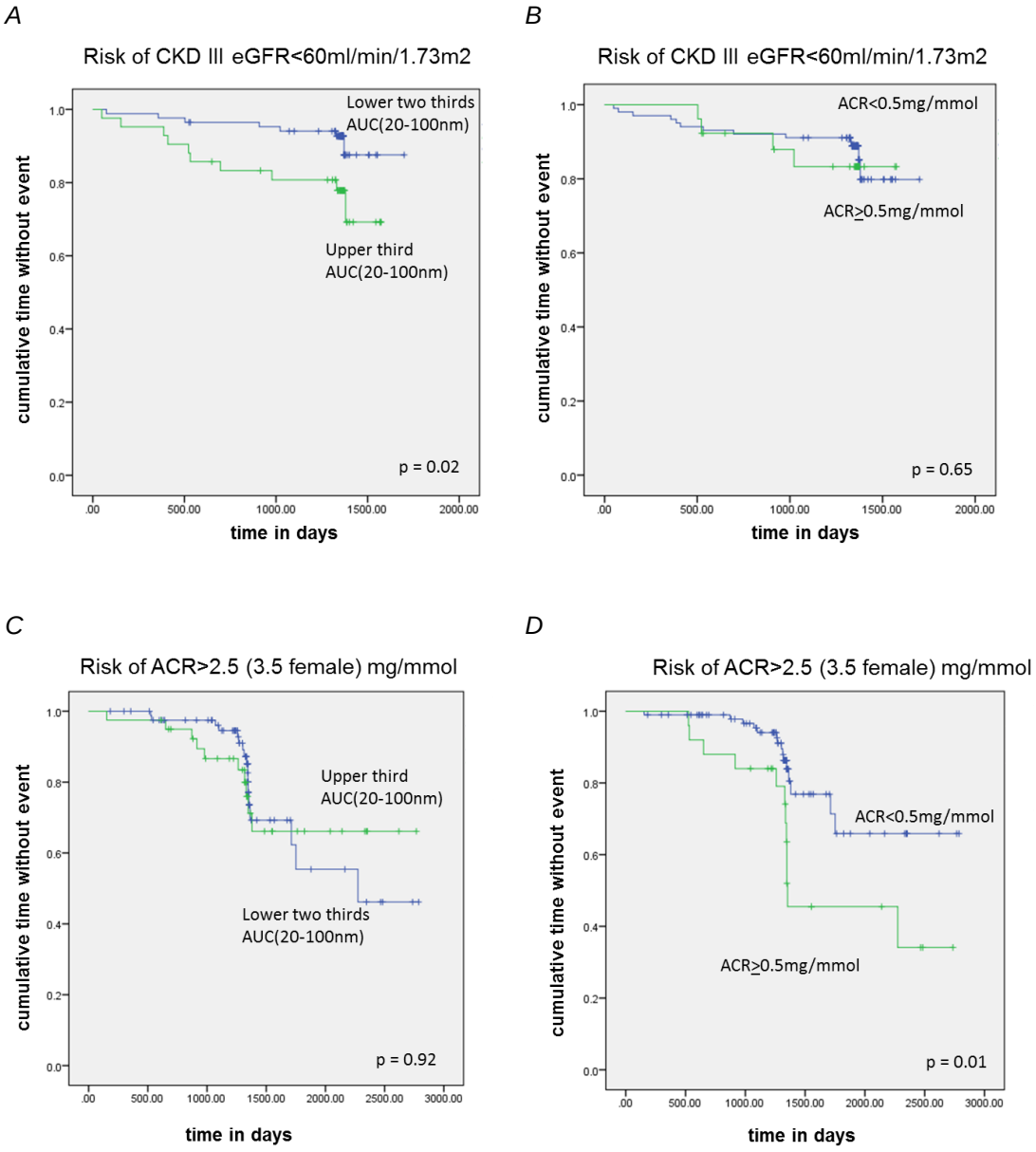

Figure 67. Kaplan Meier Curves from patients from the EDT2D study with no CKD at baseline demonstrating the risk for developing incident CKD III defined as eGFR<60ml/min/1.72m^2 in (A) and (B) or albuminuria defined as ACR > 2.5mg/mmol (> 3.5 mg/mmol for females) in (C) and (D) during a period of four years. The upper third of patients with the highest total exosome concentration had a significantly increased risk for incident CKD (A) but not albuminuria (C). Conversely, the presence of albuminuria (>0.5 mg/mmol) did not indicate a risk for incident CKD (B) but did for the development of micro-/macroalbuminuria.

Urinary exosomes are independently associated with incident CKD III

The calculated hazard ratio for development of CKD III was significantly increased in the upper third of total urinary exosome to creatinine ratio. This association remained significant after adjustment for the variables albuminuria, eGFR, sex, age and urinary KIM-1 at baseline (Table 37). After additional adjustment for HbA1c, duration of diabetes and systolic and diastolic blood pressure the association was not significant anymore (Hazard Ratio 1.9 [0.7-5.9], p=0.23, not shown), however, with regard to the number of outcomes an adjustment for so many variables is statistically not recommended and would require a higher number of participants and outcomes.

Table 37: Cox regression analysis for total exosome concentration in the ET2D subset

Ln_AUC(20-100nm) Upper third	**Incident eGFR<60ml/min/1.73m^2**	
	unadjusted	adjusted*
Hazard ratio	2.54	2.91
CI	(1.09 to 5.90)	(1.20 to 7.03)
p-value	0.030	0.041

Table 37. Hazard ratio demonstrates an increased risk of developing CKD III defined as eGFR<60ml/min/1.73m^2 for patients in the upper third according to total exosome concentration compared to the lower two thirds. *After adjustment for presence of albuminuria >0.5mmg/mmol, eGFR at baseline, age and sex

3.4.6 Protocol for the measurement of microvesicles

As microvesicles (100-1000nm) are larger than exosomes (20-100nm), they can be detected on a modified flow cytometer (Attune).

Since the concentration of microvesicles with a size range of 300nm-1000nm (approximate detection threshold of the Attune) is about only a tenth of total

extracellular vesicle (20nm-1000nm) concentration in urine (Dragovic, Gardiner et al. 2011), an enrichment protocol as described by Burger et al. (Burger, Thibodeau et al. 2014) with slight adaptions was performed and results were checked by NanoSight. Following enrichment, the concentration of microvesicles ($AUC_{300-1000nm}$) increased ten-fold, while concentration of smaller vesicles ($AUC_{20-200nm}$) did not increase significantly (Figure 68).

Next, a gating strategy for microvesicles was applied as published by Burger et al. with small adaptions. The first step was to define a threshold for detection of Bodipy-Maleimide (a dye that is incorporated into membranes and acts as a pan-marker for microvesicles) positive particles. This was achieved by measuring the signal from diluent (PBS) with the dye, a sample without dye and the combination of dye and sample. Then the size of the gate was defined by using 200nm and 1000nm polystyrene beads at a concentration of 10^5/ul which was chosen after several dilutions steps had been tested (Figure 69).

Figure 68: Enrichment of urinary microvesicles

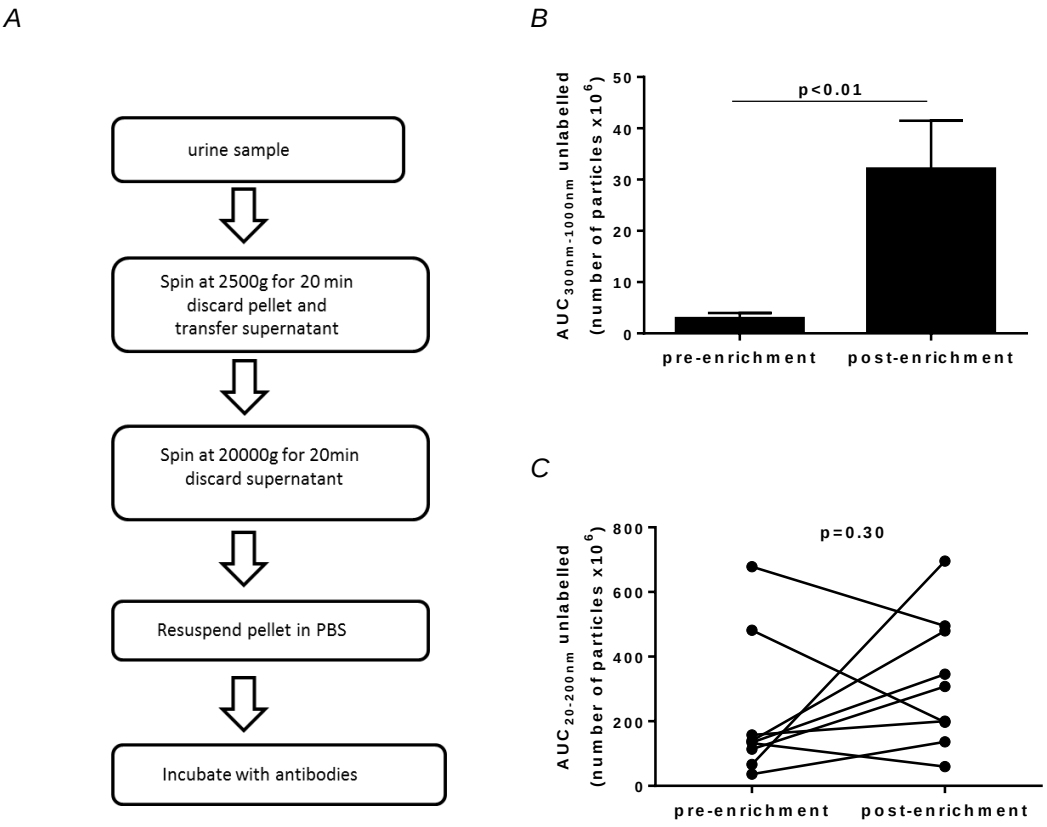

Figure 68. A) Schematic protocol for the enrichment of microvesicles (300nm-1000nm) in urine. B) The mean±SEM concentration of microvesicles in urinary samples significantly increased after application of the protocol while C) the change in exosome concentration was not significant. n=9.

Figure 69: Gating for urinary microvesicles using the Attune FCM (Life Technologies)

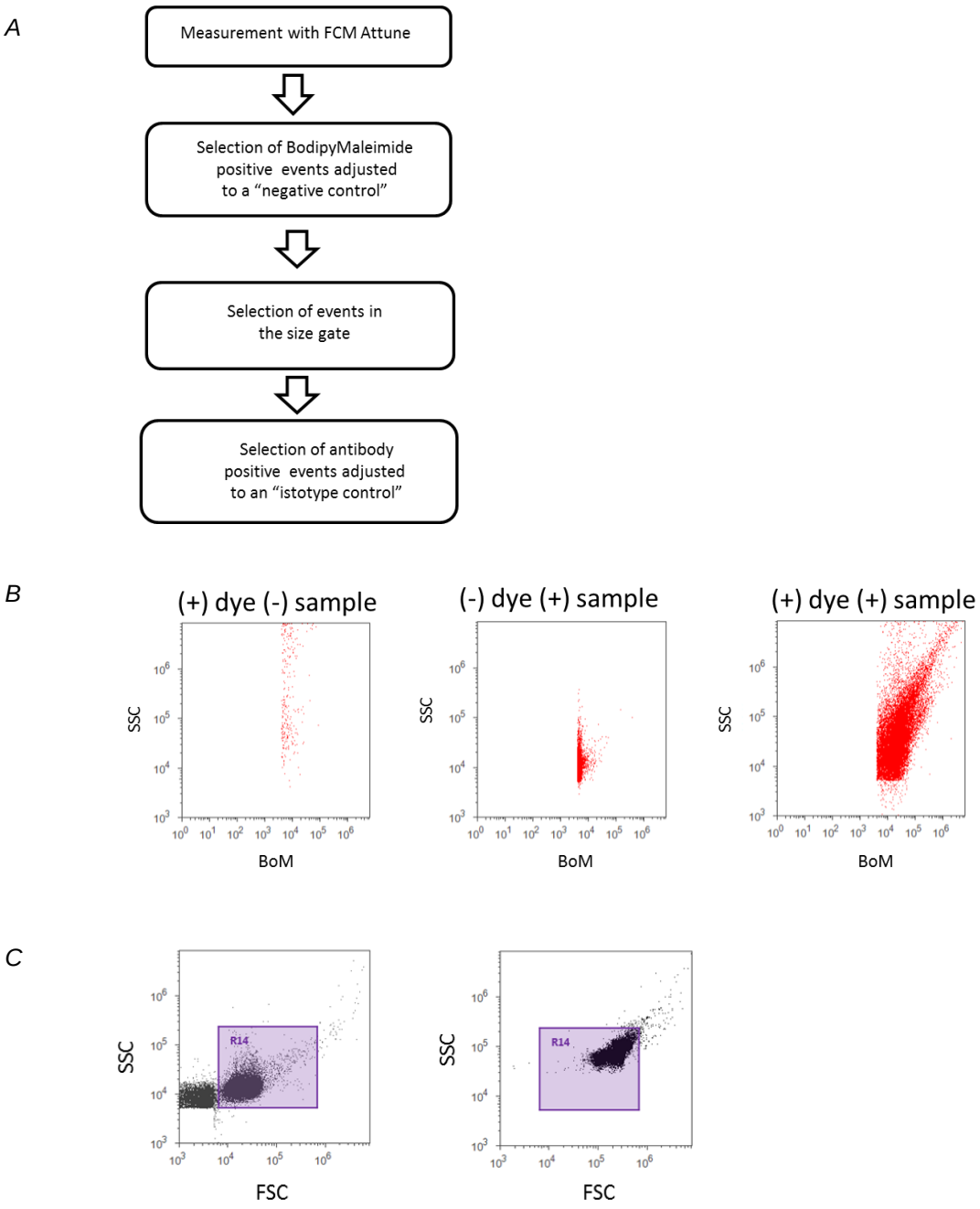

Figure 69. A) Schematic protocol for the analysis process for measurement of microvesicles in urine. B,C) Representative traces from flow cytometry analysis of microvesicles derived from human urinary samples. B) The threshold for Bodipy-Maleimide (BoM) positive events was set by comparing diluent with dye and an urinary sample measured without dye (autofluorescent control) with the combinatory measurement of dye and sample. BoM positivity is regarded as recorded events above the threshold. C) The gate for size (R14) was set to capture microvesicles in the 200-1000nm range using 200nm (left figure) and 1000nm diameter silica beads (right figure). SSC, side scatter; FSC, forward scatter; BoM, Bodipy Maleimide.

Coefficient of Variationof BoM and comparison with Annexin V Pacific blue

The coefficient of variation (CV) of the measurement for BoM positive events was 16.9% and below the maximum accepted value of 20%, which is in contrast to the CV of all (stained+unstained) recorded events (29.2%). Unstained events may represent background noise (Figure 70).

Annexin V is an established marker for microvesicles though its dependence on a high concentration of calcium can affect measurements (Enjeti, Lincz et al. 2008). Here it was tested whether Annexin V Pacific Blue could be replaced by Bodipy-Maleimide adequately as described by Enjeti et al. for blood samples (Enjeti, Lincz et al. 2008). Urinary samples were divided into two equal parts and stained by each marker separately. The recorded number of positive events did not differ significantly between the two staining techniques. A strong correlation between both markers was confirmed by double staining (Figure 70).

Figure 70: CoV of Bodipy Maleimide measurements and correlation with Annexin V - Pacific blue

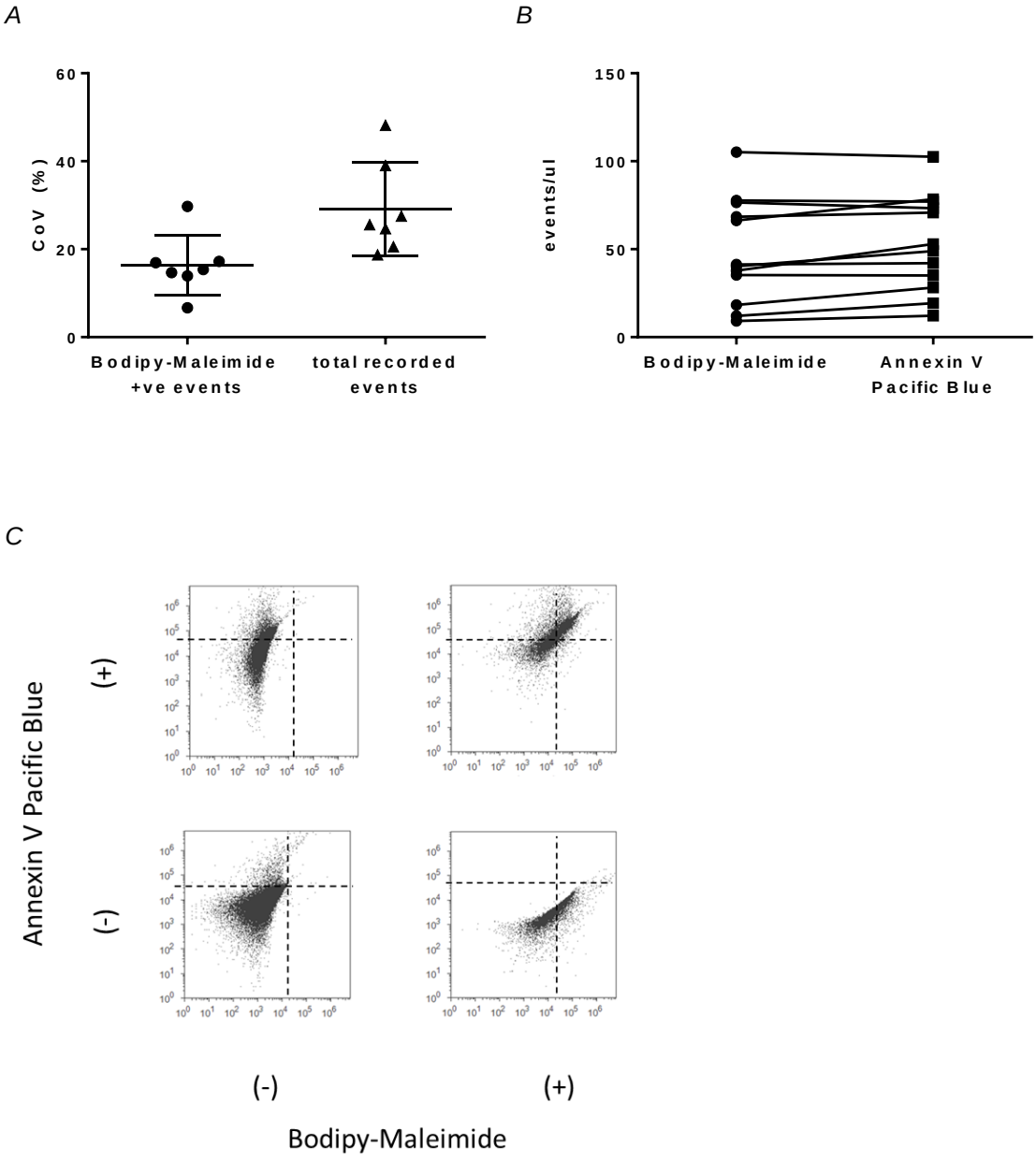

Figure 70. A) The coefficient of Variation (CoV) was calculated by repeating measurements of the same sample for total events (stained and unstained) and Bodipy-Maleimide positive events. N=7 samples with 6 repeats each. Data is presented as mean±SEM B) Number of Bodipy-Maleimide and Annexin V- Pacific blue positive events in the same urinary samples (n=12) incubated with each dye separately did not differ significantly. C) Representative urinary sample incubated with each marker alone or with both markers together. The vast majority of particles that bind annexin V also bind Bodipy-Maleimide (upper right gate).

3.4.7 BodipyMaleimide positive particles in the DM+HTN rat model

For measurement of microvesicles in the urine samples of the Cyp1a1mRen2 DN rat model a pre-dilution to correct for large variation in 24 hours urinary volume was performed as already described for the exosome measurements. The concentration of BodipyMaleimide positive events increased significantly in the combinatory diabetes + hypertension group in comparison to control. The level of total recorded events (stained+unstained) remained unchanged in the 200-1000nm size gate which was encouraging as total recorded events assumedly comprise stained microvesicles and unstained non-specific background noise. BodipyMaleimide positive events and the concentration of unlabelled particles ($AUC_{300\text{-}1000nm}$) as measured by NanoSight were positively correlated (Figure 71).

Figure 71: Measurement of Bodipy Maleimide positive events in the Cyp1a1mRen2 DN model

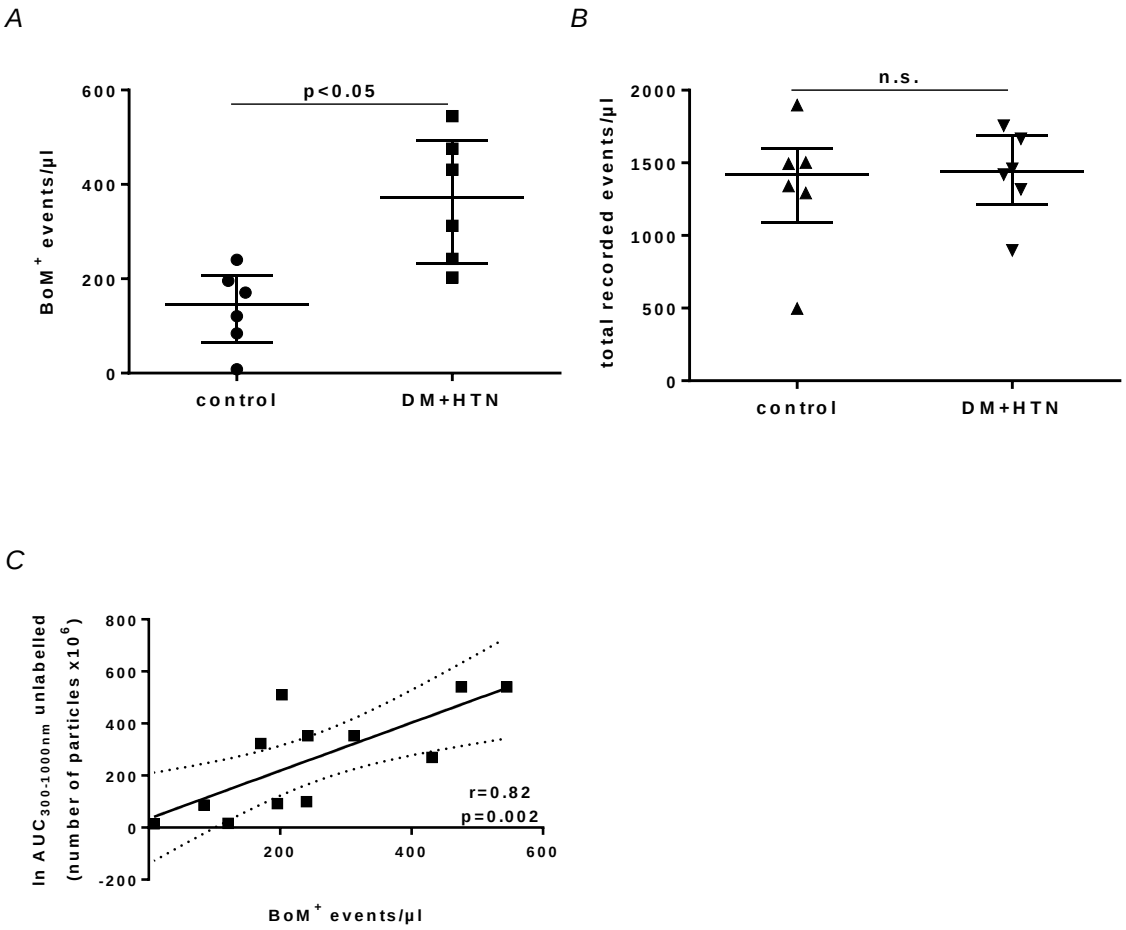

Figure 71. A) Bodipy-Maleimide positive events in urine samples increase in the group with Diabetes+Hypertension compared to control samples in the Cyp1a1mRen2 DN model. B) Concentration of total (stained+unstained) recorded events in the 200nm-1000nm size gate did not differ between the groups. Data is presented as median and IQR C) Positive Pearson correlation of microvesicle concentration between measurement by Nanosight and Attune FCM. Concentration is expressed per events/µl (Attune) or as area under curve (Nanosight). N=6 in each group. BoM – Bodipy maleimide. . In C) a linear regression line is drawn with a 95 % confidence interval (dotted line).

3.4.8 BoM and podocalyxin positive particles in a subset of the RDS study

As proof of principle of the ability to translate some of the findings from the rodent model into human disease, BodipyMaleimide and podocalyxin-like (PODXL) PerCP positive events were next measured in a subset (20%, n=34) of urine samples from patients recruited from the RDS study. These comprised 17 patients with moderately reduced renal function (CKD III, mean eGFR 46.0 (+/-8.5 SD) ml/min/1.73^2; mean age 67.5 (+/- 11.0 SD) years; 18% female) and 17 patients with severely reduced renal function (CKD IV or V, mean eGFR 21.7 (+/- 4.9 SD) ml/min/1.73^2; mean age 66.5 (+/- 24.5 SD) years; 35% female). The rationale for the selection of patients with reduced renal function was to have positive control as PODXL positive microvesicles concentration is expected to increase in patients with renal impairment (Burger, Thibodeau et al. 2014).

There was a weak, but significant positive correlation between BoM^+ events and unlabelled particles ($AUC_{300\text{-}1000nm}$) measured by the NanoSight, but not with BoM^+PODXL^+ positive events and unlabelled particles ($AUC_{300\text{-}1000nm}$). The concentration of BoM^+PODXL^+ positive events but not of BoM^+ events was significantly increased in patients with severely reduced renal function compared to patients with moderately reduced renal function. Correspondingly, the concentration of BoM^+PODXL^+ positive events also correlated negatively with eGFR in this subset of patients. (Figure 72). Of note, neither BoM^+ nor BoM^+PODXL^+ positive events were significantly correlated with urinary creatinine (Spearman's rho r=0.22 p=0.15 and r=-0.23 p=0.18, respectively).

Figure 72: Measurement of BodipyMaleimide positive and BiodipyMaleimide and Podocalyxin double positive particles in a subset of patients from the RDS study

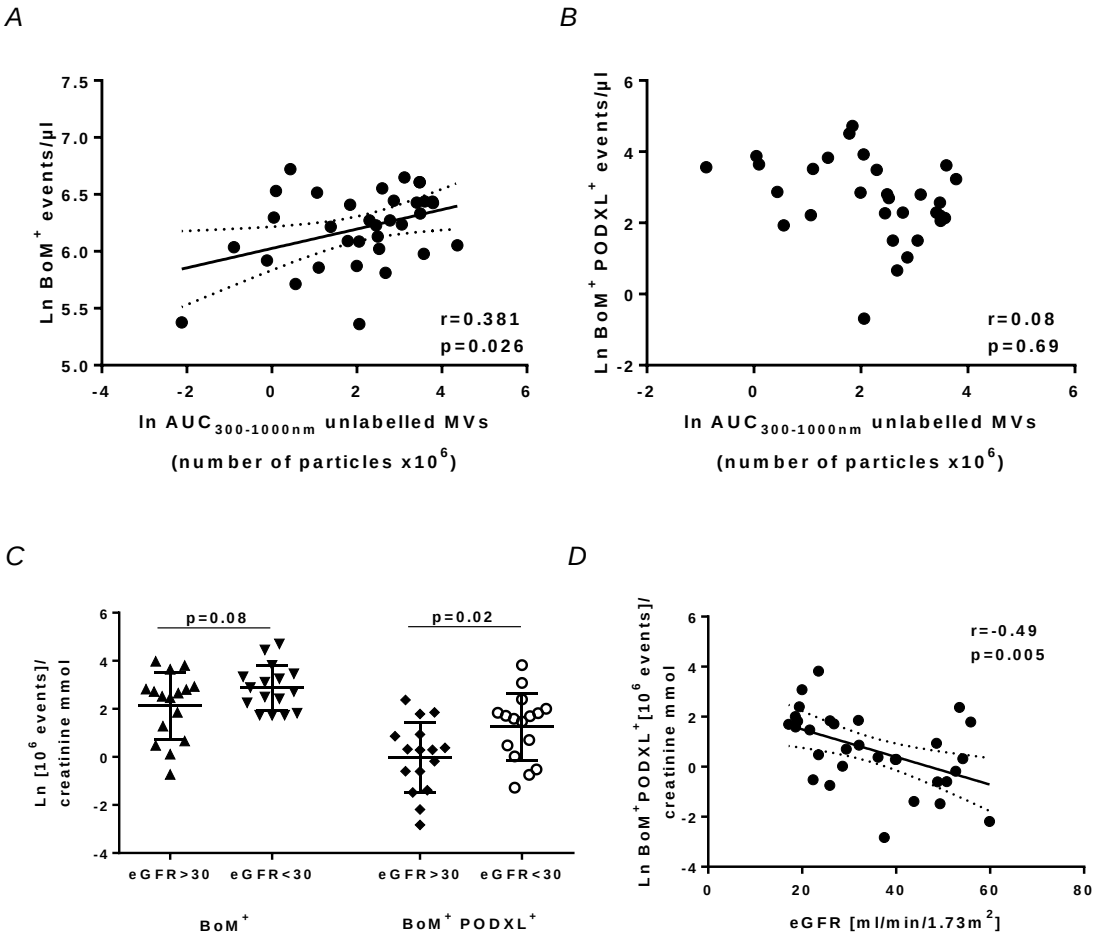

Figure 72. A, B) Pearson correlation between the concentrations of (A) Bodipy-Maleimide positive events [significantly positive] and (B) Bodipy-Maleimide and podocalyxin-like positive events [not significant] and unlabeled particles ($AUC_{300\text{-}1000nm}$) measured by NanoSight. (N=34) C) Concentration of Bodipy-Maleimide positive events and Bodipy-Maleimide and podocalyxin-like dual positive events in patients with moderately (n =17) and severely (n=17) reduced renal function. Data is presented as mean±SEM D) Negative Pearson correlation between the concentration of Bodipy-Maleimide and podocalyxin-like positive events corrected for urinary creatinine and eGFR (n=34). . In A) and D) a linear regression line is drawn with a 95 % confidence interval (dotted line). MV - microvesicle; BoM – Bodipy Maleimide; PODXL – podocalyxin-like; AUC – area under curve

3.4.9 Discussion

This chapter focuses on microparticles (20nm-1000nm) as potential biomarkers. They are readily present in urine and pathway analysis from genes and urinary peptides in the Cyp1a1mRen2 DN reversal model indicate an increasing concentration in microparticle-derived proteins during the injury phase. Using NanoSight Tracking Technology total and antibody-specific exosome concentration was demonstrated to increase during the injury phase in the model. Moreover, urinary exosomes seem to not only correlate with current renal function in patients with kidney disease but might predictive of future renal deterioration.

Quality control of exosome analysis

Due to their small size the reliable quantification of urinary exosomes is challenging. Methods like Western-Blotting or electron microscopy offer qualitative but only semi-quantitative information.

According to the guidelines of the International Society for Extracellular Vesicles (ISEV), Nanotracking Technology is a recognized way for sizing and quantifying exosomes. While the a reasonable accuracy of the NTA had been demonstrated before(van der Pol, Coumans et al. 2014), for biomarker analysis a high level of precision is mandatory as sample measurements must be comparable within runs and between runs (from different days or even labs). Therefore, the first priority was to determine the intra-run, inter-run and total precision on the NanoSight to assess reproducibility: silica beads were employed as standards in these studies. They were preferred to polystyrene beads due to their refractive index being more similar to vesicles in fresh urine (Gardiner, Ferreira et al. 2013, van der Pol, Coumans et al.

2014). Precision ranged between 10% (intra-assay) and 17% (total within-laboratory). Oosthuyzen et al. reported an intra-assay variation in unprocessed urine for light-scattered measurement of up to 47%, however the number of repeats was not given and there was no processing of urine, which was highly diluted (Oosthuyzen, Sime et al. 2013). Gardiner et al. report a variation of around 20% with no detailed information about how this was calculated (Gardiner, Ferreira et al. 2013). Hole et al. determined the inter-laboratory CV in for 100nm diameter silica beads to be around 10% (Hole, Sillence et al. 2013), which is in line with the CV obtained with similar size beads in this work. In summary, the degree of variation was considered to be acceptable, being below 20% and concordant with thresholds from other laboratories. To ensure standardisation of before each new run of samples silica beads with a known concentration (50nm and 100nm) were analysed.

For studies using antibodies, an isotype control was employed to ensure that the signal detected was not due to non-specific binding. The signal with the isotype was 10-fold less than with the actual antibodies. The optimal incubation time required to label antibodies with Qdots (15-30min) was in line with previous publications from other groups (Dragovic, Gardiner et al. 2011, Oosthuyzen, Sime et al. 2013).

Potential role of urinary nephrin and cubilin positive exosomes as a non-invasive biomarker of renal injury

Nephrin is located at the lateral site of the podocyte foot process. The 180kD protein is a constituting part of the slit diaphragm. Increased intrarenal and urinary expression is associated with glomerular/podocyte damage (Sekulic and Pichler Sekulic 2013). In FVB/NJ Akita mice or in rats injected with STZ as rodent models

of diabetic nephropathy an elevated level of urinary nephrin is associated with renal damage (Chang, Paik et al. 2012) and intra-renal nephrin-mRNA upregulation (Aaltonen, Luimula et al. 2001) and might even precede albuminuria as a marker of glomerular damage(Sekulic and Pichler Sekulic 2013). This is in line with the current study in which urinary nephrin positive exosome-like particles were increased during injury assessed by nanoparticle tracking analysis.

Cubilin is an app. 460kD membrane glycoprotein expressed at the luminal site of proximal tubular cells. Forming a complex with the transmembrane protein megalin it re-absorbs most of the filtered small-molecular weight proteins, most importantly albumin but also other molecules, such as hormones and lipoproteins (Thrailkill, Nimmo et al. 2009). While in rodent models of diabetic nephropathy a decrease of cubilin in renal tissue is observed (Feng, Zhang et al. 2006, Ke, Li et al. 2014) which could partly contribute to albuminuria, there were no reports on urinary cubilin excretion. In humans the presence of cubilin in urinary exosomes has been demonstrated in many publications (listed in Vesiclepedia at www.microvesicles.org and Pisktun et al. (Pisitkun, Shen et al. 2004)). In patients with type 1 diabetes urinary cubilin concentration increased with the development of albuminuria (Thrailkill, Nimmo et al. 2009). This is in line with findings in the present study of a robust increase of cubilin positive exosomes- in the rodent DN model.

Potential role of urinary aquaporin 2 positive exosomes as biomarkers of collecting duct injury and impaired urinary concentrating ability

Exosome aquaporin 2 (AQP2) excretion has previously been shown to correlate with urinary osmolality when assessed by NanoSight technique (Oosthuyzen, Sime et al.

2013) or exosome-specific ELISA (Salih, Fenton et al. 2016). A decreased ability to concentrate urine was associated with decreased urinary AQP2 excretion in patients suffering type 2 diabetes (Nakamura, Saito et al. 2002). Consequently, a decrease in urinary AQP2 positive particle concentration was expected in DM+HTN animals that excreted large volumes of urine (Conway, Betz et al. 2014). However, in this study a small increase in DM+HTN animals was measured. Results from the human study were in line with the animal data with AQP2 correlating inversely with renal dysfunction as assessed by eGFR. AQP2 concentration was corrected by the urinary pan-exosomal marker CD 24 (Keller, Rupp et al. 2007, Oosthuyzen, Sime et al. 2013, Salih, Zietse et al. 2014), as employed by Oosthuyzen. In a similar way CD9 was used as a pan-marker for the AQP2 ELISA (Salih, Fenton et al. 2016). Reasons for the positive correlation with renal dysfunction could be explained by the fact that increased exosome shedding could be an indicator of cellular damage (Borges, Melo et al. 2013). Tubular damage is well described in the rat model (Conway, Betz et al. 2014) and is probably present in most patients from the human RDS pilot study. Urinary Cystatine C to creatinine ratio (uCystC:Cr) is markedly increased in patients with tubulointerstitial diseases(Conti, Moutereau et al. 2006, Herget-Rosenthal, van Wijk et al. 2007) or CKD patients with a metabolic syndrome(Satoh-Asahara, Suganami et al. 2011) compared to patients with primarily glomerular diseases or healthy controls. uCystC:Cr is a predictor of renal outcome in patients with DN(Kim, Song et al. 2013). Hence uCystC:Cr might be a marker of renal impairment caused by tubular dysfunction. In the current study there was a significant positive correlation between uCystC:Cr and total exosome:creatinine and Aquaporin2:CD24

exosome concentration potentially supporting the hypothesis of increased exosome and Aquaporin2 excretion from tubular cells upon damage.

Total urinary exosome concentration and markers of renal function in humans

The current work demonstrates an association between renal function and total urinary exosome concentration in patients with mild (ET2D-subcohort) and advanced (RDS study) CKD. Correspondingly, urinary exosome concentration correlated with urinary markers of renal dysfunction like Cystatin C or albumin. The fact that these results were obtained from to different cohorts strengthens the validity of the results. In the ET2D subgroup urinary exosome concentration did not correlate with uEGF which is regarded to be a marker of renal mass, but correlated with urinary KIM-1 that is regarded to be a marker of renal injury. This is in line with the fact that cells tend to release more microparticles upon direct damage (Borges, Melo et al. 2013).

Dimuccio et al. compared total urinary exosome concentration in patients at day one and day seven after renal transplant detecting no significant difference (Dimuccio, Ranghino et al. 2014). Their measurements might have been affected by firstly the fact that the urine required processing and therefore a significant particle loss could not be excluded, and secondly the fact that the sample was taken from a six-hours and not 24 hours collection, thereby possibly neglecting diurnal fluctuations of exosome excretion.

Over a time period of four years, the tertile with the highest exosome concentration had a significantly higher risk for developing CKD III defined by eGFR<60 ml/min/1.73m^2. However, the presence of albumin in urine was not a risk factor. On the other hand albuminuria was a risk factor for developing moderately to severely

increased albuminuria, while concentration of exosomes was not. This might indicate that urinary exosomes are a marker for tubular rather than glomerular cell damage.

The association between urinary exosomes and incident CKD III remained significant after adjusting for age, sex, eGFR and albuminuria in the Cox regression analysis. Including additional predictors (systolic BP, diastolic BP, HbA1c, duration of diabetes) rendered the association non-significant. However, such a step would result in an outcome event per predictor variable (EVP) ratio below 5 and is statistically not advisable due to loss of power (Vittinghoff and McCulloch 2007). Instead, future work will focus on increasing number of participants and outcome events thereby allowing the inclusion of more potentially confounding variables.

Limitations

A limitation of this work is the single use of methodology for measurement of urinary exosomes. A contamination with non-exosome particles like protein-aggregates (Filipe, Hawe et al. 2010) and lipoproteins (Gardiner, Ferreira et al. 2013) cannot be excluded especially when the scatter-mode is used. Therefore it is recommended to combine two different methods (Lotvall, Hill et al. 2014, van der Pol, Coumans et al. 2014). At the moment no recognized gold standard for measurement of extracellular vesicles exists and there are advantages and disadvantages for every methodology (van der Pol, Coumans et al. 2014). The established methods for measurement of microparticles like western blot (WB), flow cytometry or transmission electron microscopy (TEM) are either technically or logistically not feasible for exosome analysis in a high-throughput approach. WB and TEM require multiple processing steps including ultracentrifugation before

measurement which might also result in a substantial loss of exosomes. Additionally since there is no consensus pan-marker for exosomes therefore quantitative assessment by WB or FCM remains difficult. Recently, ELISA kits for exosome measurement have been developed that might allow high-throughput measurement even in unprocessed urine (Isobe, Mori et al. 2013, Duijvesz, Versluis et al. 2015, Salih, Fenton et al. 2016). Future studies should compare performance of ELISA-kits using pan-marker candidates like CD9, CD24 or CD63 with the measurements of urinary exosomes by NanoSight LM10.

Measurement and analysis of microvesicles in urine

In contrast to exosomes, microvesicles with a size range from 100nm-1000nm are much less abundant in urine (Oosthuyzen, Sime et al. 2013). For valid measurement urinary MVs must be above a certain concentration threshold (Burger, Thibodeau et al. 2014). Therefore, in the current work a concentrating procedure proposed by Burger et al. (Burger, Thibodeau et al. 2014) is employed with modifications and then applied in the Cyp1a1mRen2 DN model and in a subset of patients from the RDS study as a proof-of-principle. 20.000g spin was enough to pellet larger microparticles (Zhou, Yuen et al. 2006). Exosome-like particles were not enriched as most were retained in the supernatant, however some also appeared in the pellet. This might be due to Tamm-Horsfall protein that forms a polymer-network entrapping and pelleting exosomes(Fernandez-Llama, Khositseth et al. 2010). Contamination with exosomes was considered to be negligible for further analysis since exosomes are below the detectable range of the Attune flow cytometer (Danielson, Estanislau et al. 2016) (Burger, Schock et al. 2013). The mean coefficient of variation for the measurement method was well below 20% which is regarded to be an acceptable

level of repeatability of results. Annexin-V (AV) and Bodipy-Maleimide (BoM) can be used for staining MPs interchangeably in blood (Enjeti, Lincz et al. 2008). Similar results were obtained for urine for the first time in the current work. Gating for size was performed using non-fluorescent beads as described before (Nielsen, Beck-Nielsen et al. 2014) including several dilution steps to avoid swarm detection(van der Pol, Coumans et al. 2014).

Microvesicles as potential urinary biomarkers

Whilst urinary MV concentrations were massively higher in the diabetes and hypertension group of the Cyp1a1mRen2 DN model compared to control, total events (BoM^+ and BoM^-) in the gating window (200nm-1000nm) did not significantly differ between the groups, implying that this was specific for microvesicles. The results are in line with Burger et al. who demonstrated an increase of AV positive particles in three mouse models after induction of diabetic nephropathy (Burger, Thibodeau et al. 2014). The significant positive correlation between BoM^+ microvesicle and $AUC_{300\text{-}1000nm}$ measured by NanoSight not only strengthened the validity of the results but also the validity of the methodology of isolation.

In a subset of the RDS study which included patients with moderately to severely reduced renal function similar results were obtained as in the rodent study with a significant but lower correlation factor between NanoSight and Attune measurements. This could be explained by interferences such as medication or impurities from contamination during the non-sterile way of collection as Nanosight measured all events (BoM^+ and BoM^-) in the specific size range.

Blood from patients with severe CKD IV-V has increased concentration of Annexin V^+ positive particles (Trappenburg, van Schilfgaarde et al. 2012): They originated mainly from platelets and endothelial cells, with the cytotoxic effect of uraemia potentially being a contributing cause. In subset of the RDS study in this work, the concentration of BoM^+ tended to be higher in the urine of patients with CKD stage IV-V patients however this was not significant. On the other hand, the concentration of BoM^+ and $PODXL^+$ (podocalyxin-like protein) microvesicles negatively correlated with renal function. This is in line with other studies suggesting that glomerular damage promotes increased release of particles (Hara, Yanagihara et al. 2005, Burger, Thibodeau et al. 2014). It is intriguing to speculate that cells of other renal compartments might behave similarly. If this was true, then a panel with antibodies against renal compartment-specific surface markers could not only detect early cell stress/injury but also help to localize it. The panel might also contain an injury specific marker like KIM-1 or NGAL. Alvarez et al. demonstrated that uNGAL is also present in the urinary microparticle fraction and might be a more sensitive indicator for renal function than total urinary NGAL concentration (Alvarez, Suazo et al. 2013). At the moment there is, to the author's knowledge, no full characterization of the microparticle profile in urine. Unfortunately, none of the kidney-specific antibodies tested in this work beside podocalyxin could render a sufficient signal for MV detection (data not shown). The challenging task remains to find antibodies that target the correct externalized peptide sequence of the antigen on MVs and that are conjugated appropriately to comprise a panel. Another clear limitation of the present MV study is the small number of patients, so the results warrant validation in larger cohorts. However, the aim of the present study was to

demonstrate the feasibility of the modified protocol to enrich and measure urinary microvesicles. As a proof-of-principle a correlation between $BoM^{+}PODXL^{+}$ microvesicle concentration with renal function in a RDS subset was demonstrated.

3.4.10 Summary

In this chapter it had been demonstrated that labelled and unlabelled exosomes might be useful markers to inform about renal injury and function in the rodent Cyp1a1mRen2 DN model and in patient cohorts with mild (ET2D subgroup) and advanced (RDS study) renal damage. In the former group urinary exosomes might indicate the risk for decline in renal function. Larger study cohorts are necessary to confirm these results. Even more importantly, validation by another methodology of measurement is required with the recently published ELISA(Isobe, Mori et al. 2013, Duijvesz, Versluis et al. 2015, Salih, Fenton et al. 2016) probably the best fit for high-throughput biomarker approach.

A protocol for the measurement of microvesicles by Attune flow cytometry was developed and successfully applied in urine samples from the Cyp1a1mRen2 DN model and in samples from patients with reduced renal function. In humans, concentrations of podocalyxin positive MVs correlated with renal impairment.

4. GENERAL SUMMARY AND FUTURE WORK

4.1 Summary

In this thesis a novel transgenic rat Cyp1a1mRen2 model of diabetic nephropathy has been utilized to study markers of progression and regression of diabetic nephropathy. Analysis of transcriptomic data from the rodent model identified key pathways involved in renal inflammation and fibrosis and these were biochemically validated. The transcriptomic data was then integrated with the urinary peptidomic profile to identify urinary biomarkers which may reflect the underlying renal pathophysiology. The urinary biomarkers were quantified in patients with DN and linked with clinical outcome. Figure 73 summarizes major findings that had been described in this work and their relation to each other. The removal of damaging stimuli caused significant changes as depicted in Figure 74.

Figure 73: Pathways and biomarkers of progression predominate during the "Injury Phase" in the Cyp1a1mRen2 reversal model of diabetic nephropathy

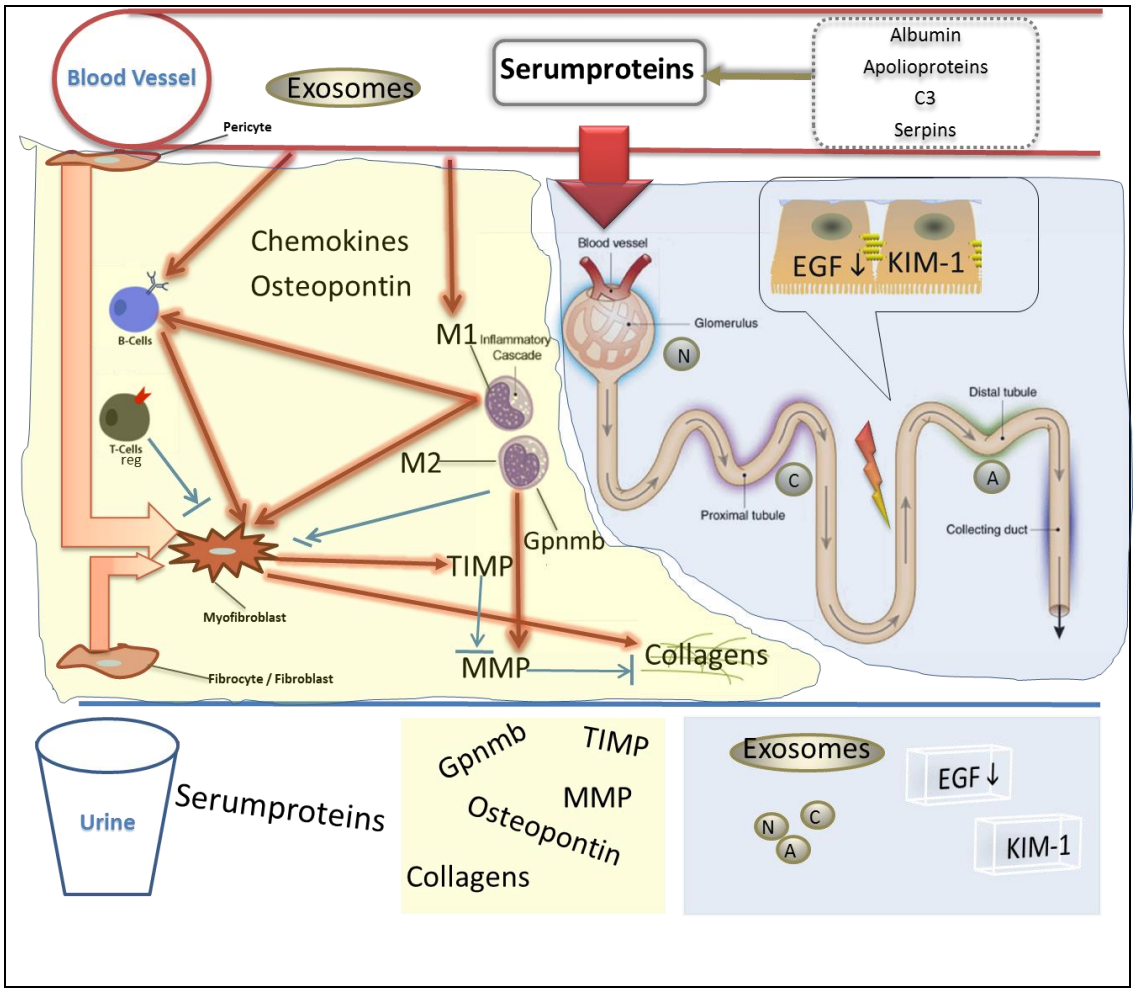

Figure 73. Simplified schematic illustration of pathophysiological pathways in the “injury phase” of the Cyp1a1mRen2 model of DN tailored to the findings of this work. Hyperglycemia and advanced glycation end products as well as glomerular hypertension are regarded the initiators of pathophysiologic changes (as outlined in more detail in the introduction section). One consequence is increased permeability of the glomerular barrier (large red arrow). In addition the inflammatory cascade is initiated which in turn activates pro-fibrotic pathways. All these factors result in cellular damage and destruction of renal architecture that can be assessed by the reduction of structural constitutively expressed proteins and increase of injury markers. Markers for all these changes can be measured in the urine. Of note, markers of tissue repair are increased during the injury stage indicating the presence of MMPs, phagocytic Macrophages and regulatory T-cells. So during injury phase, the foundations for renal repair are already laid out.

Figure 74: Pathway and markers of regression predominant during the "Reversal Phase" in the Cyp1a1mRen2 reversal model of diabetic nephropathy

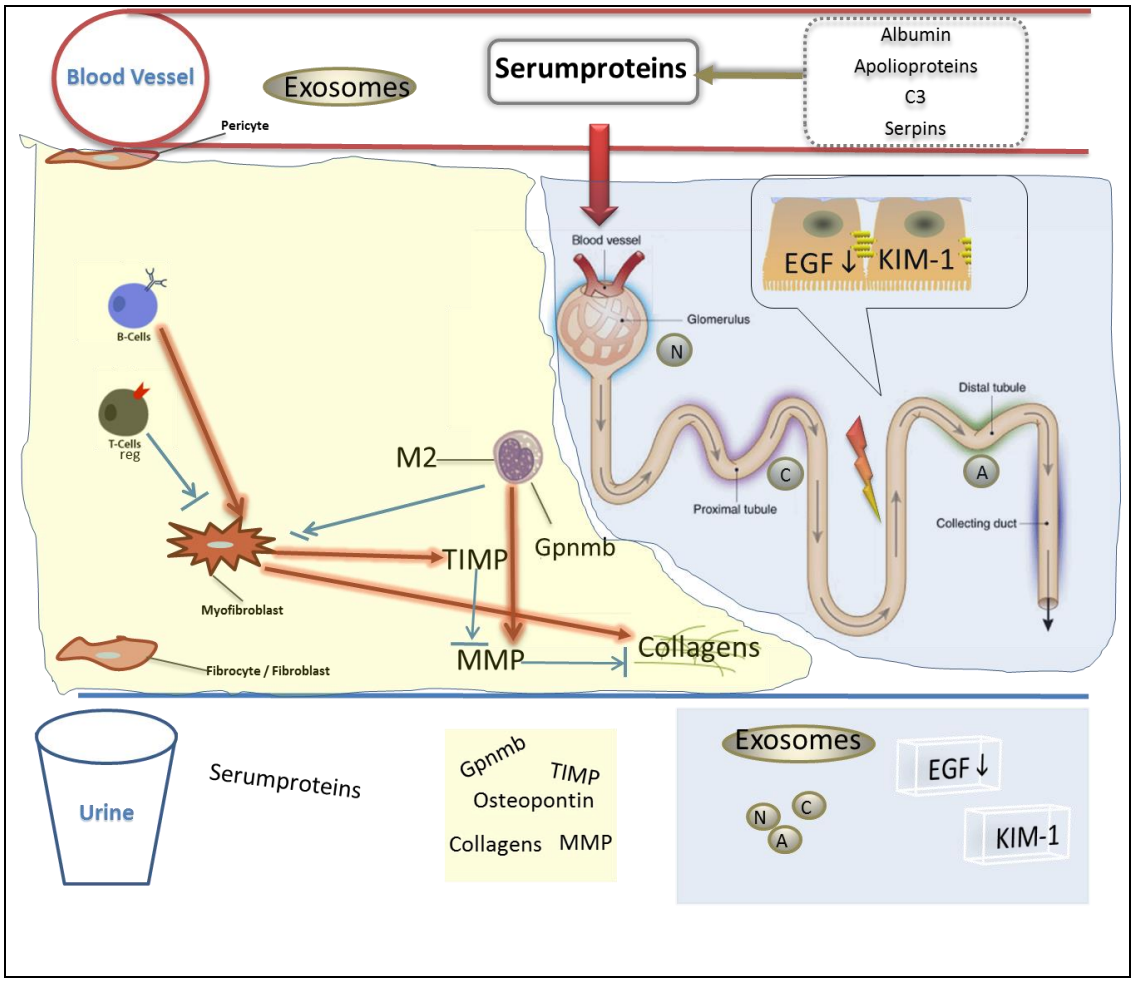

Figure 74. Schematic illustration of the assumed pathophysiological situation during the "reversal phase" of the Cyp1a1mRen2 model of DN. After the damaging stimuli had been removed the intraglomerular pressure lowers and the leakage of plasma proteins through the filtration barrier is reduced (reduced large red arrow). The removal of injurious stimuli down-regulates genetic expression of pro-inflammatory markers and of pro-fibrotic markers. This is reflected by a reduction of many inflammatory and pro-fibrotic markers in the urine. However myofibroblasts as well as TIMPs persists what might explain the failure of collagen/ECM degradation. The persistently reduced concentration of structural markers in the urine confirms the unaltered histological findings of tissue fibrosis in the reversal phase.

MMP and Gpnmb have not been detected in rat urine but in patients with DN. C3 – complement factor C3, EGF – epidermal growth factor, KIM1 – kidney injury molecule 1, MMP – metalloproteinase, TIMP – Tissue inhibitor of MMP, Treg – regulatory lymphocyte, M1 – classically activated macrophages type 1, M2- alternatively activated macrophages type 2, Gpnmb - glycoprotein (transmembrane) nmb, exosomes – unlabeled total exosomes, (C) – cubulin positive exosomes, (N) – nephrin positive exosomes, (A) – aquaporin2 positive exosomes

In summary, the pathological stimuli hypertension and hyperglycaemia do not only activate injurious but also reparative pathways in the kidney. During disease progression, renal damage increases and ECM accumulates as the reparative pathways are assumedly either blocked or outnumbered by injurious ones. Removal of the injurious stimuli may facilitate regression of disease. The persistent fibrosis observed despite a period of normotension and normoglycaemia may reflect persistent inhibition of reparative pathways, such as by Timp1. This might explain clinical observations that regression of renal fibrosis can be demonstrated only after ten years of normoglycaemia in patients with pancreatic transplants.

In urine samples from the DN model peptidomic analysis was performed at basline, injury phase (Figure 73) and reversal phase (Figure 74). In the injury phase many peptides with increased and decreased peak intensities compared to baseline were identified and could be linked to pathophysiological pathways in the kidney. Peptidomic analysis in patients with DN reflected the increased peak intensities of some of these markers. Pathophysiological alterations during the reversal phase were to a certain degree resonated by changes in the urinary peptidomic profile with a reduction of serum derived and inflammatory markers but a persistently low excretion of structural markers. The regulation of EGF, a structural marker for renal (tubular) mass, was confirmed by ELISA and IHC in the model.

Markers for inflammation (osteopontin, Gpnmb), ECM metabolism (MMP7) and renal cellular integrity and damage (EGF, KIM-1) that had been identified in the transcriptomic and/or peptidomic analysis of the DN model were measured in urine samples from patients of the ET2D study cohort. uEGF independently correlated with renal function and was associated with an increased mortality risk. In study

participants with sustained renal function increased uEGF was significantly associated with incident CKD III and/or a rapid decline in renal function even after adjustment for major risk factors like eGFR and ACR.

In pathway analysis microvesicle categories were found to be amongst the most significantly enriched for genes and urinary peptides with increased expression or peak intensities respectively during DN compared to control. Nanoparticle tracking analysis confirmed an increased total unlabelled urinary exosome-like particles (20-100nm) concentration in the injury phase of the DN model compared with baseline. $Nephrin^{+}$, $Cubilin^{+}$ and $AQP2^{+}$ urinary exosomes that might originate from different compartments of the tubule are also elevated in the injury phase (Figure 74). In the RDS study unlabelled and labelled urinary exosome concentration correlated with reduced renal function and in the ET2D study exosome concentration might be an early sensitive biomarker for renal deterioration.

The urinary microvesicles concentration measured by the Attune FCM as BoM positive events with 300-1000nm diameter also increases in the Cyp1a1mRen2 DN model compared to control. However, in a proof-of-principle study in patients with reduced renal function, only urinary levels of microvesicles that also expressed a kindey-specific surface marker (podocalyxin) correlated with renal function.

4.2 Limitations and Future Work

Extending the reversal phase

The short time period for the reversal compared to injury phase is a limitation of the study. For future work it would be intriguing to prolong the reversal period to

potentially achieve histologic regression of fibrosis. However, performing such an experiment that would exceed a year, (e.g. 28 weeks injury phase followed by 28 weeks reversal phase) would be technically very challenging to perform. The number of animals would have to be increased to ensure statistical significance since a considerable dropout due to stress/illness or severe hypo-/hyperglycemia is likely to happen throughout the experiment. To compensate for the confounding effects of aging an additional untreated control for the complete duration of the experiment also needs to be added. Recently, a mouse DN model employing combined hyperglycemia and hypertension has been published using TTRhRen mice(Thibodeau, Holterman et al. 2014). TTRhRen mice may develop biochemical and pathological evidence of DN earlier than Cyp1a1mRen2 rats, and might therefore be an alternative model for extending the experimental time frame. However the transcriptome of the TTRhRen model has not yet been characterized to demonstrate relevance to human DN.

Repeating the experiment it might be also useful to include partial reversal groups in which either hypertension or hyperglycaemia alone persist. In this way the individual contribution of these two components in preventing regression of fibrosis could be dissected.

Markers deriving from serum and renal tissue

A limitation of the urinary analysis is the inability to determine whether changes in marker concentrations stem from alterations in renal expression or in leakage of serum proteins across a disrupted glomerular barrier. In fact, both components might influence urinary biomarker concentration, and especially if occuring in opposite

directions, this might explain the our inability to detect altered urinary concentration of important tissue markers like MMP7 and osteopontin. Unless kidney specific variants of these proteins can be identified and detected, their use as urinary markers for renal pathophysiological processes will remain limited.

The identification of peptides C3 in the urine could easily be explained as serum-derived. However, increased expression of the C3 gene in the Cyp1a1mRen2 reversal DN model and in humans with DN indicates that both markers could play a pathophysiological role within the kidney. For C3, an involvement in the inflammatory cascade had been postulated(Wada and Nangaku 2013). Though limited in fully reflecting the complex interaction of different cell types involved in the development of diabetic nephropathy, *in vitro* models can be very helpful in supporting hypotheses. The novel RPTEC/TERT1 DN model based on the renal proximal tubule epithelial cells (RPTEC) that had been immortalized by using a human telomerase reverse transcriptase (hTERT) seems to recapitulate many features of human DN (Slyne, Slattery et al. 2015). Here the increased expression of C3 in a hyperglycemic milieu might be another important hint for its pathophysiological role and prompt further investigations.

Manipulating the inflammatory and profibrotic cascades

One limitation is that the suggested involvement of B- and T-cells and macrophages and the production and degradation of fibrosis are descriptive. There is no definitive proof for the hypothesized functions of these immune cells in the progression or regression of the disease. For macrophages, a lineage tracing approach could support the suggested regulation of M1 and M2 activated macrophages during the reversal

phase of the experiment. This could for example clarify whether M2 macrophages stem from the M1 phenotype or derive from resident macrophages or a different type of circulating monocytes. Unfortunately, the markers of specific macrophage subsets are not yet well characterized in rats. The depletion of B-cells as performed in other studies of renal fibrosis (Novobrantseva, Majeau et al. 2005) might help to further characterize their potential pro-fibrotic role in DN. Similarly, specific depletion of T-cells especially regulatory T-cells (Hobeika, Morse et al. 2011) could help to understand the involvement of the T-cells in DN.

The results in chapter 3 suggest that silencing of TIMP is an effective way to fasten degradation of ECM. However, such an experiment would have pharmaceutically to target both TIMP1 and TIMP2 at the same time as they appear to be able to compensate for each other(Kim, Oda et al. 2001). On the other hand a pan-TIMP blockade might be counterproductive as TIMP3 has been demonstrated to anti-inflammatory and anti-fibrotic characteristics (Wang, Famulski et al. 2014).

Potential effect of alternative splicing in the DM+HTN model

Given the fact that more than 94% of human genes can be alternatively spliced, abnormal regulation of alternative splicing (AS) is most likely involved in the pathogenesis of DN and there is evolving evidence in literature supporting this assumption (Stevens and Oltean 2016).

Gerold et al. demonstrate that the splice variant CTLA-4 potentiates regulatory T-cell function and delays the development of type 1 diabetes in a mice DN model (Gerold, Zheng et al. 2011). Notably, regulatory T-cells are assumed to play a protective role in the DM+HTN rat DN model as they are present during injury and reversal phase.

EGF activates SR-Protein kinases which in turn phosphorylate normally inactive SR proteins massively modifying AS patterns in the nucleus (Zhou, Qiu et al. 2012). This could be one potential mechanism by which EGF exerts its protective effect in renal disease.

An alternative splicing isoform of VEGF-A is VEGF-A165b that has anti-angiogenic properties. VEGF-A165b is increased in early but not in late DN stages and helps to stabilize the glomerular filtration barrier (Oltean, Qiu et al. 2015). Interestingly, in the hypertensive & hyperglycaemic DN model, that reflects moderately advanced human DN, total VEGF-A gene expression is markedly reduced (Conway, Rennie et al. 2012), however no AS isoforms have been differentiated in this work.

Finally, the AS isoform in the extradomain (EDA+) of fibronectin which is an important contributor to extracellular matrix is increased by TGF-beta1 stimulation via PI3 kinase-AKT signalling and SRp40 expression in human primary proximal tubule epithelial cells (Phanish, Heidebrecht et al. 2015). In the DM+HTN rat model TGF-beta1 and fibronectin gene expression were up-regulated but the AS isoforms of fibronectin had not been analysed.

In conclusion, the investigation of AS in the DM+HTN rat model might help to detect and explore novel pathophysiological pathways in DN what could result in the development of new treatment strategies.

Markers of tubular cell loss – more than biomarkers?

EGF and meprinA might not only indicate loss of renal cell mass but also have pathophysiological functions. Mathew et al. hypothesize that in the db/db mouse DN model meprinA in the renal tubules might directly mediate the therapeutical effects

of angiotensin-converting-enzyme-inhibitor (ACI) or ARB treatment (Mathew, Futterweit et al. 2005). As many ET2D patients had received ACI or ARB as first-line therapy for hypertension (2013), it might be possible to demonstrate a correlation between meprinA concentration, renal function and renin-angiotensin blockade in the study cohort.

In a model of early diabetic nephropathy the administration of EGF has proven to be protective against renal damage in an early model of diabetic nephropathy (Suarez-Pinzon, Yan et al. 2005). In addition, EGF administration prevented diabetes recurrence in NOD mice after transplantation with syngeneic islets (Suarez-Pinzon and Rabinovitch 2008) and improved wound-healing in diabetic NOD mice (Nagy, Nagashima et al. 2001). The administration of exogenous EGF in the Cyp1a1mRen2 model might be an interesting therapeutic experiment.

Peptidomics – beyond urinary analysis

As it has already been discussed in the respective result chapter, the exclusion of higher molecular-weight proteins by passing urine through a 10kDa exclusion filter might have reduced the spectrum of detectable proteins and hampered quantification in the LC-MS/MS analysis. The removal of abundant proteins (esp. albumin) is necessary to detect less abundant peptides, however targeted removal of albumin remains technically challenging (Filip, Vougas et al. 2015), therefore alternative approaches are needed. One option favoured by Raimondo et al. is to perform the analysis on urinary exosomes (Raimondo, Corbetta et al. 2013), however this potentially useful approach is complicated by the time-consuming process of exosome isolation. Proteomics/peptidomics in serum might be less “kidney-specific”

in patients with diabetes mellitus as the proteins will be derived from multiple organs, most importantly from the liver, but it could provide complementary information to the urinary peptidomics. Although - similar to urine - the abundance of serum albumin and immunoglobulins imposes technical challenges in sample preparation, several studies with promising biomarker panels have been published recently (e.g. Looker et al.(Looker, Colombo et al. 2015) and reviewed by Pena et al. (Pena, Mischak et al. 2016)). Direct analysis of renal tissue might circumvent the problem of abundant albumin in serum and urine. Beside the detection of new marker candidates (Zubiri, Posada-Ayala et al. 2015), it might in the Cyp1a1mRen2 reversal DN model help to gain deeper insight into the dissociation in the results between transcriptomic and immunohistochemistry/zymography analysis that was observed during the reversal phase - for example the fibrotic response persisted despite a marked reduction in collagen gene expression. Peptidomic analysis in tissue has been problematic due to its rapid degradation, but recently a new elegant protocol for peptidomic tissue analysis has been published that might forward the field (Secher, Kelstrup et al. 2016).

Extracellular vesicles – a potential new class of biomarkers

It is known that exosomes may pass from the serum to the urine (Oosthuyzen, Scullion et al. 2016), therefore whether unlabelled exosomes originate from serum or renal tissue cannot be distinguished. A further characterization of the exosomes urinary profile requires the labelling of exosomes for blood or kidney specific markers (e.g. nephrin, cubilin and aquarporin 2). The correct normalization of labelled exosome concentrations might be however a difficult task in large cohort studies: correcting for urinary creatinine is problematic since the total exosome

concentration does not well correlate with urinary creatinine as demonstrated in the ET2D cohort. Alternatively, correction can be made by reference to a "pan-exosomal marker" like CD24 or by measurement of the total exosome concentration. These options are time-consuming since the Nanosight LM10 can only measure light scatter or a single fluorochrome at a time and hence these methodologies are not feasible for high throughput cohort studies. Other methods of measurement are dynamic light scattering, resistive pulse sensing or, with some restriction due to the higher threshold of size detection, flow cytometry (van der Pol, Coumans et al. 2014) (Erdbrugger and Le 2016). However, the practicability for application in large studies remains to be elucidated for most of these techniques. The immunoassay based methodology for measurement of exosomes that has been published recently by Salih et al.(Salih, Fenton et al. 2016) seems to be quick and highly applicable for use in clinical studies. A comparative study between the immunoassay and NTA in larger cohorts for validation would be very informative.

The potential involvement of exosomes in the pathophysiology of DN was not investigated in this work but they probably play a role considering studies that demonstrate their modulating function in renal diseases (Salih, Zietse et al. 2014, Erdbrugger and Le 2016, Morrison, Bailey et al. 2016, Oosthuyzen, Scullion et al. 2016).

Microvesicles (100-1000nm) are measured by Flow Cytometry in many studies (Salih, Zietse et al. 2014) and this methodology seems reliable and applicable for large study cohorts. However, the construction of a panel of antibodies containing cell-specific surface markers from different renal compartments (cubilin, nephrin, aquaporin 2) and an injury-related marker (KIM-1) is challenging. At the moment,

only podocalyxin antibody seems to produce a signal that is sufficient for reliable measurement. Future work needs to focus on testing antibodies to find those target peptide sequences that are externalized by microvesicles. The coupling of Imaging with FCM (IFCM) might be a promising technical advance in the field because it has the potential to increase sensitivity and reduce the background noise at the lower size range of microvesicles (Erdbrugger, Rudy et al. 2014).

4.3 Concluding remark

Only recently, Ju et al. (Ju, Nair et al. 2015) applied an integrative transcriptomic approach to identify urinary EGF as a very sensitive and specific marker for renal deterioration in patients with CKD due to various aetiologies. Their work is complementary to this thesis that focuses on the predictive value of uEGF in patients with CKD due to Diabetes mellitus. Though uEGF as a marker needs further confirmation in other study cohorts including a prospective approach, it may in the future help to identify patients at risk for renal deterioration. This could support clinical decision-making relating to diagnosis (e.g. the necessity for renal biopsy) and intensification of therapeutic treatment and measurements. uEGF might be also useful in clinical research to select participants who are at higher risk of progression thereby reducing the number of patients required to achieve adequate power in the randomized-controlled trials of new therapeutics for CKD .

Future work will have to elaborate whether other markers discussed in this work have a similar potential.

5. REFERENCES

Aaltonen, P., P. Luimula, E. Astrom, T. Palmen, T. Gronholm, E. Palojoki, I. Jaakkola, H. Ahola, I. Tikkanen and H. Holthofer (2001). "Changes in the expression of nephrin gene and protein in experimental diabetic nephropathy." Lab Invest **81**(9): 1185-1190.

Advani, A., K. J. Wiggins, A. J. Cox, Y. Zhang, R. E. Gilbert and D. J. Kelly (2011). "Inhibition of the epidermal growth factor receptor preserves podocytes and attenuates albuminuria in experimental diabetic nephropathy." Nephrology (Carlton) **16**(6): 573-581.

Afkarian, M., M. Bhasin, S. T. Dillon, M. C. Guerrero, R. G. Nelson, W. C. Knowler, R. Thadhani and T. A. Libermann (2010). "Optimizing a proteomics platform for urine biomarker discovery." Mol Cell Proteomics **9**(10): 2195-2204.

Agarwal, R. and M. J. Andersen (2006). "Prognostic importance of ambulatory blood pressure recordings in patients with chronic kidney disease." Kidney Int **69**(7): 1175-1180.

Ahmed, A. K., J. L. Haylor, A. M. El Nahas and T. S. Johnson (2007). "Localization of matrix metalloproteinases and their inhibitors in experimental progressive kidney scarring." Kidney Int **71**(8): 755-763.

Aksun, S. A., D. Ozmen, B. Ozmen, Z. Parildar, I. Mutaf, N. Turgan, S. Habif, K. Kumanliogluc and O. Bayindir (2004). "Beta2-microglobulin and cystatin C in type 2 diabetes: assessment of diabetic nephropathy." Exp Clin Endocrinol Diabetes **112**(4): 195-200.

Alter, M. L., A. Kretschmer, K. Von Websky, O. Tsuprykov, C. Reichetzeder, A. Simon, J. P. Stasch and B. Hocher (2012). "Early urinary and plasma biomarkers for experimental diabetic nephropathy." Clin Lab **58**(7-8): 659-671.

Alvarez, M. L., M. Khosroheidari, R. Kanchi Ravi and J. K. DiStefano (2012). "Comparison of protein, microRNA, and mRNA yields using different methods of urinary exosome isolation for the discovery of kidney disease biomarkers." Kidney Int **82**(9): 1024-1032.

Alvarez, S., C. Suazo, A. Boltansky, M. Ursu, D. Carvajal, G. Innocenti, A. Vukusich, M. Hurtado, S. Villanueva, J. E. Carreno, A. Rogelio and C. E. Irarrazabal (2013). "Urinary exosomes as a source of kidney dysfunction biomarker in renal transplantation." Transplant Proc **45**(10): 3719-3723.

American Diabetes, A. (2016). "9. Microvascular Complications and Foot Care." Diabetes Care **39 Suppl 1**: S72-80.

Anders, H. J. and M. Ryu (2011). "Renal microenvironments and macrophage phenotypes determine progression or resolution of renal inflammation and fibrosis." Kidney Int **80**(9): 915-925.

Andresdottir, G., M. L. Jensen, B. Carstensen, H. H. Parving, K. Rossing, T. W. Hansen and P. Rossing (2014). "Improved survival and renal prognosis of patients with type 2 diabetes and nephropathy with improved control of risk factors." Diabetes Care **37**(6): 1660-1667.

Araki, S., M. Haneda, D. Koya, T. Sugaya, K. Isshiki, S. Kume, A. Kashiwagi, T. Uzu and H. Maegawa (2013). "Predictive effects of urinary liver-type fatty acid-binding protein for deteriorating renal function and incidence of cardiovascular disease in type 2 diabetic patients without advanced nephropathy." Diabetes Care **36**(5): 1248-1253.

Atrih, A., M. A. Mudaliar, P. Zakikhani, D. J. Lamont, J. T. Huang, S. E. Bray, G. Barton, S. Fleming and G. Nabi (2014). "Quantitative proteomics in resected renal cancer tissue for biomarker discovery and profiling." Br J Cancer **110**(6): 1622-1633.

Ban, C. R., S. M. Twigg, B. Franjic, B. A. Brooks, D. Celermajer, D. K. Yue and S. V. McLennan (2010). "Serum MMP-7 is increased in diabetic renal disease and diabetic diastolic dysfunction." Diabetes Res Clin Pract **87**(3): 335-341.

Barutta, F., M. Tricarico, A. Corbelli, L. Annaratone, S. Pinach, S. Grimaldi, G. Bruno, D. Cimino, D. Taverna, M. C. Deregibus, M. P. Rastaldi, P. C. Perin and G. Gruden (2013). "Urinary exosomal microRNAs in incipient diabetic nephropathy." PLoS One **8**(11): e73798.
Beretov, J., V. C. Wasinger, E. K. Millar, P. Schwartz, P. H. Graham and Y. Li (2015). "Proteomic Analysis of Urine to Identify Breast Cancer Biomarker Candidates Using a Label-Free LC-MS/MS Approach." PLoS One **10**(11): e0141876.
Berkman, J. and H. Rifkin (1973). "Unilateral nodular diabetic glomerulosclerosis (Kimmelstiel-Wilson): report of a case." Metabolism **22**(5): 715-722.
Beroniade, V. C., R. Lefebvre and P. Falardeau (1987). "Unilateral nodular diabetic glomerulosclerosis: recurrence of an experiment of nature." Am J Nephrol **7**(1): 55-59.
Betz, B. and B. R. Conway (2014). "Recent advances in animal models of diabetic nephropathy." Nephron Exp Nephrol **126**(4): 191-195.
Betz, B. and B. R. Conway (2016). "An Update on the Use of Animal Models in Diabetic Nephropathy Research." Curr Diab Rep **16**(2): 18.
Betz, B. B., S. J. Jenks, A. D. Cronshaw, D. J. Lamont, C. Cairns, J. R. Manning, J. Goddard, D. J. Webb, J. J. Mullins, J. Hughes, S. McLachlan, M. W. Strachan, J. F. Price and B. R. Conway (2016). "Urinary peptidomics in a rodent model of diabetic nephropathy highlights epidermal growth factor as a biomarker for renal deterioration in patients with type 2 diabetes." Kidney Int **89**(5): 1125-1135.
Bhensdadia, N. M., K. J. Hunt, M. F. Lopes-Virella, J. Michael Tucker, M. R. Mataria, J. L. Alge, B. A. Neely, M. G. Janech, J. M. Arthur and g. Veterans Affairs Diabetes Trial study (2013). "Urine haptoglobin levels predict early renal functional decline in patients with type 2 diabetes." Kidney Int **83**(6): 1136-1143.
Bonventre, J. V. (2009). "Kidney injury molecule-1 (KIM-1): a urinary biomarker and much more." Nephrol Dial Transplant **24**(11): 3265-3268.
Borges, F. T., S. A. Melo, B. C. Ozdemir, N. Kato, I. Revuelta, C. A. Miller, V. H. Gattone, 2nd, V. S. LeBleu and R. Kalluri (2013). "TGF-beta1-containing exosomes from injured epithelial cells activate fibroblasts to initiate tissue regenerative responses and fibrosis." J Am Soc Nephrol **24**(3): 385-392.
Braga, T. T., J. S. Agudelo and N. O. Camara (2015). "Macrophages During the Fibrotic Process: M2 as Friend and Foe." Front Immunol **6**: 602.
Brosius, F. C., 3rd (2008). "New insights into the mechanisms of fibrosis and sclerosis in diabetic nephropathy." Rev Endocr Metab Disord **9**(4): 245-254.
Brosius, F. C., 3rd, C. E. Alpers, E. P. Bottinger, M. D. Breyer, T. M. Coffman, S. B. Gurley, R. C. Harris, M. Kakoki, M. Kretzler, E. H. Leiter, M. Levi, R. A. McIndoe, K. Sharma, O. Smithies, K. Susztak, N. Takahashi, T. Takahashi and C. Animal Models of Diabetic Complications (2009). "Mouse models of diabetic nephropathy." J Am Soc Nephrol **20**(12): 2503-2512.
Brosius, F. C. and S. Pennathur (2013). "How to find a prognostic biomarker for progressive diabetic nephropathy." Kidney Int **83**(6): 996-998.
Burger, D., S. Schock, C. S. Thompson, A. C. Montezano, A. M. Hakim and R. M. Touyz (2013). "Microparticles: biomarkers and beyond." Clin Sci (Lond) **124**(7): 423-441.
Burger, D., J. F. Thibodeau, C. E. Holterman, K. D. Burns, R. M. Touyz and C. R. Kennedy (2014). "Urinary podocyte microparticles identify prealbuminuric diabetic glomerular injury." J Am Soc Nephrol **25**(7): 1401-1407.
Calvo, S. E., D. J. Pagliarini and V. K. Mootha (2009). "Upstream open reading frames cause widespread reduction of protein expression and are polymorphic among humans." Proc Natl Acad Sci U S A **106**(18): 7507-7512.

Cantley, L. G., C. M. Colangelo, K. L. Stone, L. Chung, J. Belcher, T. Abbott, J. L. Cantley, K. R. Williams and C. R. Parikh (2016). "Development of a Targeted Urine Proteome Assay for kidney diseases." Proteomics Clin Appl **10**(1): 58-74.
Chang, J. H., S. Y. Paik, L. Mao, W. Eisner, P. J. Flannery, L. Wang, Y. Tang, N. Mattocks, S. Hadjadj, J. M. Goujon, P. Ruiz, S. B. Gurley and R. F. Spurney (2012). "Diabetic kidney disease in FVB/NJ Akita mice: temporal pattern of kidney injury and urinary nephrin excretion." PLoS One **7**(4): e33942.
Chesher, D. (2008). "Evaluating assay precision." Clin Biochem Rev **29 Suppl 1**: S23-26.
Chevalier, R. L., M. S. Forbes and B. A. Thornhill (2009). "Ureteral obstruction as a model of renal interstitial fibrosis and obstructive nephropathy." Kidney Int **75**(11): 1145-1152.
Chou, K. M., C. C. Lee, C. H. Chen and C. Y. Sun (2013). "Clinical value of NGAL, L-FABP and albuminuria in predicting GFR decline in type 2 diabetes mellitus patients." PLoS One **8**(1): e54863.
Chow, F. Y., D. J. Nikolic-Paterson, R. C. Atkins and G. H. Tesch (2004). "Macrophages in streptozotocin-induced diabetic nephropathy: potential role in renal fibrosis." Nephrol Dial Transplant **19**(12): 2987-2996.
Cochrane, A. L., M. M. Kett, C. S. Samuel, N. V. Campanale, W. P. Anderson, D. A. Hume, M. H. Little, J. F. Bertram and S. D. Ricardo (2005). "Renal structural and functional repair in a mouse model of reversal of ureteral obstruction." J Am Soc Nephrol **16**(12): 3623-3630.
Cohen, C. D., M. T. Lindenmeyer, F. Eichinger, A. Hahn, M. Seifert, A. G. Moll, H. Schmid, E. Kiss, E. Grone, H. J. Grone, M. Kretzler, T. Werner and P. J. Nelson (2008). "Improved elucidation of biological processes linked to diabetic nephropathy by single probe-based microarray data analysis." PLoS One **3**(8): e2937.
Conserva, F., L. Gesualdo and M. Papale (2016). "A Systems Biology Overview on Human Diabetic Nephropathy: From Genetic Susceptibility to Post-Transcriptional and Post-Translational Modifications." J Diabetes Res **2016**: 7934504.
Conti, M., S. Moutereau, M. Zater, K. Lallali, A. Durrbach, P. Manivet, P. Eschwege and S. Loric (2006). "Urinary cystatin C as a specific marker of tubular dysfunction." Clin Chem Lab Med **44**(3): 288-291.
Conway, B. and J. Hughes (2012). "Cellular orchestrators of renal fibrosis." QJM **105**(7): 611-615.
Conway, B. R., B. Betz, T. A. Sheldrake, J. R. Manning, D. R. Dunbar, A. Dobyns, J. Hughes and J. J. Mullins (2014). "Tight blood glycaemic and blood pressure control in experimental diabetic nephropathy reduces extracellular matrix production without regression of fibrosis." Nephrology (Carlton) **19**(12): 802-813.
Conway, B. R., D. Manoharan, D. Manoharan, S. Jenks, J. W. Dear, S. McLachlan, M. W. Strachan and J. F. Price (2012). "Measuring urinary tubular biomarkers in type 2 diabetes does not add prognostic value beyond established risk factors." Kidney Int **82**(7): 812-818.
Conway, B. R., J. Rennie, M. A. Bailey, D. R. Dunbar, J. R. Manning, C. O. Bellamy, J. Hughes and J. J. Mullins (2012). "Hyperglycemia and renin-dependent hypertension synergize to model diabetic nephropathy." J Am Soc Nephrol **23**(3): 405-411.
Cook, N. R. (2008). "Statistical evaluation of prognostic versus diagnostic models: beyond the ROC curve." Clin Chem **54**(1): 17-23.
Cox, J. and M. Mann (2008). "MaxQuant enables high peptide identification rates, individualized p.p.b.-range mass accuracies and proteome-wide protein quantification." Nat Biotechnol **26**(12): 1367-1372.
Dagogo-Jack, S., S. M. Marshall, P. Kendall-Taylor and K. G. Alberti (1989). "Urinary excretion of human epidermal growth factor in the various stages of diabetic nephropathy." Clin Endocrinol (Oxf) **31**(2): 167-173.

Dallas, D. C., A. Guerrero, E. A. Parker, R. C. Robinson, J. Gan, J. B. German, D. Barile and C. B. Lebrilla (2015). "Current peptidomics: applications, purification, identification, quantification, and functional analysis." Proteomics **15**(5-6): 1026-1038.
Danielson, K. M., J. Estanislau, J. Tigges, V. Toxavidis, V. Camacho, E. J. Felton, J. Khoory, S. Kreimer, A. R. Ivanov, P. Y. Mantel, J. Jones, P. Akuthota, S. Das and I. Ghiran (2016). "Diurnal Variations of Circulating Extracellular Vesicles Measured by Nano Flow Cytometry." PLoS One **11**(1): e0144678.
Dear, J. W. (2014). "Urinary exosomes join the fight against infection." J Am Soc Nephrol **25**(9): 1889-1891.
Diabetes, C., I. Complications Trial/Epidemiology of Diabetes, G. Complications Research, D. M. Nathan, B. Zinman, P. A. Cleary, J. Y. Backlund, S. Genuth, R. Miller and T. J. Orchard (2009). "Modern-day clinical course of type 1 diabetes mellitus after 30 years' duration: the diabetes control and complications trial/epidemiology of diabetes interventions and complications and Pittsburgh epidemiology of diabetes complications experience (1983-2005)." Arch Intern Med **169**(14): 1307-1316.
Dimuccio, V., A. Ranghino, L. Pratico Barbato, F. Fop, L. Biancone, G. Camussi and B. Bussolati (2014). "Urinary CD133+ extracellular vesicles are decreased in kidney transplanted patients with slow graft function and vascular damage." PLoS One **9**(8): e104490.
Dragovic, R. A., C. Gardiner, A. S. Brooks, D. S. Tannetta, D. J. Ferguson, P. Hole, B. Carr, C. W. Redman, A. L. Harris, P. J. Dobson, P. Harrison and I. L. Sargent (2011). "Sizing and phenotyping of cellular vesicles using Nanoparticle Tracking Analysis." Nanomedicine **7**(6): 780-788.
Driver, T. H., M. G. Shlipak, R. Katz, L. Goldenstein, M. J. Sarnak, A. N. Hoofnagle, D. S. Siscovick, B. Kestenbaum, I. H. de Boer and J. H. Ix (2014). "Low serum bicarbonate and kidney function decline: the Multi-Ethnic Study of Atherosclerosis (MESA)." Am J Kidney Dis **64**(4): 534-541.
Duffield, J. S. (2014). "Cellular and molecular mechanisms in kidney fibrosis." J Clin Invest **124**(6): 2299-2306.
Duffield, J. S., S. J. Forbes, C. M. Constandinou, S. Clay, M. Partolina, S. Vuthoori, S. Wu, R. Lang and J. P. Iredale (2005). "Selective depletion of macrophages reveals distinct, opposing roles during liver injury and repair." J Clin Invest **115**(1): 56-65.
Duijvesz, D., C. Y. Versluis, C. A. van der Fels, M. S. Vredenbregt-van den Berg, J. Leivo, M. T. Peltola, C. H. Bangma, K. S. Pettersson and G. Jenster (2015). "Immuno-based detection of extracellular vesicles in urine as diagnostic marker for prostate cancer." Int J Cancer **137**(12): 2869-2878.
Edgar, J. R. (2016). "Q&A: What are exosomes, exactly?" BMC Biol **14**(1): 46.
Enjeti, A. K., L. Lincz and M. Seldon (2008). "Bio-maleimide as a generic stain for detection and quantitation of microparticles." Int J Lab Hematol **30**(3): 196-199.
Erdbrugger, U. and T. H. Le (2016). "Extracellular Vesicles in Renal Diseases: More than Novel Biomarkers?" J Am Soc Nephrol **27**(1): 12-26.
Erdbrugger, U., C. K. Rudy, M. E. Etter, K. A. Dryden, M. Yeager, A. L. Klibanov and J. Lannigan (2014). "Imaging flow cytometry elucidates limitations of microparticle analysis by conventional flow cytometry." Cytometry A **85**(9): 756-770.
Fallowfield, J. A., M. Mizuno, T. J. Kendall, C. M. Constandinou, R. C. Benyon, J. S. Duffield and J. P. Iredale (2007). "Scar-associated macrophages are a major source of hepatic matrix metalloproteinase-13 and facilitate the resolution of murine hepatic fibrosis." J Immunol **178**(8): 5288-5295.

Feng, M., Z. Zhang, P. Fu, S. M. Huang, Y. B. Yang, K. L. Su, Z. J. Chen and W. X. Tang (2006). "[Expression level of cubilin in the rat model of diabetic nephropathy]." Sichuan Da Xue Xue Bao Yi Xue Ban **37**(5): 738-741.
Fernandez-Llama, P., S. Khositseth, P. A. Gonzales, R. A. Star, T. Pisitkun and M. A. Knepper (2010). "Tamm-Horsfall protein and urinary exosome isolation." Kidney Int **77**(8): 736-742.
Filip, S., K. Vougas, J. Zoidakis, A. Latosinska, W. Mullen, G. Spasovski, H. Mischak, A. Vlahou and J. Jankowski (2015). "Comparison of Depletion Strategies for the Enrichment of Low-Abundance Proteins in Urine." PLoS One **10**(7): e0133773.
Filipe, V., A. Hawe and W. Jiskoot (2010). "Critical evaluation of Nanoparticle Tracking Analysis (NTA) by NanoSight for the measurement of nanoparticles and protein aggregates." Pharm Res **27**(5): 796-810.
Fioretto, P. and M. Mauer (2007). "Histopathology of diabetic nephropathy." Semin Nephrol **27**(2): 195-207.
Fioretto, P., M. W. Steffes, D. E. Sutherland, F. C. Goetz and M. Mauer (1998). "Reversal of lesions of diabetic nephropathy after pancreas transplantation." N Engl J Med **339**(2): 69-75.
Fioretto, P., D. E. Sutherland, B. Najafian and M. Mauer (2006). "Remodeling of renal interstitial and tubular lesions in pancreas transplant recipients." Kidney Int **69**(5): 907-912.
Fliser, D., J. Novak, V. Thongboonkerd, A. Argiles, V. Jankowski, M. A. Girolami, J. Jankowski and H. Mischak (2007). "Advances in urinary proteome analysis and biomarker discovery." J Am Soc Nephrol **18**(4): 1057-1071.
Fu, J., J. J. Keurentjes, H. Bouwmeester, T. America, F. W. Verstappen, J. L. Ward, M. H. Beale, R. C. de Vos, M. Dijkstra, R. A. Scheltema, F. Johannes, M. Koornneef, D. Vreugdenhil, R. Breitling and R. C. Jansen (2009). "System-wide molecular evidence for phenotypic buffering in Arabidopsis." Nat Genet **41**(2): 166-167.
Fufaa, G. D., E. J. Weil, K. V. Lemley, W. C. Knowler, F. C. Brosius, 3rd, B. Yee, M. Mauer and R. G. Nelson (2016). "Structural Predictors of Loss of Renal Function in American Indians with Type 2 Diabetes." Clin J Am Soc Nephrol **11**(2): 254-261.
Gandolfo, M. T., H. R. Jang, S. M. Bagnasco, G. J. Ko, P. Agreda, S. R. Satpute, M. T. Crow, L. S. King and H. Rabb (2009). "Foxp3+ regulatory T cells participate in repair of ischemic acute kidney injury." Kidney Int **76**(7): 717-729.
Gang, X., K. Ueki, S. Kon, M. Maeda, T. Naruse and Y. Nojima (2001). "Reduced urinary excretion of intact osteopontin in patients with IgA nephropathy." Am J Kidney Dis **37**(2): 374-379.
Gardiner, C., Y. J. Ferreira, R. A. Dragovic, C. W. Redman and I. L. Sargent (2013). "Extracellular vesicle sizing and enumeration by nanoparticle tracking analysis." J Extracell Vesicles **2**.
Gene Ontology, C. (2015). "Gene Ontology Consortium: going forward." Nucleic Acids Res **43**(Database issue): D1049-1056.
Gerold, K. D., P. Zheng, D. B. Rainbow, A. Zernecke, L. S. Wicker and S. Kissler (2011). "The soluble CTLA-4 splice variant protects from type 1 diabetes and potentiates regulatory T-cell function." Diabetes **60**(7): 1955-1963.
Ghazalpour, A., B. Bennett, V. A. Petyuk, L. Orozco, R. Hagopian, I. N. Mungrue, C. R. Farber, J. Sinsheimer, H. M. Kang, N. Furlotte, C. C. Park, P. Z. Wen, H. Brewer, K. Weitz, D. G. Camp, 2nd, C. Pan, R. Yordanova, I. Neuhaus, C. Tilford, N. Siemers, P. Gargalovic, E. Eskin, T. Kirchgessner, D. J. Smith, R. D. Smith and A. J. Lusis (2011). "Comparative analysis of proteome and transcriptome variation in mouse." PLoS Genet **7**(6): e1001393.
Gilbert, R. E. and M. E. Cooper (1999). "The tubulointerstitium in progressive diabetic kidney disease: more than an aftermath of glomerular injury?" Kidney Int **56**(5): 1627-1637.

Giusti, I., S. D'Ascenzo and V. Dolo (2013). "Microvesicles as potential ovarian cancer biomarkers." Biomed Res Int **2013**: 703048.
Good, D. M., P. Zurbig, A. Argiles, H. W. Bauer, G. Behrens, J. J. Coon, M. Dakna, S. Decramer, C. Delles, A. F. Dominiczak, J. H. Ehrich, F. Eitner, D. Fliser, M. Frommberger, A. Ganser, M. A. Girolami, I. Golovko, W. Gwinner, M. Haubitz, S. Herget-Rosenthal, J. Jankowski, H. Jahn, G. Jerums, B. A. Julian, M. Kellmann, V. Kliem, W. Kolch, A. S. Krolewski, M. Luppi, Z. Massy, M. Melter, C. Neususs, J. Novak, K. Peter, K. Rossing, H. Rupprecht, J. P. Schanstra, E. Schiffer, J. U. Stolzenburg, L. Tarnow, D. Theodorescu, V. Thongboonkerd, R. Vanholder, E. M. Weissinger, H. Mischak and P. Schmitt-Kopplin (2010). "Naturally occurring human urinary peptides for use in diagnosis of chronic kidney disease." Mol Cell Proteomics **9**(11): 2424-2437.
Gordin, D., C. Forsblom, N. M. Panduru, M. C. Thomas, M. Bjerre, A. Soro-Paavonen, N. Tolonen, N. Sandholm, A. Flyvbjerg, V. Harjutsalo, P. H. Groop and G. FinnDiane Study (2014). "Osteopontin is a strong predictor of incipient diabetic nephropathy, cardiovascular disease, and all-cause mortality in patients with type 1 diabetes." Diabetes Care **37**(9): 2593-2600.
Hadler-Olsen, E., P. Kanapathippillai, E. Berg, G. Svineng, J. O. Winberg and L. Uhlin-Hansen (2010). "Gelatin in situ zymography on fixed, paraffin-embedded tissue: zinc and ethanol fixation preserve enzyme activity." J Histochem Cytochem **58**(1): 29-39.
Hara, M., T. Yanagihara, I. Kihara, K. Higashi, K. Fujimoto and T. Kajita (2005). "Apical cell membranes are shed into urine from injured podocytes: a novel phenomenon of podocyte injury." J Am Soc Nephrol **16**(2): 408-416.
Harder, J. L., J. B. Hodgin and M. Kretzler (2015). "Integrative Biology of Diabetic Kidney Disease." Kidney Dis (Basel) **1**(3): 194-203.
Hartner, A., N. Cordasic, B. Klanke, M. Wittmann, R. Veelken and K. F. Hilgers (2007). "Renal injury in streptozotocin-diabetic Ren2-transgenic rats is mainly dependent on hypertension, not on diabetes." Am J Physiol Renal Physiol **292**(2): F820-827.
He, W., R. J. Tan, Y. Li, D. Wang, J. Nie, F. F. Hou and Y. Liu (2012). "Matrix metalloproteinase-7 as a surrogate marker predicts renal Wnt/beta-catenin activity in CKD." J Am Soc Nephrol **23**(2): 294-304.
Heilig, C. W., L. A. Concepcion, B. L. Riser, S. O. Freytag, M. Zhu and P. Cortes (1995). "Overexpression of glucose transporters in rat mesangial cells cultured in a normal glucose milieu mimics the diabetic phenotype." J Clin Invest **96**(4): 1802-1814.
Herget-Rosenthal, S., J. A. van Wijk, M. Brocker-Preuss and A. Bokenkamp (2007). "Increased urinary cystatin C reflects structural and functional renal tubular impairment independent of glomerular filtration rate." Clin Biochem **40**(13-14): 946-951.
Hesketh, E. E., D. C. Kluth and J. Hughes (2014). "Apoptotic cell administration is detrimental in murine renal ischaemia reperfusion injury." J Inflamm (Lond) **11**(1): 31.
Hesketh, E. E., M. A. Vernon, P. Ding, S. Clay, G. Borthwick, B. Conway and J. Hughes (2014). "A murine model of irreversible and reversible unilateral ureteric obstruction." J Vis Exp(94).
Hiemstra, T. F., P. D. Charles, T. Gracia, S. S. Hester, L. Gatto, R. Al-Lamki, R. A. Floto, Y. Su, J. N. Skepper, K. S. Lilley and F. E. Karet Frankl (2014). "Human urinary exosomes as innate immune effectors." J Am Soc Nephrol **25**(9): 2017-2027.
Hobeika, A. C., M. A. Morse, T. Osada, S. Peplinski, H. K. Lyerly and T. M. Clay (2011). "Depletion of human regulatory T cells." Methods Mol Biol **707**: 219-231.
Hodgin, J. B., V. Nair, H. Zhang, A. Randolph, R. C. Harris, R. G. Nelson, E. J. Weil, J. D. Cavalcoli, J. M. Patel, F. C. Brosius, 3rd and M. Kretzler (2013). "Identification of cross-

species shared transcriptional networks of diabetic nephropathy in human and mouse glomeruli." Diabetes **62**(1): 299-308.
Hogan, M. C., K. L. Johnson, R. M. Zenka, M. C. Charlesworth, B. J. Madden, D. W. Mahoney, A. L. Oberg, B. Q. Huang, A. A. Leontovich, L. L. Nesbitt, J. L. Bakeberg, D. J. McCormick, H. R. Bergen and C. J. Ward (2014). "Subfractionation, characterization, and in-depth proteomic analysis of glomerular membrane vesicles in human urine." Kidney Int **85**(5): 1225-1237.
Hole, P., K. Sillence, C. Hannell, C. M. Maguire, M. Roesslein, G. Suarez, S. Capracotta, Z. Magdolenova, L. Horev-Azaria, A. Dybowska, L. Cooke, A. Haase, S. Contal, S. Mano, A. Vennemann, J. J. Sauvain, K. C. Staunton, S. Anguissola, A. Luch, M. Dusinska, R. Korenstein, A. C. Gutleb, M. Wiemann, A. Prina-Mello, M. Riediker and P. Wick (2013). "Interlaboratory comparison of size measurements on nanoparticles using nanoparticle tracking analysis (NTA)." J Nanopart Res **15**: 2101.
Huang da, W., B. T. Sherman and R. A. Lempicki (2009). "Systematic and integrative analysis of large gene lists using DAVID bioinformatics resources." Nat Protoc **4**(1): 44-57.
Hudkins, K. L., W. Pichaiwong, T. Wietecha, J. Kowalewska, M. C. Banas, M. W. Spencer, A. Muhlfeld, M. Koelling, J. W. Pippin, S. J. Shankland, B. Askari, M. E. Rabaglia, M. P. Keller, A. D. Attie and C. E. Alpers (2010). "BTBR Ob/Ob mutant mice model progressive diabetic nephropathy." J Am Soc Nephrol **21**(9): 1533-1542.
Humphreys, B. D., S. L. Lin, A. Kobayashi, T. E. Hudson, B. T. Nowlin, J. V. Bonventre, M. T. Valerius, A. P. McMahon and J. S. Duffield (2010). "Fate tracing reveals the pericyte and not epithelial origin of myofibroblasts in kidney fibrosis." Am J Pathol **176**(1): 85-97.
Iimura, O., H. Takahashi, T. Yashiro, S. Madoiwa, Y. Sakata, Y. Asano and E. Kusano (2004). "Effect of ureteral obstruction on matrix metalloproteinase-2 in rat renal cortex." Clin Exp Nephrol **8**(3): 223-229.
Isobe, K., T. Mori, T. Asano, H. Kawaguchi, S. Nonoyama, N. Kumagai, F. Kamada, T. Morimoto, M. Hayashi, E. Sohara, T. Rai, S. Sasaki and S. Uchida (2013). "Development of enzyme-linked immunosorbent assays for urinary thiazide-sensitive Na-Cl cotransporter measurement." Am J Physiol Renal Physiol **305**(9): F1374-1381.
Ito, K., J. Chen, M. El Chaar, J. M. Stern, S. V. Seshan, J. J. Khodadadian, I. Richardson, M. J. Hyman, E. D. Vaughan, Jr., D. P. Poppas and D. Felsen (2004). "Renal damage progresses despite improvement of renal function after relief of unilateral ureteral obstruction in adult rats." Am J Physiol Renal Physiol **287**(6): F1283-1293.
Jaksik, R., M. Iwanaszko, J. Rzeszowska-Wolny and M. Kimmel (2015). "Microarray experiments and factors which affect their reliability." Biol Direct **10**: 46.
Ju, W., V. Nair, S. Smith, L. Zhu, K. Shedden, P. X. Song, L. H. Mariani, F. H. Eichinger, C. C. Berthier, A. Randolph, J. Y. Lai, Y. Zhou, J. J. Hawkins, M. Bitzer, M. G. Sampson, M. Thier, C. Solier, G. C. Duran-Pacheco, G. Duchateau-Nguyen, L. Essioux, B. Schott, I. Formentini, M. C. Magnone, M. Bobadilla, C. D. Cohen, S. M. Bagnasco, L. Barisoni, J. Lv, H. Zhang, H. Y. Wang, F. C. Brosius, C. A. Gadegbeku, M. Kretzler, C. P. N. Ercb and P. K.-I. Consortium (2015). "Tissue transcriptome-driven identification of epidermal growth factor as a chronic kidney disease biomarker." Sci Transl Med **7**(316): 316ra193.
Kadoglou, N. P., N. Sailer, G. Fotiadis, A. Kapelouzou and C. D. Liapis (2014). "The impact of type 2 diabetes and atorvastatin treatment on serum levels of MMP-7 and MMP-8." Exp Clin Endocrinol Diabetes **122**(1): 44-49.
Kalani, A., A. Mohan, M. M. Godbole, E. Bhatia, A. Gupta, R. K. Sharma and S. Tiwari (2013). "Wilm's tumor-1 protein levels in urinary exosomes from diabetic patients with or without proteinuria." PLoS One **8**(3): e60177.
Kamijo-Ikemori, A., T. Sugaya, T. Yasuda, T. Kawata, A. Ota, S. Tatsunami, R. Kaise, T. Ishimitsu, Y. Tanaka and K. Kimura (2011). "Clinical significance of urinary liver-type fatty

acid-binding protein in diabetic nephropathy of type 2 diabetic patients." Diabetes Care **34**(3): 691-696.
Kanehisa, M., Y. Sato, M. Kawashima, M. Furumichi and M. Tanabe (2016). "KEGG as a reference resource for gene and protein annotation." Nucleic Acids Res **44**(D1): D457-462.
Kantachuvesiri, S., S. Fleming, J. Peters, B. Peters, G. Brooker, A. G. Lammie, I. McGrath, Y. Kotelevtsev and J. J. Mullins (2001). "Controlled hypertension, a transgenic toggle switch reveals differential mechanisms underlying vascular disease." J Biol Chem **276**(39): 36727-36733.
Kanwar, Y. S., L. Sun, P. Xie, F. Y. Liu and S. Chen (2011). "A glimpse of various pathogenetic mechanisms of diabetic nephropathy." Annu Rev Pathol **6**: 395-423.
Kawaguchi, M., Y. Kamiya, J. Ito, T. Fujii, F. Hayakawa, N. Sakuma and T. Fujinami (1993). "Excretion of urinary epidermal growth factor in non-insulin dependent diabetes mellitus." Life Sci **52**(14): 1181-1186.
KDIGO, C. W. G. (2013). "KDIGO 2012 Clinical Practice Guideline for the Evaluation and Management of Chronic Kidney Disease." Kidney Int Suppl (2011) **3**(1): 4.
Ke, J. T., M. Li, S. Q. Xu, W. J. Zhang, Y. W. Jiang, L. Y. Cheng, L. Chen, J. N. Lou and W. Wu (2014). "Gliquidone decreases urinary protein by promoting tubular reabsorption in diabetic Goto-Kakizaki rats." J Endocrinol **220**(2): 129-141.
Keller, S., C. Rupp, A. Stoeck, S. Runz, M. Fogel, S. Lugert, H. D. Hager, M. S. Abdel-Bakky, P. Gutwein and P. Altevogt (2007). "CD24 is a marker of exosomes secreted into urine and amniotic fluid." Kidney Int **72**(9): 1095-1102.
Kelly, D. J., A. J. Cox, M. Tolcos, M. E. Cooper, J. L. Wilkinson-Berka and R. E. Gilbert (2002). "Attenuation of tubular apoptosis by blockade of the renin-angiotensin system in diabetic Ren-2 rats." Kidney Int **61**(1): 31-39.
Kelly, D. J., J. L. Wilkinson-Berka, T. J. Allen, M. E. Cooper and S. L. Skinner (1998). "A new model of diabetic nephropathy with progressive renal impairment in the transgenic (mRen-2)27 rat (TGR)." Kidney Int **54**(2): 343-352.
Kelly, D. J., J. L. Wilkinson-Berka, S. D. Ricardo, A. J. Cox and R. E. Gilbert (2002). "Progression of tubulointerstitial injury by osteopontin-induced macrophage recruitment in advanced diabetic nephropathy of transgenic (mRen-2)27 rats." Nephrol Dial Transplant **17**(6): 985-991.
Khokha, R., A. Murthy and A. Weiss (2013). "Metalloproteinases and their natural inhibitors in inflammation and immunity." Nat Rev Immunol **13**(9): 649-665.
Kikuchi, Y., R. Ikee, N. Hemmi, N. Hyodo, T. Saigusa, T. Namikoshi, M. Yamada, S. Suzuki and S. Miura (2004). "Fractalkine and its receptor, CX3CR1, upregulation in streptozotocin-induced diabetic kidneys." Nephron Exp Nephrol **97**(1): e17-25.
Kim, H., T. Oda, J. Lopez-Guisa, D. Wing, D. R. Edwards, P. D. Soloway and A. A. Eddy (2001). "TIMP-1 deficiency does not attenuate interstitial fibrosis in obstructive nephropathy." J Am Soc Nephrol **12**(4): 736-748.
Kim, S. S., S. H. Song, I. J. Kim, Y. K. Jeon, B. H. Kim, I. S. Kwak, E. K. Lee and Y. K. Kim (2013). "Urinary cystatin C and tubular proteinuria predict progression of diabetic nephropathy." Diabetes Care **36**(3): 656-661.
Kimura, F., G. Hasegawa, H. Obayashi, T. Adachi, H. Hara, M. Ohta, M. Fukui, Y. Kitagawa, H. Park, N. Nakamura, K. Nakano and T. Yoshikawa (2003). "Serum extracellular superoxide dismutase in patients with type 2 diabetes: relationship to the development of micro- and macrovascular complications." Diabetes Care **26**(4): 1246-1250.
Kisseleva, T., M. Cong, Y. Paik, D. Scholten, C. Jiang, C. Benner, K. Iwaisako, T. Moore-Morris, B. Scott, H. Tsukamoto, S. M. Evans, W. Dillmann, C. K. Glass and D. A. Brenner

(2012). "Myofibroblasts revert to an inactive phenotype during regression of liver fibrosis." Proc Natl Acad Sci U S A **109**(24): 9448-9453.
Klein, J., J. L. Bascands, H. Mischak and J. P. Schanstra (2016). "The role of urinary peptidomics in kidney disease research." Kidney Int **89**(3): 539-545.
Klein, J., T. Papadopoulos, H. Mischak and W. Mullen (2014). "Comparison of CE-MS/MS and LC-MS/MS sequencing demonstrates significant complementarity in natural peptide identification in human urine." Electrophoresis **35**(7): 1060-1064.
Kolset, S. O., F. P. Reinholt and T. Jenssen (2012). "Diabetic nephropathy and extracellular matrix." J Histochem Cytochem **60**(12): 976-986.
Korrapati, M. C., B. E. Shaner, B. A. Neely, J. L. Alge, J. M. Arthur and R. G. Schnellmann (2012). "Diabetes-induced renal injury in rats is attenuated by suramin." J Pharmacol Exp Ther **343**(1): 34-43.
Kowal, J., M. Tkach and C. Thery (2014). "Biogenesis and secretion of exosomes." Curr Opin Cell Biol **29**: 116-125.
Kriz, W., B. Kaissling and M. Le Hir (2011). "Epithelial-mesenchymal transition (EMT) in kidney fibrosis: fact or fantasy?" J Clin Invest **121**(2): 468-474.
Krolewski, A. S., M. A. Niewczas, J. Skupien, T. Gohda, A. Smiles, J. H. Eckfeldt, A. Doria and J. H. Warram (2014). "Early progressive renal decline precedes the onset of microalbuminuria and its progression to macroalbuminuria." Diabetes Care **37**(1): 226-234.
Kundu, S., Y. S. Aulchenko, C. M. van Duijn and A. C. Janssens (2011). "PredictABEL: an R package for the assessment of risk prediction models." Eur J Epidemiol **26**(4): 261-264.
Leichtle, A. B., J. F. Dufour and G. M. Fiedler (2013). "Potentials and pitfalls of clinical peptidomics and metabolomics." Swiss Med Wkly **143**: w13801.
Lev-Ran, A., D. L. Hwang, J. D. Miller and Z. Josefsberg (1990). "Excretion of epidermal growth factor (EGF) in diabetes." Clin Chim Acta **192**(3): 201-206.
Levey, A. S., L. A. Stevens, C. H. Schmid, Y. L. Zhang, A. F. Castro, 3rd, H. I. Feldman, J. W. Kusek, P. Eggers, F. Van Lente, T. Greene, J. Coresh and E. P. I. Ckd (2009). "A new equation to estimate glomerular filtration rate." Ann Intern Med **150**(9): 604-612.
Li, B., A. P. Castano, T. E. Hudson, B. T. Nowlin, S. L. Lin, J. V. Bonventre, K. D. Swanson and J. S. Duffield (2010). "The melanoma-associated transmembrane glycoprotein Gpnmb controls trafficking of cellular debris for degradation and is essential for tissue repair." FASEB J **24**(12): 4767-4781.
Li, C., C. W. Yang, C. W. Park, H. J. Ahn, W. Y. Kim, K. H. Yoon, S. H. Suh, S. W. Lim, J. H. Cha, Y. S. Kim, J. Kim, Y. S. Chang and B. K. Bang (2003). "Long-term treatment with ramipril attenuates renal osteopontin expression in diabetic rats." Kidney Int **63**(2): 454-463.
Li, F. and T. E. Curry, Jr. (2009). "Regulation and function of tissue inhibitor of metalloproteinase (TIMP) 1 and TIMP3 in periovulatory rat granulosa cells." Endocrinology **150**(8): 3903-3912.
Lin, S. L., T. Kisseleva, D. A. Brenner and J. S. Duffield (2008). "Pericytes and perivascular fibroblasts are the primary source of collagen-producing cells in obstructive fibrosis of the kidney." Am J Pathol **173**(6): 1617-1627.
Lindenmeyer, M. T., M. Kretzler, A. Boucherot, S. Berra, Y. Yasuda, A. Henger, F. Eichinger, S. Gaiser, H. Schmid, M. P. Rastaldi, R. W. Schrier, D. Schlondorff and C. D. Cohen (2007). "Interstitial vascular rarefaction and reduced VEGF-A expression in human diabetic nephropathy." J Am Soc Nephrol **18**(6): 1765-1776.
Looker, H. C., M. Colombo, S. Hess, M. J. Brosnan, B. Farran, R. N. Dalton, M. C. Wong, C. Turner, C. N. Palmer, E. Nogoceke, L. Groop, V. Salomaa, D. B. Dunger, F. Agakov, P. M. McKeigue, H. M. Colhoun and S. Investigators (2015). "Biomarkers of rapid chronic kidney disease progression in type 2 diabetes." Kidney Int **88**(4): 888-896.

Lorenzen, J., R. Shah, A. Biser, S. A. Staicu, T. Niranjan, A. M. Garcia, A. Gruenwald, D. B. Thomas, I. F. Shatat, K. Supe, R. P. Woroniecki and K. Susztak (2008). "The role of osteopontin in the development of albuminuria." J Am Soc Nephrol **19**(5): 884-890.
Lotvall, J., A. F. Hill, F. Hochberg, E. I. Buzas, D. Di Vizio, C. Gardiner, Y. S. Gho, I. V. Kurochkin, S. Mathivanan, P. Quesenberry, S. Sahoo, H. Tahara, M. H. Wauben, K. W. Witwer and C. Thery (2014). "Minimal experimental requirements for definition of extracellular vesicles and their functions: a position statement from the International Society for Extracellular Vesicles." J Extracell Vesicles **3**: 26913.
Lurbe, E., J. Redon, A. Kesani, J. M. Pascual, J. Tacons, V. Alvarez and D. Batlle (2002). "Increase in nocturnal blood pressure and progression to microalbuminuria in type 1 diabetes." N Engl J Med **347**(11): 797-805.
Maahs, D. M., J. Siwy, A. Argiles, M. Cerna, C. Delles, A. F. Dominiczak, N. Gayrard, A. Iphofer, L. Jansch, G. Jerums, K. Medek, H. Mischak, G. J. Navis, J. M. Roob, K. Rossing, P. Rossing, I. Rychlik, E. Schiffer, R. E. Schmieder, T. C. Wascher, B. M. Winklhofer-Roob, L. U. Zimmerli, P. Zurbig and J. K. Snell-Bergeon (2010). "Urinary collagen fragments are significantly altered in diabetes: a link to pathophysiology." PLoS One **5**(9).
Macisaac, R. J., E. I. Ekinci and G. Jerums (2014). "Markers of and risk factors for the development and progression of diabetic kidney disease." Am J Kidney Dis **63**(2 Suppl 2): S39-62.
Marioni, R. E., M. W. Strachan, R. M. Reynolds, G. D. Lowe, R. J. Mitchell, F. G. Fowkes, B. M. Frier, A. J. Lee, I. Butcher, A. Rumley, G. D. Murray, I. J. Deary and J. F. Price (2010). "Association between raised inflammatory markers and cognitive decline in elderly people with type 2 diabetes: the Edinburgh Type 2 Diabetes Study." Diabetes **59**(3): 710-713.
Mathew, R., S. Futterweit, E. Valderrama, A. A. Tarectecan, J. E. Bylander, J. S. Bond and H. Trachtman (2005). "Meprin-alpha in chronic diabetic nephropathy: interaction with the renin-angiotensin axis." Am J Physiol Renal Physiol **289**(4): F911-921.
Mathiesen, E. R., E. Nexo, E. Hommel and H. H. Parving (1989). "Reduced urinary excretion of epidermal growth factor in incipient and overt diabetic nephropathy." Diabet Med **6**(2): 121-126.
Mauer, M. and P. Fioretto (2013). "Pancreas transplantation and reversal of diabetic nephropathy lesions." Med Clin North Am **97**(1): 109-114.
McKittrick, I. B., Y. Bogaert, K. Nadeau, J. Snell-Bergeon, A. Hull, T. Jiang, X. Wang, M. Levi and K. S. Moulton (2011). "Urinary matrix metalloproteinase activities: biomarkers for plaque angiogenesis and nephropathy in diabetes." Am J Physiol Renal Physiol **301**(6): F1326-1333.
McLennan, S. V., D. J. Kelly, A. J. Cox, Z. Cao, J. G. Lyons, D. K. Yue and R. E. Gilbert (2002). "Decreased matrix degradation in diabetic nephropathy: effects of ACE inhibition on the expression and activities of matrix metalloproteinases." Diabetologia **45**(2): 268-275.
McLennan, S. V., D. J. Kelly, M. Schache, M. Waltham, V. Dy, R. G. Langham, D. K. Yue and R. E. Gilbert (2007). "Advanced glycation end products decrease mesangial cell MMP-7: a role in matrix accumulation in diabetic nephropathy?" Kidney Int **72**(4): 481-488.
McLennan, S. V., X. Y. Wang, V. Moreno, D. K. Yue and S. M. Twigg (2004). "Connective tissue growth factor mediates high glucose effects on matrix degradation through tissue inhibitor of matrix metalloproteinase type 1: implications for diabetic nephropathy." Endocrinology **145**(12): 5646-5655.
Meex, R. C., A. J. Hoy, A. Morris, R. D. Brown, J. C. Lo, M. Burke, R. J. Goode, B. A. Kingwell, M. J. Kraakman, M. A. Febbraio, J. W. Greve, S. S. Rensen, M. P. Molloy, G. I. Lancaster, C. R. Bruce and M. J. Watt (2015). "Fetuin B Is a Secreted Hepatocyte Factor Linking Steatosis to Impaired Glucose Metabolism." Cell Metab **22**(6): 1078-1089.

Meran, S. and R. Steadman (2011). "Fibroblasts and myofibroblasts in renal fibrosis." Int J Exp Pathol **92**(3): 158-167.
Merchant, M. L., B. A. Perkins, G. M. Boratyn, L. H. Ficociello, D. W. Wilkey, M. T. Barati, C. C. Bertram, G. P. Page, B. H. Rovin, J. H. Warram, A. S. Krolewski and J. B. Klein (2009). "Urinary peptidome may predict renal function decline in type 1 diabetes and microalbuminuria." J Am Soc Nephrol **20**(9): 2065-2074.
Merl, J., M. Ueffing, S. M. Hauck and C. von Toerne (2012). "Direct comparison of MS-based label-free and SILAC quantitative proteome profiling strategies in primary retinal Muller cells." Proteomics **12**(12): 1902-1911.
Miranda, K. C., D. T. Bond, M. McKee, J. Skog, T. G. Paunescu, N. Da Silva, D. Brown and L. M. Russo (2010). "Nucleic acids within urinary exosomes/microvesicles are potential biomarkers for renal disease." Kidney Int **78**(2): 191-199.
Mischak, H., C. Delles, A. Vlahou and R. Vanholder (2015). "Proteomic biomarkers in kidney disease: issues in development and implementation." Nat Rev Nephrol **11**(4): 221-232.
Mischak, H. and J. P. Schanstra (2011). "CE-MS in biomarker discovery, validation, and clinical application." Proteomics Clin Appl **5**(1-2): 9-23.
Mogensen, C. E. (1998). "Combined high blood pressure and glucose in type 2 diabetes: double jeopardy. British trial shows clear effects of treatment, especially blood pressure reduction." BMJ **317**(7160): 693-694.
Mogensen, C. E. (2003). "Microalbuminuria and hypertension with focus on type 1 and type 2 diabetes." J Intern Med **254**(1): 45-66.
Mogensen, C. E., R. Osterby and H. J. Gundersen (1979). "Early functional and morphologic vascular renal consequences of the diabetic state." Diabetologia **17**(2): 71-76.
Molitch, M. E., A. I. Adler, A. Flyvbjerg, R. G. Nelson, W. Y. So, C. Wanner, B. L. Kasiske, D. C. Wheeler, D. de Zeeuw and C. E. Mogensen (2015). "Diabetic kidney disease: a clinical update from Kidney Disease: Improving Global Outcomes." Kidney Int **87**(1): 20-30.
Morrison, E. E., M. A. Bailey and J. W. Dear (2016). "Renal extracellular vesicles: from physiology to clinical application." J Physiol.
Nagai, Y., L. Yao, H. Kobori, K. Miyata, Y. Ozawa, A. Miyatake, T. Yukimura, T. Shokoji, S. Kimura, H. Kiyomoto, M. Kohno, Y. Abe and A. Nishiyama (2005). "Temporary angiotensin II blockade at the prediabetic stage attenuates the development of renal injury in type 2 diabetic rats." J Am Soc Nephrol **16**(3): 703-711.
Nagy, A., H. Nagashima, S. Cha, G. E. Oxford, T. Zelles, A. B. Peck and M. G. Humphreys-Beher (2001). "Reduced oral wound healing in the NOD mouse model for type 1 autoimmune diabetes and its reversal by epidermal growth factor supplementation." Diabetes **50**(9): 2100-2104.
Nakamura, T., T. Saito, I. Kusaka, M. Higashiyama, S. Nagasaka, S. Ishibashi and S. E. Ishikawa (2002). "Decrease in urinary excretion of aquaporin-2 associated with impaired urinary concentrating ability in diabetic nephropathy." Nephron **92**(2): 445-448.
Naseeb, U., J. Axelsson, T. Jagerbrink, J. Shafqat, S. Zarina and H. Jornvall (2015). "Complementary LC-MS/MS Proteomic Analysis of Uremic Plasma Proteins." J Coll Physicians Surg Pak **25**(8): 606-609.
Nguyen, T. Q., L. Tarnow, A. Jorsal, N. Oliver, P. Roestenberg, Y. Ito, H. H. Parving, P. Rossing, F. A. van Nieuwenhoven and R. Goldschmeding (2008). "Plasma connective tissue growth factor is an independent predictor of end-stage renal disease and mortality in type 1 diabetic nephropathy." Diabetes Care **31**(6): 1177-1182.
NICE, N. C. G. C. (2014). Chronic Kidney Disease (Partial Update): Early Identification and Management of Chronic Kidney Disease in Adults in Primary and Secondary Care. Chronic

Kidney Disease (Partial Update): Early Identification and Management of Chronic Kidney Disease in Adults in Primary and Secondary Care. London.
Nicholas, S. B., J. Liu, J. Kim, Y. Ren, A. R. Collins, L. Nguyen and W. A. Hsueh (2010). "Critical role for osteopontin in diabetic nephropathy." Kidney Int **77**(7): 588-600.
Nielsen, M. H., H. Beck-Nielsen, M. N. Andersen and A. Handberg (2014). "A flow cytometric method for characterization of circulating cell-derived microparticles in plasma." J Extracell Vesicles **3**.
Nielsen, S. E., H. Reinhard, D. Zdunek, G. Hess, O. M. Gutierrez, M. Wolf, H. H. Parving, P. K. Jacobsen and P. Rossing (2012). "Tubular markers are associated with decline in kidney function in proteinuric type 2 diabetic patients." Diabetes Res Clin Pract **97**(1): 71-76.
Niewczas, M. A., T. Gohda, J. Skupien, A. M. Smiles, W. H. Walker, F. Rosetti, X. Cullere, J. H. Eckfeldt, A. Doria, T. N. Mayadas, J. H. Warram and A. S. Krolewski (2012). "Circulating TNF receptors 1 and 2 predict ESRD in type 2 diabetes." J Am Soc Nephrol **23**(3): 507-515.
Nkuipou-Kenfack, E., A. Bhat, J. Klein, V. Jankowski, W. Mullen, A. Vlahou, M. Dakna, T. Koeck, J. P. Schanstra, P. Zurbig, K. L. Rudolph, B. Schumacher, A. Pich and H. Mischak (2015). "Identification of ageing-associated naturally occurring peptides in human urine." Oncotarget **6**(33): 34106-34117.
Norden, A. G., M. Lapsley and R. J. Unwin (2014). "Urine retinol-binding protein 4: a functional biomarker of the proximal renal tubule." Adv Clin Chem **63**: 85-122.
Nosadini, R., M. Velussi, E. Brocco, M. Bruseghin, C. Abaterusso, A. Saller, M. Dalla Vestra, A. Carraro, E. Bortoloso, M. Sambataro, I. Barzon, F. Frigato, B. Muollo, M. Chiesura-Corona, G. Pacini, B. Baggio, F. Piarulli, A. Sfriso and P. Fioretto (2000). "Course of renal function in type 2 diabetic patients with abnormalities of albumin excretion rate." Diabetes **49**(3): 476-484.
Novobrantseva, T. I., G. R. Majeau, A. Amatucci, S. Kogan, I. Brenner, S. Casola, M. J. Shlomchik, V. Koteliansky, P. S. Hochman and A. Ibraghimov (2005). "Attenuated liver fibrosis in the absence of B cells." J Clin Invest **115**(11): 3072-3082.
O'Seaghdha, C. M., S. J. Hwang, M. G. Larson, J. B. Meigs, R. S. Vasan and C. S. Fox (2013). "Analysis of a urinary biomarker panel for incident kidney disease and clinical outcomes." J Am Soc Nephrol **24**(11): 1880-1888.
Obro, N. F., U. Lademann, K. Birkenkamp-Demtroder, L. Holten-Andersen, N. Brunner and H. Offenberg (2008). "A TIMP-1 splice variant transcript: possible role in regulation of TIMP-1 expression." Cancer Lett **262**(1): 64-70.
Ohta, S., J. C. Bukowski-Wills, L. Sanchez-Pulido, L. Alves Fde, L. Wood, Z. A. Chen, M. Platani, L. Fischer, D. F. Hudson, C. P. Ponting, T. Fukagawa, W. C. Earnshaw and J. Rappsilber (2010). "The protein composition of mitotic chromosomes determined using multiclassifier combinatorial proteomics." Cell **142**(5): 810-821.
Oltean, S., Y. Qiu, J. K. Ferguson, M. Stevens, C. Neal, A. Russell, A. Kaura, K. P. Arkill, K. Harris, C. Symonds, K. Lacey, L. Wijeyaratne, M. Gammons, E. Wylie, R. P. Hulse, C. Alsop, G. Cope, G. Damodaran, K. B. Betteridge, R. Ramnath, S. C. Satchell, R. R. Foster, K. Ballmer-Hofer, L. F. Donaldson, J. Barratt, H. J. Baelde, S. J. Harper, D. O. Bates and A. H. Salmon (2015). "Vascular Endothelial Growth Factor-A165b Is Protective and Restores Endothelial Glycocalyx in Diabetic Nephropathy." J Am Soc Nephrol **26**(8): 1889-1904.
Oosthuyzen, W., K. M. Scullion, J. R. Ivy, E. E. Morrison, R. W. Hunter, P. J. Starkey Lewis, E. O'Duibhir, J. M. Street, A. Caporali, C. D. Gregory, S. J. Forbes, D. J. Webb, M. A. Bailey and J. W. Dear (2016). "Vasopressin Regulates Extracellular Vesicle Uptake by Kidney Collecting Duct Cells." J Am Soc Nephrol.

Oosthuyzen, W., N. E. Sime, J. R. Ivy, E. J. Turtle, J. M. Street, J. Pound, L. E. Bath, D. J. Webb, C. D. Gregory, M. A. Bailey and J. W. Dear (2013). "Quantification of human urinary exosomes by nanoparticle tracking analysis." J Physiol **591**(Pt 23): 5833-5842.
Parikh, C. R. and H. Thiessen-Philbrook (2014). "Key concepts and limitations of statistical methods for evaluating biomarkers of kidney disease." J Am Soc Nephrol **25**(8): 1621-1629.
Park, M., M. G. Shlipak, R. Katz, S. Agarwal, J. H. Ix, C. Y. Hsu and C. A. Peralta (2012). "Subclinical cardiac abnormalities and kidney function decline: the multi-ethnic study of atherosclerosis." Clin J Am Soc Nephrol **7**(7): 1137-1144.
Parving, H. H., J. B. Lewis, M. Ravid, G. Remuzzi, L. G. Hunsicker and D. investigators (2006). "Prevalence and risk factors for microalbuminuria in a referred cohort of type II diabetic patients: a global perspective." Kidney Int **69**(11): 2057-2063.
Pena, M. J., A. Heinzel, G. Heinze, A. Alkhalaf, S. J. Bakker, T. Q. Nguyen, R. Goldschmeding, H. J. Bilo, P. Perco, B. Mayer, D. de Zeeuw and H. J. Lambers Heerspink (2015). "A panel of novel biomarkers representing different disease pathways improves prediction of renal function decline in type 2 diabetes." PLoS One **10**(5): e0120995.
Pena, M. J., H. Mischak and H. J. Heerspink (2016). "Proteomics for prediction of disease progression and response to therapy in diabetic kidney disease." Diabetologia.
Perkins, B. A., L. H. Ficociello, B. Roshan, J. H. Warram and A. S. Krolewski (2010). "In patients with type 1 diabetes and new-onset microalbuminuria the development of advanced chronic kidney disease may not require progression to proteinuria." Kidney Int **77**(1): 57-64.
Perkins, B. A., L. H. Ficociello, K. H. Silva, D. M. Finkelstein, J. H. Warram and A. S. Krolewski (2003). "Regression of microalbuminuria in type 1 diabetes." N Engl J Med **348**(23): 2285-2293.
Phanish, M. K., F. Heidebrecht, M. E. Nabi, N. Shah, I. Niculescu-Duvaz and M. E. Dockrell (2015). "The Regulation of TGFbeta1 Induced Fibronectin EDA Exon Alternative Splicing in Human Renal Proximal Tubule Epithelial Cells." J Cell Physiol **230**(2): 286-295.
Pichaiwong, W., K. L. Hudkins, T. Wietecha, T. Q. Nguyen, C. Tachaudomdach, W. Li, B. Askari, T. Kobayashi, K. D. O'Brien, J. W. Pippin, S. J. Shankland and C. E. Alpers (2013). "Reversibility of structural and functional damage in a model of advanced diabetic nephropathy." J Am Soc Nephrol **24**(7): 1088-1102.
Pickering, J. W. and Z. H. Endre (2012). "New metrics for assessing diagnostic potential of candidate biomarkers." Clin J Am Soc Nephrol **7**(8): 1355-1364.
Pisitkun, T., R. F. Shen and M. A. Knepper (2004). "Identification and proteomic profiling of exosomes in human urine." Proc Natl Acad Sci U S A **101**(36): 13368-13373.
Price, J. F., R. M. Reynolds, R. J. Mitchell, R. M. Williamson, F. G. Fowkes, I. J. Deary, A. J. Lee, B. M. Frier, P. C. Hayes and M. W. Strachan (2008). "The Edinburgh Type 2 Diabetes Study: study protocol." BMC Endocr Disord **8**: 18.
Qi, Z., H. Fujita, J. Jin, L. S. Davis, Y. Wang, A. B. Fogo and M. D. Breyer (2005). "Characterization of susceptibility of inbred mouse strains to diabetic nephropathy." Diabetes **54**(9): 2628-2637.
Raila, J., A. Henze, J. Spranger, M. Mohlig, A. F. Pfeiffer and F. J. Schweigert (2007). "Microalbuminuria is a major determinant of elevated plasma retinol-binding protein 4 in type 2 diabetic patients." Kidney Int **72**(4): 505-511.
Raimondo, F., S. Corbetta, L. Morosi, C. Chinello, E. Gianazza, G. Castoldi, C. Di Gioia, C. Bombardi, A. Stella, C. Battaglia, C. Bianchi, F. Magni and M. Pitto (2013). "Urinary exosomes and diabetic nephropathy: a proteomic approach." Mol Biosyst **9**(6): 1139-1146.
Ramachandran, P., A. Pellicoro, M. A. Vernon, L. Boulter, R. L. Aucott, A. Ali, S. N. Hartland, V. K. Snowdon, A. Cappon, T. T. Gordon-Walker, M. J. Williams, D. R. Dunbar, J. R. Manning,

N. van Rooijen, J. A. Fallowfield, S. J. Forbes and J. P. Iredale (2012). "Differential Ly-6C expression identifies the recruited macrophage phenotype, which orchestrates the regression of murine liver fibrosis." Proc Natl Acad Sci U S A **109**(46): E3186-3195.
Rappsilber, J., Y. Ishihama and M. Mann (2003). "Stop and go extraction tips for matrix-assisted laser desorption/ionization, nanoelectrospray, and LC/MS sample pretreatment in proteomics." Anal Chem **75**(3): 663-670.
Reidy, K., H. M. Kang, T. Hostetter and K. Susztak (2014). "Molecular mechanisms of diabetic kidney disease." J Clin Invest **124**(6): 2333-2340.
Retnakaran, R., C. A. Cull, K. I. Thorne, A. I. Adler, R. R. Holman and U. S. Group (2006). "Risk factors for renal dysfunction in type 2 diabetes: U.K. Prospective Diabetes Study 74." Diabetes **55**(6): 1832-1839.
Rouillon, J., A. Zocevic, T. Leger, C. Garcia, J. M. Camadro, B. Udd, B. Wong, L. Servais, T. Voit and F. Svinartchouk (2014). "Proteomics profiling of urine reveals specific titin fragments as biomarkers of Duchenne muscular dystrophy." Neuromuscul Disord **24**(7): 563-573.
Salih, M., R. A. Fenton, J. Knipscheer, J. W. Janssen, M. S. Vredenbregt-van den Berg, G. Jenster, R. Zietse and E. J. Hoorn (2016). "An Immunoassay for Urinary Extracellular Vesicles." Am J Physiol Renal Physiol: ajprenal 00463 02015.
Salih, M., R. Zietse and E. J. Hoorn (2014). "Urinary extracellular vesicles and the kidney: biomarkers and beyond." Am J Physiol Renal Physiol **306**(11): F1251-1259.
Satoh-Asahara, N., T. Suganami, T. Majima, K. Kotani, Y. Kato, R. Araki, K. Koyama, T. Okajima, M. Tanabe, M. Oishi, A. Himeno, S. Kono, A. Sugawara, M. Hattori, Y. Ogawa, A. Shimatsu, O. Japan and G. Metabolic Syndrome Study (2011). "Urinary cystatin C as a potential risk marker for cardiovascular disease and chronic kidney disease in patients with obesity and metabolic syndrome." Clin J Am Soc Nephrol **6**(2): 265-273.
Schanstra, J. P., P. Zurbig, A. Alkhalaf, A. Argiles, S. J. Bakker, J. Beige, H. J. Bilo, C. Chatzikyrkou, M. Dakna, J. Dawson, C. Delles, H. Haller, M. Haubitz, H. Husi, J. Jankowski, G. Jerums, N. Kleefstra, T. Kuznetsova, D. M. Maahs, J. Menne, W. Mullen, A. Ortiz, F. Persson, P. Rossing, P. Ruggenenti, I. Rychlik, A. L. Serra, J. Siwy, J. Snell-Bergeon, G. Spasovski, J. A. Staessen, A. Vlahou, H. Mischak and R. Vanholder (2015). "Diagnosis and Prediction of CKD Progression by Assessment of Urinary Peptides." J Am Soc Nephrol **26**(8): 1999-2010.
Schlatzer, D., D. M. Maahs, M. R. Chance, J. E. Dazard, X. Li, F. Hazlett, M. Rewers and J. K. Snell-Bergeon (2012). "Novel urinary protein biomarkers predicting the development of microalbuminuria and renal function decline in type 1 diabetes." Diabetes Care **35**(3): 549-555.
Schlatzer, D. M., J. E. Dazard, M. Dharsee, R. M. Ewing, S. Ilchenko, I. Stewart, G. Christ and M. R. Chance (2009). "Urinary protein profiles in a rat model for diabetic complications." Mol Cell Proteomics **8**(9): 2145-2158.
Scilabra, S. D., L. Troeberg, K. Yamamoto, H. Emonard, I. Thogersen, J. J. Enghild, D. K. Strickland and H. Nagase (2013). "Differential regulation of extracellular tissue inhibitor of metalloproteinases-3 levels by cell membrane-bound and shed low density lipoprotein receptor-related protein 1." J Biol Chem **288**(1): 332-342.
Secher, A., C. D. Kelstrup, K. W. Conde-Frieboes, C. Pyke, K. Raun, B. S. Wulff and J. V. Olsen (2016). "Analytic framework for peptidomics applied to large-scale neuropeptide identification." Nat Commun **7**: 11436.
Sekulic, M. and S. Pichler Sekulic (2013). "A compendium of urinary biomarkers indicative of glomerular podocytopathy." Patholog Res Int **2013**: 782395.
Sheen, Y. J. and W. H. Sheu (2014). "Risks of rapid decline renal function in patients with type 2 diabetes." World J Diabetes **5**(6): 835-846.

Shlipak, M. G., R. Katz, B. Kestenbaum, D. Siscovick, L. Fried, A. Newman, D. Rifkin and M. J. Sarnak (2009). "Rapid decline of kidney function increases cardiovascular risk in the elderly." J Am Soc Nephrol **20**(12): 2625-2630.
Siwy, J., C. Zoja, J. Klein, A. Benigni, W. Mullen, B. Mayer, H. Mischak, J. Jankowski, R. Stevens, A. Vlahou, S. Kossida, P. Perco and F. H. Bahlmann (2012). "Evaluation of the Zucker diabetic fatty (ZDF) rat as a model for human disease based on urinary peptidomic profiles." PLoS One **7**(12): e51334.
Slyne, J., C. Slattery, T. McMorrow and M. P. Ryan (2015). "New developments concerning the proximal tubule in diabetic nephropathy: in vitro models and mechanisms." Nephrol Dial Transplant **30 Suppl 4**: iv60-67.
Stevens, M. and S. Oltean (2016). "Alternative Splicing in CKD." J Am Soc Nephrol **27**(6): 1596-1603.
Stevens, P. E., A. Levin and M. Kidney Disease: Improving Global Outcomes Chronic Kidney Disease Guideline Development Work Group (2013). "Evaluation and management of chronic kidney disease: synopsis of the kidney disease: improving global outcomes 2012 clinical practice guideline." Ann Intern Med **158**(11): 825-830.
Suarez-Pinzon, W. L. and A. Rabinovitch (2008). "Combination therapy with epidermal growth factor and gastrin delays autoimmune diabetes recurrence in nonobese diabetic mice transplanted with syngeneic islets." Transplant Proc **40**(2): 529-532.
Suarez-Pinzon, W. L., Y. Yan, R. Power, S. J. Brand and A. Rabinovitch (2005). "Combination therapy with epidermal growth factor and gastrin increases beta-cell mass and reverses hyperglycemia in diabetic NOD mice." Diabetes **54**(9): 2596-2601.
Sun, A. L., J. T. Deng, G. J. Guan, S. H. Chen, Y. T. Liu, J. Cheng, Z. W. Li, X. H. Zhuang, F. D. Sun and H. P. Deng (2012). "Dipeptidyl peptidase-IV is a potential molecular biomarker in diabetic kidney disease." Diab Vasc Dis Res **9**(4): 301-308.
Sun, S. Z., Y. Wang, Q. Li, Y. J. Tian, M. H. Liu and Y. H. Yu (2006). "Effects of benazepril on renal function and kidney expression of matrix metalloproteinase-2 and tissue inhibitor of metalloproteinase-2 in diabetic rats." Chin Med J (Engl) **119**(10): 814-821.
Szklarczyk, D., A. Franceschini, S. Wyder, K. Forslund, D. Heller, J. Huerta-Cepas, M. Simonovic, A. Roth, A. Santos, K. P. Tsafou, M. Kuhn, P. Bork, L. J. Jensen and C. von Mering (2015). "STRING v10: protein-protein interaction networks, integrated over the tree of life." Nucleic Acids Res **43**(Database issue): D447-452.
Takamiya, Y., K. Fukami, S. Yamagishi, Y. Kaida, Y. Nakayama, N. Obara, R. Iwatani, R. Ando, K. Koike, T. Matsui, Y. Nishino, S. Ueda, M. E. Cooper and S. Okuda (2013). "Experimental diabetic nephropathy is accelerated in matrix metalloproteinase-2 knockout mice." Nephrol Dial Transplant **28**(1): 55-62.
Tapmeier, T. T., K. L. Brown, Z. Tang, S. H. Sacks, N. S. Sheerin and W. Wong (2008). "Reimplantation of the ureter after unilateral ureteral obstruction provides a model that allows functional evaluation." Kidney Int **73**(7): 885-889.
ter Meulen, C. G., H. J. Bilo, G. J. van Kamp, R. O. Gans and A. J. Donker (1994). "Urinary epidermal growth factor excretion is correlated to renal function loss per se and not to the degree of diabetic renal failure." Neth J Med **44**(1): 12-17.
Tervaert, T. W., A. L. Mooyaart, K. Amann, A. H. Cohen, H. T. Cook, C. B. Drachenberg, F. Ferrario, A. B. Fogo, M. Haas, E. de Heer, K. Joh, L. H. Noel, J. Radhakrishnan, S. V. Seshan, I. M. Bajema, J. A. Bruijn and S. Renal Pathology (2010). "Pathologic classification of diabetic nephropathy." J Am Soc Nephrol **21**(4): 556-563.
Tesch, G. H. (2010). "Macrophages and diabetic nephropathy." Semin Nephrol **30**(3): 290-301.

Thery, C., M. Ostrowski and E. Segura (2009). "Membrane vesicles as conveyors of immune responses." Nat Rev Immunol **9**(8): 581-593.
Thibodeau, J. F., C. E. Holterman, D. Burger, N. C. Read, T. L. Reudelhuber and C. R. Kennedy (2014). "A novel mouse model of advanced diabetic kidney disease." PLoS One **9**(12): e113459.
Thomas, M. C., M. E. Cooper and P. Zimmet (2016). "Changing epidemiology of type 2 diabetes mellitus and associated chronic kidney disease." Nat Rev Nephrol **12**(2): 73-81.
Thrailkill, K. M., R. Clay Bunn and J. L. Fowlkes (2009). "Matrix metalloproteinases: their potential role in the pathogenesis of diabetic nephropathy." Endocrine **35**(1): 1-10.
Thrailkill, K. M., T. Nimmo, R. C. Bunn, G. E. Cockrell, C. S. Moreau, S. Mackintosh, R. D. Edmondson and J. L. Fowlkes (2009). "Microalbuminuria in type 1 diabetes is associated with enhanced excretion of the endocytic multiligand receptors megalin and cubilin." Diabetes Care **32**(7): 1266-1268.
Thulesen, J., P. E. Jorgensen, O. Torffvit, E. Nexo and S. S. Poulsen (1997). "Urinary excretion of epidermal growth factor and Tamm-Horsfall protein in three rat models with increased renal excretion of urine." Regul Pept **72**(2-3): 179-186.
Titan, S. M., J. M. Vieira, Jr., W. V. Dominguez, S. R. Moreira, A. B. Pereira, R. T. Barros and R. Zatz (2012). "Urinary MCP-1 and RBP: independent predictors of renal outcome in macroalbuminuric diabetic nephropathy." J Diabetes Complications **26**(6): 546-553.
Togashi, Y. and Y. Miyamoto (2013). "Urinary cystatin C as a biomarker for diabetic nephropathy and its immunohistochemical localization in kidney in Zucker diabetic fatty (ZDF) rats." Exp Toxicol Pathol **65**(5): 615-622.
Torffvit, O., P. E. Jorgensen, A. L. Kamper, N. H. Holstein-Rathlou, P. P. Leyssac, S. S. Poulsen and S. Strandgaard (1998). "Urinary excretion of Tamm-Horsfall protein and epidermal growth factor in chronic nephropathy." Nephron **79**(2): 167-172.
Trappenburg, M. C., M. van Schilfgaarde, F. C. Frerichs, H. M. Spronk, H. ten Cate, C. W. de Fijter, W. E. Terpstra and A. Leyte (2012). "Chronic renal failure is accompanied by endothelial activation and a large increase in microparticle numbers with reduced procoagulant capacity." Nephrol Dial Transplant **27**(4): 1446-1453.
Tse, G. H., C. J. Johnston, D. Kluth, M. Gray, D. Gray, J. Hughes and L. P. Marson (2015). "Intrarenal B Cell Cytokines Promote Transplant Fibrosis and Tubular Atrophy." Am J Transplant **15**(12): 3067-3080.
Tuttle, K. R., G. L. Bakris, R. W. Bilous, J. L. Chiang, I. H. de Boer, J. Goldstein-Fuchs, I. B. Hirsch, K. Kalantar-Zadeh, A. S. Narva, S. D. Navaneethan, J. J. Neumiller, U. D. Patel, R. E. Ratner, A. T. Whaley-Connell and M. E. Molitch (2014). "Diabetic kidney disease: a report from an ADA Consensus Conference." Diabetes Care **37**(10): 2864-2883.
Tyanova, S., T. Temu, P. Sinitcyn, A. Carlson, M. Y. Hein, T. Geiger, M. Mann and J. Cox (2016). "The Perseus computational platform for comprehensive analysis of (prote)omics data." Nat Methods.
Urbanelli, L., A. Magini, S. Buratta, A. Brozzi, K. Sagini, A. Polchi, B. Tancini and C. Emiliani (2013). "Signaling pathways in exosomes biogenesis, secretion and fate." Genes (Basel) **4**(2): 152-170.
van der Pol, E., F. A. Coumans, A. E. Grootemaat, C. Gardiner, I. L. Sargent, P. Harrison, A. Sturk, T. G. van Leeuwen and R. Nieuwland (2014). "Particle size distribution of exosomes and microvesicles determined by transmission electron microscopy, flow cytometry, nanoparticle tracking analysis, and resistive pulse sensing." J Thromb Haemost **12**(7): 1182-1192.
Vittinghoff, E. and C. E. McCulloch (2007). "Relaxing the rule of ten events per variable in logistic and Cox regression." Am J Epidemiol **165**(6): 710-718.

Wada, J. and H. Makino (2013). "Inflammation and the pathogenesis of diabetic nephropathy." Clin Sci (Lond) **124**(3): 139-152.
Wada, T. and M. Nangaku (2013). "Novel roles of complement in renal diseases and their therapeutic consequences." Kidney Int **84**(3): 441-450.
Wang, Z., K. Famulski, J. Lee, S. K. Das, X. Wang, P. Halloran, G. Y. Oudit and Z. Kassiri (2014). "TIMP2 and TIMP3 have divergent roles in early renal tubulointerstitial injury." Kidney Int **85**(1): 82-93.
Woroniecka, K. I., A. S. Park, D. Mohtat, D. B. Thomas, J. M. Pullman and K. Susztak (2011). "Transcriptome analysis of human diabetic kidney disease." Diabetes **60**(9): 2354-2369.
Xu, X., L. Xiao, P. Xiao, S. Yang, G. Chen, F. Liu, Y. S. Kanwar and L. Sun (2014). "A glimpse of matrix metalloproteinases in diabetic nephropathy." Curr Med Chem **21**(28): 3244-3260.
Yamamoto, K., G. Murphy and L. Troeberg (2015). "Extracellular regulation of metalloproteinases." Matrix Biol **44-46**: 255-263.
Zhang, J., L. Xin, B. Shan, W. Chen, M. Xie, D. Yuen, W. Zhang, Z. Zhang, G. A. Lajoie and B. Ma (2012). "PEAKS DB: de novo sequencing assisted database search for sensitive and accurate peptide identification." Mol Cell Proteomics **11**(4): M111 010587.
Zhang, Z. X., K. Shek, S. Wang, X. Huang, A. Lau, Z. Yin, H. Sun, W. Liu, B. Garcia, S. Rittling and A. M. Jevnikar (2010). "Osteopontin expressed in tubular epithelial cells regulates NK cell-mediated kidney ischemia reperfusion injury." J Immunol **185**(2): 967-973.
Zhao, H. J., S. Wang, H. Cheng, M. Z. Zhang, T. Takahashi, A. B. Fogo, M. D. Breyer and R. C. Harris (2006). "Endothelial nitric oxide synthase deficiency produces accelerated nephropathy in diabetic mice." J Am Soc Nephrol **17**(10): 2664-2669.
Zhao, L., F. Wu, L. Jin, T. Lu, L. Yang, X. Pan, C. Shao, X. Li and Z. Lin (2014). "Serum CXCL16 as a novel marker of renal injury in type 2 diabetes mellitus." PLoS One **9**(1): e87786.
Zhou, H., P. S. Yuen, T. Pisitkun, P. A. Gonzales, H. Yasuda, J. W. Dear, P. Gross, M. A. Knepper and R. A. Star (2006). "Collection, storage, preservation, and normalization of human urinary exosomes for biomarker discovery." Kidney Int **69**(8): 1471-1476.
Zhou, Z., J. Qiu, W. Liu, Y. Zhou, R. M. Plocinik, H. Li, Q. Hu, G. Ghosh, J. A. Adams, M. G. Rosenfeld and X. D. Fu (2012). "The Akt-SRPK-SR axis constitutes a major pathway in transducing EGF signaling to regulate alternative splicing in the nucleus." Mol Cell **47**(3): 422-433.
Zubiri, I., M. Posada-Ayala, A. Benito-Martin, A. S. Maroto, M. Martin-Lorenzo, P. Cannata-Ortiz, F. de la Cuesta, L. Gonzalez-Calero, M. G. Barderas, B. Fernandez-Fernandez, A. Ortiz, F. Vivanco and G. Alvarez-Llamas (2015). "Kidney tissue proteomics reveals regucalcin downregulation in response to diabetic nephropathy with reflection in urinary exosomes." Transl Res **166**(5): 474-484 e474.
Zubiri, I., M. Posada-Ayala, A. Sanz-Maroto, E. Calvo, M. Martin-Lorenzo, L. Gonzalez-Calero, F. de la Cuesta, J. A. Lopez, B. Fernandez-Fernandez, A. Ortiz, F. Vivanco and G. Alvarez-Llamas (2014). "Diabetic nephropathy induces changes in the proteome of human urinary exosomes as revealed by label-free comparative analysis." J Proteomics **96**: 92-102.
Zurbig, P., G. Jerums, P. Hovind, R. J. Macisaac, H. Mischak, S. E. Nielsen, S. Panagiotopoulos, F. Persson and P. Rossing (2012). "Urinary proteomics for early diagnosis in diabetic nephropathy." Diabetes **61**(12): 3304-3313.

6. APPENDICES

i. Study information and consent form for the RDS-study

South East Scotland SAHSC BioResource

Participant Information Sheet Information for the collection of Tissue, Biospecimens and Data for Research

You are being invited to donate tissue samples to the South East Scotland SAHSC BioResource. Before you decide whether or not to do this, please take time to read the following information carefully and talk to others such as family, friends, your GP or healthcare team about the study if you wish. Please contact us if there is anything that is not clear or if you would like more information.

What is the purpose of the study?

SAHSC (Scottish Academic Health Sciences Collaboration) is funded by the CSO (Chief Scientist Office) which is part of the Scottish Government Health Directorates. This is a collaboration which has been set up between Scottish Universities and Health Boards. Its aim is to help translate discoveries made in research laboratories into improved care for patients.

The South East Scotland SAHSC BioResource will collect and store **biospecimens** (small pieces of tissue, cells and samples of body fluids) and build up a collection for use in research and education. This BioResource is being run by NHS Lothian, and has been approved by a Research Ethics Committee. The samples will only ever be used in research applications which have been approved by a scientific review committee.

What is tissue and why is it required for research and education?

The human body is made up of cells which are the basic building blocks for tissues. Organs such as lungs, liver, kidney and appendix are made up of tissue. There are many different types of cells and tissues in the human body. Body fluids such as blood, urine and saliva contain cells. Material taken during a cervical smear test also contains cells. Doctors and scientists need human tissue and other biospecimens for medical research. From these they can see and understand how diseases start and develop. They can also try out different drugs and tests on the tissue. This may help them find new medicines and treatments, and possibly even ways of diagnosing diseases earlier.

As well as providing care and treatment for patients, the NHS is also responsible for educating and training doctors, nurses and other healthcare workers. Human tissue is needed for this as well.

Why have I been asked to take part?

You are currently in hospital or attending a clinic and may be due to have an operation or medical procedure during which you may have some cells or tissue removed. If some cells or tissue are left over, and you agree, we would like to use this material for research.

What will this involve?

During your investigation(s) or operation(s), which are part of your treatment the doctor may take some tissue from your body. This piece of tissue will be sent to a pathologist for diagnosis. A pathologist is a doctor who specialises in the examination of tissue, to diagnose or confirm what is wrong with you. Some of the tissue is used for your tests, and then becomes part of your medical record. This means that it can be looked at again if you are ill in the future.

However, some tissue is usually left over and would normally be disposed of. We are asking you to donate this surplus tissue for medical research and education.

During your treatment, the doctor may also take body fluids e.g. blood and urine for testing. Some of these may also be "left over" and if you agree, could also be used for medical research and teaching.

We may ask you to provide us with an extra blood sample, and this could possibly mean an extra venepuncture. We may also ask you to provide a urine sample.

The piece of tissue taken for the BioResource is usually about the size of a pound coin, or about two to four teaspoonfuls of fluid.

We would also like to use some information from your medical notes. This will be information about your physical condition, treatment and diagnosis but not about your mental health.

Your name and address and anything else that could identify you will be removed before allowing researchers to use any of your samples or data.

Do I have to do this?

No, it is entirely up to you if you want to donate to the BioResource. When you come into hospital or attend a clinic and we ask if you agree to let us use your surplus tissue for education or research, simply say no. We will not put you under any pressure, and you do not have to give a reason. **Please be assured that your decision will not affect your healthcare.**

You can also change your mind at any time, without giving a reason. If you change your mind later on however, some of your samples may already have been used. It would be too late for us to stop your sample being used, but we would dispose of any tissue that hadn't been used yet.

What are the benefits of taking part?

It is unlikely that you will personally benefit from the research. This research often involves testing large numbers of samples from many different people to try to identify factors that influence medical conditions and disease, and it can take many years to produce advances in treatmentd. However, if at any point during the programme this information becomes of use in guiding your treatment, the clinical care team looking after you in the hospital will be made aware of this and they will explain the information to you

You can benefit from the knowledge that you are personally helping research to prevent or treat illness. The tests and treatments being used for you were developed with the help of patients who took part in research years ago. Research might make faster progress as more human samples are studied, helping the health of future generations

What are the possible disadvantages or risks of taking part?

The only risks would be the possibility of some pain or bruising from giving an extra blood sample. Otherwise, there will be nothing extra happening to you as the BioResource would only collect and store tissue that would normally have been removed and disposed of anyway.

Where will my tissue sample be used?

- The NHS
- Universities
- Research Institutions
- Commercial companies

Tissue samples may also be sent abroad. You can be sure, however, that all researchers whether in this country or abroad must have proof that they are following legal and ethical guidelines for their research. Researchers working abroad will be required to sign a form agreeing to follow the same rules and regulations which apply in the UK.
Your donated tissue will not be used in animal research, research about termination of pregnancy, or reproductive cloning.

How long will tissue be stored?

The tissue you donate will stay in the NHS, or with approved researchers until it is all used, or disposed of should you decide to withdraw your consent. All tissues will be disposed of lawfully and respectfully, and a record will be kept of this. If you decide to withdraw consent, you can tell a member of your healthcare team, or contact us at the BioResource on the telephone number or email address in the "Further Information" section.

Will my taking part be confidential?

Yes, only the BioResource staff will be able to identify you. They will abide by the Data Protection Act 1998 at all times and make sure your name, address, and any other information that would identify you are removed from your medical information before it is given to any researchers. The information held on computer will be kept secure, and all written information will be held in locked filing cabinets.

Will my medical notes be used?

Medical research is of more value if the researcher has information about the medical history of the person who donated the tissue. We would like your permission to use and store information from your medical notes now, and possibly in the future as a follow up. All information collected and stored will be kept strictly confidential. Your personal information like your name and address will be removed from your medical notes before being given to anyone for their research. Only the BioResource staff and your Healthcare team will be able to link your information to your medical notes.

Can researchers find new information about my health?

It is possible, but the research on your tissue will normally have nothing to do with your own care or treatment. Future research may give us information about what type of treatment would be most suitable for particular medical conditions but this data is primarily intended for research and it is very unlikely that your sample alone will give us this type of information. However, if any information might be of use in your clinical care, the doctors looking after you may discuss how the information could be used to guide your treatment.

Will researchers carry out genetic tests on my tissue?

Genetic testing on your DNA may be carried out on the donated tissue. A lot of research today focuses on the study of genetic material from healthy individuals compared to people with known diseases. This comparison helps researchers to discover genetic differences which in turn help in the development of new drugs and treatments.

Will anyone make money from my tissues?
It is illegal to sell tissue for profit. The NHS may charge researchers a fee for your tissue, but this is to cover the costs of running the BioResource.
If researchers develop a new drug, treatment or test, a pharmaceutical company or other researcher may then make a profit. It will not be possible to claim any money because you donated tissue, but any new drug, treatment, or test would potentially help us all in the future.

I want to donate…what should I do next?
When you come into hospital or attend a clinic, you will be asked if you agree to let your surplus tissue from any investigation(s) or operation(s) be used for medical research. You will then be asked to sign a consent form. You should keep a copy of this Patient Information Sheet and Consent Form for your records.

What if there is a problem?
If you believe that you have been harmed in any way by taking part in this study, speak to the research team in the first instance. If you are still unhappy, you have the right to pursue a complaint and seek any resulting compensation through NHS Lothian which is acting as the research sponsor. Details about this are available from the research team. Also as a patient of the NHS, you have the right to pursue a complaint through the usual NHS process. To do so, you can submit a written complaint to the Patient Liaison Manager, NHS Lothian Complaints Office, 2nd Floor, Waverley Gate, Edinburgh telephone 0131 465 5708. Note that the NHS has no legal liability for non-negligent harm. However, if you are harmed and this is due to someone's negligence, you may have grounds for a legal action against NHS Lothian, but you may have to pay your legal costs.

Who has reviewed the study?
The Tayside Committee on Medical Research Ethics B, has examined the proposal and has raised no objections from the point of view of medical ethics. It is a requirement that your records in this research together with any relevant medical records, be made available for scrutiny by monitors whose role is to check that research is properly conducted and the interests of those taking part are adequately protected.

Further Information
If you have any questions about the donation of samples and information on the possible uses of them, please ask the person discussing donation with you and seeking your consent.
If you think of anything else later, you can contact us at 0131 537 3363 or email rie.tissuegovernance@luht.scot.nhs.uk

We will endeavour to supply this information in different languages and formats if requested.

Thank you for taking the time to read this Information Sheet and for considering taking part in this study.

South East Scotland SAHSC BioResource

The collection of Tissue, Biospecimens and Data for Research

PARTICIPANT CONSENT FORM

Explanation of consent procedure

You are being invited to donate tissue to the South East Scotland SAHSC BioResource and should have had time to read the Participant Information Sheet (Version 1.2) and discuss it with your healthcare team, GP, family and friends.
If you decide to participate, please initial the boxes for numbers 1 to 7, circle YES or NO for numbers 8 and 9, and sign at the bottom (overleaf).
All of your information will be treated strictly confidentially, and all BioResource staff will follow the principles of the Data Protection Act 1998.

Please Initial

1. I confirm that I have read this consent form and Participant Information Sheet (Version 1.2) and have had the opportunity to ask questions about them. ☐
2. I understand that some surplus tissue or body fluids may be left over during the course of my operation(s) / investigation(s) within NHS Lothian and I agree to donate this surplus material to the South East Scotland BioResource for future research use. ☐
3. I declare that I have given my consent voluntarily to the storage of this surplus tissue and understand that I am free to withdraw at any time without giving any reason, and that my medical care will not be affected. ☐
4. I agree that my donated sample(s) may be used by clinical, academic or commercial researchers, and may be used abroad. ☐
5. I give the SAHSC BioResource permission to access and store information about my general physical health, past, present and future illness, diagnosis and treatment from my medical records. I understand that all information collected will be kept strictly confidential by the BioResource research team. ☐
6. I understand that the information obtained through any research conducted is unlikely to have any direct medical benefit to me, but I agree to my clinical care team being informed if research tests on my samples could have direct impact on my care during the course of my treatment ☐
7. I understand that I will not benefit financially if this research leads to the development of a new treatment or medical test or product. ☐

8. I agree that my surplus tissue or other biospecimen may be stored and used for future DNA testing including genetic analysis.
Please clearly circle YES or NO

YES / NO

9. I agree to provide an extra blood sample, by venepuncture, and/or urine sample if necessary.
Please clearly circle YES or NO.

YES / NO

Name of patient (please print)	**Signature**	**Date**
.....	.....	.....

Name of person witnessing consent	**Signature**	**Date**
.....	.....	.....

Thank you for agreeing to take part in this research

3 Copies:
1 to Participant, 1 to South East Scotland SAHSC BioResource, Original to be stored in Patient File

Contact details for BioResource team:

The Tissue Governance Manager
ECMC
WTCRF
Western General Hospital
Crewe Road South
Edinburgh EH4 2XU

Tel 0131 537 3363
Email rie.tissuegovernance@luht.scot.nhs.uk

Study ID label:

ii. Genes upregulated specifically during injury phase in the Cyp1a1mRen2 reversal model

The list has been published(Conway, Betz et al. 2014) and is available online at: http://onlinelibrary.wiley.com/doi/10.1111/nep.12335/suppinfo

iii. Genes upregulated during the injury and reversal phase in the Cyp1a1mRen2 reversal model

The list has been published (Conway, Betz et al. 2014) and is available online at: http://onlinelibrary.wiley.com/doi/10.1111/nep.12335/suppinfo

iv. Urinary Peptides significantly changed in precursor peak intensities between baseline and injury phase and injury and reversal phase in the Cyp1a1mRen2 reversal model

Mean intensity per group, p-value between two respective groups, peptide sequence are provided. The group indicates the significance between baseline and injury and between injury and reversal phase. The respective numbers per group are given in the table.

group	injury to baseline	reversal to injury	number of peptides
1	increase	unchanged	29
2	increase	decrease	26
3	decrease	unchanged	120
4	decrease	increase	13
5	increase	increase	3
6	decrease	decrease	3
7	unchanged	increase	47
8	unchanged	decrease	13

peptide sequence	protein symbol	gene symbol	protein names	p-value baseline-injury	p-value control-reversal	p-value injury-reversal	mean peak intensity control	mean peak intensity injury	meanpeak intensity reversal	groups
SPVASVESASGEVLHSPK	P24090	Ahsg	Alpha-2-HS-glycoprotein	0.00025	0	0.978874008	1.79E+06	1.92E+09	1.62E+09	1
SVESASGEVLHSPK	P24090	Ahsg	Alpha-2-HS-glycoprotein	0.032904762	0.010151899	0.582085926	4.91E+05	4.80E+08	2.09E+08	1
VASVESASGEVLHSPK	P24090	Ahsg	Alpha-2-HS-glycoprotein	0.015089552	0.007934211	0.732908629	0.00E+00	7.10E+08	2.47E+08	1
AEFQPLVEEPK	P02770	Alb	Serum albumin	0.00032	0	0.808848341	3.08E+06	1.71E+09	1.32E+09	1
ATIDQNLEDLR	P02651	Apoa4	Apolipoprotein A-IV	0.000210526	0.003640625	0.968861682	7.11E+05	2.06E+09	6.11E+08	1
NLAPLVEDVQSK	P02651	Apoa4	Apolipoprotein A-IV	0	9.38E-05	0.121588889	0.00E+00	5.13E+09	9.27E+08	1
EDVPAADLSDQVPDTDSETR	M0RBJ7	C3		0.000227273	0.028457143	0.241641278	0.00E+00	1.49E+09	1.66E+08	1
SEETKQNEGFSLTAK	M0RBJ7	C3	Complement C3	0	6.67E-05	0.293689888	9.00E+05	4.58E+09	7.93E+08	1
TLDPEHLGQGGVQR	M0RBJ7	C3		0	5.00E-04	0.24688835	0.00E+00	1.64E+09	3.77E+08	1
TLDPEHLGQGGVQREDVPAADLS	M0RBJ7	C3		0	0.016604396	0.190298817	0.00E+00	2.00E+09	5.31E+08	1
TENYEEQFEMFK	Q62930	C9	Complement component C9	0.029024691	0	0.431849265	0.00E+00	2.32E+09	3.86E+09	1
SLLNSLEEAK	P05371	Clu	Clusterin	0.003565217	6.45E-05	0.832206857	2.60E+06	1.87E+09	9.91E+08	1
SLLNSLEEAKK	P05371	Clu	Clusterin	0.000238095	0.000225	0.675897119	2.60E+06	5.19E+09	7.66E+08	1
ILGSDVQQIAVT	Q01177	Plg	Plasminogen	0	0.000509804	0.739911392	0.00E+00	1.59E+09	4.41E+08	1
ILGSDVQQIAVTK	Q01177	Plg	T	0	0	0.190354167	0.00E+00	1.28E+10	2.45E+09	1
LKEAQLPVIENK	Q01177	Plg	Plasminogen	0.000710526	0.019483871	0.395829588	0.00E+00	9.95E+08	1.97E+08	1
LVLEPNDADIALLK	Q01177	Plg	Plasminogen	0.000125	0.012870588	0.065184834	0.00E+00	1.18E+09	2.59E+08	1
VLEPNDADIAL	Q01177	Plg	Plasminogen	0.000333333	0.007527778	0.247891304	1.19E+06	1.40E+09	4.48E+08	1
VLEPNDADIALL	Q01177	Plg	Plasminogen	0.000527778	0.001	0.437732639	0.00E+00	8.33E+08	4.51E+08	1
VLEPNDADIALLK	Q01177	Plg	Plasminogen	0.000344828	0.026058252	0.081465217	1.72E+07	5.64E+09	8.43E+08	1
IVESETQSPLFVGK	P17475	Serpina1	Alpha-1-antiproteinase	0.003959184	0.000111111	0.812716895	1.27E+07	2.04E+09	1.77E+09	1
LYQAEAFVADFK	P05545	Serpina3k	Serine protease inhibitor A3K	0.015897059	0.034517857	0.490461412	0.00E+00	9.56E+08	2.86E+08	1
DGILGRDTLPHEDQGKGR	P05545	Serpina3k	Serine protease inhibitor A3K	0	0.000574074	0.413306422	9.21E+07	7.41E+09	3.61E+09	1
FIDKEQPILSEFQEK	P05544	Serpina3k	Serine protease inhibitor A3K	0.000235294	0.047635593	0.5111504	2.08E+07	2.20E+09	1.90E+09	1
IDELYLPK	P09006	Serpina3n	Serine protease inhibitor A3N	0.026948052	0.004942029	0.919797325	0.00E+00	1.47E+09	2.34E+08	1
ATEEDVLEQKVPEATNRR	Q5M7T5	Serpinc1		0.004377358	0.000205128	0.737663706	0.00E+00	9.02E+08	7.47E+08	1
LGNQDLGDHATLK	Q68FT8	Serpinf2		0.002837209	0.008636364	0.731014085	3.45E+05	1.11E+09	2.77E+08	1
DTGESGVDLADRLDLVEK	Q08420	Sod3	Extracellular superoxide dismutase [Cu-Zn]	0.000424242	0.019431579	0.146329932	0.00E+00	8.69E+08	2.07E+08	1
DAVATWLKPDPSQK	P08721	Spp1	Osteopontin	0.000133333	0.008641026	0.089618257	0.00E+00	1.05E+09	2.16E+08	1
AKPALDDLGQGL	P04639	Apoa1	Apolipoprotein A-I	0.001853659	99	0.002411765	0.00E+00	1.41E+09	1.59E+06	2
LTEIKNHPTL	P04639	Apoa1	Apolipoprotein A-I	0.008737705	0.578393293	0.007615385	0.00E+00	9.84E+08	1.14E+07	2
NLEKETDWLRNE	P04639	Apoa1	Apolipoprotein A-I	0.004230769	0.562376766	0	0.00E+00	5.50E+08	2.22E+07	2
DEFQEKWNEEVE	P04639	Apoa1	Apolipoprotein A-I	0.040522727	0.74486783	0.006787879	0.00E+00	4.23E+08	2.18E+07	2
DEPQSQWDRVKD	P04639	Apoa1	Apolipoprotein A-I	0.030414634	0.46570674	0.005821429	2.98E+06	9.86E+08	2.66E+06	2
HLDEFQEKWNEE	P04639	Apoa1	Apolipoprotein A-I	0	0.578737762	0.003857143	0.00E+00	2.42E+09	1.46E+08	2
NHPTLIEYHTK	P04639	Apoa1	Apolipoprotein A-I	0.014515152	0.971180685	0.009	0.00E+00	6.13E+08	5.03E+07	2
LEPLGTELHK	P04639	Apoa1	Apolipoprotein A-I	0.006517241	0.866504225	0.012890625	3.84E+06	1.60E+09	4.12E+07	2
DSGDVESHLSF	P02651	Apoa4	Apolipoprotein A-IV	0.033253012	0.613960813	0.006034483	0.00E+00	5.65E+08	9.44E+06	2
DDPGSSALLDTVQEHL	G3V8D4	Apoc2		0.016828571	0.734637046	0.0095	0.00E+00	7.33E+08	3.86E+07	2
DEGEGSLLLGSMQGYMEQASK	P06759	Apoc3	Apolipoprotein C-III	0.005875	0.864176966	0.009095238	0.00E+00	4.61E+08	5.52E+07	2
SSLTETIEGADAEDGHSPGEQQK	G3V615	C2		0.000357143	99	0.007710526	0.00E+00	3.30E+09	0.00E+00	2

peptide sequence	protein symbol	gene symbol	protein names	p-value baseline-injury	p-value control-reversal	p-value injury-reversal	mean peak intensity control	mean peak intensity injury	meanpeak intensity reversal	groups
SSPTVFRL	M0RBJ7	C3	Complement C3	0.003901961	99	0.003954545	0.00E+00	1.06E+09	0.00E+00	2
TLDPEHLGQGGVQRE	M0RBJ7	C3		0.011435484	0.21417734	0.049186047	2.65E+05	5.57E+08	9.46E+07	2
TLDPEHLGQGGVQRED	M0RBJ7	C3		0	0.079917293	0.044403727	1.38E+06	2.20E+09	1.56E+08	2
TLDPEHLGQGGVQREDVPAADLSD	M0RBJ7	C3		0.000322581	0.58527931	0.0161	0.00E+00	9.18E+08	1.46E+08	2
DNELQELSTQGSR	P05371	Clu	Clusterin	0.020520548	0.281612565	0.016494505	2.28E+06	2.13E+09	4.40E+06	2
DTGTTSEFIEAGGDIR	F7EUB6	Fga	Fibrinogen alpha chain	0.000648649	0.931207082	0.010490196	0.00E+00	7.69E+08	2.70E+07	2
DNSDRPPLQEGALPQ	Q99PS8	Hrg	Histidine-rich glycoprotein	0	0.931023622	0.030625	0.00E+00	2.84E+09	2.43E+07	2
DNSDRPPLQEGALPQM	Q99PS8	Hrg	Histidine-rich glycoprotein	0	0.149101266	0.007028571	0.00E+00	2.86E+09	8.00E+07	2
DGILGRDTLPHEDQG	P05545	Serpina3k	Serine protease inhibitor A3K	0.011253968	0.683910547	0.00988	0.00E+00	5.83E+08	7.10E+07	2
LQVLAEFQEK	P09006	Serpina3n	Serine protease inhibitor A3N	0.005894737	0	0.001365854	2.73E+07	2.65E+10	1.51E+10	2
DLPGQQPVSEQAQQKLPPL	Q68FT8	Serpinf2		0.026855263	0.550759171	0.006911765	0.00E+00	6.12E+08	9.85E+07	2
SQESDEAIKVIPVAQR	P08721	Spp1	Osteopontin	0.000974359	0.45323506	0.047957576	1.06E+07	1.87E+09	2.40E+08	2
GLQPDPNGGQIGV	G3V947	Vcsa1	SMR1 protein	0.005589041	0	0.04928655	2.54E+07	2.81E+08	1.17E+06	2
DGVLDSVTDQDSKDSTYSM	P01836		Ig kappa chain C region, A allele	0.006348993	0	0.018938144	1.96E+07	2.29E+07	0.00E+00	2
DHVGEAIREK	Q6AYQ2	Akr1c21	Aldo-keto reductase family 1 member C21	0.03044	0.009326667	99	3.12E+06	0.00E+00	0.00E+00	3
EAPVASSEQSVAVKE	Q05175	Basp1	Brain acid soluble protein 1	0.00995092	0.005083969	99	1.13E+07	0.00E+00	0.00E+00	3
DLEDVAGHGGR	B4F7A5	Cd99		0.011680473	0.004722222	99	1.42E+07	0.00E+00	0.00E+00	3
DRDLEDVAGHGGR	B4F7A5	Cd99		0	0	0.752125155	7.63E+07	1.13E+07	2.81E+06	3
SITGPGADKPPVG	Q9R0T4	Cdh1	Cadherin-1	0	0	99	2.85E+07	0.00E+00	0.00E+00	3
DADLEPAFR	G3V7L4	Cdh16		0.015583333	0.004867188	99	8.77E+06	0.00E+00	0.00E+00	3
TDADLEPAFR	G3V7L4	Cdh16		0.016132597	0.005037594	99	2.24E+07	0.00E+00	0.00E+00	3
SQADFDKAAEEVK	P11030	Dbi	Acyl-CoA-binding protein	0.0001875	0.001270833	0.618698571	3.27E+07	1.96E+06	1.81E+06	3
ERLITEGVD	F1M959	Egf		0	0	99	7.70E+07	0.00E+00	5.32E+05	3
HMHFDGTDYKT	F1M959	Egf	Pro-epidermal growth factor	4.65E-05	0	99	8.06E+07	1.60E+06	0.00E+00	3
ALDYDPVESK	F1M959	Egf	Pro-epidermal growth factor	0.033769608	0.001607843	0.319774194	3.58E+07	2.03E+07	6.52E+05	3
EGLAVDWIGR	F1M959	Egf	Pro-epidermal growth factor	0	0	0.895002033	1.02E+08	0.00E+00	1.51E+07	3
RIYWTDSGK	F1M959	Egf	Pro-epidermal growth factor	3.51E-05	0.003512821	0.936175153	1.97E+07	0.00E+00	1.16E+07	3
TPEGLAVDWIGR	F1M959	Egf	Pro-epidermal growth factor	2.86E-05	0.003855932	0.262608911	1.07E+08	2.17E+06	4.78E+07	3
HMHFDGTDYK	F1M959	Egf	Pro-epidermal growth factor	0	0.000827586	0.51575817	1.53E+08	4.69E+07	9.29E+07	3
DNVGTESTKPQSQEAQDGLR	Q04807	Glycam1	Glycosylation-dependent cell adhesion molecule 1	0.003731884	9.26E-05	0.238108642	2.37E+07	1.43E+07	1.71E+05	3
DIDSINEELQ	Q62781	Kap	Kidney androgen-regulated protein	0.011637427	0.004464	99	6.09E+06	0.00E+00	0.00E+00	3
SLDIDSINEELQ	Q62781	Kap	Kidney androgen-regulated protein	0	0	0.526435484	3.81E+08	4.85E+06	3.22E+07	3
SPENSQEQPQQTNPEEKPPAPK	D4A0S3	LOC100365252	Submandibular gland secretory Glx-rich protein CA	5.00E-05	0	99	2.79E+07	0.00E+00	1.25E+05	3
NNMVCAGFLEGGKDS	D4A5M0	LOC100366131		0.011959538	0.001625	0.879969795	1.12E+09	4.26E+07	7.73E+07	3
REKIEENGSMR	P02761	LOC100909412	Major urinary protein	0.016763736	0.029762431	0.484551155	1.06E+07	1.05E+06	2.41E+06	3
DRFTGSGSGTDFT	F1LZH0	LOC100912707		0.038307692	0.011279221	99	1.39E+07	0.00E+00	2.54E+06	3
DDVDVGEQQKDISEINS	Q64230	Mep1a	Meprin A subunit alpha	0.001605263	0.009708609	0.857281849	3.82E+07	1.86E+06	5.40E+06	3
EREIQNAGDQAQENR	F1M7H2	Pigr	Polymeric immunoglobulin receptor	0.006317568	0.001221053	99	2.45E+06	0.00E+00	0.00E+00	3
EVSQVPEFPNDTH	F1M7H2	Pigr	Polymeric immunoglobulin receptor	0.00696	0.000405063	0.18525228	1.44E+07	5.92E+06	0.00E+00	3
ADEREIQNAGDQAQENR	F1M7H2	Pigr	Polymeric immunoglobulin receptor	0.003318182	9.62E-05	0.229246851	1.47E+07	1.37E+07	6.30E+05	3
DEREIQNAGDQAQENR	F1M7H2	Pigr	Polymeric immunoglobulin receptor	0.000295455	0.00160396	0.348700413	2.95E+08	1.37E+08	2.08E+07	3

peptide sequence	protein symbol	gene symbol	protein names	p-value baseline-injury	p-value control-reversal	p-value injury-reversal	mean peak intensity control	mean peak intensity injury	meanpeak intensity reversal	groups
EVEQLILHE	Q3KR76	Plau	Urokinase-type plasminogen activator	0.000526316	0.00028169	0.543976994	1.28E+07	2.67E+06	3.81E+06	3
EDFAQELVECKSSR	D3ZLD7	Ppp2r3a		0.00076699	0.000487805	0.69874328	8.13E+08	5.45E+06	9.60E+06	3
DQELTITSEAIR	E9PT75	Prp2l1		7.81E-05	0	99	3.46E+07	2.88E+06	0.00E+00	3
DQELTLSSQPHG	E9PT75	Prp2l1		0.007072368	0.003431034	99	9.43E+06	0.00E+00	0.00E+00	3
HEVTGPPLGHGQVH	E9PT75	Prp2l1		0.013446328	0.003967213	99	3.92E+06	0.00E+00	0.00E+00	3
TPDKIYLH	E9PT75	Prp2l1		0.004545455	0.001119565	99	1.32E+07	0.00E+00	0.00E+00	3
NENFEEYLR	P02696	Rbp1	Retinol-binding protein 1	0.018854054	0.004298387	99	4.88E+06	0.00E+00	0.00E+00	3
QRIDEFEAM	E9PT65	Rdx	Ezrin	4.26E-05	0.0021875	0.659042818	1.48E+07	0.00E+00	5.01E+06	3
GSGSGTDFTLTIDPVEA	M0RCN6	RGD1563231		0.000554455	9.52E-05	99	1.25E+07	0.00E+00	0.00E+00	3
TFNDPNERIM	D3ZS19	RGD1565709		0.010006173	0.000837209	0.460446309	2.93E+07	1.63E+07	5.37E+06	3
ETEVIDPQDLLEGR	P34901	Sdc4	Syndecan-4	3.13E-05	1.00E-04	0.615182209	3.23E+07	5.90E+06	1.04E+07	3
DLSQFGQQRQ	Q6P6X2	Semg1	Seminal vesicle secretory protein 2	0.008151899	0.001621359	99	8.10E+06	0.00E+00	0.00E+00	3
GFSQQTQQKG	Q6P6X2	Semg1	Seminal vesicle secretory protein 2	0.023162304	0.002646018	0.315785558	3.52E+06	1.16E+06	1.28E+05	3
LKGGSEEAAEESIFMQ	Q6P6X2	Semg1	Seminal vesicle secretory protein 2	0.007201299	0.047385787	0.723934469	9.67E+07	0.00E+00	6.87E+06	3
KGQVSQLKSQESQIKS	Q6P6X2	Semg1	Seminal vesicle secretory protein 2	0.033802956	0.019576687	0.678199454	1.58E+07	6.32E+06	7.34E+06	3
TEGAAATAVTAALK	P05545	Serpina3k	Serine protease inhibitor A3K	4.35E-05	0.00550365	0.441181159	4.38E+07	0.00E+00	3.27E+07	3
DKNVVFSPL	P05544	Serpina3k	Serine protease inhibitor A3K	0.001092593	0.0004375	99	1.32E+07	0.00E+00	1.31E+06	3
DKNVVFSPLS	P05544	Serpina3k	Serine protease inhibitor A3K	0.00025	0.001223404	0.442846552	1.85E+07	0.00E+00	4.96E+06	3
NPDKNVVF	P05544	Serpina3k	Serine protease inhibitor A3K	4.00E-05	9.68E-05	0.51161465	3.53E+07	9.73E+06	1.31E+07	3
DGTLGRDTLSH	P05544	Serpina3l	Serine protease inhibitor A3L	0.00056	0.003941667	0.539294299	1.31E+07	0.00E+00	2.77E+06	3
DLSPEEIQLR	O70377	Snap23	Synaptosomal-associated protein 23	3.03E-05	0	0.39269434	2.70E+07	0.00E+00	1.04E+06	3
DELVRDKPY	P02783	Svs4	Seminal vesicle secretory protein 4	0.000256098	0.000105263	99	3.81E+06	0.00E+00	4.80E+05	3
EEASEEISSRR	P02783	Svs4	Seminal vesicle secretory protein 4	0.002464	0.000107143	99	6.85E+07	9.36E+05	0.00E+00	3
EKYSQSEEVVSE	P02783	Svs4	Seminal vesicle secretory protein 4	0.000234568	8.89E-05	99	9.61E+06	2.86E+06	0.00E+00	3
EKYSQSEEVVSESFAS	P02783	Svs4	Seminal vesicle secretory protein 4	0.000144737	0.00327193	99	1.57E+07	0.00E+00	1.65E+06	3
EVVSESFASGPSSGSS	P02783	Svs4	Seminal vesicle secretory protein 4	0.000303371	0.001609524	99	1.00E+07	0.00E+00	1.11E+06	3
GSFGEEASEEISSRR	P02783	Svs4	Seminal vesicle secretory protein 4	0.000189873	0.000102041	99	3.31E+07	0.00E+00	0.00E+00	3
YSQSEEVVS	P02783	Svs4	Seminal vesicle secretory protein 4	0.000298851	1.00E-04	99	8.58E+06	0.00E+00	0.00E+00	3
EKYSQSEEVVS	P02783	Svs4	Seminal vesicle secretory protein 4	0	0	0.862645304	2.92E+08	0.00E+00	1.24E+07	3
SEEVVSESFASGPSSGSS	P02783	Svs4	Seminal vesicle secretory protein 4	0.000253012	9.38E-05	0.490564648	6.92E+07	9.31E+06	1.96E+07	3
SSGGSNMEGESSYAK	P02783	Svs4	Seminal vesicle secretory protein 4	0.004177305	0.008932886	0.609927746	9.19E+06	2.34E+05	2.58E+06	3
SSGGSNMEGESSYAKK	P02783	Svs4	Seminal vesicle secretory protein 4	0.000114286	0.00149	0.829453502	1.29E+07	0.00E+00	3.07E+06	3
FGEEASEEISSR	P02783	Svs4	Seminal vesicle secretory protein 4	0.012829545	0.004945736	0.894428571	2.27E+08	1.69E+08	9.41E+07	3
FGEEASEEISSRR	P02783	Svs4	Seminal vesicle secretory protein 4	0.018919355	0.009809211	0.499151007	2.17E+08	4.92E+07	7.54E+07	3
GGSFGEEASEEISSR	P02783	Svs4	Seminal vesicle secretory protein 4	0.013730337	0.000287879	0.759532436	6.27E+09	2.88E+09	2.07E+09	3
GSFGEEASEEISSR	P02783	Svs4	Seminal vesicle secretory protein 4	2.78E-05	0	0.726443878	3.01E+08	5.63E+07	7.99E+07	3
SFGEEASEEISSR	P02783	Svs4	Seminal vesicle secretory protein 4	5.26E-05	0	0.916955624	1.74E+08	4.26E+07	5.58E+07	3
SRFAQDVLN	P02783	Svs4	Seminal vesicle secretory protein 4	0.000903846	0.005075758	0.329104803	3.69E+08	2.35E+07	2.75E+08	3
DPYSENMNLK	P04812	Svs5	Seminal vesicle secretory protein 5	0.00055102	0.000279412	0.45374744	2.26E+07	5.23E+06	6.03E+06	3
EDPYSENMNLKI	P04812	Svs5	Seminal vesicle secretory protein 5	0.000112676	0	99	3.13E+07	4.23E+06	0.00E+00	3
EDPYSENMNLK	P04812	Svs5	Seminal vesicle secretory protein 5	4.88E-05	0.005183824	0.663176552	2.25E+07	0.00E+00	8.02E+06	3

peptide sequence	protein symbol	gene symbol	protein names	p-value baseline-injury	p-value control-reversal	p-value injury-reversal	mean peak intensity control	mean peak intensity injury	meanpeak intensity reversal	groups
SEMSSTSSHFGLK	P04812	Svs5	Seminal vesicle secretory protein 5	0.018456522	0.00159434	0.485327842	1.73E+07	8.47E+06	6.81E+06	3
DFSSESSEAK	D3ZJA4	Svs6		0.003503704	9.80E-05	0.185752266	5.81E+06	1.04E+06	2.39E+06	3
SVIHEDVYE	D3ZJA4	Svs6		0.000135135	0.000101695	0.393141777	1.45E+07	0.00E+00	2.74E+06	3
VIHEDVYEEKK	D3ZJA4	Svs6		0.002515873	9.43E-05	0.296910515	4.32E+06	1.57E+06	2.06E+06	3
DFSSESSEAKIPKS	D3ZJA4	Svs6		0	0	0.688172087	1.27E+08	1.41E+07	1.32E+07	3
VIHEDVYEEK	D3ZJA4	Svs6		0.001890756	0.000493827	0.422234973	1.23E+07	1.06E+06	2.96E+06	3
DFSSESSEAKIPK	D3ZJA4	Svs6		0.001557522	0.025202312	0.896052953	3.69E+08	2.48E+08	1.97E+08	3
SLSAGEIER	D3ZJA4	Svs6		0.011290909	0.001454545	0.947951466	9.44E+07	4.61E+07	1.98E+07	3
DTDEEYLFR	Q9ESG3	Tmem27	Collectrin	4.17E-05	0	99	2.09E+07	0.00E+00	0.00E+00	3
GNFIDQTRV	P27590	Umod	Uromodulin	0.002	0.036285714	0.873473461	7.85E+08	1.16E+08	8.16E+07	3
NFIDQTRV	P27590	Umod	Uromodulin	0.000541667	0.039072917	0.56384858	5.84E+08	2.83E+08	4.79E+08	3
VLNLGPITR	P27590	Umod	Uromodulin	0.00027907	0.006143885	0.100376068	3.84E+08	8.12E+07	1.83E+08	3
GFITGPPLVVQ	G3V947	Vcsa1	SMR1 protein	0	9.09E-05	99	3.23E+07	0.00E+00	4.88E+06	3
GFITGPPLVVQG	G3V947	Vcsa1	SMR1 protein	0	0	99	4.35E+07	0.00E+00	0.00E+00	3
GTTEYQYQW	G3V947	Vcsa1	SMR1 protein	0.000536082	0.001131868	0.190677326	2.97E+07	2.65E+07	2.92E+06	3
ITGPPLVVQ	G3V947	Vcsa1	SMR1 protein	0.001844828	0.000275362	0.569575301	2.94E+07	2.68E+07	1.62E+07	3
LQPDPNGGQIGVT	G3V947	Vcsa1	SMR1 protein	0.003447761	0.021470238	0.392122411	9.74E+07	1.90E+07	7.41E+06	3
LTAPDPTPLS	G3V947	Vcsa1	SMR1 protein	3.92E-05	0	99	1.37E+07	0.00E+00	0.00E+00	3
QLTAPDPTPL	G3V947	Vcsa1	SMR1 protein	3.45E-05	0.000106383	0.176110063	6.85E+07	5.24E+06	1.72E+06	3
QWQLTAPDPTPLS	G3V947	Vcsa1	SMR1 protein	3.70E-05	0.000104167	0.238237624	3.47E+07	3.42E+06	5.03E+06	3
TGPPLVVQGTTEYQ	G3V947	Vcsa1	SMR1 protein	0	0	99	2.85E+07	0.00E+00	0.00E+00	3
TTATTQNSTDIFEGGG	G3V947	Vcsa1	SMR1 protein	4.76E-05	0	99	1.72E+07	0.00E+00	0.00E+00	3
TTEYQYQWQLTAPDPTPLS	G3V947	Vcsa1	SMR1 protein	3.28E-05	0	99	1.57E+07	0.00E+00	0.00E+00	3
WQLTAPDPTPLS	G3V947	Vcsa1	SMR1 protein	3.85E-05	0	99	1.72E+07	0.00E+00	0.00E+00	3
YQWQLTAPDPTPLS	G3V947	Vcsa1	SMR1 protein	6.35E-05	0.001663551	99	9.44E+06	0.00E+00	1.56E+06	3
FITGPPLVVQ	G3V947	Vcsa1	SMR1 protein	0	0	0.743392677	2.33E+08	2.86E+07	1.53E+07	3
GTTEYQYQWQL	G3V947	Vcsa1	SMR1 protein	0.000340659	0	0.190566372	5.77E+07	4.65E+07	6.70E+06	3
QLTAPDPTPLS	G3V947	Vcsa1	SMR1 protein	0	0	0.528564743	6.44E+08	1.59E+07	1.53E+07	3
TTEYQYQWQ	G3V947	Vcsa1	SMR1 protein	0.001491071	0	0.208225275	5.88E+07	5.71E+07	1.03E+07	3
DPSTLPHY	G3V947	Vcsa1	SMR1 protein	4.44E-05	0.001144444	0.399324627	6.49E+08	1.22E+08	1.19E+08	3
DPSTLPHYL	G3V947	Vcsa1	SMR1 protein	0.030651741	0.02247929	0.815157159	3.99E+08	1.96E+08	1.03E+08	3
DPSTLPHYLG	G3V947	Vcsa1	SMR1 protein	4.17E-05	0.000103448	0.815950116	4.95E+09	4.60E+08	2.27E+09	3
FITGPPLVVQG	G3V947	Vcsa1	SMR1 protein	0	0	0.539912037	3.83E+08	2.42E+07	8.14E+06	3
ITGPPLVVQG	G3V947	Vcsa1	SMR1 protein	3.39E-05	0	0.196937322	7.21E+07	7.18E+07	1.43E+07	3
QDPSTLPHYLG	G3V947	Vcsa1	SMR1 protein	4.08E-05	0.000702381	0.512053055	1.57E+08	1.27E+08	1.05E+08	3
TTEYQYQWQL	G3V947	Vcsa1	SMR1 protein	0.000141026	0	0.470058236	9.22E+07	8.85E+07	1.50E+07	3
DGVLDSVTDQDSKD	P01836		Ig kappa chain C region, A allele	3.33E-05	0	99	3.85E+07	0.00E+00	0.00E+00	3
DGVLDSVTDQDSKDS	P01836		Ig kappa chain C region, A allele	0.001028302	0.002163636	0.390632887	1.23E+07	1.03E+07	8.64E+06	3
GNLDVAKL	P02761		Major urinary protein	5.13E-05	0	99	1.92E+08	0.00E+00	0.00E+00	3
IDGSEQRDGVLDSVTDQDSKDSTY	P01836		Ig kappa chain C region, A allele	6.45E-05	0.004284553	99	1.29E+07	0.00E+00	2.56E+06	3
NWYQQKPDGTIKP	M0R8G6			2.94E-05	0	0.303754425	5.53E+07	0.00E+00	4.66E+06	3

peptide sequence	protein symbol	gene symbol	protein names	p-value baseline-injury	p-value control-reversal	p-value injury-reversal	mean peak intensity control	mean peak intensity injury	meanpeak intensity reversal	groups
STLSLTKVE	P01836		Ig kappa chain C region, A allele	9.09E-05	0	99	2.58E+07	0.00E+00	0.00E+00	3
STLSLTKVEY	P01836		Ig kappa chain C region, A allele	3.45E-05	0.015063291	0.371244618	1.14E+07	0.00E+00	4.31E+06	3
SVTDQDSKDSTYSMSSTL	P01836		Ig kappa chain C region, A allele	9.23E-05	0	99	1.98E+07	1.39E+06	0.00E+00	3
SVTDQDSKDSTYSMSSTLS	P01836		Ig kappa chain C region, A allele	4.00E-05	0.027775281	0.372011834	1.32E+07	0.00E+00	7.32E+06	3
TLSLTKVEY	P01836		Ig kappa chain C region, A allele	3.77E-05	4.65E-05	99	2.86E+07	0.00E+00	5.23E+06	3
DGVLDSVTDQ	P01836		Ig kappa chain C region, A allele	0	0.000811765	0.714710938	6.15E+07	1.30E+07	2.76E+07	3
DGVLDSVTDQDSKDSTY	P01836		Ig kappa chain C region, A allele	0.000333333	0.03079235	0.72427668	1.20E+08	3.51E+07	1.02E+07	3
DGVLDSVTDQDSKDSTYS	P01836		Ig kappa chain C region, A allele	0	0.000271429	0.379413655	9.69E+07	5.23E+07	6.42E+07	3
DGVLDSVTDQDSKDSTYSMS	P01836		Ig kappa chain C region, A allele	0	0.000292308	0.895460446	1.24E+08	0.00E+00	2.39E+07	3
ERHNLYTCEVVHK	P01836		Ig kappa chain C region, A allele	0.001201835	0.00769863	0.917093194	7.29E+06	9.73E+05	3.61E+06	3
IDGSEQRDGVLDSVTD	P01836		Ig kappa chain C region, A allele	0	0.003840336	0.851379464	1.12E+08	0.00E+00	4.24E+07	3
GEACKALEGSVLSPGPAGDFPMA	F1M8B2	Adad2		0.04850463	0.436078585	0.031227848	6.55E+07	5.97E+07	1.47E+08	4
SVIEMADLDGSK	F1M959	Egf	Pro-epidermal growth factor	0.045140845	0.548925	0.026986667	1.69E+07	8.13E+06	1.46E+08	4
IQTFQGDSDHNWK	Q64230	Mep1a	Meprin A subunit alpha	0.003053846	0.663195862	0.005981481	1.89E+07	1.13E+07	2.71E+08	4
KKIEGNWR	P15399-2	Pbsn	Probasin	0.000123288	0.694844648	0.031075	4.23E+07	2.65E+06	1.06E+08	4
GHLNFGLK	Q6P6X2	Semg1	Seminal vesicle secretory protein 2	0.014497207	0.946996805	0.013815385	4.59E+07	3.37E+07	2.79E+08	4
KQFDDDDLSVQQK	Q6P6X2	Semg1	Seminal vesicle secretory protein 2	0.001074766	0.15784669	0.048842697	3.68E+08	1.00E+08	6.10E+08	4
EDAQETDTSQQDQSPTYR	P17475	Serpina1	Alpha-1-antiproteinase	0.000146667	0.4353	0.001435897	1.03E+08	3.19E+07	1.19E+09	4
ELFSELDER	P05545	Serpina3k	Serine protease inhibitor A3K	0.045221698	0.097092199	0.000307692	6.03E+07	1.45E+07	6.21E+08	4
TLASSNTDFALS	P05544	Serpina3l	Serine protease inhibitor A3L	0.000555556	0.787633172	0.007589286	2.79E+07	2.59E+07	2.73E+08	4
VLNLGPIT	P27590	Umod	Uromodulin	4.55E-05	0.620203438	0.030192308	3.19E+07	0.00E+00	9.94E+07	4
NLDWYQQK	D3ZMS7			4.35E-05	0.896103261	0.013757576	8.22E+06	0.00E+00	2.16E+08	4
WKIDGSEQR	P01836		Ig kappa chain C region, A allele	0	0.332874419	0.000896552	4.27E+07	1.61E+06	2.23E+08	4
DGVLDSVTDQDSK	P01836		Ig kappa chain C region, A allele	0.000142857	0.313014528	0.013111111	2.09E+08	8.93E+07	6.37E+08	4
ASDSSINWNNLKG	P12346	Tf	Serotransferrin	0.004570423	4.17E-05	0	9.05E+05	1.51E+06	1.04E+09	5
SSTKDLLFR	P12346	Tf	Serotransferrin	0.044900474	0.000117647	9.09E-05	0.00E+00	1.33E+07	1.14E+09	5
STPTLTVFPPSTEELQGNK	P20767		Ig lambda-2 chain C region	0.020673797	0.002603175	0.000518519	1.06E+06	4.27E+07	5.64E+08	5
GLQPDPNGGQIG	G3V947	Vcsa1	SMR1 protein	0.007119205	0	0.025732143	5.55E+07	3.61E+07	0.00E+00	6
TEYQYQWQ	G3V947	Vcsa1	SMR1 protein	0	0	0.028733871	7.45E+07	1.08E+07	0.00E+00	6
TEYQYQWQL	G3V947	Vcsa1	SMR1 protein	0.001837607	0	0.012967742	1.11E+08	8.23E+07	0.00E+00	6
ETGLMAFTNLK	P14046	A1i3	Alpha-1-inhibitor 3	99	0.007621622	0.004612245	0.00E+00	6.97E+07	2.21E+09	7
DKLVLATEKLEAEDR	P01015	Agt	Angiotensinogen	0.904315663	0.000297872	0.001181818	0.00E+00	5.37E+08	1.17E+09	7
LSTLLGAEANLGK	P01015	Agt	Angiotensinogen	99	0.026039604	0.023712329	0.00E+00	3.35E+08	7.68E+08	7
SLDLSTDPVLAAQK	P01015	Agt	Angiotensinogen	0.618752363	0.00052	0	4.87E+06	2.85E+08	1.81E+09	7
EAHKSEIAHRFK	P02770	Alb	Serum albumin	0.653332727	0.033645455	0.000785714	8.07E+04	4.21E+05	6.96E+08	7
FKDLGEQHF	P02770	Alb	Serum albumin	0.889361858	0	0.001194444	5.66E+05	3.85E+08	8.70E+09	7
QTALAELVK	P02770	Alb	Serum albumin	0.640332215	0.001	0.009965517	4.23E+06	1.77E+08	2.36E+09	7
FKDLGEQHFKG	P02770	Alb	Serum albumin	0.765244767	0	0	4.21E+06	4.36E+07	7.79E+09	7
SSPSIVLGQEQDTYGGGFDK	P23680	Apcs	Serum amyloid P-component	99	0.004823529	0.001809524	0.00E+00	4.23E+07	3.62E+08	7
GLSQSLSVQWDEK	Q63678	Azgp1	Zinc-alpha-2-glycoprotein	0.854294469	0.000304348	0.001	1.17E+07	2.42E+08	9.53E+08	7
AAVFNHFISDGVKK	M0RBJ7	C3	Complement C3	99	9.09E-05	1.00E-04	0.00E+00	5.84E+08	4.48E+09	7

peptide sequence	protein symbol	gene symbol	protein names	p-value baseline-injury	p-value control-reversal	p-value injury-reversal	mean peak intensity control	mean peak intensity injury	meanpeak intensity reversal	groups
RVPVVTQGSDAQALTQDDGVAK	M0RBJ7	C3	Complement C3	99	0.0036	0.005673077	0.00E+00	3.07E+08	8.75E+08	7
VLIEDGSGEAVLSRK	M0RBJ7	C3	Complement C3	99	0.000785714	0.001421053	0.00E+00	5.35E+08	1.14E+09	7
GYTQQLAFK	M0RBJ7	C3	Complement C3	0.85038009	0.000238095	0.00462	0.00E+00	3.92E+07	6.09E+08	7
SDVDEDIIPEEDIISR	M0RBJ7	C3	Complement C3	0.131503497	0.000114286	0	1.11E+07	1.01E+10	1.65E+10	7
KALYSEYTDGTFTK	G3V7K3	Cp	Ceruloplasmin	99	0	0	0.00E+00	2.47E+09	6.55E+09	7
MFTTAPENVDKEDEDFQESNK	G3V7K3	Cp	Ceruloplasmin	0.927195479	0	0	0.00E+00	5.44E+08	5.98E+09	7
RDTANLFPHK	G3V7K3	Cp	Ceruloplasmin	99	0.028679245	0.002869565	0.00E+00	0.00E+00	1.75E+08	7
ALYSEYTDGTFTK	G3V7K3	Cp	Ceruloplasmin	0.812310734	0	0	3.24E+06	3.30E+09	5.07E+09	7
SSTVAPTLPGEVR	G3V7K3	Cp	Ceruloplasmin	0.563906504	0.01545977	0.007327273	5.96E+06	8.24E+07	2.49E+09	7
NTEPVMDSDGSFFMYSK	P20761	Igh-1a	Ig gamma-2B chain C region	99	0.000232558	0	0.00E+00	0.00E+00	1.18E+09	7
AREVAFDVEIPK	B2RYM3	Itih1		99	3.85E-05	0	0.00E+00	1.33E+09	2.56E+09	7
EVQLVESGGGLVQPKG	F1M5X4	LOC100362687		99	0.029850467	0.012532258	0.00E+00	6.84E+07	1.98E+08	7
YNAELESGNQFVLYR	P01048	Map1	T-kininogen 1	0.355719072	0.019864583	0.001162162	2.03E+06	7.06E+07	5.55E+08	7
DGAETLYSFK	P01048	Map1	T-kininogen 1	0.916773224	0	0.000217391	0.00E+00	1.27E+08	1.19E+09	7
SVDGKEDSIQELLR	E9PST1	RGD1310507		99	0.010725	0.01580597	0.00E+00	6.53E+08	1.05E+09	7
SAILYFPK	P17475	Serpina1	Alpha-1-antiproteinase	0.897899576	0.000490566	0.018695652	0.00E+00	4.11E+08	1.10E+09	7
SVKVPMMK	P05544	Serpina3k	Serine protease inhibitor A3K	0.055651786	0.000690909	0	2.60E+06	9.95E+06	9.59E+08	7
MQQVESSLQPETLK	P05544	Serpina3k	Serine protease inhibitor A3K	0.898764624	0.000311111	0.028792208	6.69E+06	4.15E+08	2.60E+09	7
MQQVESSLQPETLKK	P05544	Serpina3k	Serine protease inhibitor A3K	0.783331395	0	0.016632353	5.15E+06	1.12E+09	5.02E+09	7
EELSCSVLELK	P05544	Serpina3k	Serine protease inhibitor A3K	99	0.021092784	0.005215686	0.00E+00	9.75E+06	2.09E+08	7
IINDLRMPK	P05544	Serpina3l	Serine protease inhibitor A3L	99	0.046179487	0.036134146	0.00E+00	2.19E+08	4.49E+08	7
ALYQAEAFIADFK	P05544	Serpina3l	Serine protease inhibitor A3L	0.917272851	0.003727273	0.038604651	8.69E+05	4.70E+08	1.83E+09	7
EAFIADFKQPNEAK	P05544	Serpina3l	Serine protease inhibitor A3L	0.918166891	0.002344262	0.022142857	6.86E+06	2.11E+08	7.31E+08	7
FSISTDYSLK	P05544	Serpina3l	Serine protease inhibitor A3L	0.863599407	0	0	2.26E+06	5.99E+08	4.12E+09	7
KIDELYLPR	F1LR92	Serpina3m	Serine protease inhibitor A3M	99	0.004477612	0.002244444	0.00E+00	1.09E+09	1.88E+09	7
KLINDYVSK	P09006	Serpina3n	Serine protease inhibitor A3N	0.915229858	0.000162162	0.011491525	7.55E+05	4.88E+08	7.10E+08	7
GTDFQLNQLQGK	P12346	Tf	Serotransferrin	99	3.57E-05	0	0.00E+00	1.06E+08	1.23E+09	7
GTDFQLNQLQGKK	P12346	Tf	Serotransferrin	99	3.70E-05	0	0.00E+00	2.90E+07	1.81E+09	7
GYYAVAVVK	P12346	Tf	Serotransferrin	99	0	0	0.00E+00	1.50E+08	2.28E+09	7
KGTDFQLNQLQGKK	P12346	Tf	Serotransferrin	0.07507438	0	0	0.00E+00	3.34E+07	1.88E+09	7
SKDFQLFGSPLGK	P12346	Tf	Serotransferrin	0.609915385	0.000227273	0.000208333	1.01E+06	1.35E+09	3.47E+09	7
ASDSSINWNNLK	P12346	Tf	Serotransferrin	0.362038363	0	0	3.61E+06	1.01E+08	7.56E+09	7
DSAFGLLR	P12346	Tf	Serotransferrin	0.315169399	0.000243902	0.002162791	0.00E+00	1.81E+08	1.01E+09	7
KTADGSWEPFASGK	P02767	Ttr	Transthyretin	0.062665236	0	0	0.00E+00	2.33E+07	1.01E+10	7
TADGSWEPFASGK	P02767	Ttr	Transthyretin	0.080285714	0.000367347	0.001142857	0.00E+00	1.71E+07	7.20E+08	7
TAESGELHGLTTDEKFTEGVYR	P02767	Ttr	Transthyretin	99	0.020918367	0.011633333	0.00E+00	3.08E+07	1.83E+09	7
PPPPGPPPP	O08816	Enah	Neural Wiskott-Aldrich syndrome protein	0.812879688	0.000291667	0.00755	1.19E+07	7.87E+07	1.18E+06	8
SDRPPLQEGALPQM	Q99PS8	Hrg	Histidine-rich glycoprotein	0.092228571	0.036268421	0.001333333	1.65E+06	7.73E+08	0.00E+00	8
THEIGCPPPPEGKDNSDRPPLQ	Q99PS8	Hrg	Histidine-rich glycoprotein	0.263177143	0.02822905	0.012984127	1.61E+07	6.23E+08	0.00E+00	8
DIVENVDSLK	F1LWZ1	LOC690507		0.970301688	0.022930233	0.027795082	4.01E+06	7.97E+07	0.00E+00	8
FIDKEQPI	P05544	Serpina3k	Serine protease inhibitor A3K	0.965488636	0.000337838	0.002625	4.36E+07	3.17E+08	0.00E+00	8

peptide sequence	protein symbol	gene symbol	protein names	p-value baseline-injury	p-value control-reversal	p-value injury-reversal	mean peak intensity control	mean peak intensity injury	meanpeak intensity reversal	groups
LQPLDFKENPEQS	Q5M7T5	Serpinc1		0.131541667	0.000287671	0.025540541	3.84E+06	8.96E+07	0.00E+00	8
TEEDVLEQKVPEATNR	Q5M7T5	Serpinc1		0.870838663	0.003983471	0.015894118	7.79E+07	9.58E+08	3.77E+07	8
DQDQEDSALLAL	E9PU79	Spt1		0.535733475	0.001731481	0.030669173	1.00E+07	4.85E+07	2.91E+06	8
LGLQPDPNGGQIGVT	G3V947	Vcsa1	SMR1 protein	0.161082192	0.006678322	0.012934426	1.53E+07	9.60E+08	2.80E+06	8
GLQPDPNGGQIGVT	G3V947	Vcsa1	SMR1 protein	0.089519685	0	0.013273973	1.44E+08	4.13E+08	3.21E+06	8
QDPSTLPHY	G3V947	Vcsa1	SMR1 protein	0.727851536	0.000368421	0.0015	6.48E+07	3.94E+08	2.87E+06	8
TAPDPTPLSNPPTQ	G3V947	Vcsa1	SMR1 protein	0.401797561	9.84E-05	0.030813433	2.62E+07	2.63E+08	2.34E+06	8
TAPDPTPLSNPPTQL	G3V947	Vcsa1	SMR1 protein	0.926967366	0.001034091	0.002428571	1.64E+07	3.31E+08	1.77E+06	8

v. List of the peptide sequences that were significantly different in precursor peak intensities between healthy volunteers and patients with DN

Peptide sequence, gene symbol, protein name are provided p-value and mean intensity per group are provided. Only the significantly different peptides between healthy volunteers and patients with DN are listed.

Significantly increased in diabetic nephropathy vs control					
Gene Names	**Protein Names**	**Sequence**	**p-value**	**mean peak intensity control**	**mean peak intensity DN**
AHCTF1	Protein ELYS	YEVCQEMGLME	0.004735	4.57E+06	1.92E+09
AHSG	Alpha-2-HS-glycoprotein;Alpha-2-HS-glycoprotein chain A;Alpha-2-HS-glycoprotein chain B	MGVVSLGSPSGEVSHP	0.00025	9.66E+06	7.29E+08
AHSG	Alpha-2-HS-glycoprotein;Alpha-2-HS-glycoprotein chain A;Alpha-2-HS-glycoprotein chain B	MGVVSLGSPSGEVSHPR	0.000458	1.90E+08	1.87E+09
AHSG	Alpha-2-HS-glycoprotein;Alpha-2-HS-glycoprotein chain A;Alpha-2-HS-glycoprotein chain B	VVSLGSPSGEVSHPR	0.002404	7.25E+06	1.02E+09
AMBP	Protein AMBP;Alpha-1-microglobulin;Inter-alpha-trypsin inhibitor light chain;Trypstatin	ADRGECVPGEQEPEPILIPR	0.004658	6.23E+07	6.91E+08
AMBP	Protein AMBP;Alpha-1-microglobulin;Inter-alpha-trypsin inhibitor light chain;Trypstatin	ADRGECVPGEQEPEPILIPRV	0.007155	6.29E+07	2.01E+08
APOA1	Apolipoprotein A-I;Truncated apolipoprotein A-I	DEPPQSPWDRVKDL	0.009811	1.32E+07	1.32E+09
APOA1	Apolipoprotein A-I;Truncated apolipoprotein A-I	DEPPQSPWDRVKDLA	0.002366	4.69E+08	7.57E+08
APOA1	Apolipoprotein A-I;Truncated apolipoprotein A-I	DEPPQSPWDRVKDLAT	0.00261	8.50E+07	3.86E+09
APOA1	Apolipoprotein A-I;Truncated apolipoprotein A-I	HLAPYSDELR	0.003387	1.77E+08	7.05E+08
APOA1	Apolipoprotein A-I;Truncated apolipoprotein A-I	LEALKENGGAR	0.004838	1.22E+07	1.33E+09
APOA1	Apolipoprotein A-I;Truncated apolipoprotein A-I	LSALEEYTKK	0.000279	9.05E+07	1.67E+09
APOA1	Apolipoprotein A-I;Truncated apolipoprotein A-I	LSALEEYTKKLNTQ	0.003014	6.56E+05	1.53E+09
APOA1	Apolipoprotein A-I;Truncated apolipoprotein A-I	SALEEYTK	0.004739	6.07E+05	5.22E+08
APOA1	Apolipoprotein A-I;Truncated apolipoprotein A-I	SALEEYTKK	0.006946	4.59E+06	1.77E+07
APOA2	Apolipoprotein A-II;Truncated apolipoprotein A-II	EPCVESLVSQY	0.009767	4.08E+06	6.89E+07
APOA2	Apolipoprotein A-II;Truncated apolipoprotein A-II	FVELGTQPATQ	0.0002	1.35E+07	1.94E+07
APOA2	Apolipoprotein A-II;Truncated apolipoprotein A-II	QAKEPCVESLVSQY	0.000375	6.95E+06	4.50E+07
APOA4	Apolipoprotein A-IV	ALVQQMEQL	0.000386	3.65E+06	3.02E+09
APOA4	Apolipoprotein A-IV	EVSADQVATVMWD	0.000461	2.45E+07	2.65E+07
APOA4	Apolipoprotein A-IV	FKEKESQDK	0.002313	3.48E+06	2.81E+09
APOA4	Apolipoprotein A-IV	FSTFKEKESQDK	0.003844	1.36E+06	2.16E+09
APOA4	Apolipoprotein A-IV	KVKIDQTVEEL	0.000272	9.74E+06	7.86E+07
APOA4	Apolipoprotein A-IV	LGPHAGDVEGHLS	0.002635	1.37E+07	1.73E+07
APOA4	Apolipoprotein A-IV	LGPHAGDVEGHLSF	0.002758	2.21E+06	9.29E+08
APOA4	Apolipoprotein A-IV	NKALVQQMEQL	0.00289	8.14E+07	2.65E+08
APOA4	Apolipoprotein A-IV	SLAELGGHLDQQVEEF	0.00442	3.63E+07	6.87E+08
APOA4	Apolipoprotein A-IV	TFKEKESQDK	0.00542	1.32E+08	1.17E+09
APOA4	Apolipoprotein A-IV	TLSLPELEQQQEQQQEQQQEQVQ	0.007826	6.61E+07	1.67E+09
APOA4	Apolipoprotein A-IV	TLSLPELEQQQEQQQEQQQEQVQM	0.009604	1.93E+07	8.10E+08
APOC3	Apolipoprotein C-III	WDLDPEVRPTSAVA	0.002431	1.33E+08	1.39E+08
B2M	Beta-2-microglobulin;Beta-2-microglobulin form pI 5.3	NGERIEKVEHSDLSFSKDWS	0.0027	4.62E+06	1.96E+08
B2M	Beta-2-microglobulin;Beta-2-microglobulin form pI 5.3	YVSGFHPSDIEVD	0.002823	5.42E+06	7.09E+07
CALR	Calreticulin	IHPEIDNPEYSPDPSIY	0.003527	6.10E+06	1.41E+07
CD99	CD99 antigen	EGEEADAPGVIPGIVGAV	0.006513	2.83E+07	3.15E+07
CD99	CD99 antigen	KEGEEADAPGVIPGIVGAV	0.007331	4.63E+06	2.56E+07
CD99	CD99 antigen	KEGEEADAPGVIPGIVGAVV	0.007565	6.08E+07	7.96E+07
CDH1	Cadherin-1;E-Cad/CTF1;E-Cad/CTF2;E-Cad/CTF3	FSHAVSSNGNAVEDPMEIL	0.000281	1.55E+07	6.02E+07
CDH1	Cadherin-1;E-Cad/CTF1;E-Cad/CTF2;E-Cad/CTF3	KVTDADAPNTPAWEAVY	0.00821	4.14E+07	2.48E+08

Significantly increased in diabetic nephropathy vs control					
Gene Names	**Protein Names**	**Sequence**	**p-value**	**mean peak intensity control**	**mean peak intensity DN**
CDH11	Cadherin-11	AVDRDTNRPLEPPSEF	0.00963	7.17E+05	3.93E+08
CFB	Complement factor B;Complement factor B Ba fragment;Complement factor B Bb fragment	LSSLTETIEGVDAEDGHGPGEQ	6.08E-08	4.45E+06	1.34E+07
CFB	Complement factor B;Complement factor B Ba fragment;Complement factor B Bb fragment	LSSLTETIEGVDAEDGHGPGEQQ	0.000411	9.24E+06	2.53E+07
CFB	Complement factor B;Complement factor B Ba fragment;Complement factor B Bb fragment	LSSLTETIEGVDAEDGHGPGEQQK	0.002912	5.90E+06	2.46E+07
CFB	Complement factor B;Complement factor B Ba fragment;Complement factor B Bb fragment	LSSLTETIEGVDAEDGHGPGEQQKR	0.003297	8.28E+05	1.22E+08
CFD	Complement factor D	RAVPHPDSQPDTIDHDLL	0.00717	1.63E+07	1.56E+08
CLU	Clusterin;Clusterin beta chain;Clusterin alpha chain;Clusterin	ASHTSDSDVPSGVTEVVVK	0.006086	4.05E+06	8.57E+06
CLU	Clusterin;Clusterin beta chain;Clusterin alpha chain;Clusterin	ASHTSDSDVPSGVTEVVVKL	0.0078	2.25E+07	2.36E+08
CLU	Clusterin;Clusterin beta chain;Clusterin alpha chain;Clusterin	FDSDPITVTVPVE	0.00811	1.56E+07	4.84E+07
CLU	Clusterin;Clusterin beta chain;Clusterin alpha chain;Clusterin	FDSDPITVTVPVEVS	0.007204	5.84E+07	1.10E+08
CLU	Clusterin;Clusterin beta chain;Clusterin alpha chain;Clusterin	FDSDPITVTVPVEVSR	0.007803	1.11E+07	2.39E+07
CLU	Clusterin;Clusterin beta chain;Clusterin alpha chain;Clusterin	HTSDSDVPSGVTEVVVKL	0.008315	4.77E+06	1.07E+08
CLU	Clusterin;Clusterin beta chain;Clusterin alpha chain;Clusterin	SDSDVPSGVTEVVVKL	0.000365	9.76E+06	2.64E+07
CLU	Clusterin;Clusterin beta chain;Clusterin alpha chain;Clusterin	SHTSDSDVPSGVTEVVVK	0.00242	2.92E+07	5.17E+07
CLU	Clusterin;Clusterin beta chain;Clusterin alpha chain;Clusterin	SHTSDSDVPSGVTEVVVKL	0.003227	1.02E+07	1.03E+07
CLU	Clusterin;Clusterin beta chain;Clusterin alpha chain;Clusterin	TSDSDVPSGVTEVVVKL	0.004103	7.59E+06	7.91E+07
CLU	Clusterin;Clusterin beta chain;Clusterin alpha chain;Clusterin	TVASHTSDSDVPSGVTEVVVKL	0.007029	5.78E+07	6.37E+07
COL15A1	Collagen alpha-1(XV) chain;Endostatin	GATETASQGHLDLTQL	0.000293	2.43E+07	2.86E+08
COL18A1	Collagen alpha-1(XVIII) chain;Endostatin	DDILASPPRLPEPQPYPGAP	0.000377	1.63E+07	4.63E+08
COL18A1	Collagen alpha-1(XVIII) chain;Endostatin	DDILASPPRLPEPQPYPGAPHHS	0.002648	1.68E+07	2.35E+07
COL18A1	Collagen alpha-1(XVIII) chain;Endostatin	DDILASPPRLPEPQPYPGAPHHSS	0.002672	4.44E+06	7.12E+07
COL18A1	Collagen alpha-1(XVIII) chain;Endostatin	ERISEEVGLLQ	0.00381	1.79E+07	3.58E+08
COL1A1	Collagen alpha-1(I) chain	GDKGETGEQGDR	0.004643	2.77E+07	3.22E+08
CXCL16	C-X-C motif chemokine 16	EAGENQKQPEKNAGPTAR	0.000309	2.94E+08	3.71E+08
FETUB	Fetuin-B	FLEPMEEKL	0.0027	1.03E+08	8.31E+08
FGB	Fibrinogen beta chain;Fibrinopeptide B;Fibrinogen beta chain	DKKREEAPSLRPAPPPISGGGY	0.00509	1.93E+07	1.79E+08
GSN	Gelsolin	WVGTGASEAEKTGAQEL	0.006616	8.26E+07	2.27E+08
HLA-C	HLA class I histocompatibility antig Cw-1 alpha chain	Color [DarkGray]	0.009893	2.80E+08	3.67E+08
IGF2	Insulin-like growth factor II;Insulin-like growth factor II;Insulin-like growth factor II Ala-25 Del;Preptin	PAHGGAPPEMASN	2.7E-05	3.39E+08	7.39E+08
INS	Insulin;Insulin B chain;Insulin A chain	EAEDLQVGQVELGGGPGAGSLQ	0.000461	5.86E+08	4.77E+10
ITGA7	Integrin alpha-7;Integrin alpha-7 heavy chain;Integrin alpha-7 light chain;Integrin alpha-7 70 kDa form	ELEPPEQQEPGERQEPSMSW	0.003973	2.86E+08	5.05E+08
ITIH2	Inter-alpha-trypsin inhibitor heavy chain H2	FEIPINGLSE	0.006861	4.24E+08	2.49E+09
KNG1	Kininogen-1;Kininogen-1 heavy chain;T-kinin;Bradykinin;Lysyl-bradykinin;Kininogen-1 light chain;Low mol	KRPPGFSPF	0.007539	9.57E+07	4.41E+08
KNG1	Kininogen-1;Kininogen-1 heavy chain;T-kinin;Bradykinin;Lysyl-bradykinin;Kininogen-1 light chain;Low mol	KRPPGFSPFR	0.008866	2.02E+08	3.76E+09
KNG1	Kininogen-1;Kininogen-1 heavy chain;T-kinin;Bradykinin;Lysyl-bradykinin;Kininogen-1 light chain;Low mol	RPPGFSPF	0.00899	2.16E+08	7.12E+09
KNG1	Kininogen-1;Kininogen-1 heavy chain;T-kinin;Bradykinin;Lysyl-bradykinin;Kininogen-1 light chain;Low mol	RPPGFSPFR	0.002593	3.31E+08	4.45E+08
LMAN2	Vesicular integral-membrane protein VIP36	FGASAGTGDLSDNHDIIS	4.23E-06	1.25E+08	4.67E+08
LMAN2	Vesicular integral-membrane protein VIP36	FGASAGTGDLSDNHDIISMK	0.000264	1.00E+08	1.73E+08
LMAN2	Vesicular integral-membrane protein VIP36	FGASAGTGDLSDNHDIISMKL	0.002584	2.10E+08	4.22E+08

Significantly increased in diabetic nephropathy vs control					
Gene Names	**Protein Names**	**Sequence**	**p-value**	**mean peak intensity control**	**mean peak intensity DN**
LMAN2	Vesicular integral-membrane protein VIP36	LDTYPNDETTERVFPY	0.002669	4.53E+08	8.13E+08
LMAN2	Vesicular integral-membrane protein VIP36	MVEHTPDEESIDWTKIEPSVN	0.003137	3.64E+06	3.06E+08
MB	Myoglobin	GKVEADIPGHGQEVL	0.005096	8.50E+06	2.92E+08
MB	Myoglobin	NVWGKVEADIPGHGQEVL	0.007638	3.08E+06	8.76E+08
PCSK1N	ProSAAS;KEP;Big SAAS;Little SAAS;Big PEN-LEN;PEN;Little LEN;Big LEN	DHDVGSELPPEGVLGAL	0.004301	8.89E+06	3.50E+08
PI16	Peptidase inhibitor 16	LMVELHNL	0.006692	2.60E+06	6.30E+08
RBP4	Retinol-binding protein 4;Plasma retinol-binding protein(1-182);Plasma retinol-binding protein(1-181);Pla	AKKDPEGLFLQDNIVAE	0.002362	7.74E+06	5.49E+08
RBP4	Retinol-binding protein 4;Plasma retinol-binding protein(1-182);Plasma retinol-binding protein(1-181);Pla	KDPEGLFLQDNIVAE	0.005394	3.70E+07	2.08E+08
RUSC2	Iporin	GVGEPGLGDLYDDSIGD	0.002332	3.63E+06	4.75E+07
SERPINA1	Alpha-1-antitrypsin;Short peptide from AAT	DAAQKTDTSHHDQDHPTFNK	0.007246	1.17E+06	1.52E+09
SERPINA1	Alpha-1-antitrypsin;Short peptide from AAT	EAIPMSIPPEVK	0.007695	1.96E+06	1.28E+08
SERPINA1	Alpha-1-antitrypsin;Short peptide from AAT	EDPQGDAAQKTDTSHHDQDHPTFNK	0.000264	2.31E+06	3.48E+08
SERPINA1	Alpha-1-antitrypsin;Short peptide from AAT	LRTLNQPDSQLQLTTGNGL	0.000346	1.49E+07	1.32E+08
SERPINA1	Alpha-1-antitrypsin;Short peptide from AAT	MIEQNTKSPLFMGKVVNPTQK	0.005572	3.34E+07	1.25E+08
SERPINA1	Alpha-1-antitrypsin;Short peptide from AAT	TDTSHHDQDHPTFNK	0.007847	1.42E+07	5.34E+08
SERPINA1	Alpha-1-antitrypsin;Short peptide from AAT	TEIPEAQIHEGFQEL	0.002455	1.36E+07	3.44E+08
SERPINA1	Alpha-1-antitrypsin;Short peptide from AAT	TIDEKGTEAAGAMF	0.003589	3.86E+07	8.32E+08
SERPINA1	Alpha-1-antitrypsin;Short peptide from AAT	TIDEKGTEAAGAMFL	0.002357	2.92E+06	1.56E+08
SERPINA1	Alpha-1-antitrypsin;Short peptide from AAT	VKELDRDTVF	0.003053	7.24E+06	4.92E+07
SERPINA6	Corticosteroid-binding globulin	AKSDTSLEMTMGNAL	0.003251	6.57E+06	1.26E+08
SERPINA6	Corticosteroid-binding globulin	YVDETTVVKVPM	0.003611	6.39E+06	4.88E+08
SERPINC1	Antithrombin-III	SKLPGIVAEGRDDL	0.004011	1.43E+07	3.03E+08
SERPINC1	Antithrombin-III	YQHLADSKNDNDNIFLSPLSISTA	0.005153	1.15E+06	3.53E+08
SERPING1	Plasma protease C1 inhibitor	ELTETGVEAAAASAISVAR	0.007091	3.16E+06	9.24E+07
SERPING1	Plasma protease C1 inhibitor	WDQQHKFPV	0.008942	3.28E+05	5.41E+08
SH3BGRL3	SH3 domain-binding glutamic acid-rich-like protein 3	FVEAVEQNTLQEF	1.89E-05	2.12E+07	1.61E+08
SPINK5	Serine protease inhibitor Kazal-type 5;Hemofiltrate peptide HF6478;Hemofiltrate peptide HF7665	ENDPVLGPDGKTHGNK	0.002755	2.75E+07	2.24E+08
SPP1;opn	Osteopontin	AIPVAQDLNAPSDWDSR	0.003065	9.90E+07	1.79E+08
SPP1;opn	Osteopontin	AQDLNAPSDWDSR	0.003082	7.21E+06	1.12E+08
SPP1;opn	Osteopontin	GKDSYETSQLDDQSAETHSHKQS	0.004415	1.36E+06	3.04E+09
TMSB4X	Thymosin beta-4;Hematopoietic system regulatory peptide	KTETQEKNPLPSKETIEQEKQAGES	0.005479	1.23E+06	6.46E+07
TMSB4X	Thymosin beta-4;Hematopoietic system regulatory peptide	TETQEKNPLPSKETIEQEKQAGES	0.006731	1.53E+06	5.40E+08
TMSB4X;TMSL4	Thymosin beta-4;Hematopoietic system regulatory peptide	SDKPDMAEIEKFDK	0.007015	1.55E+06	1.23E+07
TMSB4X;TMSL4	Thymosin beta-4;Hematopoietic system regulatory peptide	SDKPDMAEIEKFDKSK	0.008009	2.21E+06	2.49E+06
TMSB4X;TMSL4	Thymosin beta-4;Hematopoietic system regulatory peptide	SDKPDMAEIEKFDKSKLK	0.000479	9.52E+06	1.03E+07
TSTD1	Thiosulfate sulfurtransferase/rhodanese-like domain-containing protein 1	YSAEKPKLEDEHLV	0.003111	1.67E+06	1.70E+10
TTR	Transthyretin	ALLSPYSYSTTA	0.003439	4.75E+06	3.89E+07
TTR	Transthyretin	ALLSPYSYSTTAVVTNPKE	0.004638	4.78E+05	7.36E+08
TTR	Transthyretin	GISPFHEHAEVV	0.002757	7.45E+06	1.16E+08

Significantly increased in diabetic nephropathy vs control					
Gene Names	**Protein Names**	**Sequence**	**p-value**	**mean peak intensity control**	**mean peak intensity DN**
TTR	Transthyretin	LLSPYSYSTTAVVTNPKE	0.00515	2.04E+06	1.09E+07
TTR	Transthyretin	LSPYSYSTTAVVTNPKE	3.68E-06	5.64E+05	5.19E+09
UMOD	Uromodulin;Uromodulinsecreted form	Color [DarkGray]	2E-05	2.75E+06	2.70E+08

Significantly increased in control vs diabetic nephropathy

Gene Names	**Protein Names**	**Sequence**	**p-value**	**mean peak intensity control**	**mean peak intensity DN**
MGP	Matrix Gla protein	ACDDYRLCE	0.008745	1.03E+08	5.31E+06
PGRMC1	Membrane-associated progesterone receptor component 1	DDDEPPPLPRL	0.000743	3.06E+08	2.15E+07
VEGFA;VEGF	Vascular endothelial growth factor A	RCGGCCNDEGLECVPT	0.002518	2.92E+08	2.11E+07
FXYD2	Sodium/potassium-transporting ATPase subunit gamma	TGLSMDGGGSPK	0.000145	8.16E+07	9.04E+06
ANGPTL2	Angiopoietin-related protein 2	EFIYLNRY	0.000528	8.76E+08	2.40E+07
CD59	CD59 glycoprotein	CWKFEHCN	0.001737	7.81E+08	5.93E+06
TSPAN9	Tetraspanin-9	EGLLLYHTENNVGL	0.000591	3.16E+08	2.82E+05

vi. Urinary peptides that were significantly different between the groups control, diabetes (DM), hypertension (HTN) and the combinatory diabetes and hypertension (DM+HTN)

Peptide sequence, protein symbol and uniprot name, mean intensity per group, p-value, description are provided. The complete list of peptides detected in the control group and diabetes and hypertension group has been published (Betz, Jenks et al. 2016) and is available online at: http://www.sciencedirect.com/science/article/pii/S0085253816002969.

References

Betz, B. B., S. J. Jenks, A. D. Cronshaw, D. J. Lamont, C. Cairns, J. R. Manning, J. Goddard, D. J. Webb, J. J. Mullins, J. Hughes, S. McLachlan, M. W. Strachan, J. F. Price and B. R. Conway (2016). "Urinary peptidomics in a rodent model of diabetic nephropathy highlights epidermal growth factor as a biomarker for renal deterioration in patients with type 2 diabetes." Kidney Int **89**(5): 1125-1135.

Conway, B. R., B. Betz, T. A. Sheldrake, J. R. Manning, D. R. Dunbar, A. Dobyns, J. Hughes and J. J. Mullins (2014). "Tight blood glycaemic and blood pressure control in experimental diabetic nephropathy reduces extracellular matrix production without regression of fibrosis." Nephrology (Carlton) **19**(12): 802-813.

Protein	Sequence	mean peak intensity control	mean peak intensity DM	mean peak intensity HTN	mean peak intensity DM+HTN	Description	control vs all	DM vs control	HTN vs control	HTN+DM vs control
Q6P6X2	SQGGQLQSYGQMK	3.12E+06	0.00E+00	0.00E+00	2.40E+05	Protein Semg1 OS=Rattus norvegicus GN=Semg1 PE=2 SV=1	9.27E-05			
Q63461	DQELTITSEAIR	1.13E+07	0.00E+00	5.79E+06	8.55E+06	Proline-rich protein (Fragment) n=1 Tax=Rattus norvegicus RepID=Q63461_RAT	1.11E-04			
P08568	SPENSQEQPQQTNPEEKPPAPK	1.42E+07	3.31E+06	0.00E+00	4.95E+06	Submandibular gland secretory Glx-rich protein CA n=1 Tax=Rattus norvegicus RepID=GRPA_RAT	1.13E-04			
G3V947	LQPDPNGGQIGVT	7.63E+07	9.27E+06	8.94E+06	1.03E+07	SMR1 protein (Fragment) OS=Rattus norvegicus GN=Vcsa1 PE=4 SV=2	1.76E-04			
Q5I0L0	TGSGGIENYNDAAQVR	2.85E+07	1.41E+07	4.67E+06	1.91E+06	Amy1a protein OS=Rattus norvegicus GN=Amy1a PE=2 SV=1	4.78E-04			
P02783	GGSFGEEASEEISSR	8.77E+06	0.00E+00	7.85E+06	5.77E+06	Seminal vesicle secretory protein 4 n=1 Tax=Rattus norvegicus RepID=SVS4_RAT	4.82E-04			
Q6P6X2	KQFDDDDLSVQQK	2.24E+07	4.05E+06	1.53E+07	2.21E+07	Protein Semg1 OS=Rattus norvegicus GN=Semg1 PE=2 SV=1	1.97E-03			
P02783	GGSFGEEASEEISSR	3.27E+07	6.46E+06	1.29E+07	6.66E+06	Seminal vesicle secretory protein 4 n=1 Tax=Rattus norvegicus RepID=SVS4_RAT	3.60E-03			
Q9ESG3	DTDEEYLFR	7.70E+08	6.41E+06	6.52E+07	5.18E+06	Collectrin OS=Rattus norvegicus GN=Tmem27 PE=1 SV=2	3.82E-03			
P18897	EEVSNAEISDVKQQPDS	3.82E+08	8.03E+06	1.60E+07	2.52E+06	SMR2 protein n=1 Tax=Rattus norvegicus RepID=SMR2_RAT	5.07E-03			
P07522	DYDPVESKIY	2.45E+08	1.94E+07	4.22E+07	3.66E+06	Pro-epidermal growth factor n=1 Tax=Rattus norvegicus RepID=EGF_RAT	6.44E-03			
I3PMS6	ESIRETEVIDPQDLLEGR	1.02E+09	0.00E+00	1.12E+08	1.81E+07	Syndecan (Fragment) OS=Rattus exulans GN=SDC4 PE=2 SV=1	6.79E-03			
Q6IFV4	TRLEQEIATYR	1.47E+07	2.65E+06	0.00E+00	4.13E+06	Keratin, type I cytoskeletal 13 n=1 Tax=Rattus norvegicus RepID=K1C13_RAT	6.82E-03			
Q6P6X2	KQFDDDDLSVQQK	2.95E+08	0.00E+00	9.40E+07	4.98E+05	Protein Semg1 OS=Rattus norvegicus GN=Semg1 PE=2 SV=1	6.90E-03			
P02783	GGSFGEEASEEISSR	1.28E+09	0.00E+00	3.78E+08	9.86E+07	Seminal vesicle secretory protein 4 n=1 Tax=Rattus norvegicus RepID=SVS4_RAT	7.55E-03			
M0R8W8	TAHLSVVSEDGSAVAAT	1.66E+08	0.00E+00	1.00E+08	3.45E+07	Gamma-glutamyltranspeptidase 1 (Fragment) OS=Rattus norvegicus GN=Ggt1 PE=4 SV=1	9.72E-03			
Q01177	ILGSDVQQIAVT	2.60E+06	7.93E+08	2.11E+09	1.75E+08	Plasminogen n=1 Tax=Rattus norvegicus RepID=PLMN_RAT		2.68E-05	0.002052	3.01E-09
P05545	DQAEINTGSALFIDK	0.00E+00	2.20E+10	1.07E+08	2.66E+07	Serine protease inhibitor A3K n=1 Tax=Rattus norvegicus RepID=SPA3K_RAT		1.17E-04	0.000165	4.38E-09
B2RYM3	DGSEIVVAGRI	0.00E+00	2.56E+08	4.33E+07	2.36E+06	Inter-alpha trypsin inhibitor, heavy chain 1 (Predicted), isoform CRA_a n=1 Tax=Rattus norvegicus RepID=B2RYM3_RAT		3.16E-04	0.001086	8.87E-09
M0R8A9	DSGDVESHLSFLEK	0.00E+00	2.87E+08	5.02E+07	9.25E+06	Apolipoprotein A-IV n=1 Tax=Rattus norvegicus RepID=M0R8A9_RAT		1.08E-03	0.001514	1.26E-08
P01015	DKLVLATEKLEAEDR	2.60E+06	3.30E+07	3.51E+07	6.62E+07	Angiotensinogen n=1 Tax=Rattus norvegicus RepID=ANGT_RAT		1.95E-03	0.003277	3.38E-08
P24090	TDCTGQEVTDPAKC	2.60E+06	3.89E+07	2.25E+08	2.59E+08	Alpha-2-HS-glycoprotein n=1 Tax=Rattus norvegicus RepID=FETUA_RAT		2.38E-03	0.008707	4.90E-08
E0A3N4	SLRPSMIDELYLPK	0.00E+00	1.06E+07	4.80E+07	6.74E+07	Serpina3n-like protein n=1 Tax=Rattus norvegicus RepID=E0A3N4_RAT		3.03E-03	4.15E-07	1.05E-07
Q01177	VLEPNDADIALLK	0.00E+00	2.97E+06	1.30E+07	3.88E+06	Plasminogen n=1 Tax=Rattus norvegicus RepID=PLMN_RAT		3.55E-03	0.001444	1.41E-07
P05544	DQVEINTGSALF	0.00E+00	4.98E+07	1.54E+08	1.12E+07	Serine protease inhibitor A3L n=1 Tax=Rattus norvegicus RepID=SPA3L_RAT		4.62E-03	1.86E-05	1.55E-07
E0A3N4	LQVLAEFQEKA	0.00E+00	1.38E+08	3.35E+07	5.70E+07	Serpina3n-like protein n=1 Tax=Rattus norvegicus RepID=E0A3N4_RAT		5.76E-03	0.000101	5.29E-07
F1LM19	SPVASVESASGEVLH	1.19E+06	2.71E+07	1.65E+07	2.43E+07	Alpha-2-HS-glycoprotein n=1 Tax=Rattus norvegicus RepID=F1LM19_RAT		6.51E-03	0.000104	7.45E-07
P24090	AFSPVASVESASGEVL	0.00E+00	3.59E+08	4.90E+07	1.44E+06	Alpha-2-HS-glycoprotein n=1 Tax=Rattus norvegicus RepID=FETUA_RAT		7.48E-03	0.0012	8.89E-07
Q01177	VILGAHEER	1.72E+06	8.16E+08	6.92E+07	2.34E+08	Plasminogen n=1 Tax=Rattus norvegicus RepID=PLMN_RAT		7.84E-03	0.001501	1.03E-06
Q5M7T5	DDICIAKPR	1.27E+06	1.49E+07	8.66E+07	6.18E+06	Protein Serpinc1 OS=Rattus norvegicus GN=Serpinc1 PE=2 SV=1		9.97E-03	0.004451	1.21E-06
P17475	IVESETQSPLFVGK	0.00E+00	6.86E+06	2.86E+08	2.34E+08	Alpha-1-antiproteinase n=1 Tax=Rattus norvegicus RepID=A1AT_RAT		5.39E-03	0.005176	1.61E-06
P09006	DSLRPSMIDELYLP	9.21E+05	5.30E+07	3.14E+07	6.18E+06	Serine protease inhibitor A3N n=1 Tax=Rattus norvegicus RepID=SPA3N_RAT		3.97E-04	0.00706	1.83E-06
Q80ZA3	LAAAVSNFGYDLYR	2.08E+05	2.35E+08	5.46E+08	3.25E+07	Alpha-2 antiplasmin OS=Rattus norvegicus GN=Serpinf1 PE=2 SV=1		6.40E-07	5.60E-04	2.59E-06
P05544	EAFIADFKQPNE	0.00E+00	8.62E+07	7.07E+07	1.11E+07	Serine protease inhibitor A3L n=1 Tax=Rattus norvegicus RepID=SPA3L_RAT		4.11E-05	4.29E-03	2.80E-06
Q6IFV4	QSVEADINGLR	0.00E+00	3.80E+08	1.58E+09	3.47E+07	Keratin, type I cytoskeletal 13 n=1 Tax=Rattus norvegicus RepID=K1C13_RAT		9.71E-03	9.92E-03	3.13E-06
P06759	WESGPEDQLTTPTLE	3.45E+05	6.11E+06	2.33E+09	6.41E+07	Apolipoprotein C-III n=1 Tax=Rattus norvegicus RepID=APOC3_RAT		1.57E-03	5.13E-04	3.35E-06
Q63556	IDELYLPR	0.00E+00	1.65E+07	6.71E+08	2.11E+07	Serine protease inhibitor A3M (Fragment) n=1 Tax=Rattus norvegicus RepID=SPA3M_RAT		4.77E-07	5.84E-05	3.61E-06
P04639	KPALDDLGQQGL	0.00E+00	3.79E+07	1.95E+08	2.22E+07	Apolipoprotein A-I n=1 Tax=Rattus norvegicus RepID=APOA1_RAT		4.82E-03	8.97E-03	3.73E-06
P02770	LAEIEHDNIPADLPSIAADFVEDK	0.00E+00	1.08E+07	1.29E+08	3.13E+07	Serum albumin n=1 Tax=Rattus norvegicus RepID=ALBU_RAT		7.89E-04	0.000178	5.06E-06
P01015	DKLVLATEKLEAEDR	0.00E+00	3.01E+06	6.85E+07	1.40E+08	Angiotensinogen n=1 Tax=Rattus norvegicus RepID=ANGT_RAT		1.66E-03	0.005153	6.68E-06
A1EC93	TCAELCSGDWDCGPGEQCVSTGCSNVCATS	0.00E+00	7.61E+05	1.93E+07	1.22E+08	Protein LOC360228 OS=Rattus norvegicus GN=LOC360228 PE=4 SV=1		1.92E-03	0.001408	7.14E-06
Q80ZA3	LAAAVSNFGYDLY	0.00E+00	5.40E+08	1.16E+07	2.84E+07	Alpha-2 antiplasmin OS=Rattus norvegicus GN=Serpinf1 PE=2 SV=1		4.42E-03	0.005672	7.80E-06
Q01177	LVLEPNDADIALLK	2.98E+05	4.98E+07	2.27E+06	2.41E+07	Plasminogen n=1 Tax=Rattus norvegicus RepID=PLMN_RAT		1.00E+00	0.00811	
P02770	TCVADENAENCDK	0.00E+00	9.14E+07	2.38E+07	1.12E+07	Serum albumin n=1 Tax=Rattus norvegicus RepID=ALBU_RAT		8.59E-03	2.7E-05	
P02770	GLVLIAFSQYLQK	0.00E+00	2.07E+09	1.73E+07	0.00E+00	Serum albumin n=1 Tax=Rattus norvegicus RepID=ALBU_RAT		1.99E-03	4.5E-05	
P02767	TADGSWEPFASGK	3.84E+06	8.88E+06	1.24E+08	7.14E+07	Transthyretin n=1 Tax=Rattus norvegicus RepID=TTHY_RAT		5.00E-03	0.00227	
Q7M0D3	SIVHPSYNSN	0.00E+00	2.97E+08	3.68E+07	2.69E+07	Dentin phosphophoryn OS=Rattus norvegicus PE=1 SV=1		5.53E-03	0.002431	
P01026	LLWESGSLL	0.00E+00	1.45E+09	2.13E+07	2.28E+07	Complement C3 n=1 Tax=Rattus norvegicus RepID=CO3_RAT		3.85E-03	0.00261	
P12346	SKDFQLFGSPLG	0.00E+00	1.30E+08	2.86E+08	6.29E+07	Serotransferrin n=1 Tax=Rattus norvegicus RepID=TRFE_RAT		4.06E-03	0.003844	
M0R8A9	NLAPLVEDVQSKL	0.00E+00	5.71E+08	7.79E+07	5.37E+06	Apolipoprotein A-IV n=1 Tax=Rattus norvegicus RepID=M0R8A9_RAT		1.62E-05	0.00717	
M0RBF1	VGLVAVDKGVFVLN	0.00E+00	2.93E+08	1.06E+08	1.12E+06	Complement C3 OS=Rattus norvegicus GN=C3 PE=4 SV=1		6.17E-04	0.000177	
M0R8A9	VQEQVQEQVQPKPLES	2.65E+05	9.34E+07	0.00E+00	1.40E+07	Apolipoprotein A-IV n=1 Tax=Rattus norvegicus RepID=M0R8A9_RAT		0.000393		2.31E-05
P04639	WNEEVEAYR	1.38E+06	1.23E+08	4.00E+07	4.81E+07	Apolipoprotein A-I n=1 Tax=Rattus norvegicus RepID=APOA1_RAT		0.000345		2.53E-05
P02454	GDRGETGPAGPAGPIGPAG	0.00E+00	1.64E+07	1.88E+08	1.23E+08	Collagen alpha-1(I) chain n=1 Tax=Rattus norvegicus RepID=CO1A1_RAT		0.002338		2.77E-05
P04639	LDNWDTLGSTVGR	2.28E+06	3.61E+07	4.09E+07	1.00E+07	Apolipoprotein A-I n=1 Tax=Rattus norvegicus RepID=APOA1_RAT		0.000281		2.91E-05
P01026	LWESGSLLR	0.00E+00	3.24E+07	1.07E+07	2.78E+07	Complement C3 n=1 Tax=Rattus norvegicus RepID=CO3_RAT		0.003288		2.93E-05
P04639	DYVSQFESSTLGK	0.00E+00	8.58E+07	0.00E+00	1.25E+07	Apolipoprotein A-I n=1 Tax=Rattus norvegicus RepID=APOA1_RAT		0.00365		3.20E-05
UPI0002AB826B	DLQLLHQKVEEQ	0.00E+00	1.34E+07	4.36E+08	7.27E+07	UPI0002AB826B related cluster n=1 Tax=Rattus norvegicus RepID=UPI0002AB826B		0.008		3.67E-05
P08721	DAVATWLKPDP	0.00E+00	1.08E+07	9.08E+07	1.84E+07	Osteopontin n=1 Tax=Rattus norvegicus RepID=OSTP_RAT		0.000939		3.97E-05
G3V615	VKDMEDLENVFYK	0.00E+00	5.85E+08	9.08E+07	2.07E+08	Complement factor B, isoform CRA_b OS=Rattus norvegicus GN=C2 PE=3 SV=1		0.001393		4.57E-05

Protein	Sequence	mean peak intensity control	mean peak intensity DM	mean peak intensity HTN	mean peak intensity DM+HTN	Description	control vs all	DM vs control	HTN vs control	HTN+DM vs control
A1L114	DTGTTSEFIEAGGDIR	0.00E+00	1.60E+07	5.79E+08	3.76E+07	Fga protein OS=Rattus norvegicus GN=Fga PE=2 SV=1		8.53E-05		4.73E-05
G3V836	EQEFSDNELQELSTQGSRY	1.06E+06	4.01E+06	1.25E+09	3.13E+08	Clusterin OS=Rattus norvegicus GN=Clu PE=3 SV=1		0.005206		5.83E-05
F1LM19	HAFSPVASVESASGEVLHSPK	2.54E+07	3.20E+07	1.10E+08	2.69E+07	Alpha-2-HS-glycoprotein n=1 Tax=Rattus norvegicus RepID=F1LM19_RAT		0.005664		6.17E-05
Q64240	DNVPTLPDIQVQENFNEAR	1.96E+06	1.92E+07	9.75E+07	1.93E+07	Protein AMBP n=1 Tax=Rattus norvegicus RepID=AMBP_RAT		0.003392		6.35E-05
A1L114	MSPVPDLVPGSFK	9.05E+04	9.13E+05	0.00E+00	5.91E+07	Fga protein OS=Rattus norvegicus GN=Fga PE=2 SV=1		0.009787		7.06E-05
P05544	LSQPEDQVEINTGSAL	0.00E+00	4.63E+07	4.89E+06	5.43E+07	Serine protease inhibitor A3L n=1 Tax=Rattus norvegicus RepID=SPA3L_RAT		0.00019		7.36E-05
P24090	AFSPVASVESASGEVLH	1.06E+06	4.53E+06	0.00E+00	4.85E+07	Alpha-2-HS-glycoprotein n=1 Tax=Rattus norvegicus RepID=FETUA_RAT		0.000214		7.82E-05
B3DM95	SVEAAAELSAK	0.00E+00	8.84E+06	5.23E+07	6.00E+07	Parathymosin OS=Rattus norvegicus GN=Ptms PE=2 SV=1		0.007199		8.47E-05
P13635	ELISVDTEQSNFYLR	0.00E+00	1.03E+08	0.00E+00	2.42E+07	Ceruloplasmin n=1 Tax=Rattus norvegicus RepID=CERU_RAT		0.000627		8.63E-05
Q6P6X2	KSQGGQLQSYGQMK	2.70E+06	2.42E+07	0.00E+00	9.12E+06	Protein Semg1 OS=Rattus norvegicus GN=Semg1 PE=2 SV=1		8.65E-05		
P17475	IVESETQSPLFVGK	0.00E+00	7.18E+07	0.00E+00	4.71E+07	Alpha-1-antiproteinase n=1 Tax=Rattus norvegicus RepID=A1AT_RAT		9.00E-05		
M0RBF1	TLDPEHLGQGGVQRE	0.00E+00	3.19E+07	1.03E+08	1.50E+08	Complement C3 OS=Rattus norvegicus GN=C3 PE=4 SV=1			7.32E-06	9.03E-05
M0R8A9	GSPDQPLALPLPEQVQ	0.00E+00	0.00E+00	4.38E+08	7.61E+05	Apolipoprotein A-IV n=1 Tax=Rattus norvegicus RepID=M0R8A9_RAT			0.003424	9.52E-05
Q01177	VLEPNDADIAL	0.00E+00	0.00E+00	4.31E+08	3.09E+06	Plasminogen n=1 Tax=Rattus norvegicus RepID=PLMN_RAT			0.005206	1.03E-04
Q5M7T5	ATEEDVLEQKVPEATNR	0.00E+00	0.00E+00	1.80E+08	2.19E+07	Protein Serpinc1 OS=Rattus norvegicus GN=Serpinc1 PE=2 SV=1			2.55E-07	1.04E-04
A1L114	DEAASEAHQEGDTR	0.00E+00	0.00E+00	1.57E+08	4.80E+05	Fga protein OS=Rattus norvegicus GN=Fga PE=2 SV=1			0.001393	1.08E-04
Q01177	LVLEPNDADIALLK	0.00E+00	0.00E+00	9.11E+07	4.41E+05	Plasminogen n=1 Tax=Rattus norvegicus RepID=PLMN_RAT			0.002735	1.18E-04
P05544	VLDVDETGTEATAATGVAT	0.00E+00	0.00E+00	2.68E+08	1.14E+06	Serine protease inhibitor A3L n=1 Tax=Rattus norvegicus RepID=SPA3L_RAT			0.002975	1.26E-04
F1LR92	ALYQVEAFTADFQQPR	0.00E+00	0.00E+00	7.62E+07	4.29E+07	Serine protease inhibitor A3M (Fragment) n=2 Tax=Rattus norvegicus RepID=F1LR92_RAT			0.003138	1.28E-04
P17475	MIVESETQSPLFVGK	8.63E+05	0.00E+00	2.37E+08	1.08E+08	Alpha-1-antiproteinase n=1 Tax=Rattus norvegicus RepID=A1AT_RAT			0.004663	1.37E-04
P02651	VQEQVQEQVQPKPLE	0.00E+00	0.00E+00	2.15E+07	6.57E+07	Apolipoprotein A-IV n=1 Tax=Rattus norvegicus RepID=APOA4_RAT			0.001153	1.45E-04
P02770	AEFQPLVEEPK	0.00E+00	0.00E+00	4.85E+06	1.55E+07	Serum albumin n=1 Tax=Rattus norvegicus RepID=ALBU_RAT			0.008303	1.47E-04
Q6P6X2	QFDDDDLSVQQK	0.00E+00	0.00E+00	8.36E+07	1.93E+08	Protein Semg1 OS=Rattus norvegicus GN=Semg1 PE=2 SV=1			0.008865	1.58E-04
A1L114	TSDSDIFTDIENPSSHVPEFSSSS	0.00E+00	0.00E+00	3.02E+08	1.00E+09	Fga protein OS=Rattus norvegicus GN=Fga PE=2 SV=1			0.004757	1.68E-04
P05544	FSISTDYSLKE	0.00E+00	0.00E+00	5.12E+07	7.83E+07	Serine protease inhibitor A3L n=1 Tax=Rattus norvegicus RepID=SPA3L_RAT			0.000426	1.74E-04
F1M7X5	VLEDNSALDK	0.00E+00	0.00E+00	8.32E+06	7.76E+07	Dipeptidyl peptidase 4 OS=Rattus norvegicus GN=Dpp4 PE=2 SV=1			0.003899	1.83E-04
P02651	TDVTQQLNTLFQDK	0.00E+00	0.00E+00	4.22E+06	9.72E+06	Apolipoprotein A-IV n=1 Tax=Rattus norvegicus RepID=APOA4_RAT			0.004087	1.96E-04
Q01177	LVLEPNDADIAL	0.00E+00	0.00E+00	5.28E+07	2.42E+08	Plasminogen n=1 Tax=Rattus norvegicus RepID=PLMN_RAT			0.008718	2.04E-04
Q01177	LVLEPNDADIAL	0.00E+00	0.00E+00	3.63E+07	1.14E+09	Plasminogen n=1 Tax=Rattus norvegicus RepID=PLMN_RAT			0.000115	2.17E-04
P17475	EDAQETDTSQQDQSPTYR	0.00E+00	0.00E+00	9.64E+07	1.64E+08	Alpha-1-antiproteinase n=1 Tax=Rattus norvegicus RepID=A1AT_RAT			0.005876	2.32E-04
P02783	EEASEEISSR	2.74E+07	0.00E+00	1.37E+08	4.13E+08	Seminal vesicle secretory protein 4 n=1 Tax=Rattus norvegicus RepID=SVS4_RAT			0.006879	2.37E-04
P17475	TDTSQQDQSPTYR	0.00E+00	0.00E+00	1.70E+07	9.65E+08	Alpha-1-antiproteinase n=1 Tax=Rattus norvegicus RepID=A1AT_RAT			0.008106	2.40E-04
P24090	ESASGEVLHSPK	0.00E+00	0.00E+00	1.27E+08	8.62E+06	Alpha-2-HS-glycoprotein n=1 Tax=Rattus norvegicus RepID=FETUA_RAT			0.008516	2.45E-04
F1LM05	AVLDVAETGTEAAAATGV	0.00E+00	0.00E+00	1.07E+09	2.03E+06	Protein LOC299282 n=1 Tax=Rattus norvegicus RepID=F1LM05_RAT			1.95E-05	2.61E-04
P17475	EDAQETDTSQQDQSPTYR	0.00E+00	0.00E+00	2.89E+08	8.09E+07	Alpha-1-antiproteinase n=1 Tax=Rattus norvegicus RepID=A1AT_RAT			2.63E-04	
P02770	EAHKSEIAHR	0.00E+00	9.42E+07	7.42E+08	1.50E+07	Serum albumin n=1 Tax=Rattus norvegicus RepID=ALBU_RAT			2.92E-04	
P24090	DCTGQEVTDPAKC	1.28E+06	0.00E+00	5.27E+08	7.95E+07	Alpha-2-HS-glycoprotein n=1 Tax=Rattus norvegicus RepID=FETUA_RAT			3.03E-04	
P17475	EDAQETDTSQQDQSPTYRK	8.64E+06	4.12E+05	4.58E+08	1.14E+08	Alpha-1-antiproteinase n=1 Tax=Rattus norvegicus RepID=A1AT_RAT			3.22E-04	
P17475	EDAQETDTSQQDQSPTYR	1.77E+08	0.00E+00	1.32E+09	1.99E+08	Alpha-1-antiproteinase n=1 Tax=Rattus norvegicus RepID=A1AT_RAT			3.32E-04	
P02770	EKCCAEGDPPAC	9.06E+06	0.00E+00	1.86E+09	1.21E+08	Serum albumin n=1 Tax=Rattus norvegicus RepID=ALBU_RAT			3.43E-04	
P17475	EDAQETDTSQQDQSPTYRK	5.45E+07	0.00E+00	8.38E+08	1.16E+08	Alpha-1-antiproteinase n=1 Tax=Rattus norvegicus RepID=A1AT_RAT			3.44E-04	
P02770	DICTLPDKE	1.34E+07	0.00E+00	1.38E+09	1.97E+08	Serum albumin n=1 Tax=Rattus norvegicus RepID=ALBU_RAT			3.63E-04	
P12346	HQTVLENTNGK	3.79E+06	0.00E+00	5.53E+08	1.03E+08	Serotransferrin n=1 Tax=Rattus norvegicus RepID=TRFE_RAT			3.67E-04	
M0R620	LNGDWFSIVVASNKR	1.36E+07	0.00E+00	9.91E+08	0.00E+00	Protein LOC100912565 n=1 Tax=Rattus norvegicus RepID=M0R620_RAT			3.75E-04	
P17475	EDAQETDTSQQDQSPTYRK	8.69E+06	0.00E+00	1.13E+09	4.77E+08	Alpha-1-antiproteinase n=1 Tax=Rattus norvegicus RepID=A1AT_RAT			3.84E-04	
P12346	VSTVLTAQK	6.11E+07	0.00E+00	1.19E+09	9.95E+07	Serotransferrin n=1 Tax=Rattus norvegicus RepID=TRFE_RAT			4.27E-04	
P12346	DGGGDVAFVK	7.09E+07	0.00E+00	1.92E+09	4.57E+07	Serotransferrin n=1 Tax=Rattus norvegicus RepID=TRFE_RAT			4.40E-04	
G3V836	SLLNSLEEA	8.04E+06	8.69E+05	6.50E+08	9.66E+06	Clusterin OS=Rattus norvegicus GN=Clu PE=3 SV=1			4.69E-04	
F1LS40	GIDGRPGPIGPAGPRGEAG	5.39E+06	4.58E+06	4.14E+06	1.84E+07	Collagen alpha-2(I) chain OS=Rattus norvegicus GN=Col1a2 PE=2 SV=2				4.80E-04
P04639	HLDEFQEKWNEE	1.00E+06	0.00E+00	0.00E+00	1.09E+08	Apolipoprotein A-I n=1 Tax=Rattus norvegicus RepID=APOA1_RAT				4.96E-04
F1LNT3	HPPPPPPPP	0.00E+00	1.92E+07	4.97E+07	1.38E+08	Protein R3hdm1 OS=Rattus norvegicus GN=R3hdm1 PE=2 SV=1				5.12E-04
P02454	DRGETGPAGPAGPIGPAG	0.00E+00	3.29E+07	2.05E+08	5.24E+07	Collagen alpha-1(I) chain n=1 Tax=Rattus norvegicus RepID=CO1A1_RAT				5.27E-04
P02651	NLAPLVEDVQSK	5.68E+05	3.69E+07	0.00E+00	5.99E+07	Apolipoprotein A-IV n=1 Tax=Rattus norvegicus RepID=APOA4_RAT				5.35E-04
Q99PS8	DNSDRPPLQEGALPQ	0.00E+00	4.39E+07	7.66E+05	5.26E+06	Histidine-rich glycoprotein OS=Rattus norvegicus GN=Hrg PE=2 SV=1				5.52E-04
M0RBF1	SEETKQNEGFSLTAK	1.18E+06	1.58E+08	1.76E+06	1.14E+08	Complement C3 OS=Rattus norvegicus GN=C3 PE=4 SV=1				5.61E-04
P02651	RAVEPLGDKFN	1.26E+07	3.60E+08	6.82E+07	1.60E+08	Apolipoprotein A-IV n=1 Tax=Rattus norvegicus RepID=APOA4_RAT				5.68E-04
P17475	VFNNDADLSGITEDAPLK	0.00E+00	0.00E+00	9.55E+06	1.09E+07	Alpha-1-antiproteinase n=1 Tax=Rattus norvegicus RepID=A1AT_RAT				5.83E-04
M0RBF1	EDVPAADLSDQVPDTDSETR	2.31E+07	8.90E+07	2.51E+08	1.42E+08	Complement C3 OS=Rattus norvegicus GN=C3 PE=4 SV=1				5.89E-04
Q99PS8	DNSDRPPLQEGALPQMLPGHSGPSGTN	0.00E+00	2.24E+07	1.08E+08	1.03E+08	Histidine-rich glycoprotein OS=Rattus norvegicus GN=Hrg PE=2 SV=1				6.15E-04
P24090	SPVASVESASGEVLHSPK	0.00E+00	7.20E+07	1.56E+07	1.75E+07	Alpha-2-HS-glycoprotein n=1 Tax=Rattus norvegicus RepID=FETUA_RAT				6.23E-04

Protein	Sequence	mean peak intensity control	mean peak intensity DM	mean peak intensity HTN	mean peak intensity DM+HTN	Description	control vs all	DM vs control	HTN vs control	HTN+DM vs control
M0R8A9	VQEQVQEQVQPKPLES	0.00E+00	0.00E+00	1.25E+08	2.39E+08	Apolipoprotein A-IV n=1 Tax=Rattus norvegicus RepID=M0R8A9_RAT				6.23E-04
M0RBF1	TLDPEHLGQGGVQRED	0.00E+00	3.02E+07	4.14E+07	1.82E+07	Complement C3 OS=Rattus norvegicus GN=C3 PE=4 SV=1				6.30E-04
A1L114	DTGTTSEFIEAGGDIR	6.99E+05	4.68E+07	4.05E+08	1.38E+07	Fga protein OS=Rattus norvegicus GN=Fga PE=2 SV=1				6.33E-04
P02651	ATIDQNLEDLR	2.19E+06	3.86E+07	4.75E+07	3.82E+07	Apolipoprotein A-IV n=1 Tax=Rattus norvegicus RepID=APOA4_RAT				6.52E-04
P04639	KLEPLGTELHK	6.22E+06	5.23E+09	2.80E+08	6.88E+07	Apolipoprotein A-I n=1 Tax=Rattus norvegicus RepID=APOA1_RAT				6.96E-04
P15083	FADEREIQNAGDQAQENR	0.00E+00	2.46E+08	3.36E+08	9.73E+07	Polymeric immunoglobulin receptor OS=Rattus norvegicus GN=Pigr PE=1 SV=1				7.06E-04
P02651	KGSPDQPLALPLPEQVQ	0.00E+00	2.26E+08	8.59E+07	1.03E+07	Apolipoprotein A-IV n=1 Tax=Rattus norvegicus RepID=APOA4_RAT				7.21E-04
P17475	MIVESETQSPLFVGK	0.00E+00	7.40E+07	8.72E+06	2.55E+07	Alpha-1-antiproteinase n=1 Tax=Rattus norvegicus RepID=A1AT_RAT				7.49E-04
Q5M7T5	ATEEDVLEQKVPEATNRR	0.00E+00	6.24E+07	2.53E+07	4.43E+07	Protein Serpinc1 OS=Rattus norvegicus GN=Serpinc1 PE=2 SV=1				7.59E-04
Q6P6X2	FGQDGGDMAQTSVSQEHTGVK	0.00E+00	7.96E+07	3.25E+07	2.62E+07	Protein Semg1 OS=Rattus norvegicus GN=Semg1 PE=2 SV=1				7.65E-04
P09034	TQDPAKAPNTPDVLEIE	7.40E+05	0.00E+00	6.12E+07	2.12E+07	Argininosuccinate synthase OS=Rattus norvegicus GN=Ass1 PE=2 SV=1				7.79E-04
Q68FT8	DLPGQQPVSEQAQQKLPPL	7.78E+05	4.21E+07	3.86E+07	1.24E+08	Protein Serpinf2 OS=Rattus norvegicus GN=Serpinf2 PE=2 SV=1				8.53E-04
Q08420	SDTGESGVDLADRLDLVEK	0.00E+00	1.30E+07	2.95E+07	4.55E+07	Extracellular superoxide dismutase [Cu-Zn] n=1 Tax=Rattus norvegicus RepID=SODE_RAT				8.69E-04
P04639	DEFQEKWNEEVEAY	0.00E+00	1.65E+07	3.08E+08	2.72E+08	Apolipoprotein A-I n=1 Tax=Rattus norvegicus RepID=APOA1_RAT				9.15E-04
P08721	DAIDSAEKPDAIDSAERSDAIDSQASSK	0.00E+00	1.76E+07	4.21E+08	2.14E+08	Osteopontin n=1 Tax=Rattus norvegicus RepID=OSTP_RAT				9.21E-04
Q68FT8	RLDQNDKADIPGGK	0.00E+00	8.03E+06	7.68E+08	6.22E+08	Protein Serpinf2 OS=Rattus norvegicus GN=Serpinf2 PE=2 SV=1				9.55E-04
D3ZVB6	LEGQDLQSENQR	0.00E+00	1.33E+08	1.11E+08	1.12E+08	Protein LOC690326 OS=Rattus norvegicus GN=LOC690326 PE=4 SV=1				9.83E-04
P05545	DGILGRDTLPHEDQGKGR	0.00E+00	1.06E+09	0.00E+00	5.76E+06	Serine protease inhibitor A3K n=1 Tax=Rattus norvegicus RepID=SPA3K_RAT				9.85E-04
Q5BKC4	TENYEEQFEMFK	0.00E+00	0.00E+00	2.77E+08	4.92E+07	C9 protein OS=Rattus norvegicus GN=C9 PE=2 SV=1				1.01E-03
P02454	AVGPAGKDGEAGAQGAPGPAGPAGERGEQGPAG	0.00E+00	0.00E+00	1.13E+07	6.31E+07	Collagen alpha-1(I) chain n=1 Tax=Rattus norvegicus RepID=CO1A1_RAT				1.03E-03
Q5BKC4	TENYEEQFEMFK	0.00E+00	1.33E+07	0.00E+00	1.73E+08	C9 protein OS=Rattus norvegicus GN=C9 PE=2 SV=1				1.09E-03
P17475	IVESETQSPLFVGKVIDPT	0.00E+00	9.30E+06	7.05E+06	4.82E+06	Alpha-1-antiproteinase n=1 Tax=Rattus norvegicus RepID=A1AT_RAT				1.11E-03
Q5M7T5	EEGSEAAASTSVVITGR	0.00E+00	6.40E+07	9.68E+06	7.18E+07	Protein Serpinc1 OS=Rattus norvegicus GN=Serpinc1 PE=2 SV=1				1.14E-03
P02650	ELEEQLGPVAEETR	3.15E+06	2.04E+07	4.56E+08	3.69E+08	Apolipoprotein E n=1 Tax=Rattus norvegicus RepID=APOE_RAT				1.14E-03
P02770	TVDETYVPKEF	0.00E+00	4.55E+06	3.49E+08	3.56E+07	Serum albumin n=1 Tax=Rattus norvegicus RepID=ALBU_RAT				1.16E-03
P02770	TQKAPQVSTPTLVEAAR	3.37E+06	1.44E+08	2.79E+07	3.41E+07	Serum albumin n=1 Tax=Rattus norvegicus RepID=ALBU_RAT				1.18E-03
P24090	SPVASVESASGEVLHSP	0.00E+00	4.33E+08	1.10E+08	2.65E+08	Alpha-2-HS-glycoprotein n=1 Tax=Rattus norvegicus RepID=FETUA_RAT				1.21E-03
F1LM19	SPVASVESASGEVLH	0.00E+00	3.02E+07	1.01E+07	3.35E+06	Alpha-2-HS-glycoprotein n=1 Tax=Rattus norvegicus RepID=F1LM19_RAT				1.29E-03
P05544	AEAFIADFKQPNE	0.00E+00	0.00E+00	5.26E+07	4.76E+07	Serine protease inhibitor A3L n=1 Tax=Rattus norvegicus RepID=SPA3L_RAT				1.29E-03
P04639	EQLGPVTQEF	0.00E+00	0.00E+00	0.00E+00	1.50E+07	Apolipoprotein A-I n=1 Tax=Rattus norvegicus RepID=APOA1_RAT				1.32E-03
Q6P734	DSEVTSHSSQDPLVVQEGSR	4.87E+05	0.00E+00	2.63E+08	1.62E+07	Plasma protease C1 inhibitor OS=Rattus norvegicus GN=Serping1 PE=2 SV=1				1.36E-03
Q68FT8	MDLPGQQPVSEQAQQKLPPL	1.78E+05	1.10E+08	1.59E+08	1.58E+06	Protein Serpinf2 OS=Rattus norvegicus GN=Serpinf2 PE=2 SV=1				1.44E-03
Q6P734	DSEVTSHSSQDPLVVQEGSR	0.00E+00	0.00E+00	9.25E+06	2.18E+07	Plasma protease C1 inhibitor OS=Rattus norvegicus GN=Serping1 PE=2 SV=1				1.46E-03
Q6P734	DSEVTSHSSQDPLVVQEGSR	0.00E+00	1.39E+07	0.00E+00	9.77E+06	Plasma protease C1 inhibitor OS=Rattus norvegicus GN=Serping1 PE=2 SV=1				1.50E-03
P04639	DYVSQFESSTLGKQ	1.55E+06	1.33E+07	0.00E+00	1.30E+07	Apolipoprotein A-I n=1 Tax=Rattus norvegicus RepID=APOA1_RAT				1.50E-03
P04639	QKLEPLGTELHK	0.00E+00	2.97E+06	1.40E+06	2.79E+06	Apolipoprotein A-I n=1 Tax=Rattus norvegicus RepID=APOA1_RAT				1.52E-03
P24090	SPVASVESASGEVL	5.80E+06	6.96E+07	3.62E+06	3.17E+07	Alpha-2-HS-glycoprotein n=1 Tax=Rattus norvegicus RepID=FETUA_RAT				1.60E-03
P05545	DQAEINTGSALFIDKEQP	3.57E+07	4.31E+08	1.03E+08	8.03E+07	Serine protease inhibitor A3K n=1 Tax=Rattus norvegicus RepID=SPA3K_RAT				1.65E-03
Q68FT8	LGNQDLGDHATLK	9.03E+06	1.12E+08	2.77E+08	8.97E+07	Protein Serpinf2 OS=Rattus norvegicus GN=Serpinf2 PE=2 SV=1				1.71E-03
P04639	DNWDTLGSTVGR	5.05E+07	1.32E+09	1.31E+09	3.86E+08	Apolipoprotein A-I n=1 Tax=Rattus norvegicus RepID=APOA1_RAT				1.81E-03
P24090	VASVESASGEVLHSPK	7.41E+05	4.04E+07	4.40E+06	2.02E+07	Alpha-2-HS-glycoprotein n=1 Tax=Rattus norvegicus RepID=FETUA_RAT				1.83E-03
A9UMV1	DDPGSSALLDTVQEHL	0.00E+00	3.57E+07	0.00E+00	2.77E+07	Uncharacterized protein (Fragment) OS=Rattus norvegicus GN=Apoc2 PE=2 SV=1				1.85E-03
P05545	ILGRDTLPHEDQGKGR	0.00E+00	5.21E+07	0.00E+00	1.17E+08	Serine protease inhibitor A3K n=1 Tax=Rattus norvegicus RepID=SPA3K_RAT				1.85E-03
P05545	QVESSLQPETLKK	0.00E+00	4.02E+07	0.00E+00	5.31E+07	Serine protease inhibitor A3K n=1 Tax=Rattus norvegicus RepID=SPA3K_RAT				1.89E-03
P05545	LSQPEDQAEINTGSAL	3.55E+05	1.37E+08	0.00E+00	8.28E+07	Serine protease inhibitor A3K n=1 Tax=Rattus norvegicus RepID=SPA3K_RAT				1.92E-03
D4A6E3	VVLSAPAVESELSPR	0.00E+00	6.47E+07	0.00E+00	2.47E+08	Protein LOC100911833 OS=Rattus norvegicus GN=LOC100911833 PE=2 SV=1				1.93E-03
Q5BKC4	TENYEEQFEMF	0.00E+00	8.63E+07	0.00E+00	2.03E+08	C9 protein OS=Rattus norvegicus GN=C9 PE=2 SV=1				1.93E-03
Q68FT8	RLDQNDKADIPGGKTF	1.55E+07	2.47E+08	3.59E+06	8.60E+07	Protein Serpinf2 OS=Rattus norvegicus GN=Serpinf2 PE=2 SV=1				2.01E-03
Q99PS8	SDRPPLQEGALPQM	0.00E+00	0.00E+00	4.48E+06	4.53E+08	Histidine-rich glycoprotein OS=Rattus norvegicus GN=Hrg PE=2 SV=1				2.07E-03
Q01177	ILGSDVQQIAVTK	0.00E+00	1.57E+08	0.00E+00	3.86E+07	Plasminogen n=1 Tax=Rattus norvegicus RepID=PLMN_RAT				2.09E-03
G3V947	LGLQPDPNGGQIGV	0.00E+00	1.95E+08	1.53E+06	1.20E+09	SMR1 protein (Fragment) OS=Rattus norvegicus GN=Vcsa1 PE=4 SV=2				2.11E-03
Q01177	ILGSDVQQIAVTKL	0.00E+00	5.44E+08	4.43E+06	8.82E+09	Plasminogen n=1 Tax=Rattus norvegicus RepID=PLMN_RAT				2.16E-03
M0RBF1	DLNMDVSLHLPS	0.00E+00	2.84E+07	4.42E+07	1.78E+08	Complement C3 OS=Rattus norvegicus GN=C3 PE=4 SV=1				2.17E-03
B2RYM3	YDGSEIVVAGRI	0.00E+00	6.84E+07	1.95E+06	7.09E+09	Inter-alpha trypsin inhibitor, heavy chain 1 (Predicted), isoform CRA_a n=1 Tax=Rattus norvegicus RepID=B2RYM3_RAT				2.21E-03
G3V615	SLTETIEGADAEDGHSPGEQQ	0.00E+00	1.07E+08	4.23E+06	7.70E+08	Complement factor B, isoform CRA_b OS=Rattus norvegicus GN=C2 PE=3 SV=1				2.23E-03
P02770	LTVDETYVPKEF	0.00E+00	6.97E+07	7.37E+06	5.46E+10	Serum albumin n=1 Tax=Rattus norvegicus RepID=ALBU_RAT				2.27E-03
P02651	SRLAPLAEGVQEK	0.00E+00	1.03E+08	6.42E+06	2.12E+08	Apolipoprotein A-IV n=1 Tax=Rattus norvegicus RepID=APOA4_RAT				2.37E-03
P02770	AEFQPLVEEPKN	0.00E+00	1.72E+08	6.06E+07	5.10E+08	Serum albumin n=1 Tax=Rattus norvegicus RepID=ALBU_RAT				2.37E-03
E0A3N4	DSLRPSMIDELYLPK	0.00E+00	5.54E+08	3.81E+07	7.61E+07	Serpina3n-like protein n=1 Tax=Rattus norvegicus RepID=E0A3N4_RAT				2.47E-03
Q5M7T5	EGSEAAASTSVVITGR	0.00E+00	1.16E+08	1.77E+07	1.20E+09	Protein Serpinc1 OS=Rattus norvegicus GN=Serpinc1 PE=2 SV=1				2.49E-03

Protein	Sequence	mean peak intensity control	mean peak intensity DM	mean peak intensity HTN	mean peak intensity DM+HTN	Description	control vs all	DM vs control	HTN vs control	HTN+DM vs control
P02651	FRQQLGSDSGDVESHLS	0.00E+00	5.58E+07	2.15E+07	1.33E+08	Apolipoprotein A-IV n=1 Tax=Rattus norvegicus RepID=APOA4_RAT				2.54E-03
P08721	DAIDSAEKPDAIDSAER	0.00E+00	2.16E+08	5.28E+06	2.39E+09	Osteopontin n=1 Tax=Rattus norvegicus RepID=OSTP_RAT				2.66E-03
P01835	DGVLDSVTDQDSKDSTYSMSSTL	0.00E+00	1.71E+08	3.32E+07	3.03E+07	Ig kappa chain C region, B allele n=2 Tax=Rattus norvegicus RepID=KACB_RAT				2.72E-03
P02651	AVEPLGDKFNMA	0.00E+00	5.53E+08	2.44E+07	1.86E+07	Apolipoprotein A-IV n=1 Tax=Rattus norvegicus RepID=APOA4_RAT				2.74E-03
P02651	SRLAPLAEGVQEK	5.83E+06	4.78E+08	6.48E+07	1.18E+08	Apolipoprotein A-IV n=1 Tax=Rattus norvegicus RepID=APOA4_RAT				3.07E-03
P08721	DAVATWLKPDPSQ	5.64E+05	7.69E+07	4.01E+06	6.89E+07	Osteopontin n=1 Tax=Rattus norvegicus RepID=OSTP_RAT				3.15E-03
P05544	AVLDVDETGTEATAATGVAT	0.00E+00	3.43E+08	3.91E+07	9.04E+07	Serine protease inhibitor A3L n=1 Tax=Rattus norvegicus RepID=SPA3L_RAT				3.18E-03
Q01177	KEAQLPVIENK	0.00E+00	2.27E+08	5.37E+07	1.67E+09	Plasminogen n=1 Tax=Rattus norvegicus RepID=PLMN_RAT				3.31E-03
P04639	QEQLGPVTQEF	0.00E+00	4.17E+08	1.27E+08	4.51E+07	Apolipoprotein A-I n=1 Tax=Rattus norvegicus RepID=APOA1_RAT				3.32E-03
G3V947	ISNTTATTQNSTDIFEGGG	0.00E+00	2.80E+07	2.59E+07	3.00E+08	SMR1 protein (Fragment) OS=Rattus norvegicus GN=Vcsa1 PE=4 SV=2				3.36E-03
Q01177	GSDVQQIAVTKL	0.00E+00	1.22E+08	1.68E+08	6.48E+08	Plasminogen n=1 Tax=Rattus norvegicus RepID=PLMN_RAT				3.38E-03
B4F7A5	GGGAGDRGTDGAESEGQPQGLIPGVV	5.59E+05	1.37E+08	0.00E+00	3.16E+07	Cd99 protein OS=Rattus norvegicus GN=Cd99 PE=2 SV=1				3.38E-03
P08721	DAIDSAEKPDAIDSAER	0.00E+00	3.40E+07	1.99E+06	3.36E+07	Osteopontin n=1 Tax=Rattus norvegicus RepID=OSTP_RAT				3.41E-03
P02651	AVEPLGDKFNMA	0.00E+00	2.49E+08	7.17E+07	1.82E+08	Apolipoprotein A-IV n=1 Tax=Rattus norvegicus RepID=APOA4_RAT				3.51E-03
P08721	DEAIKVIPVAQR	0.00E+00	9.18E+07	4.67E+06	4.44E+07	Osteopontin n=1 Tax=Rattus norvegicus RepID=OSTP_RAT				3.52E-03
P05545	QRLSQPEDQAEINTGSAL	1.56E+05	7.76E+07	3.15E+07	1.89E+07	Serine protease inhibitor A3K n=1 Tax=Rattus norvegicus RepID=SPA3K_RAT				3.60E-03
P02651	LPLPEQVQEQVQEQVQPKPLES	0.00E+00	8.49E+08	3.30E+07	1.27E+08	Apolipoprotein A-IV n=1 Tax=Rattus norvegicus RepID=APOA4_RAT				3.62E-03
P08721	DEQYPDATDEDLTSRM	0.00E+00	1.26E+08	1.03E+07	5.90E+07	Osteopontin n=1 Tax=Rattus norvegicus RepID=OSTP_RAT				3.65E-03
P02770	RHPDYSVSLLLR	1.32E+07	7.31E+09	6.85E+08	3.57E+07	Serum albumin n=1 Tax=Rattus norvegicus RepID=ALBU_RAT				3.66E-03
M0R8A9	EQVQEQVQPKPLE	4.38E+06	3.71E+08	8.85E+07	1.12E+08	Apolipoprotein A-IV n=1 Tax=Rattus norvegicus RepID=M0R8A9_RAT				3.68E-03
P09006	YQAEAFTADFQQSR	8.03E+06	3.00E+08	3.78E+08	7.42E+08	Serine protease inhibitor A3N n=1 Tax=Rattus norvegicus RepID=SPA3N_RAT				3.69E-03
Q99PS8	DNSDRPPLQEGALPQMLPGHSGPSGTN	1.19E+07	5.31E+07	4.45E+07	3.79E+07	Histidine-rich glycoprotein OS=Rattus norvegicus GN=Hrg PE=2 SV=1				3.71E-03
G3V947	YLGLQPDPNGGQIGVT	0.00E+00	1.09E+08	1.01E+07	4.73E+07	SMR1 protein (Fragment) OS=Rattus norvegicus GN=Vcsa1 PE=4 SV=2				3.72E-03
M0RBF1	EDVPAADLSDQVPDTDSETR	1.39E+05	0.00E+00	2.48E+06	2.97E+07	Complement C3 OS=Rattus norvegicus GN=C3 PE=4 SV=1				3.84E-03
G3V836	EQEFSDNELQELSTQGSR	0.00E+00	5.09E+05	0.00E+00	1.13E+06	Clusterin OS=Rattus norvegicus GN=Clu PE=3 SV=1				3.96E-03
G3V836	DNELQELSTQGSR	2.11E+07	2.48E+08	9.31E+07	2.72E+07	Clusterin OS=Rattus norvegicus GN=Clu PE=3 SV=1				3.99E-03
UPI0002AB826B	DDLIVTTGYSSGLA	1.21E+06	1.44E+08	5.65E+06	1.22E+08	UPI0002AB826B related cluster n=1 Tax=Rattus norvegicus RepID=UPI0002AB826B				4.08E-03
Q01177	ILGSDVQQIAVTK	1.99E+06	0.00E+00	2.05E+07	9.82E+07	Plasminogen n=1 Tax=Rattus norvegicus RepID=PLMN_RAT				4.45E-03
P05545	DQAEINTGSALFIDKEQPILSEFQEK	0.00E+00	8.26E+07	8.87E+05	1.80E+08	Serine protease inhibitor A3K n=1 Tax=Rattus norvegicus RepID=SPA3K_RAT				4.49E-03
P08721	SQESDEAIKVIPVAQR	0.00E+00	5.86E+07	0.00E+00	9.10E+07	Osteopontin n=1 Tax=Rattus norvegicus RepID=OSTP_RAT				4.69E-03
P04639	DEPQSQWDRVKDF	0.00E+00	4.96E+07	0.00E+00	8.59E+07	Apolipoprotein A-I n=1 Tax=Rattus norvegicus RepID=APOA1_RAT				4.71E-03
M0R8A9	AVEPLGDKFN	5.54E+05	1.19E+07	1.20E+07	4.82E+07	Apolipoprotein A-IV n=1 Tax=Rattus norvegicus RepID=M0R8A9_RAT				4.85E-03
P02651	VQEQVQEQVQPKPLE	1.14E+07	2.19E+08	2.35E+07	5.83E+07	Apolipoprotein A-IV n=1 Tax=Rattus norvegicus RepID=APOA4_RAT				4.93E-03
G3V8D4	GSSALLDTVQEHL	0.00E+00	0.00E+00	7.93E+07	3.25E+08	Apolipoprotein C-II (Predicted) OS=Rattus norvegicus GN=Apoc2 PE=4 SV=1				5.07E-03
P02770	YTQKAPQVSTPTLVEAAR	7.30E+05	5.47E+06	1.84E+07	2.43E+09	Serum albumin n=1 Tax=Rattus norvegicus RepID=ALBU_RAT				5.13E-03
Q7TPI9	LQPLDFKENPEQSR	0.00E+00	1.64E+07	3.29E+07	9.37E+08	Ac2-248 n=1 Tax=Rattus norvegicus RepID=Q7TPI9_RAT				5.20E-03
M0R8A9	DSGDVESHLSF	0.00E+00	1.80E+07	2.20E+07	2.95E+07	Apolipoprotein A-IV n=1 Tax=Rattus norvegicus RepID=M0R8A9_RAT				5.23E-03
Q80ZA3	TTLQDFHLDEDRTVR	0.00E+00	0.00E+00	1.06E+07	6.32E+08	Alpha-2 antiplasmin OS=Rattus norvegicus GN=Serpinf1 PE=2 SV=1				5.31E-03
Q9WUW3	SDQGGETEIETEETEMLTPDMDTERK	0.00E+00	1.20E+08	4.64E+07	8.53E+07	Complement factor I OS=Rattus norvegicus GN=Cfi PE=2 SV=1				5.32E-03
P05544	LSQPEDQVEINTGSALFIDKEQPIL	0.00E+00	2.33E+07	5.41E+08	1.51E+07	Serine protease inhibitor A3L n=1 Tax=Rattus norvegicus RepID=SPA3L_RAT				5.32E-03
UPI0002AB826B	ESYAGVTLDPR	0.00E+00	7.30E+06	3.27E+07	2.58E+07	UPI0002AB826B related cluster n=1 Tax=Rattus norvegicus RepID=UPI0002AB826B				5.32E-03
Q01177	KVILGAHEER	0.00E+00	9.55E+06	1.65E+08	2.39E+07	Plasminogen n=1 Tax=Rattus norvegicus RepID=PLMN_RAT				5.34E-03
P06759	LWESGPEDQLTTPT	0.00E+00	5.21E+07	7.08E+07	1.90E+08	Apolipoprotein C-III n=1 Tax=Rattus norvegicus RepID=APOC3_RAT				5.45E-03
G3V615	LSSLTETIEGADAEDGHSPGEQQ	0.00E+00	8.09E+07	2.22E+08	2.35E+07	Complement factor B, isoform CRA_b OS=Rattus norvegicus GN=C2 PE=3 SV=1				5.47E-03
P06759	WESGPEDQLTTPT	0.00E+00	2.09E+08	1.30E+08	8.08E+07	Apolipoprotein C-III n=1 Tax=Rattus norvegicus RepID=APOC3_RAT				5.59E-03
P02650	DQVQEELQSSQVTQEL	0.00E+00	0.00E+00	4.60E+07	2.57E+07	Apolipoprotein E n=1 Tax=Rattus norvegicus RepID=APOE_RAT				5.77E-03
Q08420	DTGESGVDLADRLDLVEK	0.00E+00	0.00E+00	5.85E+07	1.66E+08	Extracellular superoxide dismutase [Cu-Zn] n=1 Tax=Rattus norvegicus RepID=SODE_RAT				5.79E-03
P15399	TVYLAASSVEK	0.00E+00	0.00E+00	5.72E+07	6.01E+07	Probasin n=3 Tax=Rattus RepID=PBAS_RAT				5.80E-03
P09006	IDELYLPK	0.00E+00	3.30E+08	7.59E+07	9.05E+07	Serine protease inhibitor A3N n=1 Tax=Rattus norvegicus RepID=SPA3N_RAT				5.83E-03
P02770	QVSTPTLVEAAR	1.91E+05	1.34E+08	1.03E+08	5.18E+06	Serum albumin n=1 Tax=Rattus norvegicus RepID=ALBU_RAT				6.01E-03
P28902	VTVQDGDLSFPLESVK	0.00E+00	1.74E+07	6.82E+07	2.32E+08	Guanylin n=1 Tax=Rattus norvegicus RepID=GUC2A_RAT				6.07E-03
P02770	QTALAELVK	5.04E+05	0.00E+00	6.87E+06	6.57E+07	Serum albumin n=1 Tax=Rattus norvegicus RepID=ALBU_RAT				6.20E-03
P02770	VDETYVPKEF	0.00E+00	4.04E+06	9.75E+06	1.84E+07	Serum albumin n=1 Tax=Rattus norvegicus RepID=ALBU_RAT				6.34E-03
P05544	LFSDLEERTS	0.00E+00	0.00E+00	3.89E+07	1.12E+09	Serine protease inhibitor A3L n=1 Tax=Rattus norvegicus RepID=SPA3L_RAT				6.35E-03
G3V947	VVQGTTEYQYQWQL	0.00E+00	3.95E+06	2.56E+07	2.12E+07	SMR1 protein (Fragment) OS=Rattus norvegicus GN=Vcsa1 PE=4 SV=2				6.37E-03
Q99PS8	THEIGCPPPPEGK	1.88E+06	3.63E+07	4.90E+07	2.68E+07	Histidine-rich glycoprotein OS=Rattus norvegicus GN=Hrg PE=2 SV=1				6.38E-03
Q68FY8	DIDPEDEELELGPR	3.05E+06	7.15E+07	1.79E+07	1.55E+07	Protein C OS=Rattus norvegicus GN=Proc PE=2 SV=1				6.50E-03
Q68FT8	MDLPGQQPVSEQAQQK	1.84E+07	1.13E+08	4.12E+07	1.42E+08	Protein Serpinf2 OS=Rattus norvegicus GN=Serpinf2 PE=2 SV=1				6.61E-03
P24090	HAFSPVASVESASGEVLH	3.43E+05	1.74E+06	8.19E+05	2.65E+07	Alpha-2-HS-glycoprotein n=1 Tax=Rattus norvegicus RepID=FETUA_RAT				6.71E-03
Q7TP84	VVGGCVANPHSW	0.00E+00	1.54E+07	3.02E+07	2.77E+07	Ab1-346 n=1 Tax=Rattus norvegicus RepID=Q7TP84_RAT				6.84E-03

Protein	Sequence	mean peak intensity control	mean peak intensity DM	mean peak intensity HTN	mean peak intensity DM+HTN	Description	control vs all	DM vs control	HTN vs control	HTN+DM vs control
G3V836	SLLNSLEEAK	0.00E+00	1.90E+07	7.81E+07	3.09E+07	Clusterin OS=Rattus norvegicus GN=Clu PE=3 SV=1				6.87E-03
P02454	DRGETGPAGPAGPIGP	0.00E+00	0.00E+00	2.01E+07	1.91E+07	Collagen alpha-1(I) chain n=1 Tax=Rattus norvegicus RepID=CO1A1_RAT				6.92E-03
E0A3N4	DSLRPSMIDELYLPK	0.00E+00	4.06E+05	4.46E+05	7.73E+09	Serpina3n-like protein n=1 Tax=Rattus norvegicus RepID=E0A3N4_RAT				7.01E-03
D3ZBS2	FYDGSEIVVAGR	6.84E+06	6.96E+06	1.20E+07	2.55E+09	Inter-alpha-trypsin inhibitor heavy chain H3 OS=Rattus norvegicus GN=Itih3 PE=2 SV=2				7.03E-03
G3V615	LSSLTETIEGADAEDGHSPGEQQK	0.00E+00	1.10E+08	3.89E+06	2.56E+09	Complement factor B, isoform CRA_b OS=Rattus norvegicus GN=C2 PE=3 SV=1				7.37E-03
M0R8A9	LGSDSGDVESHLSF	1.00E+08	7.05E+07	4.63E+07	3.27E+09	Apolipoprotein A-IV n=1 Tax=Rattus norvegicus RepID=M0R8A9_RAT				7.41E-03
P05544	DQVEINTGSALFIDKEQP	2.69E+06	2.72E+08	1.20E+08	1.89E+07	Serine protease inhibitor A3L n=1 Tax=Rattus norvegicus RepID=SPA3L_RAT				7.59E-03
G3V947	TAPDPTPLSNPPTQL	5.63E+07	3.01E+08	1.91E+08	1.46E+08	SMR1 protein (Fragment) OS=Rattus norvegicus GN=Vcsa1 PE=4 SV=2				7.82E-03
Q5M7T5	DVLEQKVPEATNR	8.93E+06	4.94E+07	1.40E+08	9.87E+06	Protein Serpinc1 OS=Rattus norvegicus GN=Serpinc1 PE=2 SV=1				7.95E-03
P24090	FSPVASVESASGEVLH	1.67E+07	5.02E+06	0.00E+00	3.04E+07	Alpha-2-HS-glycoprotein n=1 Tax=Rattus norvegicus RepID=FETUA_RAT				8.07E-03
P05545	MQQVESSLQPETLKK	2.87E+07	1.53E+07	5.23E+07	1.62E+08	Serine protease inhibitor A3K n=1 Tax=Rattus norvegicus RepID=SPA3K_RAT				8.10E-03
P02651	KGSPDQPLALPLPEQVQEQ	0.00E+00	7.08E+07	0.00E+00	1.03E+08	Apolipoprotein A-IV n=1 Tax=Rattus norvegicus RepID=APOA4_RAT				8.13E-03
P05545	DQAEINTGSALFIDKEQPI	0.00E+00	0.00E+00	3.77E+07	1.59E+07	Serine protease inhibitor A3K n=1 Tax=Rattus norvegicus RepID=SPA3K_RAT				8.35E-03
A1L114	TSDSDIFTDIENPSSHVPEFSSSSK	0.00E+00	1.05E+07	9.65E+07	4.54E+07	Fga protein OS=Rattus norvegicus GN=Fga PE=2 SV=1				8.42E-03
P05544	AEAFIADFK	0.00E+00	2.74E+07	7.96E+07	4.59E+07	Serine protease inhibitor A3L n=1 Tax=Rattus norvegicus RepID=SPA3L_RAT				8.58E-03
Q5BKC4	NFRTENYEEQFEMF	0.00E+00	3.06E+08	3.76E+08	1.39E+07	C9 protein OS=Rattus norvegicus GN=C9 PE=2 SV=1				8.65E-03
Q6IRS6	GKSPEEPFPVQLDLTTNPQG	6.53E+06	2.74E+07	7.01E+07	7.32E+06	Fetub protein OS=Rattus norvegicus GN=Fetub PE=2 SV=1				8.69E-03
Q01177	LKEAQLPVIENK	0.00E+00	1.11E+07	4.65E+06	1.60E+07	Plasminogen n=1 Tax=Rattus norvegicus RepID=PLMN_RAT				8.75E-03
Q68FT8	DLPGQQPVSEQAQQK	0.00E+00	8.31E+07	0.00E+00	3.17E+07	Protein Serpinf2 OS=Rattus norvegicus GN=Serpinf2 PE=2 SV=1				8.91E-03
P08721	DEPSVETHSLEQSKEY	0.00E+00	6.09E+06	7.29E+07	3.13E+07	Osteopontin n=1 Tax=Rattus norvegicus RepID=OSTP_RAT				9.00E-03
P02770	YTQKAPQVSTPTLVEAAR	0.00E+00	0.00E+00	1.26E+07	4.79E+07	Serum albumin n=1 Tax=Rattus norvegicus RepID=ALBU_RAT				9.01E-03
P24090	SPVASVESASGEVLHSPK	0.00E+00	3.57E+06	1.52E+07	1.78E+08	Alpha-2-HS-glycoprotein n=1 Tax=Rattus norvegicus RepID=FETUA_RAT				9.09E-03
G3V836	EQEFSDNELQELSTQGSR	0.00E+00	3.25E+07	0.00E+00	3.42E+07	Clusterin OS=Rattus norvegicus GN=Clu PE=3 SV=1				9.17E-03
P14480	QAATTDSDKVDLSIAR	0.00E+00	0.00E+00	6.62E+06	1.85E+07	Fibrinogen beta chain n=1 Tax=Rattus norvegicus RepID=FIBB_RAT				9.19E-03
P09006	QAEAFTADFQQSR	0.00E+00	3.78E+07	5.02E+06	5.77E+06	Serine protease inhibitor A3N n=1 Tax=Rattus norvegicus RepID=SPA3N_RAT				9.20E-03
P02651	INTYADDLQNKLV	0.00E+00	0.00E+00	4.65E+07	2.84E+06	Apolipoprotein A-IV n=1 Tax=Rattus norvegicus RepID=APOA4_RAT				9.45E-03
F1LM05	TQADLSGITGDKDL	0.00E+00	9.73E+07	1.03E+08	6.77E+07	Protein LOC299282 n=1 Tax=Rattus norvegicus RepID=F1LM05_RAT				9.57E-03
M0RBF1	TLDPEHLGQGGVQRE	0.00E+00	1.82E+07	3.43E+07	1.04E+08	Complement C3 OS=Rattus norvegicus GN=C3 PE=4 SV=1				9.64E-03
P08721	HSDAVATWLKPDP	6.65E+06	1.63E+08	4.41E+07	3.96E+07	Osteopontin n=1 Tax=Rattus norvegicus RepID=OSTP_RAT				9.96E-03